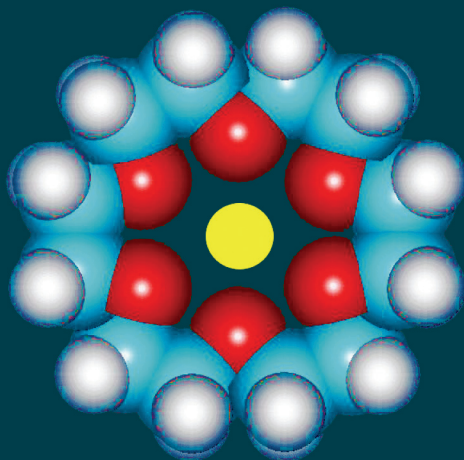


MOLECULAR RECEPTORS

Edited by

Volodymyr I. Rybachenko



MOLECULAR RECEPTORS

Collected research papers

Edited by
Volodymyr I. Rybachenko

Donetsk
«East Publisher House»
2011

УДК 541.1+547

ББК 24.2

M 75

**Reviewers: Opeida I.A. – professor
Grzesiak Piotr – professor**

Recommended for printing academic councils of L. Litvinenko Institute Physical Organic and Coal Chemistry National Academy of Science of Ukraine & Faculty of Chemistry Adam Mickiewicz University Poznan, Poland

M 75 Molecular receptors: [collected research papers] / Edited by V.I. Rybachenko. – Donetsk : «East Publisher House» Ltd, 2011. – 343 p.

ISBN 978-966-317-108-1

Functional materials with molecular receptors is a new direction in chemistry. The book presents the results of basic research on various types of molecular receptors. Discusses not only the synthesis, properties and application of these systems but also the research methods appropriate to describe the molecular receptors and their complexes.

Функціональні матеріали на підставі молекулярних рецепторів є новий напрямок в хімії. У книзі представлені результати фундаментальних досліджень різних типів молекулярних рецепторів. Обговорюється не тільки синтез, властивості і застосування цих систем, а й методи досліджень, що підходять для опису молекулярних рецепторів і їх комплексів.

УДК 541.1+547

ББК 24.2

M 75

ISBN 978-966-317-108-1

© Collective of authors, 2011

Contents

List of contributors	5
Alginate-the phenomenon of natural polysaccharide polymer	13
<i>Joanna Kurczewska</i>	
Ruthenium dyes and their application in dye-sensitized solar cells	27
<i>Maciej Zalas</i>	
Ionic liquids as electrolyte components in quasi solid state photoelectrochemical cells	39
<i>Maciej Zalas and Mariusz Walkowiak</i>	
Acceptor number of organoboron molecules - quantitative determination of Lewis acidity	53
<i>Michał Jakubczyk, Agnieszka Adamczyk-Woźniak and Andrzej Sporzyński</i>	
Sulfur-containing molecules in phenylboronic acids chemistry	69
<i>Krzysztof M. Borys, Agnieszka Adamczyk-Woźniak and Andrzej Sporzyński</i>	
The application of the energy-resolved in-source collision-induced dissociation method for examination of ion fragmentation pathways ...	87
<i>Natalia Mańkowska and Grzegorz Schroeder</i>	
Application of noble gas NMR in fullerene chemistry	105
<i>Błażej Gierczyk</i>	
Mass spectral analysis of synthetic polymers end groups by MALDI MS (matrix-assisted laser desorption/ionization mass spectrometry)	141
<i>Grażyna Bartkowiak and Grzegorz Schroeder</i>	

Selected tripodal receptors for halide anions	165
<i>Bogusława Łęska</i>	
Biological and chemical properties of semduramicin	181
<i>Radosław Pankiewicz and Bogusława Łęska</i>	
Humic acids as molecular receptors	197
<i>Svetlana Khil'ko, Rimma Semenova, Grzegorz Schroeder and Volodymyr Rybachenko</i>	
Synthesis and application of organic polyphosphates as drug carrier ..	207
<i>Viktor Anischenko, Volodymyr Rybachenko, Grzegorz Schroeder, Constantine Chotiy and Andrew Redko</i>	
Products of organic wastes thermal degradation as a source of molecular adsorbents and receptors	219
<i>Elena Lygina, Alexander Dmitruk, Leonid Galushko, Svetlana Lyubchik, Vladimir Tret'yakov and Grzegorz Schroeder</i>	
Hybrid inorganic-organic mesostructured thin films	245
<i>Agata Wawrzyńczak and Izabela Nowak</i>	
Terpyridine as molecular receptor in functional polymers	259
<i>Szymon Jasiocki and Grzegorz Schroeder</i>	
Supramolecular complexes of terpenes and their derivatives with cyclodextrins	285
<i>Leonid Yakovishin, Vladimir Grishkovets, Grzegorz Schroeder and Volodymyr Rybachenko</i>	
Mesoporous material as assisted matrix for MALDI-TOF MS	317
<i>Szymon Jasiocki, Izabela Nowak and Grzegorz Schroeder</i>	
Phosphono peptides and their host-guest chemistry. ESI MS study	329
<i>Piotr Młynarz, Bernadeta Lasek, Paweł Kafarski, Tomasz Kozik and Grzegorz Schroeder</i>	

List of contributors

Agnieszka Adamczyk-Woźniak

Warsaw University of Technology
Faculty of Chemistry
Noakowskiego 3
00-664 Warsaw
Poland

Viktor Anischenko

L.M. Litvinenko Institute of Physical-Organic and Coal Chemistry
National Academy of Sciences of Ukraine
Department of Spectrochemical Researches
R. Luxemburg 70
81-134 Donetsk
Ukraine

Grażyna Bartkowiak

Adam Mickiewicz University
Faculty of Chemistry
Grunwaldzka 6
60-780 Poznań
Poland

Krzysztof M. Borys

Warsaw University of Technology
Faculty of Chemistry
Noakowskiego 3
00-664 Warsaw
Poland

Constantine Chotiy

L.M. Litvinenko Institute of Physical-Organic and Coal Chemistry
National Academy of Sciences of Ukraine
Department of Spectrochemical Researches
R. Luxemburg 70
81-134 Donetsk
Ukraine

Alexander Dmitruk

Tugan-Baranovsky State University of Economy and Trade
Zhorsa 31
83050 Donetsk
Ukraine

Leonid Galushko

L.M. Litvinenko Institute of Physical Organic and Coal Chemistry NAS
of Ukraine
R. Luxemburg 70
83-114 Donetsk
Ukraine

Błażej Gierczyk

Adam Mickiewicz University
Faculty of Chemistry
Grunwaldzka 6
60-780 Poznań
Poland

Vladimir Grishkovets

V.I. Vernadsky Taurida National University
Vernadsky Ave. 4
Simferopol
95007 Crimea
Ukraine

Michał Jakubczyk

Warsaw University of Technology
Faculty of Chemistry
Noakowskiego 3
00-664 Warsaw
Poland

Szymon Jasiński

Adam Mickiewicz University
Faculty of Chemistry
Grunwaldzka 6
60-780 Poznań
Poland

Paweł Kafarski

Wrocław University of Technology
Faculty of Chemistry
Wybrzeże Wyspiańskiego 27
50-370 Wrocław

Svetlana Khil'ko

L.M. Litvinenko Institute of Physical Organic and Coal Chemistry NAS
of Ukraine
R. Luxemburg 70
83-114 Donetsk
Ukraine

Tomasz Kozik

Adam Mickiewicz University
Faculty of Chemistry
Grunwaldzka 6
60-780 Poznań
Poland

Joanna Kurczewska

Adam Mickiewicz University
Faculty of Chemistry
Grunwaldzka 6
60-780 Poznań
Poland

Bernadeta Lasek

Adam Mickiewicz University
Faculty of Chemistry
Grunwaldzka 6
60-780 Poznań
Poland

Elena Lygina

Tugan-Baranovsky State University of Economy and Trade
Zhorsa 31
83050 Donetsk
Ukraine

Svetlana Lyubchik

REQUIMTE-CQFB, Faculty of Sciences and Technology
New University Lisbon
Quinta da Torre
2829-516 Monte da Caparica
Portugal

Bogusława Łęska

Adam Mickiewicz University
Faculty of Chemistry
Grunwaldzka 6
60-780 Poznań
Poland

Natalia Mańkowska

Adam Mickiewicz University
Faculty of Chemistry
Grunwaldzka 6
60-780 Poznań
Poland

Piotr Młynarz

Wrocław University of Technology
Faculty of Chemistry
Wybrzeże Wyspiańskiego 27
50-370 Wrocław

Izabela Nowak

Adam Mickiewicz University
Faculty of Chemistry
Grunwaldzka 6
60-780 Poznań
Poland

Radosław Pankiewicz

Adam Mickiewicz University
Faculty of Chemistry
Grunwaldzka 6
60-780 Poznań
Poland

Andrew Redko

L.M. Litvinenko Institute of Physical-Organic and Coal Chemistry
National Academy of Sciences of Ukraine
Department of Spectrochemical Researches
R. Luxemburg 70
81-134 Donetsk
Ukraine

Volodymyr Rybachenko

L.M. Litvinenko Institute of Physical Organic and Coal Chemistry NAS
of Ukraine
R. Luxemburg 70
83-114 Donetsk
Ukraine

Grzegorz Schroeder

Adam Mickiewicz University
Faculty of Chemistry
Grunwaldzka 6
60-780 Poznań
Poland

Rimma Semenova

L.M. Litvinenko Institute of Physical Organic and Coal Chemistry NAS
of Ukraine
R. Luxemburg 70
83-114 Donetsk
Ukraine

Andrzej Sporzyński

Warsaw University of Technology
Faculty of Chemistry
Noakowskiego 3
00-664 Warsaw
Poland

Vladimir Tret'yakov

Topchiev Institute of Petrochemical Synthesis
Russian Academy of Sciences, Leninskii pr. 29
Moscow
119991 Russia

Mariusz Walkowiak

Institute of Non-Ferrous Metals Branch in Poznan CLAiO
Forteczna 12
61-362 Poznań
Poland

Agata Wawrzyńczak

Adam Mickiewicz University
Faculty of Chemistry
Grunwaldzka 6
60-780 Poznań
Poland

Leonid Yakovishin

Sevastopol National Technical University
Universitetskaya Str., 33
Sevastopol
99053 Crimea
Ukraine

Maciej Zalas

Adam Mickiewicz University
Faculty of Chemistry
Grunwaldzka 6
60-780 Poznań
Poland

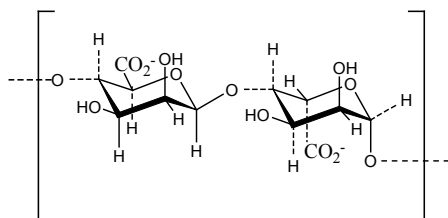
Chapter 1

Alginate-the phenomenon of natural polysaccharide polymer

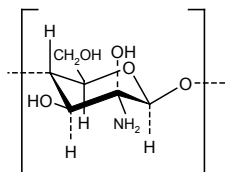
Joanna Kurczewska

*Adam Mickiewicz University, Faculty of Chemistry,
Grunwaldzka 6, 60-780 Poznań, Poland*

The chemical structure of varied synthetic and natural polymers encourages applying them for different purpose. On the one hand, the significant development of advanced synthetic methods allows designing of materials characterized by a desired functioning. On the other hand, the purification and extraction processes amplify the importance of natural products in area of biomaterials. Those biomaterials find many applications, among others as drug-delivery vehicles and tissue-engineering scaffolds [1, 2]. One of the simplest methods that guarantee biological activity is the use of polysaccharides. These compounds can be divided into two groups: non-mammalian and mammalian polysaccharides. The mammalian ones (alginate, chitin, dextran; Figure 1) are characterized by similar saccharide structure and simple procedure of material extraction, which results in costs decrease. This short review concentrates on first above mentioned naturally occurring polymer-alginate [3, 4].



ALGINATE
1-4 β-D-mannuronic acid
and 1-4 α-L-guluronic acid



CHITOSAN
1-4 β-D-glucosamine
and 1-4 β-N-acetyl-D-
glucosamine

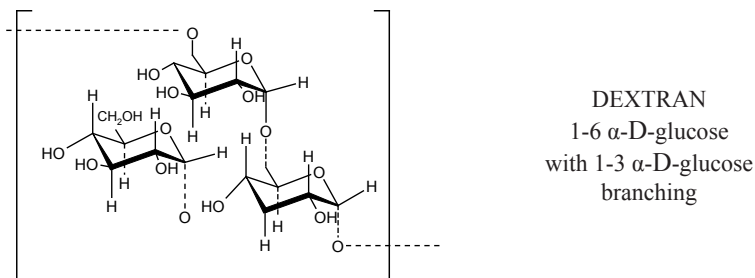


Figure 1. Non-mammalin polysaccharides

1. The characteristic of alginate

Alginate is obtained from two sources: 1. Commercial one is extracted from marine brown algae (*Laminaria hyperborean*, *Ascophyllum nodosum*, *Macrocystis pyrifera*) having about 40% of dry weight; 2. Bacterial alginates – from soil bacteria (*Azotobacter vinelandii* and some *Pseudomonas* species). Alginate from sea water exists as a mixed salt of Mg^{2+} , Ca^{2+} , Sr^{2+} , Ba^{2+} and Na^{+} , while a native one is present as an insoluble calcium gel. After mechanical harvest of algae, they are dried before further processing (with the exception of *M. Pyrifera* that is used without drying). After that algal material is treated with mineral acid in order to remove neutral homopolysaccharides, while alkaline earth cations are exchanged with protons. Next sodium carbonate is added (pH below 10.0) to change protonated form (insoluble) to sodium salt (soluble). The extraction process does not eliminate some impurities (heavy metals, proteins, polyphenols etc.). Those amounts are insignificant if only alginates are applied in food industry. However, in case of pharmaceutical application, the material requires further purification processes that are realized by several specialized manufacturers [5, 6].

The hydrophilic polysaccharide (Figure 2) consists of alternating residues of 1-4 α -L-guluronic (G-blocks) and β -D-mannuronic acid (M-blocks), which can vary in composition and sequence affecting molecular weight and physical properties of the material. Depending on the organism whose alginate is prepared from, the content of G- and M-blocks can be different. Molecular weight of alginate varies from 10 to 1000 kDa. The structure of the polymer chain is resistant to normal enzymatic degradation in mammals [7, 8].

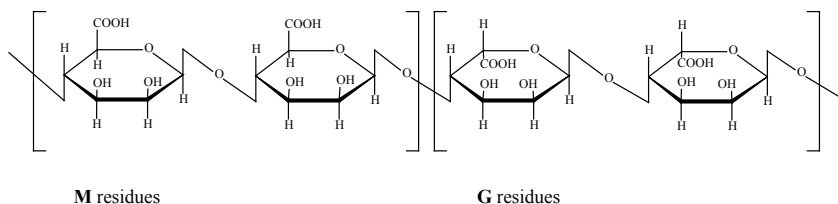


Figure 2. *M- and G-blocks of alginate structure*

2. Alginate gel formation

Gel formation of alginate is carried out under mild environment and is possible by reacting with divalent cations (Ca, Ba, Sr). The mild conditions of the process allow incorporating of proteins, cells and DNA into the matrix. Gelation process does not happen in the presence of monovalent cations and Mg^{2+} , while some divalent cations are useless due to their toxicity (Pb, Cu, Cd, Ni). Generally sodium cations (from guluronic acids) are exchanged with divalent ones and guluronic groups form egg-box structure (Figure 3). Moreover, alginate chains can dimerize to form gel networks [9,10].

Alginate applied in food industry (thickener, emulsifier, and stabilizer) is classified as a safe compound. In case of oral delivery, there is no conformity about the material biocompatibility but it is regarded as non-toxic and biodegradable.

Depending on the bead size, there are different procedures of preparation applied. Beads greater than 1.0 mm are formed by using a syringe with a needle or a pipette that influence diameter bead. Moreover, the shape of alginate beads can be influenced by sodium alginate viscosity. In case of microbead ($\gg 0.2$ mm), atomization (spraying method), emulsification and coacervation is applied. Generally, well mixed solution of sodium alginate and incorporated material (eg. proteins) is placed into a syringe linked to a pump. An atomization device is characterized by an orifice having specified diameter that guarantees desired size of droplets introduced into divalent solution. Final size of microbead depends on several agents: the pressure of nitrogen gas, the pump flow-rate, the distance between the orifice and the divalent solution. After that the procedure for all size of beads obtained is analogous, poly-L-lysine and final alginate coatings are formed. In general, alginate beads are rather inert to proteins. However, it is sometimes possible that positively charged proteins can compete with calcium cations for carboxylic acid sides taking effect in drug inactivation. In such situations, protective cover is added (anionic polymer) [11-14].

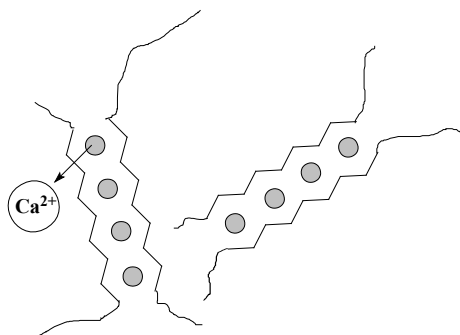


Figure 3. The scheme of egg-box structure of guluronic groups

Even though, atomization is the most popular method of microbeads preparation, the other techniques also require some attention. Oil-in-water emulsification is addressed to more stable drugs that are resistant to organic solvents (ethyl ether) used for the oil removing [15]. Complex coacervation boils down to the separation of two oppositely charged polyelectrolytes into two phases: a dense coacervate one (with microbeads) and dilute one [16].

Apart from mentioned morphologies, other ones can be also formed. “Block” gel formation is carried out as follows: alginate solution in a container is placed into divalent solution (gelation process) for several hours; then gels are cut (discs, blocks). If alginate solution is applied without proteins, then gel is immersed in the protein solution of high concentration and for a long time [17]. In case of alginate fibers, sodium alginate solution is extruded into a calcium ions solution. Very strong fibers are rolled up or chopped and find application in many wound dressings. As sodium ions are present in wound fluids, the mechanism of drug release from fibers is based on their slow conversion into sodium alginate solution [18]. The gelation process can also take place in situ, for example when applied into the eye by reacting with calcium ions present in tears [19].

Due to a variable content of guluronic and mannanuronic acid residues in alginate beads, their physical properties differ. Generally, the best parameters (mechanical strength, porosity, stability) are observed for alginate having 70% of α -L-guluronic acid that forms blocks higher than 15 long. However, alginates characterized by low α -L-guluronic acid content are more elastic [20, 21].

3. Alginate as a drug carrier

Drug release from alginate matrix proceeds through diffusion (through polymer pores) or degradation of alginate network. Diffusion method can only be applied if encapsulated molecules are characterized by appropriate molecular

weight. This method is influenced by the composition of alginate, encapsulated drug charge. The highest diffusion rates are observed for alginate beads with high G-residues content. It can be modified by drying the beads or incorporating them into acidic environment (low pH), which gives rise to pore size reduction [22, 23].

As crosslinking of alginate happens in the presence of divalent cations (mostly calcium ions), the opposite process should take place whenever Ca^{2+} ions are removed. It is achieved by the addition of chelating agent (eg. lactate, citrate), high concentration of other cations (sodium, magnesium) or phosphate buffer solution. As a result, the drug is released and the polymer starts to solubilize. Another process that destroys alginates is proton catalyzed hydrolysis, while low pH value can bring to faster degradation. The formation of strong complexes (with polycations, polypeptides, and synthetic polymers) prevents the biomaterial destruction [20, 24, 25].

From the biological point of view, there are two crucial factors that determine the application of any matrix as a drug carrier, strictly speaking immunogenicity and biocompatibility. Nowadays, alginates of different purity are purchased (ultra pure, food, research grade). Alginates applied as drug carriers should contain low M-residues and high G-residues, as well as it should be purified from mitogenic impurities (ultra-pure alginate) [26]. On the other hand, the strongest mucoadhesion (contact between two surfaces including mucosal layer) is observed for alginate if compared with other polymers (eg. polystyrene, chitosan) [27]. The covalent attachment of L-cysteine (Figure 4) in the presence of carbodiimide improves the mucoadhesive properties [28].

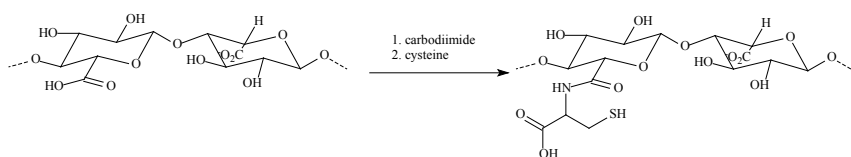


Figure 4. The synthesis of thiolated alginate

The list of possible proteins that can be successfully encapsulated in alginate matrix is impressive [29], starting with vaccines, through growth and tumor factors, cells and many others. There are also numerous of other materials that can be encapsulated, like probiotic bacteria, genes or metal ions. It is worth to mention several examples of the newest results that have been reported.

The micro shells constructed of alginate and chitosan, obtained using layer-by-layer self-assembly method, were prepared for doxorubicin encapsulation

[30]. Doxorubicin (Figure 5a) belongs to the most popular anti-cancer drugs that require an increasing of efficiency as well as a decreasing of toxic side-effects. Melamine formaldehyde was used as a template solution, around which polyelectrolyte microshells were formed. In order to obtain hollow microsphere that subsequently were filled with doxorubicin, the core was dissolved with hydrochloric acid. The release of the drug was studied by the incorporation of microshells into NaCl solution of physiological pH value. The release of the drug was controlled by the number of assembled layers. The high concentration of loaded doxorubicin guaranteed better effectiveness in cancer killing than free anti-cancer drug.

One of the theories assumes that cancerous cells are more sensitive to high temperature when compared to normal ones. Therefore, hyperthermia is a model of treatment of malignant tumors. As a source of heat, a high-frequency magnetic field can be applied. The combination of control heating and drug delivery in constructed magnetic beads should give promising results. Such a platform was designed by Brulé [31] and was composed of alginate microbeads filled with magnetic nanoheaters and doxorubicin. The temperature increase was observed after external magnetic field activation and it stimulated much faster anti-cancer drug release from microbeads in comparison to experiments carried out at room temperature. Moreover, magnetic nanoheaters are characterized by contrast properties so their position in a human body can be monitored by magnetic resonance imaging.

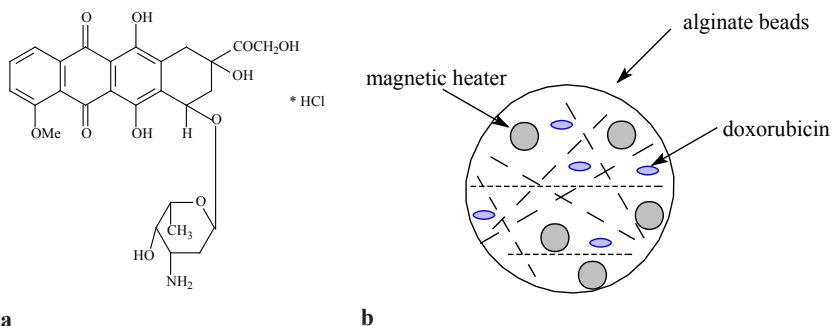


Figure 5. (a) The structure of doxorubicin; (b) The scheme of magnetic alginate beads containing doxorubicin

As it was mentioned above, alginic acid finds application as a support in a food industry. Recently, an enzyme–microbial xylanase-has become very popular in the food and beverage industries. Xylanases are the most important

enzymes responsible for xylan (the main component of hemicellulose) biodegradation. As they are large molecules, it is not possible to entrap these enzymes in alginate carrier. Therefore, it is rather recommended to immobilize the enzyme covalently. Pal [32] proposed the procedure, which requires the application of glutaraldehyde as an activator molecule of alginate beads. The enzyme was immobilized on the activated alginate beads at room temperature. After the optimization of all parameters, the results for the immobilized enzyme are promising.

Alginate can also be used in order to improve the properties of other biomaterials. Chen et al. [33] constructed hybrid cement consisted of calcium phosphate and alginate for gentamicin release. Calcium phosphate cement is known as an excellent material for bone defect repair and dental surgery. However, it is characterized by a serious defect, strictly speaking bone-defects of complex structures are rather inaccessible for a material and it is very sensitive to blood and other fluids influence. The process of calcium alginate gel formation occurs between sodium alginate and calcium phosphate cement. It was shown that the rate of the antibiotic release was extended in a hybrid cement when compared to standard calcium phosphate one.

On the other hands, there are many papers that consider methods with the object of the improvement of alginate effectiveness. The application of chitosan (the other polysaccharide having polycation properties) influences favorably mechanical properties and permeability of calcium alginate bead. However, from the practical point of view many applied methods of such microbeads formation (spray drying, coacervation, and emulsification/solidification) are useless because of oversized particles, broad size distribution of microspheres or deactivation of encapsulated drugs. Therefore, the membrane emulsification was proposed as an alternative technique that should ensure narrow size distribution [34]. However, the difficulty in this case is connected with the solidification of alginate droplets, which is not carried out directly by calcium ions solution. In order to obtain alginate-chitosan microspheres, sodium alginate water solution is passed under pressure through hydrophobic porous glass membrane (pore size 7 μm) to oil phase. Then, mini-emulsion of CaCl_2 solution is added to sodium alginate solution with uniform-sized droplets. Finally, solidified alginate gels are obtained (Figure 6). The properties of microspheres were tested with a use of a model peptide-insulin. As insulin is positively charged, it cannot be mixed with alginate directly because of aggregate formation. The experiment was carried out in a few directions: insulin was dissolved in CaCl_2 solution before mini-emulsion formation; insulin was dissolved in chitosan solution or both methods were combined. According to the results obtained, the best loading efficiency

was observed when insulin was added during the chitosan solidification process. Moreover, the use of this method guaranteed the best preservation of the immunological activity.

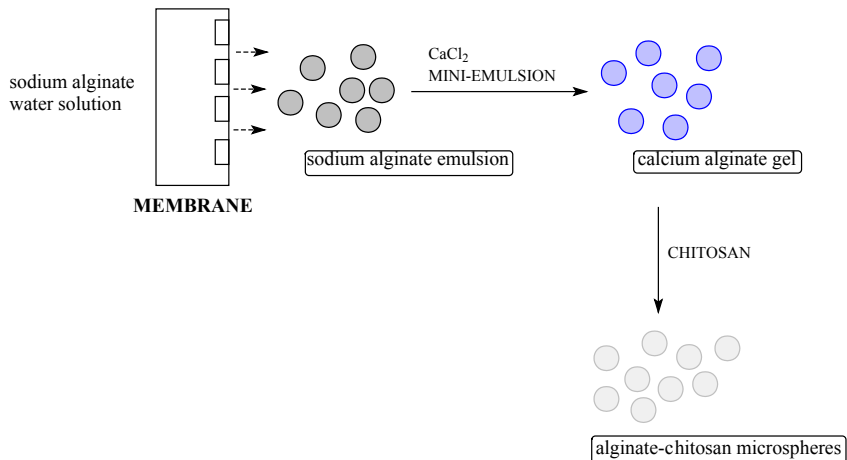


Figure 6. The procedure of alginate-chitosan microspheres preparation

4. Chemical modification of alginate

Apart from varied application of unmodified alginate, the presence of free hydroxyl and carboxyl groups in the structure encourages to synthesize the polysaccharide derivatives. Such modification influences different properties of the biopolymer, like solubility, physiochemical and biological ones. There are several possibilities to obtain alginate derivatives like oxidation, estrification or amidation of the biopolymer [35]. The oxidation process, carried out without the access of light, is used in order to increase the activity of the functional groups and the rate of degradation. It occurs on hydroxyl groups of sodium alginate in the presence of the oxidant (sodium periodate) and it takes effect in two aldehyde groups formation preceded by carbon C2-carbon C3 bond disruption (Figure 7). Such a derivative is more flexible and posses amplified number of reactive groups. However, the process must be controlled considering the concentration of the oxidant because of the possible difficulties with the gel formation in the presence of calcium ions [36-38]. The crosslinking process is achieved when the degree of oxidation is limited to 5%. The lower gel strength of oxidized alginate could explain its faster degradation when compared to unmodified polymer. The dialdehydes obtained are very sensitive to alkaline β -elimination even under physiological conditions.

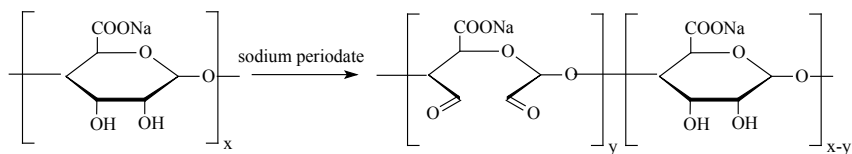


Figure 7. Alginate oxidation in the presence of sodium periodate

Very interesting derivative of the oxidized alginate was proposed by Kang et al. [39]. The reductive amination of 2,3-dialdehydic alginate with alkyl amines was applied in order to introduce alkyl groups of different lengths (C_8H_{17} -, $C_{12}H_{25}$ -, $C_{16}H_{33}$ -). The reduction of imines was carried out using sodium cyanoborohydride ($NaCNBH_3$) instead of traditional reducing agents: sodium hydroborate ($NaBH_4$), selenophenol ($PhSeH$) or pentarboronyl ions in alcoholic potassium hydroxide, which were less reactive and selective (Figure 8). The presence of long alkyl chains took effect in an appearance of amphiphilic characteristics of the polymers. The surfactants were able to solubilize of solid azobenzene as well as to adsorb cobalt cations from the solution.

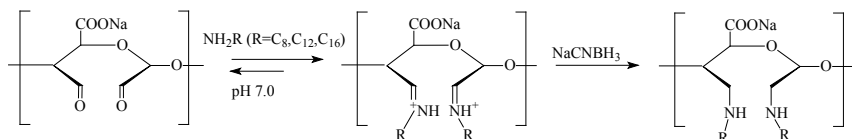


Figure 8. Synthesis of alginate-derived polymeric surfactants

The alginate modified with alkyl groups can participate in further synthesis. The one functionalized with octyl amine ($C_8H_{17}-NH_2$), 2,3-dioctyl amine alginate, was used to obtain alginate-poly(ethylene glycol) copolymer (Figure 9), [40]. Initially polyethyleneglycol monomethyl ether (PEG) was treated with succinic anhydride and pyridine (catalyst), giving PEG-COOH derivative. The coupling between 2,3-dioctyl amine alginate and PEG-COOH was carried out with 1-ethyl-dimethylaminopropyl-carbodiimide (EDC). Such prepared derivative retains the characteristics of gelation.

Chemical modification of hydroxyl groups is also carried on to obtain superabsorbent polymers. These polymers are characterized by the ability of absorption of vary large amount of water and retaining of water even under pressure. They find application not only as infant diapers, hygiene products, but also as controlled release devices. Yang et al. [41] described the synthesis of sodium alginate/ Na^+ rectorite grafted acrylic acid composite superabsorbent

by $^{60}\text{Co}\gamma$ -irradiation. The copolymerization of synthetic and natural polymers is much desired as the first ones are inexpensive, bio-degradable, friendly to the environment, while the second ones have large water absorbing capacities. Additionally, rectorite used for the superabsorbent preparation is characterized by good mechanical and thermal properties, as well as excellent UV resistance. The synthesis was carried out in several steps. Initially, rectorite was reacted with sodium pyrophosphate to obtain Na^+ rectorite, and then the product took part in the reaction with sodium alginate to get sodium alginate/ Na^+ rectorite. Finally acrylic acid was added and the mixture was irradiated under gamma-rays in order to obtain composite superabsorbent (Figure 10).

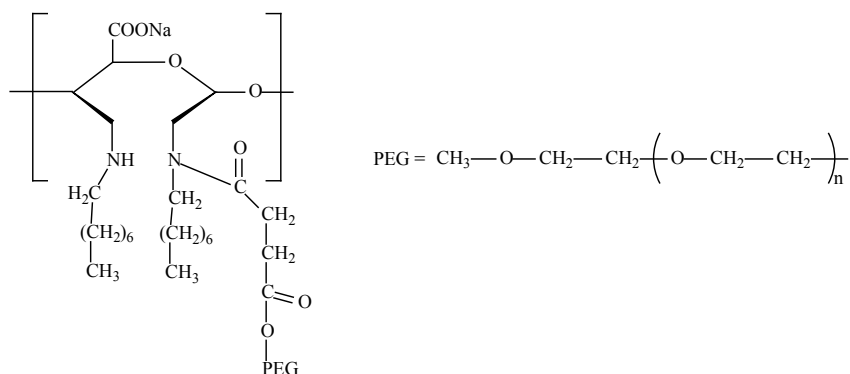


Figure 9. The scheme of alginate-poly(ethylene glycol) copolymer

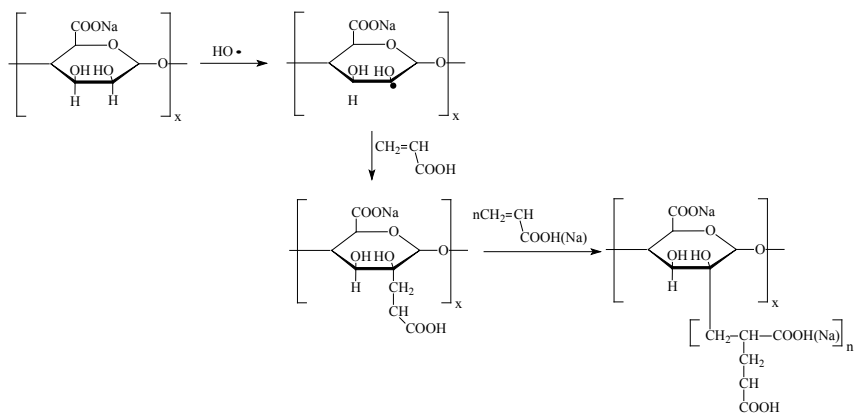


Figure 10. Synthesis of sodium alginate/acrylic acid copolymer

The other functional group in alginate structure, carboxylic one, usually undergoes esterification or amidation reaction. Generally, esterification is used to incorporate alkyl groups for increasing of the hydrophobic properties. The reaction is conducted directly in the presence of a catalyst and an alcohol in excess (Figure 11).

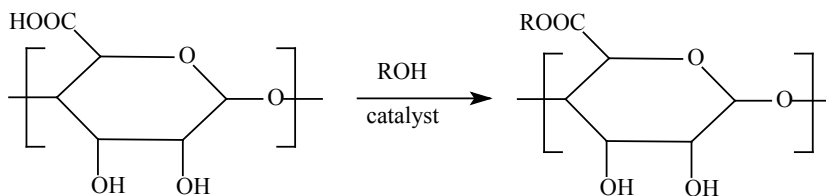


Figure 11. Esterification reaction between alginic acid and alcohol

Long alkyl chains (dodecyl and octadecyl) were attached to the alginate by Pelletier et al. [42]. Initially, carboxylic groups were transformed into their tetrabutylammonium salts and then reacted with alkyl halides, giving long alkyl chains linked to the backbone of the polymer via ester function. Broderick et al. [43] used direct esterification of alginate using butanol in excess (30:1) and concentrated sulphuric acid (catalyst). The derivative obtained possesses better hydrophobic properties with a retention of stable beads formation and non-toxic properties.

Alginate-amide derivatives can be synthesized with a coupling agent presence, eg. 2-chloro-1-methylpyridinium iodide (CMPI). Vallée et al. [44] carried on in this way covalent attachment of dodecylamine via amide linkage. On the other hand, Yao et al. modified sodium alginate to get a carrier for a drug release [45]. In this case, sodium alginate was dissolved in a buffer solution (pH 6.0) and reaction catalyst were added (1-ethyl-[3-(dimethylamino)propyl]-3-ethylcarbodiimide HCl, EDC; N-hydroxysuccinimide, NHC). After 24h of stirring at room temperature, the polymer solution (amino-ended polybutyl methacrylate, PBMA-NH₂) was dialyzed. The final product was used for an immobilization of bovine serum albumin and it demonstrated prolonged release behaviour compared to unmodified alginate.

Despite long-term studies concerning naturally occurring polymer-alginate, it is still a foundation of more advanced research regarding eg. drug delivery devices. Two directions of modern carriers development are very promising, strictly speaking the chemical modification of alginate structure that did not find as yet significant attention from the practical point of view; and the combination of two different polymers (natural or synthetic), which already is successfully

applied in practice.

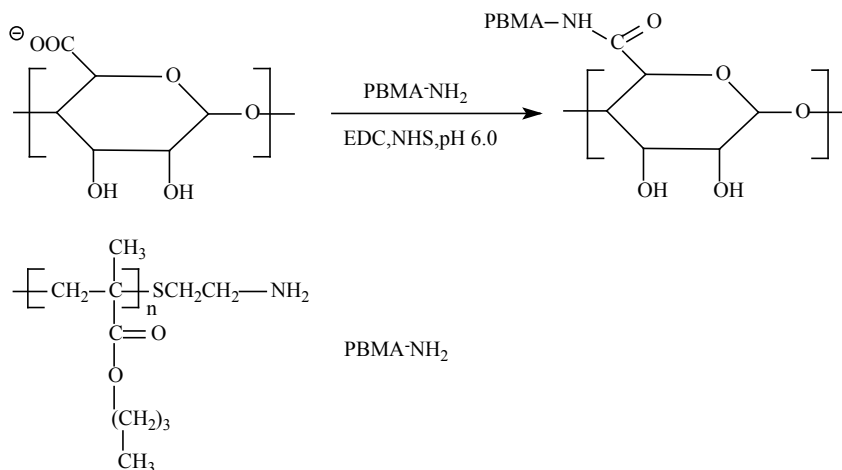


Figure 12. Synthesis of polybutyl methacrylate grafted alginate

References

1. N.A. Peppas, R. Langer, *Science*, 263, 1715-1720 (1994);
2. R.L. Reis, N.M. Neves, *Natural based polymers for biomedical applications*, CRC Press: Boca Raton, FL (2008);
3. P. Gacesa, *Carbohydr. Polym.*, 8, 161-182 (1988);
4. Y.S. Khotimchenko, V.V. Kovalev, V.O. Savchenko, O.A. Ziganshina, *R. J. Mar. Biol.*, 27, 53-64 (2001);
5. M. George, T.E. Abraham, *J. Control. Release*, 114, 1-14 (2006);
6. A.D. Baldwin, K.L. Kiick, *Biopolymers (Peptide Science)*, 94, 128-139 (2009);
7. A. Haug, B. Larsen, O. Smidsrod, *Acta Chem. Scand.*, 21, 691-704 (1967);
8. A. Haug, B. Larsen, *Acta Chem. Scand.*, 16, 1908-1918 (1962);
9. A.H. Clark, S.B. Ross-Murphy, *Adv. Polym. Sci.*, 83, 57-192 (1987);
10. D.A. Rees, *Pure Appl. Chem.*, 53, 1-14 (1981);
11. A. Martinsen, G. Skijak-Braek, O. Smidsrod, *Biotach. Bioeng.*, 33, 79-89 (1989);
12. A.A. Badwan, A. Abumaloo, E. Sallam, A. Abukalaf, O. Jawan, *Grug. Dev. Ind. Pharm.*, 11, 239-256 (1985);
13. K.K. Kwok, M.J. Groves, D.J. Burgess, *Proc. Int. Symp. Control.*

- Release Bioact. Mater., 16, 170-171 (1989);
14. K.K. Kwok, M.J. Groves, D.J. Burgess, *Pharm. Res.*, 8, 341-344 (1991);
 15. L.S. Wan, P.W. Heng, L.W. Chan, *J. Microencapsulation*, 9, 309-316 (1992);
 16. T. Alexakis, D. Boadi, D. Quong, A. Groboillot, I. O'Neill, D. Poncelet, R. Neufeld, *Appl. Biochem. Biotech.*, 50, 93-106 (1995);
 17. M. Bhakoo, S. Woerly, R. Duncan, *Proc. Int. Symp. Control. Release Bioact. Mater.*, 18, 441-442 (1991);
 18. T. Gilchrist, A.M. Martin, *Biomaterials*, 4, 317-320 (1983);
 19. S. Cohen, E. Lobel, A. Trevgoda, Y. Peled, *J. Control. Release*, 44, 201-208 (1997);
 20. O. Smidsrod, *Carbohyd. Res.*, 27, 107-118 (1973);
 21. A. Martinsen, G. Skjak-Braek, O. Smidsrod, F. Zanetti, S. Paoletti, *Carbohyd. Polym.*, 15, 171-193 (1991);
 22. H. Tanaka, M. Matsumara, I.A. Veliky, *Biotech. Bioeng.*, 26, 53-58 (1984);
 23. P. Chevalier, G.P. Consentino, J. de la Noue, S. Rakhit, *Biotech. Tech.*, 1, 201-206 (1987);
 24. I.W. Sutherland, *Alginates*, in: D. Byrom (Ed.), *Biomaterials; Novel Materials from Biological Sources*, Stockton, New York, pp. 309-331 (1991);
 25. R.J. Mumper, A.S. Hoffman, P. Puolakkainen, L.S. Bouchard, W.R. Gombotz, *J. Control. Release*, 30, 241-251 (1994);
 26. P. Soon-Shiong, M. Otterlie, G. Skjak-Braek, O. Smidsrod, R. Heintx, R. Lanza, T. Espevik, *Transplant. Proc.*, 23, 758-759 (1991);
 27. D.E. Chickering, E. Mathiowitz, *J. Control. Release*, 34, 251-261 (1995);
 28. J.R. Gum Jr, J.W. Hicks, N.W. Toribara, E.M. Rothe, R.E. Lagace, Y.S. Kim, *J. Biol. Chem.*, 267, 21375-21383 (1992);
 29. W.R. Gombotz, S.F. Wee, *Adv. Drug Deliver. Rev.*, 31, 267-285 (1998);
 30. X. Tao, H. Chen, X.-J. Sun, J.-F. Chen, W.H. Roa, *Int. J. Pharmaceut.*, 336, 376-381 (2007);
 31. S. Brulé, M. Levy, C. Wilhelm, D. Letourner, F. Gazeau, C. Ménager, C. Le Visage, *Adv. Mater.*, 23, 787-790 (2011);
 32. A. Pal, F. Khanum, *Process Biochem.*, 46, 1315-1322 (2011);
 33. Ch.-H. David Chen, Ch.-Ch. Chen, M.-Y. Shie, Ch.-H. Huang, S.-J. Ding, *Mater. Sci. Eng. C*, 31, 334-341 (2011);
 34. Y. Zhang, W. Wei, P. Lv, L. Wang, G. Ma, *Eur. J. Pharm. Biopharm.*, 77, 11-19 (2011);

35. J.-S. Yang, Y.-J. Xie, W. He, *Carbohydr. Polym.*, 84, 33-39 (2011);
36. C.G. Gomez, M. Rinaudo, M.A. Villar, *Carbohydr. Polym.*, 67, 296-304 (2007);
37. K.A. Kristiansen, A. Potthast, B.E. Christensen, *Carbohydr. Polym.*, 345, 1264-1271 (2010);
38. K.A. Kristiansen, H.B. Tomren, B.E. Christensen, *Carbohydr. Polym.*, 86, 1595-1601 (2011);
39. H.-A. Kang, G.-J. Jeon, M.-Y. Lee, J.-W. Yang, *J. Chem. Technol. Biol.*, 77, 205-210 (2002);
40. P. Laurienzo, M. Malinconico, A. Motta, A. Vicinanza, *Carbohydr. Polym.*, 62, 274-282 (2005);
41. L. Yang, X. Ma, N. Guo, *Carbohydr. Polym.*, 85, 431-418 (2011);
42. S. Pelletier, P. Hubert, F. Lapique, E. Payan, E. Dellacherie, *Carbohydr. Polym.*, 43, 343-349 (2000);
43. E. Broderick, H. Lyons, T. Pembroke, H. Byrne, B. Murray, M. Hall, *J. Colloid Interf. Sci.*, 298, 154-161 (2006);
44. F. Vallée, C. Müller, A. Durand, S. Schimchowitch, E. Dellacherie, C. Kelche, J.C. Cassel, M. Leonard, *Carbohydr. Res.*, 344, 223-228 (2009);
45. B. Yao, C. Ni, C. Xiong, C. Zhu, B. Huang, *Bioprocess Biosyst. Eng.*, 33, 457-463 (2010).

Chapter 2

Ruthenium dyes and their application in dye-sensitized solar cells

Maciej Zalas

*Adam Mickiewicz University, Faculty of Chemistry,
Grunwaldzka 6, 60-780 Poznań, Poland*

1. Introduction

Continuously growing demand for energy in view of foreseeable depletion of resources of fossil fuels such as coal, oil and/or natural gas, is one of the most important challenges for human civilization. On the other hand, degradation of the natural environment has prompted development of non-pollutant and environmentally friendly energy production technologies [1]. In general the main sources of the clean energy are:

- solar energy
- wind power
- hydropower
- geothermal
- biomass

Photovoltaic technologies utilizing solar operation as the energy source are the most promising ones and may soon replace the traditional fuels [2]. The main advantage of solar cells is direct conversion of solar energy to the electricity without any intermediate forms of the energy. This gives very good performance on the photon-to-current conversion efficiencies. The first commercial solar cell was demonstrated by Bell Telephone Laboratories in 1954 [2, 3]. This device was a silicon p-n junction type and had efficiency of about 6%. Since that time the efficiency of photocurrent production of silicon solar cells has reached 25% [4]. These values are more intelligible when compared with the maximal theoretical photoelectric conversion efficiency, which is equal 33% [5]. Almost five times increase in the efficiencies that have become very close to the theoretical maximum, achieved over the last 60 years, shows huge potential of the solar cell technologies. Unfortunately, except these undisputed advantages, silicon solar cell has a number of disadvantages. For example the manufacture of silicon

photovoltaic devices needs very sophisticated methods and ultra high purity and/or toxic chemicals, which have negative influence on the manufacturing costs and the environment [2]. For the above reasons photovoltaic technology has still a marginal importance in global energy production [5].

In 1991 Grätzel et al. have first reported dye-sensitized nanocrystalline TiO_2 based solar cell [6]. The photoconversion efficiency of this device was 7.1-7.9%. The use of low cost and commercially available materials and chemicals without of any specific treatment and purification connected with relatively high efficiency (at that time) made the dye-sensitized solar cells (DSSC) an interesting alternative to the conventional silicon devices. Enormous interest in the DSSC may be illustrated by the fact that over the first decade after first announcement by Grätzel et al., over 2500 of original works in this area were published by scientific groups all over the world. Nowadays, everyday two or three new research articles on the subject are published [5].

2. Principles of DSSC operation

In short, DSSC device (fig. 1) is made of two conductive glass electrodes [1, 2, 5, 7-11]. The first electrode is a transparent photoanode, which consist of tin conducting oxide glass (TCO) substrate coated with a thin mesoporous layer of nanocrystalline semiconducting oxide with a wide band gap (mostly TiO_2). The surface of the semiconductor is modified with a monolayer of chemisorbed dye molecules. The second electrode, the counter electrode, is made of TCO coated with an ultrathin layer of platinum. The electrolyte containing redox medium (usually I^-/I_3^- couple) is injected between these two electrodes to transfer charge between them.

There are different opinions about which part of the DSSC device, the semiconductor [7] or the dye [1, 12], plays the main role in the photoelectric process taking place in the cell upon its illumination. There is no doubt, however, that the whole operating process starts when the dye molecule absorbs a photon of visible light. After this process (see fig. 2) the electron is excited from the highest occupied molecular orbital (HOMO) to the lowest unoccupied molecular orbital (LUMO) of the dye molecule, which process leads to generation of the excited state of the dye. The excited electron is consequently injected from the LUMO orbitals of the dye to the conduction band of the semiconductor and in consequence the dye undergoes oxidation. The oxidized dye is regenerated through the electron transferred from the reduced form of redox mediator present in the electrolyte and simultaneously the oxidized form of the redox mediator is created. At the same time the photoinjected electron is transported through the nanoparticle network of the semiconductor to reach the TCO substrate. The

electrons collected on TCO are transported through the external circuit, give electric power, and finally get into the counter electrode, where they regenerate the reduced form of the redox mediator via reducing the oxidized form and close the circuit. In the ideal system the whole operation process takes place without consumption nor permanent transformation of any chemical species and theoretically it can occur until illumination is present.

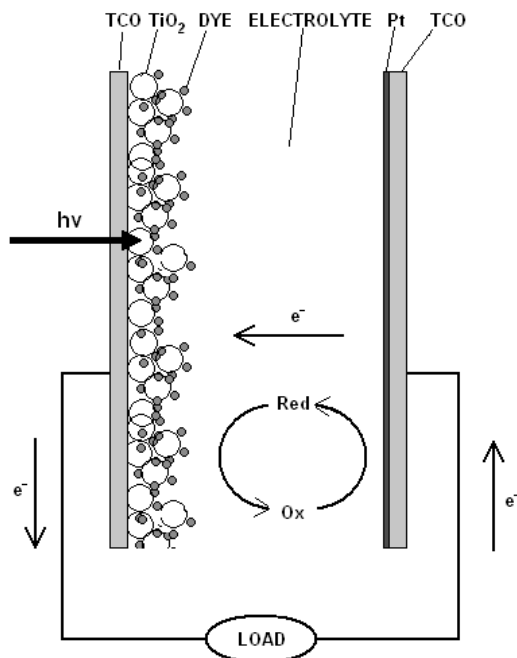


Figure 1. Schematic structure of the typical DSSC device.

Unfortunately in real systems there are some undesirable electron transfer pathways, which cause some losses. The excited dye molecules can directly recombine to reproduce the dye molecule ground state and the absorbed energy is usually emitted as heat. Another unwanted process in DSSC is the recombination of the electron injected into the semiconductor conduction band with the oxidized form of the dye. The main cause of losses is the interactions between the semiconductor nanoparticles and the redox mediator in the electrolyte. The processes described above cause a considerable decrease in the cell performance and much attention is paid to prevention of these processes.

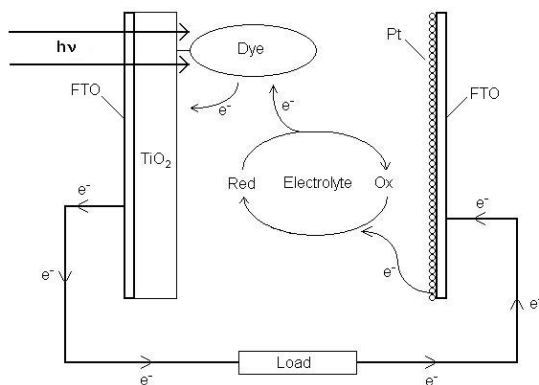


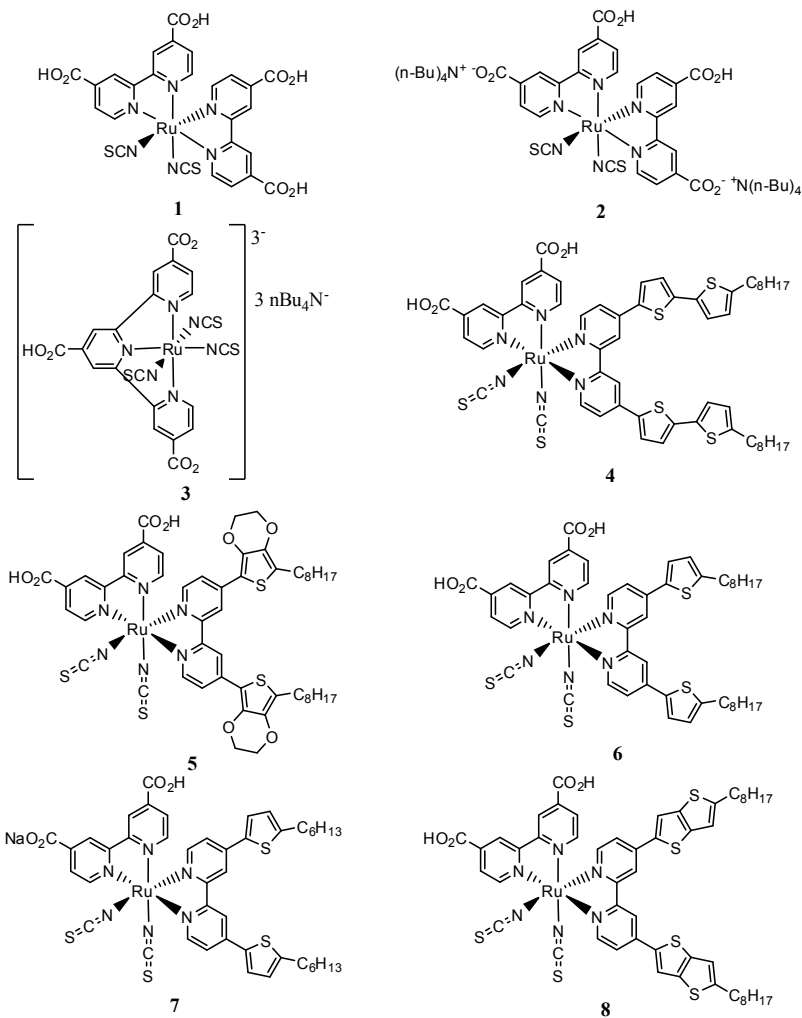
Figure 2. Mechanism of the DSSC operation

In this short review we will focus on the dye molecule, which is responsible for the most important process of the light-to-electricity conversion phenomena, namely for the light harvesting. From among many classes of dyes, such as metal complexes, organic dyes and natural dyes, we will focus on those which contain in their molecules the ruthenium atom and are applied in the most effective DSSC devices.

3. Application of ruthenium dyes in DSSC

An efficient photosensitizer should have some important features such as intensive absorption in a wide range of visible light, strong interaction with the semiconductor surface and good efficiency of the electron injection to the semiconductor's conduction band. Moreover the dye should be easily regenerated by the electrolyte redox mediator, and must be stable both in its ground and excited state [12, 13]. So far, the Ru-complexes have been the most successful family of sensitizers, in terms of performance and long-term stability, used in DSSC ever [1]. Ligands in typical Ru-complexes may be divided into two groups such as anchoring ligands and ancillary ligands [12]. The first group is first of all responsible for the adsorption of the dye molecule onto semiconductor surface, then it usually also is a chromophore. The ancillary ligands are mainly chromophores which are not directly attached to a semiconductor and are used for tuning the properties of the complexes. In d^6 metals complexes the polypyridinic ligands show strong metal to ligand charge transfer (MLCT) bands in the visible region, which supports injection of the electron to the conduction band of the semiconductor. Modification of both types of ligands (anchoring and ancillary) in polypyridinic Ru-complexes influences the sensitization properties of the dye

and, in consequence, the performance of the photovoltaic devices assembled with those sensitizers. The vast majority of the literature in the field is focused on the ancillary ligands modification, but there are some papers whose authors are concerned with the anchoring ligands.

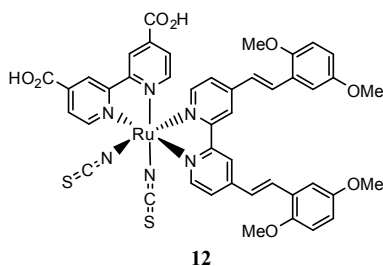
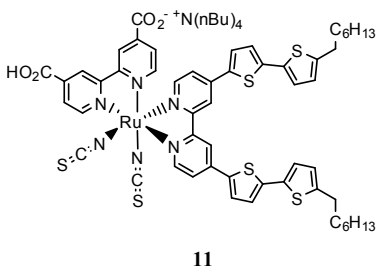
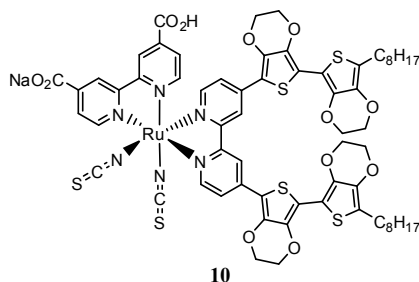
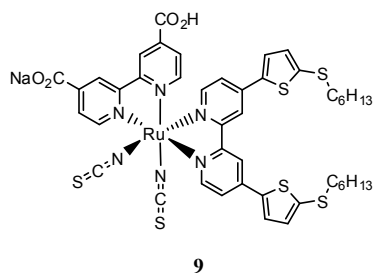


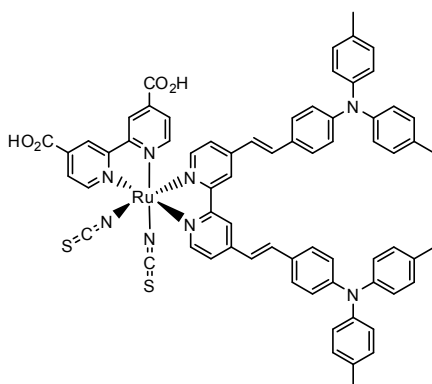
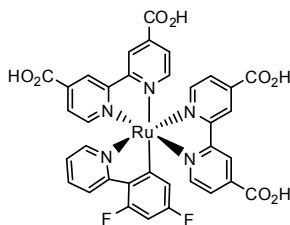
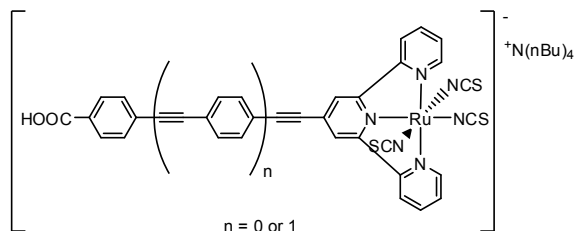
O'Regan and Grätzel in their first announcement about highly effective DSSC have used trimeric ruthenium complex, and the cell they proposed had a performance of 7.1-7.9% [6]. After a very short time Grätzel and co-workers have reported N3 (**1**) and N719 (**2**) dyes which were characterized with high photon-to-current conversion efficiencies of 10.0 and 11.2% respectively [14]. These two dyes differ only in the protonation state, N719 is a bis(tetrabutylammonium) salt of N3. Each of them has a wide absorption reaching 800 nm and the differences in the photoconversion efficiencies follow from the higher voltage in the N719 sensitized cell. In 1997 the same group reported a terpyridyl analogue of N3 and N719, the so-called "black dye" (**3**), characterised with an extended range of light harvesting, including near infrared region up to 920 nm [15]. Despite so wide range of light absorption, the efficiency of photoconversion obtained in the device sensitized with "black dye" reaches only 10.4%. The "black dyes" incident photon conversion efficiency (ICPE) for the whole visible region usually exceeds 80%, as recorded of N3, additionally the spectral response in the red and near infrared region exceeds that characteristic for N3, which resulted in higher short circuit photocurrent. Unfortunately relatively low extinction coefficient and poor coverage of the semiconductor surface leads to not very impressive photoconversion efficiency. In spite of these disadvantages the "black dye" together with N3 and N719 are still in the forefront of the dyes with best photoelectric performance and have become a kind of reference for further research to DSSC development.

Since 1997, a number of modifications of Ru-sensitizers have been developed and their efficiencies have reached up to 12.3% [1]. The attention of the researches was mainly focused on extending the chromophoric functions of ancillary ligands. A good example of this direction of research is the work by Wu et. al. who presented highly conjugated ligand substituted with alkyl thiophene groups in the the CYC-B1 dye (**4**) [16]. CYC B1 is characterised by a high absorption coefficient in the main MLTC band, what gives photoconversion efficiency 8.5%. In the device sensitised with the thiophene dye the photoconversion efficiency was by 10% higher than that of the cell based on N3, produced and studied in the same conditions. The efficiency of the cell sensitised with N3 was 7.7%. In continuation of the study on the effect of thiophene groups, the same research group in 2007 published their results on the other two complexes SJW-E1 (**5**) and CYC-B3 (**6**) [17]. These two sensitizers gave the efficiencies of 9.0 and 7.4%, while N3 in the same conditions gave 8.4%. The hitherto record efficiency is 12.3% and has been achieved for the device sensitized with mono(tetrabutylammonium) salt of CYC-B1, referred also as Z991, in the presence of dineoheksylo bis-(3,3-dimethyl-butyl)-phosphonic acid

as a co-adsorbent [18].

Grätzel [19-22] and Wang [22-24] and their co-workers studied the ligands containing systems of coupled π bonds (that enhance light absorption by sensitised TiO₂) and hydrophilic substituents (that protect the system against moisture and increase stability of solar cells). These studies resulted in presentation of a group of sensitizers C101 (**7**), C104 (**8**), C106 (**9**) C107 (**10**) and CYC-B11 (**11**) with efficiencies 11.3%, 10.5%, 11.4%, 10.7% and 11.5%, respectively. Unquestionable advantage of the systems employing above sensitizers is their extreme stability during the long-term exposure to light and relatively high temperature. These features make such cells potentially suitable for commercial outdoor applications. For example the device sensitized with C101 and employing a non-volatile electrolyte based on 3-methoxypropionitrile or ionic-liquid electrolyte has shown conversion efficiency of 9.0% and 7.4%, respectively, maintaining 95% of the initial performance for 1000h full sunlight operation at 60°C. Similar temporal stability was observed for the CYC-B11 sensitized cell with a low-volatile electrolyte in similar conditions, however a slightly lower, 7.9% overall conversion efficiency was observed. The stability of CYC-B11 device employing a solid state electrolyte was on the same level with the efficiency of 4.7%.



**13****14****15**

Nazeeruddin et. al. reported an interesting dye N954 (**12**) with photon-to-current efficiency of 10.8% [25]. The dye has a high extinction coefficient obtained thanks to the ligands with extended π -conjugation and orientation in the excited state, by tuning of the LUMO level of the ligand. The sensitizing Ru-complex, containing in its molecule a ditolylamine phenyl-ethyl-2,2'-bipyridine ligand, IJ-1 (**13**), has been studied by Yum et. al [26]. IJ-1 reached the photoconversion efficiency of 10.3%, when sensitizing nanocrystalline titania. Grätzel et. al. have studied an Ru-sensitizer YE05 in which thiocyanate groups were replaced by 2-(2,4-difluorophenyl) pyridine ligand (**14**) [18, 26]. The DSSC with a liquid-

based electrolyte and compound (**14**) exhibits an overall conversion efficiency of 10.1%. The DFT calculations shows that HOMO is located mostly on ruthenium and cyclometallated ligand, while LUMO is on the anchoring ligands. These orbital locations promote the excited electron injection into the semiconductors' conducting band. The authors postulated of that presented findings will provide new designing criteria for the next generation of Ru-dyes and will help foster widespread interest in the engineering of new sensitizers interacting effectively with the redox couple in the electrolyte.

The anchoring ligands modifications, as mentioned above, have been rarely used for design of new ruthenium sensitizers, but there are some reports about these methods. A good example of this route to obtain a new class of Ru-dyes may be the work presented by Funaki and co-workers [27]. The authors have presented two analogues of "black dye" with π expanded ligands having phenylene-ethynylene moiety (**15**). The molar extinction coefficients of these dyes were higher than that of the "black dye", but their conversion efficiencies were much lower and did not exceed 5.7%. The authors of this paper speculated that the low efficiency was due to aggregation of dye molecules on the semiconductor surface and in consequence to a decreased light harvesting. Despite of the relatively low efficiencies of so far presented sensitizers with extended anchoring ligands, this route of ligands designing seems to be an attractive way to obtain new hi-efficient ruthenium dyes for DSSC.

4. Conclusions

Ruthenium-based dyes are relatively expensive and, when DSSC seems to be low-cost alternative for silicon solar cells, this is one of their main disadvantage. In fact, the price of Ru-sensitizers depends more on difficulties with the purification of final product, during synthesis, than on the price of rare metal [1]. DSSC devices sensitized with ruthenium dyes, because of they high photoconversion efficiencies and very good stability under solar operation conditions, probably will first find commercial application. However, the costs of the Ru-dyes fabrication may be a major factor limiting of the expansion of this technology. For the above reasons further development of the Ru-dyes for DSSC sensitization should not be focused only on increasing the sensitization performance, but on improving the methods of their synthesis too. The intensive efforts on investigation of the sensitizing dyes and other DSSC materials leads to a slow evolution of the photoelectric performance and temporal stability of constructed devices, however there are still many problems, which must be solved, before DSSCs will find a wide application as a mass energy producing technology.

Acknowledgments

This work was supported by the Polish Ministry of Science and Higher Education, grant No. N N204 023538

References

1. C. Vougioukalakis, A.I. Philippopoulos, T. Stergiopoulos, P. Falaras, Contributions to the development of ruthenium-based sensitizers for dye-sensitized solar cells, *Coord. Chem. Rev.*, 255 (2011) 2602-2621.
2. B. Li, L. Wang, B. Kang, P. Wang, Y. Qiu, Review of recent progress in solid-state dye-sensitized solar cells, *Sol. Energy Mater. Sol. Cells*, 90 (2006) 549-573.
3. H. Spanggaard, F.C. Krebs, A brief history of the development of organic and polymeric photovoltaics, *Sol. Energy Mater. Sol. Cells*, 83 (2004) 125-146.
4. M.A. Green, The path to 25% silicon solar cell efficiency: History of silicon cell evolution, *Progress in Photovoltaics: Research and Applications*, 17 (2009) 183-189.
5. A. Hagfeldt, G. Boschloo, L. Sun, L. Kloo, H. Pettersson, Dye-Sensitized Solar Cells, *Chem. Rev. (Washington, DC, U. S.)*, 110 (2010) 6595-6663.
6. B. O'Regan, M. Grätzel, A low-cost, high-efficiency solar cell based on dye-sensitized colloidal TiO₂ films, *Nature*, 353 (1991) 737-740.
7. A. Hagfeldt, M. Grätzel, *Molecular Photovoltaics*, *Acc. Chem. Res.*, 33 (2000) 269-277.
8. S. Günes, N.S. Sariciftci, Hybrid solar cells, *Inorg. Chim. Acta*, 361 (2008) 581-588.
9. M. Grätzel, Dye-sensitized solar cells, *Journal of Photochemistry and Photobiology C: Photochemistry Reviews*, 4 (2003) 145-153.
10. M. Grätzel, Photoelectrochemical cells, *Nature*, 414 (2001) 338-344.
11. M. Grätzel, Sol-Gel Processed TiO₂ Films for Photovoltaic Applications, *J. Sol-Gel Sci. Technol.*, 22 (2001) 7-13.
12. A.S. Polo, M.K. Itokazu, N.Y. Murakami Iha, Metal complex sensitizers in dye-sensitized solar cells, *Coord. Chem. Rev.*, 248 (2004) 1343-1361.
13. S. Ardo, G.J. Meyer, Photodriven heterogeneous charge transfer with transition-metal compounds anchored to TiO₂ semiconductor surfaces, *Chem. Soc. Rev.*, 38 (2009) 115-164.
14. M.K. Nazeeruddin, A. Kay, I. Rodicio, R. Humphry-Baker, E. Mueller, P. Liska, N. Vlachopoulos, M. Graetzel, Conversion of light to electricity by *cis*-X₂bis(2,2'-bipyridyl-4,4'-dicarboxylate)ruthenium(II) charge-

- transfer sensitizers (X = Cl-, Br-, I-, CN-, and SCN-) on nanocrystalline titanium dioxide electrodes, *J. Am. Chem. Soc.*, 115 (1993) 6382-6390.
15. M.K. Nazeeruddin, P. Pechy, M. Gratzel, Efficient panchromatic sensitization of nanocrystalline TiO₂ films by a black dye based on a trithiocyanato-ruthenium complex, *Chem. Commun. (Cambridge, U. K.)*, (1997) 1705-1706.
 16. C.-Y. Chen, S.-J. Wu, C.-G. Wu, J.-G. Chen, K.-C. Ho, A Ruthenium Complex with Superhigh Light-Harvesting Capacity for Dye-Sensitized Solar Cells, *Angewandte Chemie International Edition*, 45 (2006) 5822-5825.
 17. C.Y. Chen, S.J. Wu, J.Y. Li, C.G. Wu, J.G. Chen, K.C. Ho, A New Route to Enhance the Light-Harvesting Capability of Ruthenium Complexes for Dye-Sensitized Solar Cells, *Adv. Mater. (Weinheim, Ger.)*, 19 (2007) 3888-3891.
 18. M. Grätzel, Recent Advances in Sensitized Mesoscopic Solar Cells, *Acc. Chem. Res.*, 42 (2009) 1788-1798.
 19. F. Gao, Y. Wang, D. Shi, J. Zhang, M. Wang, X. Jing, R. Humphry-Baker, P. Wang, S.M. Zakeeruddin, M. Grätzel, Enhance the Optical Absorptivity of Nanocrystalline TiO₂ Film with High Molar Extinction Coefficient Ruthenium Sensitizers for High Performance Dye-Sensitized Solar Cells, *J. Am. Chem. Soc.*, 130 (2008) 10720-10728.
 20. F. Gao, Y. Wang, J. Zhang, D. Shi, M. Wang, R. Humphry-Baker, P. Wang, S.M. Zakeeruddin, M. Gratzel, A new heteroleptic ruthenium sensitizer enhances the absorptivity of mesoporous titania film for a high efficiency dye-sensitized solar cell, *Chem. Commun. (Cambridge, U. K.)*, (2008) 2635-2637.
 21. C.-Y. Chen, M. Wang, J.-Y. Li, N. Postrakulchote, L. Alibabaei, C.-h. Ngoc-le, J.-D. Decoppet, J.-H. Tsai, C. Grätzel, C.-G. Wu, S.M. Zakeeruddin, M. Grätzel, Highly Efficient Light-Harvesting Ruthenium Sensitizer for Thin-Film Dye-Sensitized Solar Cells, *ACS Nano*, 3 (2009) 3103-3109.
 22. P. Wang, S.M. Zakeeruddin, J.E. Moser, M.K. Nazeeruddin, T. Sekiguchi, M. Gratzel, A stable quasi-solid-state dye-sensitized solar cell with an amphiphilic ruthenium sensitizer and polymer gel electrolyte, *Nat. Mater.*, 2 (2003) 402-407.
 23. Y. Cao, Y. Bai, Q. Yu, Y. Cheng, S. Liu, D. Shi, F. Gao, P. Wang, Dye-Sensitized Solar Cells with a High Absorptivity Ruthenium Sensitizer Featuring a 2-(Hexylthio)thiophene Conjugated Bipyridine, *The Journal of Physical Chemistry C*, 113 (2009) 6290-6297.

24. Q. Yu, S. Liu, M. Zhang, N. Cai, Y. Wang, P. Wang, An Extremely High Molar Extinction Coefficient Ruthenium Sensitizer in Dye-Sensitized Solar Cells: The Effects of π -Conjugation Extension, *The Journal of Physical Chemistry C*, 113 (2009) 14559-14566.
25. M.K. Nazeeruddin, T. Bessho, L. Cevey, S. Ito, C. Klein, F. De Angelis, S. Fantacci, P. Comte, P. Liska, H. Imai, M. Graetzel, A high molar extinction coefficient charge transfer sensitizer and its application in dye-sensitized solar cell, *Journal of Photochemistry and Photobiology A: Chemistry*, 185 (2007) 331-337.
26. T. Bessho, E. Yoneda, J.-H. Yum, M. Guglielmi, I. Tavernelli, H. Imai, U. Rothlisberger, M.K. Nazeeruddin, M. Grätzel, New Paradigm in Molecular Engineering of Sensitizers for Solar Cell Applications, *J. Am. Chem. Soc.*, 131 (2009) 5930-5934.
27. T. Funaki, M. Yanagida, N. Onozawa-Komatsuzaki, Y. Kawanishi, K. Kasuga, H. Sugihara, Ruthenium (II) complexes with [pi] expanded ligand having phenylene-ethynylene moiety as sensitizers for dye-sensitized solar cells, *Sol. Energy Mater. Sol. Cells*, 93 (2009) 729-732.

Chapter 3

Ionic liquids as electrolyte components in quasi solid state photoelectrochemical cells

Maciej Zalas¹ and Mariusz Walkowiak²

¹ *Adam Mickiewicz University, Faculty of Chemistry,
Grunwaldzka 6, 60-780 Poznań, Poland*

² *Institute of Non-Ferrous Metals Branch in Poznan CLAiO,
Forteczna 12, 61-362 Poznań, Poland*

Photoelectrochemical cells (also known as dye sensitized solar cells – DSSC) are a new type of devices for renewable energy harvesting through conversion of solar radiation into electricity. The concept of DSSCs was originally proposed by Grätzel in the early 90-ties [1]. DSSCs can be regarded as a promising alternative to conventional (so-called first-generation) photovoltaic cells, which have currently reached a high stage of development but at the same time suffering from relatively high cost, hindering their widespread adoption.

First generation solar cells has been relied on pure crystalline silicon and now constitutes about 90% of total PV (photovoltaics) market [2]. Second generation of solar cells is based on amorphous silicon, CIGS and CdTe thin films. Both first and second generation photovoltaic devices rely on single junctions. Dye sensitized solar cells are based on a totally different concept and can be regarded as a promising candidates for a third generation of photovoltaics, mainly because potentially lower cost and design flexibility.

DSSCs are composed of photoanode in the form of a thin film of mesoporous wide-gap semiconductor (typically nanostructured TiO₂), coated onto a conducting substrate (ITO glass), and a counter electrode, being most often thin platinum layer also coated onto a conducting substrate. The TiO₂ layer is coated with a monolayer of visible light absorbing dye. Between the photoanode and cathode there is an electrolyte consisting typically of a volatile organic solvents with an iodide/triiodide redox couple. Principle of operation of DSSCs has been described in numerous publications (refer for example to a recent thorough review [2]) and is also described in more detail in the other chapter of this book.

Although the general concept of DSSCs has proved to be successful, there

are several limitations for their further development and widespread commercial adoption. Apart from obstacles connected with the photoanode (ruthenium dyes are relatively expensive and sensitive to oxygen and water), there are a number of problems on the electrolyte side that must be solved urgently. First of all, the commonly used iodide/triiodide redox couple limits the performance of the device in terms of open-circuit voltage. Secondly, the commonly used liquid electrolytes are volatile and thus create technological and safety concerns, like the possibility of leakages and/or ignition.

Ionic liquids (IL) are potentially favorable alternatives for traditional volatile liquid electrolyte solutions. Ionic liquids in broader sense are all substances consisting entirely of ions and being liquid below 100 °C. Most interesting are so-called room temperature ionic liquids (RTIL) which are salts having melting temperatures below 20 °C. Advantages of ionic liquids that make them attractive for DSSCs are: low vapor pressure, non-flammability, thermal stability even to above 350 °C, wide electrochemical window (that is electrochemical stability over a large range of potentials), the ability to dissolve a wide range of substances, electric conductivity and tunable miscibility [3]. These favorable features made ILs prospective candidates for a number of technologies, including separation technologies, electrolytes (for fuel cells, metal deposition and metal finishing, batteries, photoelectrochemical cells, sensors and supercapacitors), synthesis/catalysis, cooling technologies, analytics, functional fluids and heat transfer and storage technologies. Some of these applications are still on the stage of R&D, while other have already been commercialized or are at the stage of pilot production (the case of DSSCs). Ionic liquids are generally composed of a large, asymmetrical cation (such as 1-alkyl-3-methylimidazolium, 1-alkylpyridinium, N-methyl-N-alkylpyrrolidinium, etc.) and a large variety of anions (see Fig. 1 for typical examples of anions and cations forming ILs).

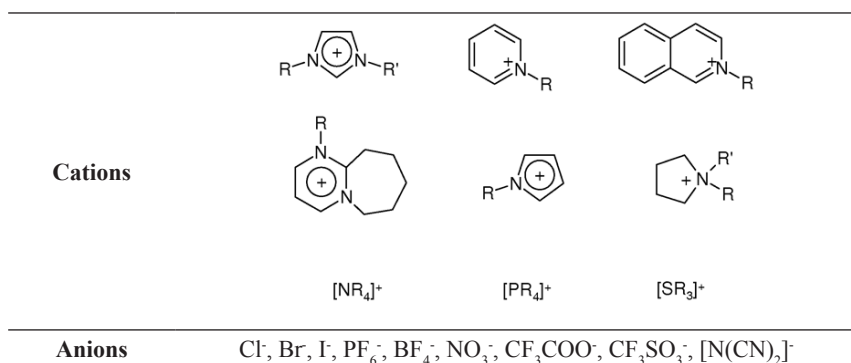


Figure 1. Typical cations and anions of simple room temperature ionic liquids

Ionic liquids were for the first time applied as electrolyte components for DSSCs by the group of Grätzel and co-workers in 1996 [6]. Imidazolium based ILs were first considered and are till now widely used (Fig. 2). Table 1 contains basic literature data on imidazolium cation-based electrolytes for DSSCs [4].

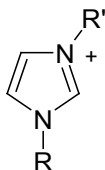
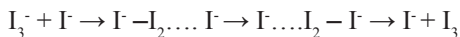


Figure 2. Structure of imidazolium cation

In their pioneering work, Grätzel and co-workers [6] examined methyl-hexyl-imidazolium iodide (MHImI) as potential electrolyte solvent for DSSC. The electrolyte was composed of 7 mM iodine in the MHImI solvent. It was found that the cells exhibited a very good stability with an estimated sensitizer turnover exceeding 50 millions. The ionic transport was found to be based on a different mechanism in comparison to organic solvent, resulting in sixteen fold increase in the effective diffusion coefficient of triiodide in the pure molten iodide salt. It was proposed that Grotthus-type charge carrier transfer occurred, involving chemical electron exchange, according to the following scheme:



This mechanism, including symmetrical transition state, was introduced for DSSC applications by Kawano et al. [19]. Thus triiodide may be transported to the counter electrode not only by diffusion but also by Grotthus-like, non-diffusional hopping mechanism. The reported results generally positioned ionic liquids as viable solution and attractive candidates for improved photoelectrochemical devices.

Ionic liquids can serve both as the source of iodide and separate solvent. In the above example MHImI was both solvent and the source of iodide ions. Other typical structures of ionic liquids being simultaneously sources of iodide anions are presented in Figs. 3-6. This is a favorable situation from the technological and safety point of view, allowing for getting rid of any volatile solvents. However, pure ionic liquids are often viscous, thus making problems with mass transport and the restoration of oxidized dye, so the photovoltaic performance of these DSSCs is often inferior to that of DSSCs using organic electrolyte solvents. The solution for this problem is either mixing IL with other low-viscosity solvent or attempts to synthesize novel IL with inherently low viscosity.

Table 1. Electrolyte compositions with imidazolium cation-based IIs and their basic photoelectrochemical parameters

Electrolyte composition	$J_{sc} / \text{mA cm}^{-2}$	V_{oc} / V	$\eta / \%$	Ref.
5 mM I2, 10% HMImI, 90% EMImTf	9.5	0.531	-	2
5 mM I2, 10% HMImI, 90% EMImTFSI	11.8	0.57	-	2
30 mM I2, 0.9 M DMHIml in EMIm-F \cdot 2.3HF	5.8	0.65	2.1	7
30 mM I2, 0.9 M DMHIml in EMImTFSI	0.9	0.50	0.36	7
0.2 M I2, 0.14 M GuanSCN, 0.5 M TBP in PMImI/EMImSCN (13 : 7 v/v)	13.3	0.746	7.0	8
0.1 M I2, 0.1 LiI, 0.45 NMBI n PMImI/EMImDCN (13 : 7 v/v)	12.8	0.707	6.6	9
I2, 0.5 M NMBI n PMImI/EMImTCM (1 : 1 v/v)	12.8	0.752	7.4	10
0.2 M I2, 0.5 NMBI, 0.1 GuanSCN n PMImI/EMImB(CN)4 (13 : 7 v/v)	13.55	0.736	7.0	11
0.8 M PMImI, 0.15 M I2, 0.1 M GuanSCN, 0.5 M NMBI in MPN	15.1	0.747	8.0	12
0.1 M HMImI2Br, 0.1 M GuanSCN, 0.5 M NMBI n HMImI	9.2	0.64	2.4	13
HMImI : I2 (10 : 1)	9.54	0.71	4.8	14
0.2 M I2, 0.5 NMBI, 0.1 GuanSCN in AllylEImI/AllylEImTFSI (13 : 7 v/v)	13.54	0.7	6.8	15
0.2 M I2 in PMImI/EMImTFSI/EMImTf (2 : 2 : 1, v/v/v)	16.13	0.612	6.67	16
0.5 M I2, 0.1 CuI n HMImI	13.6	0.538	4.54	17
0.2 M I2, 0.5 M NMBI n PMImI	13.07	0.678	6.27	18
0.2MI2, 0.5MNMBI, 0.12MGuanSCN n PMImI/EMImSCN (65 : 35 v/v)	13.99	0.707	7.05	18

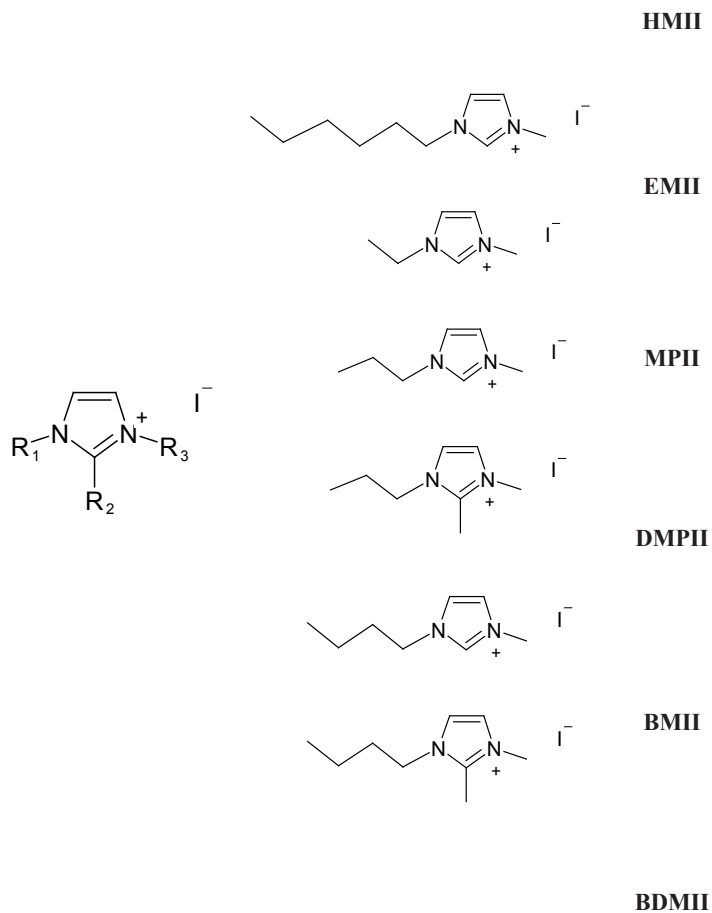


Figure 3. Imidazolium iodide derivatives

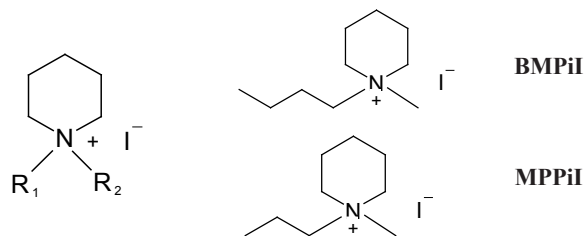


Figure 4. Piperidinium iodide derivatives

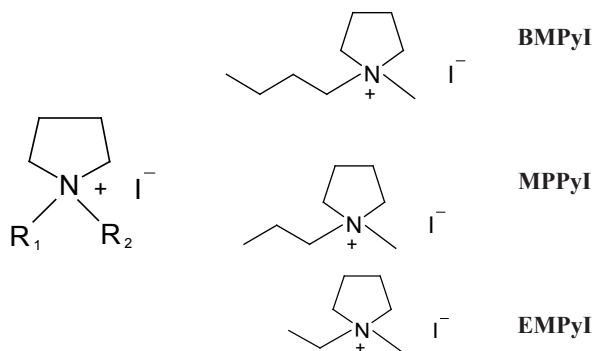


Figure 5. Pyrrolidinium iodide derivatives

As far as the first mentioned approach is concerned, a suitable diluting organic solvent is, for example, propionitrile. The problem is that the most important beneficial property of ILs, namely low vapor pressure, is dramatically compromised by adding volatile and flammable components to the system.

Example of the second approach is the development of ionic liquid IL (1-ethyl-3-methylimidazolium selenocyanate – EMISeCN) electrolyte-based $\text{SeCN}^-/(\text{SeCN})^{3-}$ redox couple [20]. The viscosity of this IL was 25 cP at 21 °C and specific conductivity at 21 °C – 14.1 mS cm⁻¹. The application of this low-viscosity and high-conductivity IL made it possible to achieve a good light-to-electricity conversion efficiency of 7.5–8.3 % (under AM 1.5 sunlight), showing path for the future developments. Nevertheless, although non-volatile, low-viscosity ILs can still be problematic in terms of potential leakages and

thus the necessity of very effective seals. Besides, some of the ILs exhibit a large degree of electrochemical instability (example: 1-ethyl-3-methylimidazoliumdicyanamide). Recently, much progress has been obtained by the application of so-called molecular volume approach, the technique allowing the prediction of melting points, viscosities, densities and conductivities of ILs [21]. In light of the fact that the total number possibly existing ionic liquids is estimated at 10^{18} , the ability of tuning their properties in a rational and predictable way seems much needed.

Quasi-solid electrolytes combine the characteristics of both liquid and solid electrolytes and have proved to be extremely viable in, for example, Li-ion battery technologies. The principal advantage of gel electrolytes is they usually exhibit satisfactorily high specific conductivities, while at the same time being to a large extent resistant to leakages and solvent evaporation. Gel electrolytes based on ionic liquids can additionally be regarded as practically non-volatile, non-flammable and thermally stable, thus giving chance for a substantial progress in the attempts to create technologically viable, safe and efficient energy conversion devices, including DSSCs. Generally speaking, gel electrolytes consist of a liquid medium (in this case ionic liquid-based electrolyte) entrapped in a polymeric matrix/network. It is said that the polymer network is swollen with liquid electrolyte. Quasi-solid-state electrolytes possess simultaneously both the cohesive property of a solid and the diffusive transport property of a liquid. The networking can be accomplished through a physical or a chemical method. Gel electrolyte formed via physical cross-linking is referred to as “entanglement network”, which is thermo-reversible. Chemical or covalent cross-linking leads to the formation of thermo-irreversible gel electrolytes [22-23].

A good example of physical cross-linking based gel electrolyte for the co-operation with ionic liquids are electrolytes relying on poly(vinylidene fluoride-co-hexafluoropropylene) (abbrev. PVdF-co-HFP) as polymeric matrix. PVdF-co-HFP based gel electrolytes are well known from Li-ion battery technologies where they have proved to be very successful. The group of Grätzel investigated the application of PVdF-co-HFP combined with PMImI or MePN-based liquid electrolyte containing for example 1,2-dimethyl-3-propyl imidazolium iodide and iodine [24-25]. It has been demonstrated that the DSSC exhibited a comparable photovoltaic performance to that of an analogous cell containing only the liquid electrolyte, with efficiencies from 5.3 to 6.1 %, which proved that the polymer matrix had no negative effect on the strictly electrical performance of DSSC, while at the same being obviously more resistant to leakage.

An interesting modification of the physically cross-linked gel electrolyte concept involves the application of ionic liquid modified silica particles.

Functionalized silica particles are embedded in the polymer matrix swollen with the liquid electrolyte. The role of this ceramic component is to further entrap the liquid component, making the resulting composite gel electrolyte even more stable and less prone to leakages and solvent evaporation. Similar idea is also known from Li-ion battery technologies. According to this general concept, Yan and co-workers [26] have recently reported the synthesis and successful application of 1-propyl-3-triethoxy silica-3-methylimidazolium iodide (TESPIm⁺I⁻) modified nanostructured silica. The prepared IL-SiO₂ material was subsequently dispersed in the polymer matrix, followed by soaking with the liquid medium to obtain the desired gel electrolytes.

Chemically cross-linked gel electrolytes have been prepared, for example, from ureasil precursor (Fig. 7) [27-30]. The unique structure of this thermosetting organic-inorganic hybrid gel electrolyte leads to high quality DSSCs, which exhibit 5–6 % light-to-electricity conversion efficiency even after several years of storage [31]. Ionic liquids as electrolyte solvents can be effectively entrapped in this type of covalent networks.

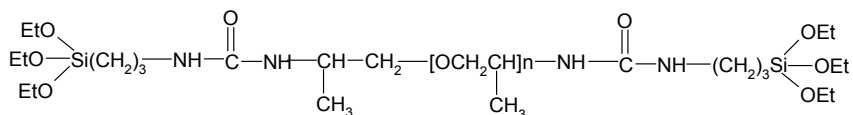


Figure 7. Structure of ureasil precursors

Further overview of the application of ionic liquids in quasi solid-state DSSCs is given in Table 2 [4].

Table 2. Quasi solid state electrolyte compositions for DSSCs and their basic photoelectrochemical parameters

Electrolyte composition	J_{sc} / mA cm ⁻²	V_{oc} / V	η / %	Ref.
0.1 M I ₂ , PVP (1.5 wt%), TBMB (4.5 wt%), PMImI (80 wt%), propionitrile (20 wt%)	10	-	-	32
0.3 M I ₂ , PVP (2 wt%), HOOC(CH ₂) ₁₆ COOH (4 wt%), H ₂ O (5 wt%) n PMImI	13.43	0.60	4.4	33
Gelator (2 wt%), 0.2 M I ₂ , 0.12 M GuanSCN, 0.5 M NMBI n PMImI/ EMImSCN (65 : 35 v/v)	12.7	0.706	6.3	34
0.3 LiI, 0.5 M I ₂ , 0.5 M NMBI, 10 wt% of gelators (see text) in HMImI	-	-	2.7-3	35
PEO, KI (20 wt%), I ₂ (10 wt% of KI) in EMImSCN	1.88	0.63	0.6	36

1 M LiI, 0.5 M I ₂ in PEO(750)MimCl	6.80	0.64	3.1	37
0.3 LiI, 0.03 M I ₂ , 0.5 M TBP, a-ZrP (6 wt%) in PMImDP	11.38	0.562	2.61	38
PVDF-HFP (10 wt%), I ₂ in PMImI	11.29	0.665	5.3	24
PVDF-HFP (5 wt%), 0.6 M DMPImI, 0.1 M I ₂ , 0.5 M NMBI in MPN	12.5	0.730	6.1	25
0.5 M I ₂ , 0.45MNMBI, SiO ₂ (5 wt%) n PMImI	12.75	0.672	6.1	39
0.5 M I ₂ , 0.45MNMBI, SiO ₂ (5 wt%) n PMImI/MPN (v : v = 13 : 7)	11.56	0.603	5.3	40
CH ₃ CO ₂ H, TMOS, 0.5MPMImI, 0.04mMNMBI, 20 mM I ₂ in PC/ Triton X-100 (molar ratio 4 : 1)	12.9	0.65	5.4	30
PEODME, SiO ₂ (9 wt%), I ₂ , PMImI	-	-	4.5	41
40 g/l of gelator, I ₂ (8.7 wt%) in HMImI	11.8	0.635	5.01	42
I ₂ (10 wt% of PMImI) n PHB/PMImI ([-O-] : PMImI = 10 : 1)	9.53	0.57	3.34	43
I ₂ /MBPyrri/succinonitrile (1 : 5 : 100 molar ratio)	7.8	0.618	6.7	44
0.35 M I ₂ , 0.02 M LiI, 0.5 M TBP, agarose (1 wt%) in PMImI	6.77	0.650	2.93	45
I ₂ , TBAI, EMImI, EC : PC (4 : 1 v/v), PEG	20.0	0.69	7.13	46
I ₂ (10 wt%) in TMS-PMImI	9.1	0.6	3.2	47
3 M TMS-PMImI, 30 M HCOOH, 3 M TMOS, 0.5 M NMBI, 1.4 M PMImI, 0.44 M I ₂	7.5	0.66	3.1	48
Poly(MHH), 0.2 M I ₂ in HMImI	8.6	0.66	3.8	49

Recently, ionic liquids with silane elements (functional groups) have also been considered as solvents and iodide sources for dye sensitized solar cells. The group of Grätzel reported three new triethoxysilanes bearing quaternary ammonium alkyl iodides: N,N,N-triethyl-3-(triethoxysilyl)propan-1-ammonium iodide, N,N,N-triheptyl-3-(triethoxysilyl)propan-1-ammonium iodide and N,N,N-tridodecyl-3-(triethoxysilyl)propan-1-ammonium iodide (see Fig. 8a) [50]. The electrolytes contained one or two silanes (in 30–60 wt%) as iodide sources together with I₂ (0.08 M), 0.1M guanidinium thiocyanate and 0.5M tert-butylpyridine in acetonitrile (AN) and I₂ (0.15M) and N-methylbenzimidazole (0.5M) for 2-methoxypropionitrile (MPN) as co-solvent. Efficiencies of up to 8.0% achieved at 0.1 Sunlight (100W/m²) intensity, which was described as promising from the point of view of low light or indoor application. The performance of the cells was reduced at higher light intensity (1 Sunlight) but efficiencies ≥5.0% were achieved for some electrolytes. The MPN-based electrolytes performed well at 1 Sunlight intensity, exhibiting smaller decreases

in performance than the AN-based electrolytes, but did show lower overall short circuit currents. Lee and co-workers [51] synthesized and studied novel ionic liquid electrolyte, 3-(iodohexyl)-1-(3-(triethoxysilyl)propylcarbamoyl)-1*H*-benzo[*d*]imidazol-3-ium iodide (see structure b in the Fig. 8). The electrolyte containing the above iodide source was gelled by heating at 60°C for 30 min in an oven. DSSC with gel electrolyte prepared this way exhibited good efficiency and significantly enhanced stability as compared to traditional liquid electrolyte. Improvement of stability was attributed to decreased volatility of the electrolyte as a result of chemical cross-linking.

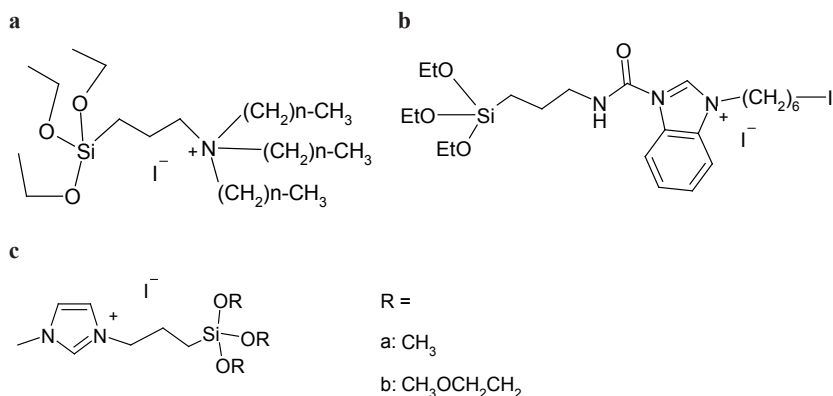


Figure 8. Structures of silane-based ionic liquids for DSSCs

Structure c (Fig. 8) is also studied, showing promising photocurrent-photovoltage characteristics and appreciable efficiencies, only slightly worse as compared to reference electrolyte based on acetonitrile (see Fig. 9) [52].

In conclusion, due to their unique properties described earlier, ionic liquids seem to be ideal for the application as electrolyte components in dye sensitized solar cells. Further progress in this field will depend on the efforts to synthesize new ILs with precisely tailored molecular structures to obtain low viscosities and high specific conductivities. The aim of this paper was to outline only the main aspects and issues associated with the application of ionic liquids in DSSCs. Some interesting recent developments have not been included in this work, like for example liquid crystals and formation of supramolecular structures. The field of ionic liquids is evolving very rapidly. Out of the total number of 10^{18} theoretically predicted ionic liquid structures only about 10 000 are considered to be of technological interest, with about 500 being today manufactured on

laboratory scale. Small percentage of the last number has been tested in DSSC so far, providing wide area for investigations.

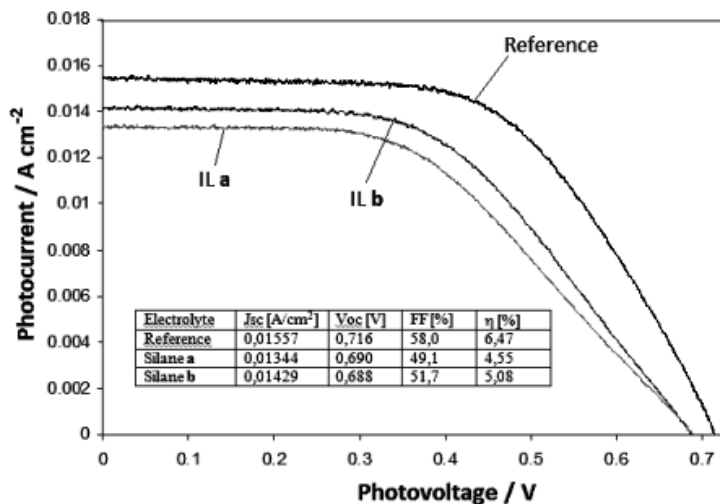


Figure 9. Voltage-current characteristics and basic photoelectrochemical data for DSSCs with electrolytes based on structures c (Fig. 8).

List of acronyms

DSSC	dye sensitized solar cell
CIGS	copper indium gallium selenium
ITO	Indium tin oxide
IL	ionic liquid
RTIL	room-temperature ionic liquid
B2-MPI	1-Butyl-2-methylpyridinium iodide
B4-MPI	1-Butyl-4-methylpyridinium iodide
BDMII	1-Butyl-2,3-dimethylimidazolium iodide
BMI	1-Butyl-3-methylimidazolium iodide
BMPiI	1-Butyl-1-methylpiperidinium iodide
BMPyI	1-Butyl-1-methylpyrrolidinium iodide
BPI	1-Butylpyridinium iodide
DMPII	1,2-Dimethyl-3-propylimidazolium iodide

EMII	1-Ethyl-3-methylimidazolium iodide
EMPyI	1-Ethyl-1-methylpyrrolidinium iodide
EPI	1-Ethylpyridinium iodide
HMII	1-Hexyl-3-methylimidazolium iodide
HPI	1-Hexylpyridinium iodide
MPII	1-Methyl-3-propylimidazolium iodide
MPPiI	1-Methyl-1-propylpiperidinium iodide
MPPyI	1-Methyl-1-propylpyrrolidinium iodide

Acknowledgements

The work has been financially supported by Polish Ministry of Science and Higher Education, grant No NN204 023538.

References

1. B. O'Regan, M. Grätzel, *Nature*, 1991, 353, 737.
2. A. Hagfeldt, G. Boschloo, L. Sun, L. Kloo, H. Pettersson, *Chem. Rev.*, 2010, 110, 6595.
3. T. Welton, *Chem. Rev.*, 2004, 248, 2459.
4. M. Gorlov, L. Kloo, *Dalton Trans.*, 2008, 2655-2666.
5. T.-Y. Cho, S.-G. Yoon, S. S. Sekhon, C.-H. Han, *Bull. Korean Chem. Soc.*, 2011, 32, 2058.
6. N. Papageorgiu, Y. Athanassov, M. Armand, P. Bonhote, H. Pettersson, A. Azam, M. Grätzel, *J. Electrochem. Soc.*, 1996, 143, 3099.
7. H. Matsumoto, T. Matsuda, T. Tsuda, R. Hagiwara, Y. Ito and Y. Miyazaki, *Chem. Lett.*, 2001, 26.
8. P. Wang, S. M. Zakeeruddin, R. Humphry-Baker and M. Grätzel, *Chem. Mater.*, 2004, 16, 2694.
9. P. Wang, S. M. Zakeeruddin, J. Moser and M. Grätzel, *J. Phys. Chem. B*, 2003, 107, 13280.
10. P. Wang, B. Wenger, R. Humphry-Baker, J. Moser, J. Teuscher, W. Kantlehner, J. Mezger, E. V. Stoyanov, S. M. Zakeeruddin and M. Grätzel, *J. Am. Chem. Soc.*, 2005, 127, 6850.
11. D. Kuang, P. Wang, S. Ito, S. M. Zakeeruddin and M. Grätzel, *J. Am. Chem. Soc.*, 2006, 128, 7732.
12. P. Wang, C. Klein, R. Humphry-Baker, S. M. Zakeeruddin and M. Grätzel, *Appl. Phys. Lett.*, 2005, 86, 123508/1.
13. M. Gorlov, H. Pettersson, A. Hagfeldt and L. Kloo, *Inorg. Chem.*, 2007,

- 46, 3566.
14. J. Xia, N. Masaki, K. Jiang, Y. Wada and S. Yanagida, *Chem. Lett.*, 2006, 35, 252.
 15. Z. Fei, D. Kuang, D. Zhao, C. Klein, W. H. Ang, S. M. Zakeeruddin, M. Grätzel and P. J. Dyson, *Inorg. Chem.*, 2006, 45, 10407.
 16. S. Ito, S.M. Zakeeruddin, R. Humphry-Baker, P. Liska, R. Charvet, P. Comte, M. K. Nazeeruddin, P. Pechy, M. Takata, H. Miura, S. Uchida and M. Grätzel, *Adv. Mater.*, 2006, 18, 1202 .
 17. L. Chen, B. Xue, X. Liu, K. Li, Y. Luo, Q. Meng, R. Wang and L. Chen, *Chin. Phys. Lett.*, 2007, 24, 555.
 18. F. Fabregat-Santiago, J. Bisquert, E. Palomares, L. Otero, D. Kuang, S. M. Zakeeruddin and M. Grätzel, *J. Phys. Chem. C*, 2007, 111, 6550.
 19. R. Kawano, M. Watanebe, *Chem. Comm.*, 2005, 2107.
 20. P. Wang, S. M. Zakeeruddin, J. E. Moser, R. H. Baker, M. Grätzel. *J. Am. Chem. Soc.* 2004, 126, 716.
 21. J. M. Slattery, C. Daguene, P. J. Dyson, T. J. S. Schubert, I. Krossing, *Angew. Chem. Int. Ed.* 2007, 46, 5384.
 22. J. Wu, Z. Lan, S. Hao, P. Li, J. Lin, M. Huang, Leqing Fang, Y. Huang, *Pure Appl. Chem.*, 2008, 80, 2241.
 23. A. F. Nogueira, C. Longo, M. A. De Paoli. *Coord. Chem. Rev.*, 2004, 248, 1455.
 24. P. Wang, S. M. Zakeeruddin, I. Exnar, M. Grätzel, *Chem. Commun.*, 2002, 2972.
 25. P. Wang, S. M. Zakeeruddin, J. E. Moser, T. Sekiguchi, M. Grätzel, *Nat. Mater.*, 2003, 2, 402 .
 26. Y. Yan, T. Jie, J. Xin, Q. Qi, *J. Appl. Polym. Sci.*, 2011, 121, 1566.
 27. E. Stathatos, P. Lianos, U. Lavrencic-Stangar, B. Orel., *Adv. Mater.*, 2002, 14, 354.
 28. E. Stathatos, P. Lianos, C. Krontiras. *J. Phys. Chem. B*, 2001, 105, 3486.
 29. E. Stathatos, P. Lianos, U. L. Stangar, B. Orel. *Adv. Funct. Mater.*, 2004, 14, 45.
 30. E. Stathatos, P. Lianos, *Chem. Mater.* , 2003, 15, 1825.
 31. J. Wu, Z. Lan, S. Hao, P. Li, J. Lin, M. Huang, L. Fang, Y. Huang, *Pure Appl. Chem.*, 2008, 80, 2241.
 32. S. Mikoshiba, S. Murai, H. Sumino, S. Hayase, *Chem. Lett.*, 2002, 31, 918.
 33. T.Kato, A. Okazaki, S. Hayase, *J. Photochem. Photobiol.*, A, 2006, 179, 42.
 34. N. Mohmeyer, D. Kuang, P. Wang, H. Schmidt, S.M. Zakeeruddin, M.

- Grätzel, J. Mater. Chem., 2006, 16, 2978.
35. L. Wang, S. Fang, Y. Lin, Polym. Adv. Technol., 2006, 17, 512.
 36. P. K. Singh, K. Kim, N. Park, H. Rhee, Macromol. Symp., 2007, 249/250, 162.
 37. M.Wang, X. Xiao, X. Zhou, X. Li, Y. Lin, Sol. Energy Mater. Sol. Cells, 2007, 91, 785.
 38. N.Wang, H. Lin, J. Li, X. Li, Appl. Phys. Lett., 2006, 89, 194104.
 39. P.Wang, S.M. Zakeeruddin, P. Comte, I. Exnar, M. Grätzel, J. Am. Chem. Soc., 2003, 125, 1166.
 40. Y. Zhao, J.Zhai, S.Tan, L.Wang,L. Jiang, D.Zhu, Nanotechnology, 2006, 17, 2090.
 41. J. H. Kim, M.-S. Kang, Y. J. Kim, J. Won, N.-G. Park, Y. S. Kang, Chem. Commun., 2004, 1662.
 42. W.Kubo, T.Kitamura, K. Hanabusa, Y.Wada, S. Yanagida, Chem. Commun., 2002, 374.
 43. Y. J. Kim, J. H. Kim, M.-S. Kang, M. J. Lee, J.Won, J. C. Lee, Y. S. Kang, Adv. Mater., 2004, 16, 1753.
 44. P.Wang, Q. Dai, S. M. Zakeeruddin, M. Forsyth, D. R. MacFarlane, M. Grätzel, J. Am. Chem. Soc., 2004, 126, 13590.
 45. K. Suzuki, M. Yamaguchi, M. Kumagai, N. Tanabe, S. Yanagida, C. R. Chim., 2006, 9, 611.
 46. H. Lee, W. Kim, S. Park, W. Shin, S. Jin, J. Lee, S. Han, K. Jung, M. Kim, Macromol. Symp., 2006, 235, 230.
 47. V. Jovanovski, E. Stathatos, B. Orel, P. Lianos, Thin Solid Films, 2006, 511–512, 634.
 48. E. Stathatos, V. Jovanovski, B. Orel, I. Jerman, P. Lianos, J. Phys. Chem. C, 2007, 111, 6528.
 49. W.Kubo, Y.Makimoto, T. Kitamura, Y.Wada, S. Yanagida, Chem. Lett., 2002, 31, 948.
 50. S.A. Cerneaux, S.M. Zakeeruddin, M. Grätzel, Y.-B. Cheng, L. Spiccia, J. Photochem. Photobiol. A: Chemistry, 2008, 198, 186.
 51. J.P. Lee, B. Yoo, T. Suresh, M.S. Kang, R. Vital, K.-J. Kim, Electrochim. Acta, 2009, 54, 4365.
 52. Unpublished results.

Chapter 4

Acceptor number of organoboron molecules - quantitative determination of Lewis acidity

Michał Jakubczyk, Agnieszka Adamczyk-Woźniak
and Andrzej Sporzyński

*Warsaw University of Technology, Faculty of Chemistry,
Noakowskiego 3, 00-664 Warsaw, Poland*

1. What is the Lewis acidity?

The IUPACS's *Compendium of Chemical Terminology* (Gold Book) [1] gives the following definition of a Lewis acid: *A molecular entity ... that is an electron-pair acceptor and therefore able to react with a Lewis base to form a Lewis adduct, by sharing the electron pair furnished by the Lewis base.* Furthermore, it describes the Lewis acidity as follows: *The thermodynamic tendency of a substrate to act as a Lewis acid. Comparative measures of this property are provided by the equilibrium constants for Lewis adduct formation of a series of Lewis acids with a common reference Lewis base.* These definitions need a comment to be fully understood. An *electron-pair acceptor* or an electrophile is a molecule which forms a so called dative bond by accepting both bonding electrons from a reaction partner. It must contain in its structure an electron deficient center. The reaction partner is often called a Lewis base or nucleophile and must provide a lone pair. This means that the concept of Lewis acidity (or basicity) is connected with the ability to form a bond, so it is the term describing a specific kind of chemical reactivity. Such description excludes any universal scale to be constituted, because Lewis acidity depends not only on the structure of the Lewis acid, but also on the structure of the reaction partner and only comparative studies of this property are possible. Since G. N. Lewis formulated his concept [2], there have been many attempts to adopt the interpretation of the Lewis acidity notion in order to make the measurements more feasible and useful in a specific field. Some of the most important will be analyzed below.

2. Fundamental approaches to quantitative determination Lewis acidity

Significant differences in the order of the investigated compounds within

different scales result from differences in the structure of the Lewis base reference compound. For example, quality of the Lewis base-center atom, analytical method (kind of the analytical signal), electronic effects (aromaticity) and the steric hindrance of the basic center, influence not only the quantitative results but often qualitative ones (ordering). The incompatibility of a particular scale with another is not, however, any disadvantage, if the model used to establish the scale corresponds with the application. Yet, there are two rather different, general approaches that have to be mentioned.

Drago and co-workers [3] proposed a following equation:

$$-\Delta H_{AB}^{\circ} / (\text{kJ} \times \text{mol}^{-1}) = E_{\text{A}} \times E_{\text{B}} + C_{\text{A}} \times C_{\text{B}},$$

which correlates the standard enthalpy of the reaction of a Lewis acid (acceptor, A) with a Lewis base (donor, B) with empirical parameters. The E and C parameters are the measure of the electrostatic interaction participation tendency and covalent bond formation tendency, respectively. Parameters E and C for a given A and B are constant regardless of the quality of A and B. Theoretically, even enthalpies of experimentally unavailable reactions can be calculated. This concept has a major, obvious disadvantage that was mentioned before. One cannot assign any general empirical coefficient to a Lewis base or acid (describing their acidity or basicity) not indicating the reference molecule towards which it is assessed. In other words, the Lewis acidity is always relative. This is especially important for organic compounds where steric factors play a significant role.

In 1937 Louis Plack Hammett published his equation [4] which describes the substituent effect in *meta* and *para* positions in the benzene ring on the rate (k) or the equilibrium (K) constant of the reaction of the side chain group. This theory was a long-expected answer to the question: how the electron charge density affects the reactivity of a molecule? Hammett proposed a two parameter equation:

$$\log(K/K_0) = \sigma \rho.$$

The σ is a substituent constant. The ρ is the reaction constant. The σ constant is assigned to a particular non-reacting substituent and is highly positive when the substituent causes an electron-withdrawing inductive effect (-I) and/or a negative mesomeric effect (-M). If one of the effects has an opposite character, then the σ constant is lower. The mid-point for which by definition $\sigma = 0$ is the hydrogen substituent. The negative value of the σ constant indicates an opposing character of both kinds of effects. The ρ constant is assigned to a specific reaction, regarding both the reaction type and a particular reaction partner. The equation is valid only for *para*- and *meta*- substituents as the *ortho* position implies a steric interaction with the reacting center not only intramolecularly but also possibly

with the other reagent. Additionally, the ρ constant depends on temperature and solvent as it is defined as follows:

$$\rho = (1/d^2 \times T) \times ([B_1/D] + B_2),$$

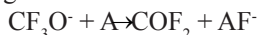
where the B_1 and B_2 depend on the reaction, D is the dielectric constant of the solvent, T is the temperature and d is defined as the distance from the substituent to the reacting group. Regarding the above, the Hammett approach can be classified as a relative method since it specifies precisely the reacting groups. Taft [5] has modified the Hammett equation and expanded its scope also to *ortho* substituents by introducing constants dependent on the steric considerations.

3. Modern approaches to qualitative assessment of the Lewis acidity

The progress of science and technology is often revealed by the availability of sophisticated instrumental methods. The last decades made quantum computations and X-ray measurements one of the top tools for chemists. The following chapter introduces two semi-empirical Lewis acidity scales that incorporate this modern techniques.

3.1. Fluoride ion affinity scale (pF⁻)

If the steric hindrance of the acidic center of a series of Lewis acids is negligible or the application assumes interactions with small molecules, the researcher can incorporate a small molecule-model for the Lewis acidity determination. The fluoride ion affinity scale[6] is a good choice, especially for water-containing mixtures of solvents. As fluoride ion is a strong Lewis base, it readily reacts with essentially all Lewis acids. The scale is expressed in terms of the enthalpy of the following reaction:



Incorporation of carbonyl fluoride in this isodesmic reaction was dictated by computational difficulties. The Lewis acids (A) affinity towards F⁻ can be calculated with high accuracy on MP2/PDZ level of theory method or higher and then converted to an absolute value using well established experimental value of the COF₂ affinity. The affinity scale is then defined as follows:

$$\text{pF}^- = \text{F}^- \text{ affinity (kcal/mol)} / 10.$$

The biggest disadvantage of this and other semi-empirical, computational concepts is that they assume a constant deviation of a particular computational method from reality, which could be not true for all investigated compounds. In other words, the quantum chemical computations deviation depend not only on the chosen level of theory, but also on the structure (size, composition) of the investigated molecule.

3.2. Tetrahedral Boron Character index (THC)

The geometrical parameters (angles, lengths) of four bonds of boron atom in a Lewis adduct vary depending on the strength of the donor-acceptor bond. The weaker the interaction between boron-Lewis acid and the Lewis base, the weaker is the dative bond and the geometry is closer to flat-pyramidal (Fig. 1).

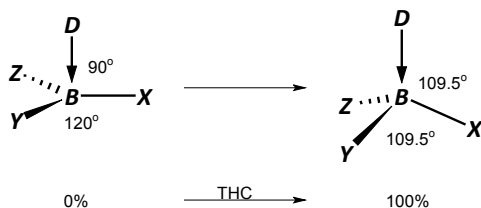


Figure 1. The change in the boron coordination from trigonal to tetrahedral can be measured in percent.

This statement is the basis of THC index (Tetrahedral Boron Character measured in percent), another Lewis acidity scale based on the boron-bond angles of crystal structures of the organoboron adducts with bases [7]. The number of available structures of Lewis adducts containing tetrahedral boron is large, enabling determination of THC index.

4. Acceptor number (AN)-the original concept

The previously cited source [1] links the *Lewis acidity* notion with the term *acceptor number (AN)* and explains it as *a quantitative measure of Lewis acidity*. Originally, the acceptor number (AN) was defined by V. Gutmann and co-workers [8] as a quantitative scale of the electrophilic properties of solvents and solvent mixtures [9]. The complementary donor number (DN) scale, based on calorimetric measurements, has been developed much earlier and will not be discussed here in details. Gutmann gave a formula that binds AN of the Lewis acid and DN of the reacting Lewis base with the coordinate bond energy:

$$\Delta H = [(DN \times AN) / 100] + \Delta \Delta H_{\text{Donor}} + \Delta \Delta H_{\text{Acceptor}} \quad [10].$$

For a comprehensive guide on the DN and Lewis basicity see Refs. [12] and [18]. The AN is a dimensionless quantity defined as follows:

$$AN = \{ (\delta_{\text{complex}} - \delta_{(1)}) / (\delta_{(2)} - \delta_{(1)}) \} \cdot 100,$$

where δ_{complex} stands for the ^{31}P NMR chemical shift of the $\text{Et}_3\text{PO} \cdots \text{Lewis acid}$ complex, $\delta_{(1)}$ and $\delta_{(2)}$ are the ^{31}P NMR chemical shifts of Et_3PO dissolved in hexane (41.0 ppm) and in SbCl_5 (86.1 ppm), respectively. Et_3PO was chosen as a NMR probe for its stability, high basicity and the fact that the actual coordination

occurs at oxygen atom, and not phosphorus, so there are no additional effects affecting the ^{31}P NMR chemical shift. The formation of the Et_3PO complex was confirmed on the basis of X-ray measurements [11]. Due to the strong solute-solute interactions (the more non-polar and non-coordinating is the solvent, the stronger they are) the δ_{complex} , $\delta_{(1)}$ and $\delta_{(2)}$ have been extrapolated to the infinite dilution of the phosphine oxide. Because the results for all solvents are always referred to hexane, an additional correction for the difference in volume susceptibilities have been applied. The values for hexane ($AN=0$) and antimony pentachloride ($AN=100$) are arbitrary fixed points within the AN scale. The established AN values have been shown to correlate with previously proposed solvents parameters such as: Z -values [12] (energy of the charge transfer band of the 1-ethyl-4-carbomethoxy pyridinium iodide ion pair), E_T -values [13] (which are the energy of the lowest electronic transition of the pyridinium- N -phenol betaine) or the Y -values [14] (based on kinetic studies on solvolysis of *tert*-butyl chloride) as well as thermodynamic quantities like: free energies of solvation, polarographic half wave potentials, reaction rate constant and Arrhenius activation energies.

It should be underlined that the Gutmann's AN scale, the above mentioned parameters (Z , E_T , Y) and many other scales that incorporate any Lewis base-partner as a molecular probe for example the above mentioned F^- affinity scale, the Childs method [15] and ^{13}C NMR- Et_2O method [16] provide relative results. In this meaning, these are no Lewis acidity scales but rather affinity scales.

5. Lewis acidity and acceptor number values of organoboron compounds

Organoboron compounds draw much attention in the last few decades. The most important boron connections including triorganoboranes (**a**), borinic acids (**b**) and their organic esters (**c**), boronic acids (**d**) and their organic esters (**e**), orthoboric acid (**f**) and its organic esters (**g**) are depicted in Fig. 2.

Nearly all chemical species (both organic and inorganic) containing trivalent boron atom are considered acids in the terms of the Lewis theory. The only four exceptions [17] are known in borylcopper species, boryllithium species, anionic dimetalloborylene species or when boron is connected to a less electronegative atoms like lithium and hydrogen. The BF_3 is an archetypical Lewis acid due to the electron deficiency on boron and large electronegativity difference between boron and fluorine [18]. The BF_3 affinity scale is one of the earliest Lewis basicity scales. The majority of boron species are characterized by low toxicity, high stability and manifest unique properties which originate from the physical and chemical properties of the boron atom, especially the presence of the vacancy in the outer shell. This makes them useful in many applications and an excellent

object for Lewis acidity studies.

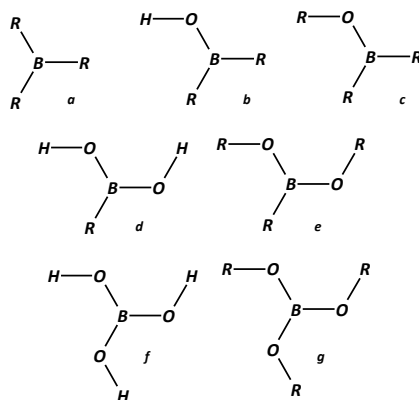


Figure 2. The most important boron containing molecules.

Organoboron compounds are utilized as therapeutic agents in synergic tumor treatment method based on a atomic reaction between boron and thermal (slow) neutron radiation (BNCT) [19]. Saccharide recognition is another application in which organoboron compounds are incorporated [20]. This issue concerns especially boronic acids (which are Lewis and not Brønsted acids regardless the presence of two hydroxyl groups) [21]. Because this topic is nowadays so broad, only brief description will be given. The basis of the sugar recognition with boronic acids is the ability to bind diols reversibly in the physiological pH according to the presented scheme (Fig. 3).

The cyclic esters of boronic acids reveal stronger Lewis acidity than the acids themselves (the pK_a lowers by about 2-4 units, which enables action of boronic esters as anion receptors) [22]. The reason for this lays in the change in the O-B-O angle upon diol binding and is connected with the difference in the energy of the planar-trigonal and tetrahedral coordination of the boron atom. The closer the O-B-O angle is to the ideal angle of 109.5° , the easier it is for the ester to adopt the tetrahedral geometry upon complex formation [23]. This concept is somewhat parent to the so-called THC index (tetrahedron boron character) described previously. Due to the release of hydronium ions, the reaction rate can be determined by the aid of a pH indicator [24]. The so-called pH depression method measures the increase in acidity of the solution, when a diol is titrated into a solution of boronic acid [25].

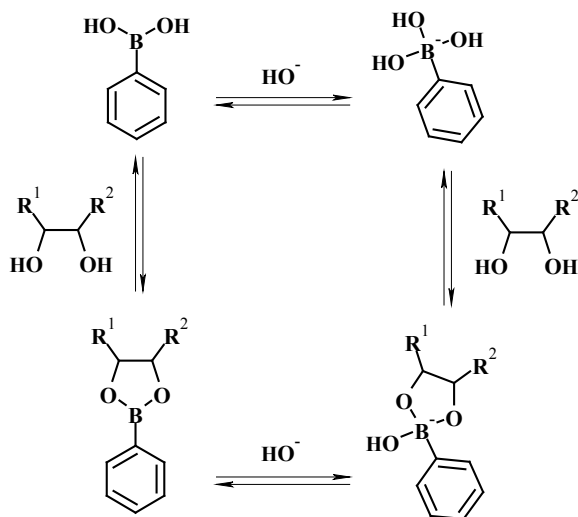


Figure 3. Equilibria of boronic acid in water in the presence of diol.

The Lewis acidity of several boron-containing species has been assessed by determination of their acceptor numbers. The *AN* values of some organoboron compounds have been shown to correlate with their activity as polymerization catalysts [26]. Lewis acidity was enabled using phenylboronic esters as additives for polymer electrolytes [27]. Table 1 presents all the so-far published ^{31}P NMR data found for complexes of organoboron compounds with Et_3PO . The records in the table are ordered by the decreasing *AN*. The aluminum, titanium and tin chlorides were cited for comparison. The significant differences in the experimental approach and the following divergence of results given by different researchers needs a comment, what is the purpose of this paper.

Table 1: Acceptor numbers of organoboron compounds along with the ^{31}P NMR chemical shift of the Et_3PO complex, appearance state in room temp., reference and measurement details.

Entry	Compound	δ / ppm	<i>AN</i>	l-liquid s-solid	Remarks	Ref.
1	BI_3	92.9	114.9	l	a	[32]
2	BBr_3	90.3	109.3	l	a	[32]
3	BCl_3	88.7	105.7	l	a	[32]
4	$\text{BF}_3 \cdot \text{THF}$	80.9	88.5	l	a	[32]

Entry	Compound	δ / ppm	<i>AN</i>	l-liquid s-solid	Remarks	Ref.
5	$B(OC_6F_5)_3$	80.9	88.4	s	b	[29]
6	$(C_6F_5)B(OC_6F_5)_2$	80.5	87.5	s	b	[29]
7	$AlCl_3$	80.3	87.0	s	a	[31]
8	$(C_6F_5)_2BOC_6F_5$	80.0	86.4	s	b	[29]
9	$C_6H_4O_2BC_6F_5$	77.8	81.5	s	c	[30]
10	$(PhMe_2SiO)_3B_3O_3$	77.5	81.0	l	d	[36]
11	$B(C_6F_5)_3$	76.6	78.9	s	b, h	[29]
12	$(MeO)_3B_3O_3$	76.4	78.5	l	a	[32]
13	$BH_3 \cdot THF$	75.8	75.8	l	a, i	[32]
14	$C_6H_4O_2BC_6H_4F_3$ -3,4,5	74.4	73.9	s	c	[30]
15	$(EtMe_2SiO)_3B_3O_3$	74.4	74.0	l	d	[36]
16	$(Ph_2MeSiO)_3B_3O_3$	74.4	74.0	l	d	[36]
17	$C_6H_4O_2BC_6H_4F_2$ -2	74.2	73.6	s	c	[30]
18	$C_6H_4O_2BC_6H_4F_2$ -2,4	74.2	73.5	s	c	[30]
19	$C_6H_4O_2BC_6H_4F_2$ -2,6	74.1	73.4	s	c	[30]
20	$(Et_3SiO)_3B_3O_3$	73.5	72.0	l	d	[36]
21	$(^nBuMe_2SiO)_3B_3O_3$	73.0	71.0	l	d	[36]
22	$TiCl_4$	72.7	70.0	s	g	[31]
23	$C_6H_4O_2BC_6H_4F_3$	72.7	70.0	s	c	[30]
24	$C_6H_4O_2BC_6H_4F_4$	72.6	70.1	s	c	[30]
25	$C_6H_4O_2BC_6H_4F_3$ -2,4,6	72.6	70.1	s	c	[30]
26	$([2-(3-cyclohexenyl)ethyl]Me_2)SiO)_3B_3O_3$	72.6	70.1	l	d	[36]
27	$B(Ph)_3$	70.6	65.6	s	c, k	[30]
28	$C_6H_4O_2BC_6H_5$	70.5	65.4	s	c	[30]
29	$(^nBuO)_3B_3O_3$	70.3	70.3	l	a	[32]
30	$(^nPr_3SiO)_3B_3O_3$	69.4	63.0	l	d	[36]
31	$B(OPh)_3$	69.4	63.0	s	b	[29]
32	$(m-NO_2C_6H_4BO)_2(^nOctMeSiO)_2$	69.0	62.0	l	e	[35]
33	$([(Me_2HC)(Me)_2C]Me_2)SiO)_3B_3O_3$	67.6	59.0	l	d	[36]
34	$(PhBO)_2(Ph_2SiO)_2$	67.6	59.0	s	e	[35]

Entry	Compound	δ / ppm	<i>AN</i>	l-liquid s-solid	Remarks	Ref.
35	SnCl ₄	67.4	58.4	s	g	[31]
36	(ⁿ Bu ₃ SiO) ₃ B ₃ O ₃	66.3	56.0	l	d	[36]
37	(ⁿ Bu ₃ SnO) ₃ B ₃ O ₃	65.4	54.0	l	d	[36]
38	(3-NO ₂ C ₆ H ₄) ₃ B ₃ O ₃	64.5	52.0	s	f	[34]
39	(p-BrC ₆ H ₄ BO) ₂ (ⁿ OctMeSiO) ₂	64.5	52.0	l	e	[35]
40	Me ₃ B ₃ O ₃	64.0	51.0	l	m	[34]
41	(4-BrC ₆ H ₄) ₃ B ₃ O ₃	63.6	50.0	s	m	[34]
42	(m-NH ₂ C ₆ H ₄ BO) ₂ (Ph ₂ SiO) ₂	63.6	50.0	s	e	[35]
43	Ph ₃ B ₃ O ₃	63.1	49.0	s	n	[34]
44	(p-BrC ₆ H ₄ BO) ₂ (Ph ₂ SiO) ₂	63.1	49.0	s	e	[35]
45	(o-MeC ₆ H ₄ BO) ₂ (Ph ₂ SiO) ₂	63.1	49.0	s	e	[35]
46	(PhBO) ₂ (ⁿ OctMeSiO) ₂	62.2	47.0	l	e	[35]
47	(m-NO ₂ C ₆ H ₄ BO) ₂ (Ph ₂ SiO) ₂	61.7	46.0	s	e	[35]
48	(ⁿ BuBO) ₂ (Ph ₂ SiO) ₂	61.7	46.0	l	e	[35]
49	(ⁿ Hex ₃ SiO) ₃ B ₃ O ₃	60.8	44.0	l	d	[36]
50	B(OSi ⁿ BuMe ₂) ₃	57.2	36.0	l	d	[36]
51	B(OSiEt ₃) ₃	56.3	34.0	l	d	[36]
52	(ⁿ Pr ₃ SiO) ₂ BC ₆ H ₄ Me-2	55.0	31.0	l	d	[36]
53	(ⁿ Bu ₃ SnO) ₂ BPh	54.5	30.0	l	d	[36]
54	(ⁿ Bu ₃ SnO) ₂ BC ₆ H ₄ Br-4	54.5	30.0	l	d	[36]
55	B(OSiPhMe ₂) ₃	54.1	29.0	l	d	[36]
56	B(OSi ⁿ Pr ₃) ₃	53.6	28.0	l	d	[36]
57	(PhBO)(MePhSiO) ₂	53.6	28.0	l	e	[35]
58	(m-NH ₂ C ₆ H ₄ BO)(MePhSiO) ₂	53.6	28.0	l	e	[35]
59	(p-BrC ₆ H ₄ BO)(MePhSiO) ₂	53.2	27.0	l	e	[35]
60	B(OSn ⁿ Bu ₃) ₃	52.3	25.0	l	d	[36]
61	B(OMe) ₃	51.4	51.4	s	a	[32]
62	B(OSi ⁿ Bu ₃) ₃	51.4	23.0	l	d	[36]
63	B(OSi([2-(3-cyclohexenyl)ethyl]Me ₂) ₃) ₃	51.4	23.0	l	d	[36]
64	(ⁿ Pr ₃ SiO) ₂ BPh	51.4	23.0	l	d	[36]

Entry	Compound	δ / ppm	AN	l-liquid s-solid	Remarks	Ref.
65	(m-NH ₂ C ₆ H ₄ BO)([p-BrC ₆ H ₄] ₂ SiO) ₂	50.9	22.0	1	e	[35]
66	B(OEt) ₃	48.7	17.1	1	j	[32]
67	2-(2-fluorophenyl)-4,4,5,5-tetramethyl-1,3,2-dioxaborolane	47.8	15.1	1	c	
68	B(O ⁿ Bu) ₃	46.3	11.8	1		[32]
69	B(NMe ₂) ₃	45.1	9.1	1	j	[32]

a- Ca. 50mg of Et₃PO in 0.5ml neat liquid.

b- Et₃PO ratio 1:1, solution in C₆D₆, the authors don't calculate AN from their measurements.

c- Solution in C₆D₆, δ used to calculate the AN was measured for different ratios of the boron compound to Et₃PO and extrapolated to infinite excess of the boron compound.

d- Et₃PO in neat liquid, authors gave only AN .

e- 50mg of Et₃PO dissolved in 1ml THF solution of 0.61M concentration (ratio 1.65 borosiloxane:Et₃PO), authors gave only AN .

f- 50 mg of Et₃PO dissolved in 1 ml THF solution

g- Excess over Et₃PO in Et₂O.

h- Britovsek *et al.*: $\delta=76.3$, $AN=78.3$; Beckett *et al.*: $\delta=83.4$, $AN=82$, solution in THF of unknown concentration.

i- 1 M solution in THF.

j- ca. 50mg of Et₃PO in 0.5 ml neat liquid.

k- Britovsek *et al.*: $\delta=65.9$, $AN=55$, acid to Et₃PO ratio 1:1, solution in C₆D₆.

m- 50 mg of Et₃PO in 1 ml THF solution.

The top of the table is occupied by boron trihalides. The next few rows contain the series investigated by Britovsek *et al.* (belonging to species **a**, **c**, **e** and **g** presented in Fig. 1) [28]. All four compounds differ from each other only by the number of oxygen-boron/carbon-boron bonds. The Lewis acidity of the boron center in compounds **5**, **6** and **8** is affected by $\pi\pi$ - $\pi\pi$ interactions between the lone pairs on the oxygen atoms and the empty p_z orbital on the boron atom. The electron-withdrawing C₆F₅ substituents decrease the electron density at oxygen. However, Britovsek has shown that there is only weak $\pi\pi$ - $\pi\pi$ interaction between boron and oxygen (double character, measure of conjunction). The rotation barrier was assessed for 35 kJ/mol. The observed order of acceptor numbers for these compounds can be rationalized in terms of Pearson's *hard soft acid base* (HSAB) classification, whereby the *hardness* or *softness* of a particular Lewis acidic or Lewis basic center is affected by the nature of the other atoms attached to it and the type of bonding between them. In the compound **5** all three aromatic rings are connected to the boron via oxygen atoms. The B-O bond is much more ionic in character than the B-C bond. The HSAB theory claims that the combination of a *hard* Lewis acid with a *hard* Lewis base or a *soft* Lewis acid with a *soft* Lewis base results in a stronger interaction than the mixed *hard-soft* interaction. The P=O double bond in Et₃PO

is a π - $d\pi$ bond, which is significantly ionic in character, what makes it a *hard* Lewis base. Thus the four compounds **11**, **8**, **6** and **5** are progressively harder, what results in a increasingly stronger interactions with Et_3PO . Compounds **31** and **36** also follow the above explanation although are of much lower acceptor number because of the lack of the electron-withdrawing fluorine substituents, which are often introduced into the phenyl ring to enhance the Lewis acidity [29]. The next very important issue is the huge difference in the acceptor number for the BPh_3 measured by Britovsek *et al.* ($AN=55$) [28] and Adamczyk-Woźniak *et al.* (entry **27**, $AN=65.6$) [30]. The reason for this lays in differences of the experimental approach. Gutmann, in the original paper from 1975 [7], have marked the dependence of the chemical shift from the concentration of the Et_3PO and assigned this to strong solute-solute interactions. He had corrected his results by extrapolation of the values to the infinite dilution from the concentrational dependence of the chemical shift. Adamczyk-Woźniak *et al.*, following the work of Beckett *et al.* and Britovsek *et al.*, have modified the Gutmann procedure for measuring the acceptor number of solid compounds. The Lewis acid and the TEPO are dissolved in an inert solvent. The assumption is that if the acceptor number of the used solvent is much lower than of the investigated Lewis acid then the solvent-Lewis base interactions are negligible. It has been shown that in the case of BPh_3 the complexation reaction leading to the adduct is a fast equilibrium (Fig. 4). In the majority of the investigated cases the fraction of the free phosphine oxide is significant as far as to the double excess of the Lewis acid. In case of catechol phenylboronate however (entry **28**) the chemical shift changes until ratio of about 3:1 (Fig. 5). This fact extorts an extrapolation of the chemical shift of the complex from the function of the molar ratio of the Lewis acid to Et_3PO , similarly to the original Gutmann's procedure, but in a three component-system. Britovsek *et al.* conducted measurements preparing a 1:1 solution of BPh_3 and Et_3PO in benzene ($AN=8.2$).

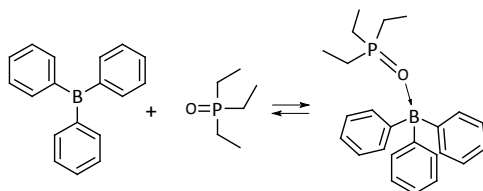


Figure 4. Complexation of triphenylborane with triethylphosphine oxide.

Thus, his result is of almost 5 ppm lower than the one recently evaluated. In contrast to the BPh_3 , the $\text{B}(\text{C}_6\text{F}_5)_3$ reacts quantitatively with the phosphine oxide.

This is confirmed by the close acceptor number of 78.9 (76.6 ppm) and 78.3 (76.3 ppm) measured for this compound by Britovsek *et al.* and Adamczyk-Woźniak *et al.* respectively (entry **11**). The higher acceptor number of $B(C_6F_5)_3$ determined by Beckett ($AN=82$)[31] is certainly caused by the use of different solvent (THF instead of C_6D_6).

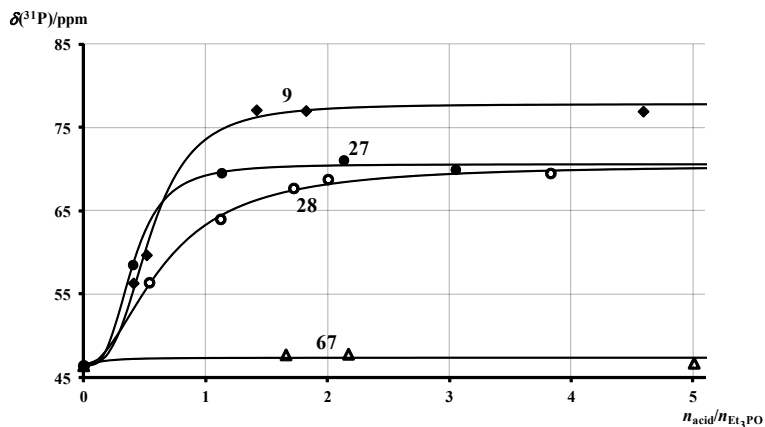


Figure 5. Measured $\delta(^{31}P)$ for different Lewis acid/ Et_3PO molar ratios and curves of fitted functions for selected derivatives.

The next part of the table is shared by three classes of organoboron compounds shown in Fig. 6: fluorinated phenylboronic esters of catechol (**a**), trialkyl (**b**), and triorganosilyl (**c**) esters of metaboric acid.

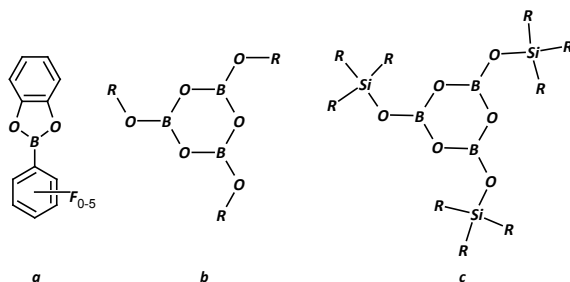


Figure 6. Fluorinated phenylboronates of catechol (**a**), trialkyl (**b**) and triorganosilyl (**c**) esters of metaboric acid.

The first series are all solids and were investigated by Adamczyk-Woźniak *et*

al. using the modified method [30]. The remaining two series investigated by Beckett *et al.* compounds are liquids [32], so the original procedure could be applied without affecting the reliability (comparability) of the determined values. The order of the acceptor number of fluorinated catechol phenylboronates is only partially rational and arranges as follows: **9**>**14**≈**17**≈**18**≈**19**>**23**≈**24**≈**25**>**28**. The pentafluorinated derivative as the strongest and the non-fluorinated derivative as the weakest Lewis acid is not surprising. Unexpected is the almost equal acceptor number of mono- and polyfluorinated derivatives. However, the experimental results have been confirmed by the authors by DFT-GIAO (Density Functional Theory -Gauge-Including Atomic Orbital) calculations on the B3LYP/6-311G(2df,p)//B3LYP/pcS-1 level of theory (geometry optimization//NMR calculation respectively). The next two series, trialkyl- and triorganosilyl metaborates have the same structural motif in common. Both consist of B₃O₃ ring with boron and oxygen atoms in turns. It is well known that the complexation of triorganoboroxines (that consist of the same ring) with an Lewis base occurs only at one boron atom at the same time [33]. The acceptor number of B-O-SiR₃ is enhanced relative to the corresponding organic esters B-O-R. The acidic strength of the latter species is weakened by the size of -R due to the steric hindrance (entries **12** and **29**), while for the bimetallic compounds the bulky groups are located away from the acidic center, so the steric effect is not pounced (entry **26**). Instead, there is some electron-withdrawing effect associated with the empty, low energy C-Si σ* orbital. The same effect occurs for the organotin (entry **37**) derivative investigated by Beckett. The Sn gives an equal effect as Si (entry **36**). The few boroxines investigated also by Beckett *et al.* reveal much lower acidic properties (entries **38**, **40**, **41**, **43**) [34].

The relative Lewis acidity of *cyclo*-diboratetrasiloxanes (**a**) is comparable to triorganoboroxines (**b**), weaker acids are the *cyclo*-boratrisiloxanes (**c**) (Fig. 7).

The two bimetallic species (**a** and **c**) are only seemingly related, what is mirrored by the significant difference in their acceptor numbers. This is easy to explain if one considers the B:Si ratio of atoms that form the central rings of these compounds[35]. The extend of π-electron density which is made available to boron atoms from the adjacent oxygens is less in the case of *cyclo*-diboratetrasiloxanes.

The overall character of the -O-Si(R₂)-O-Si(R₂)-O- linkage in *cyclo*-boratrisiloxanes is more electron-donating than the -O-Si(R₂)-O-B(R)-O-Si(R₂)-O- linkage in *cyclo*-diboratetrasiloxanes towards every boron atom present (despite the fact, that there is only one B atom in *cyclo*-boratrisiloxanes). The two borasiloxane series are separated in the table by a few triorganosilyl esters of orthoboric acid (H₃BO₃) and arylboronic acids (PhB(OH)₂) [36]. The

acceptor number of these species is of the same order as the *cyclo*-boratrisiloxanes ($AN=50-58$). The end of the table is represented by 2-(2-fluorophenyl)-4,4,5,5-tetramethyl-1,3,2-dioxaborolane (pinacol 2-fluorophenylboronic ester) and $B(NMe_2)_3$. The much lower Lewis acidity of the pinacol ester relative to other phenylboronic esters is caused by steric hindrance of the boron atom. For the same reason the pinacol diol is considered as one of the best protective group for $-B(OH)_2$ function in the literature [37]. On the other hand, the boron atom in $B(NMe_2)_3$ is linked to three tertiary nitrogen atoms. As one can expect, the lone pairs from nitrogen atoms are strongly donated to boron due to an almost perfect orbital overlapping.

Concluding, the variety of presented organoboron compounds fills up almost the whole scale of acceptor number ($AN=9-92$). In many cases the range of acceptor number for one species of compounds covers with the range for another, what increases the scope of applicability of organoboron Lewis acids. It also proves that the Gutmann method is a very sensitive, all-purpose indicator of the Lewis acidity despite its relativity. It has been shown that the Lewis acidity of the boron center can be controlled by both the steric and electronic factors. This all proves the boron atom to be a very useful and versatile acidic function in organic chemistry.

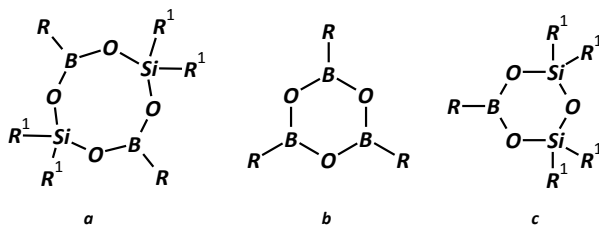


Figure 7. *Cyclo*-diboratetrasiloxanes (a), triorganoboroxines (b) and *cyclo*-boratrisiloxanes (c).

Acknowledgement

Authors acknowledge financial support by the Ministry of Science and Higher Education (Grant N N204 127938).

References

1. <http://goldbook.iupac.org>
2. G.N. Lewis, *Valence and the Structure of Atoms in Molecules*, Chemical Catalog Company, New York, 1923, p.141-142; G.N. Lewis, *J. Franklin Inst.*, 226 (1938) 293.

3. R.S. Drago, B.B. Wayland, *J. Am. Chem. Soc.*, 87 (1965) 3571. R.S. Drago, *Coord. Chem. Rev.*, 33 (1980) 251.
4. L.P. Hammett, *J. Am. Chem. Soc.*, 59 (1937) 96.
5. R.W. Taft, *J. Am. Chem. Soc.*, 74 (1952) 2729; R.W. Taft, *J. Am. Chem. Soc.*, 74 (1952) 3120; R.W. Taft, *J. Am. Chem. Soc.*, 75 (1953) 4538.
6. H. Höpfl, *J. Organomet. Chem.*, 581 (1999) 129.
7. U. Mayer, V. Gutmann, W. Gerger, *Monatsh. Chem.*, 106 (1975) 1235.
8. U. Mayer, W. Gerger, V. Gutmann, *Monatsh. Chem.*, 108 (1977) 489.
9. V. Gutmann, *Electrochim. Acta*, 21 (1976) 661.
10. M.A. Beckett, D.S. Brassington, M.E. Light, M.B. Hursthouse, *J. Chem. Soc., Dalton Trans.*, (2001) 1768.
11. E.M. Kosower, *J. Am. Chem. Soc.*, 80 (1958) 3253.
12. K. Dimroth, C. Reichardt, T. Siepmann, F. Böhlmann, *Ann. Chem.*, 661 (1963) 1.
13. E. Grunwald, S. Winstein, *J. Am. Chem. Soc.*, 70 (1948) 846.
14. K.O. Christie, D.A. Dixon, D. McLemore, W.W. Wilson, J.A. Sheehy, J.A. Boatz, *J. Fluorine Chem.*, 101 (2000) 151.
15. R.F. Childs, D. Mulholland, A. Nixon, *Can. J. Chem.*, 60 (1982) 801.
16. D. Fărcașiu, P. Lukinskas, A. Ghenciu, R. Martin, *J. Molecular Catalysis A: Chemical*, 137 (1999) 213.
17. M. Yamashita, *Angew. Chem. Int. Ed.*, 49 (2010) 2474.
18. C. Laurence, J.-F. Gal, *Lewis basicity and affinity scales. Data and measurements.*, John Wiley & Sons Ltd. Chichester, U.K., 2010.
19. A.H. Soloway, W. Tjarks, B.A. Barnum, F.-G. Rong, R.F. Barth, I.M. Codogni, G.J. Wilson, *Chem. Rev.*, 98 (1998) 1515.
20. T.D. James, M.D. Phillips, S. Shinkai, *Boronic acids in saccharide recognition*, Royal Society of Chemistry, Cambridge, 2006.
21. D.G. Hall, *Boronic Acids: Preparation and Applications in Organic Synthesis and Medicine*, Wiley-VCH, Weinheim, 2005, p. 8-10.
22. H. G. Kuivila *et al.*, *J. Org. Chem.*, 19 (1954) 780; L. I. Bosch *et al.*, *Tetrahedron*, 60 (2004) 11175; W. Ni, H. Fang, G. Springsteen, B. Wang, *J. Org. Chem.*, 69 (2004) 1999.
23. T. D. James, S. Shinkai, *Top. Curr. Chem.*, 218 (2002) 159.
24. H. Ito, Y. Kono, A. Machida, Y. Mitsumoto, K. Omori, N. Nakamura, Y. Kondo, K. Ishihara, *Inorganica Chim. Acta*, 344 (2003) 28.
25. G. Springsteen, B. Wang, *Tetrahedron*, 58 (2002) 5291.
26. C.S. Chen, B.J. Bulkin, E.M. Pearce, *J. Appl. Polym. Sci.*, 27 (1982) 1177; E.S. Lopata, S.R. Riccitiello, *J. Appl. Polym. Sci.*, 19 (1975) 1127; 21 (1977) 91.

27. H.S. Lee, X.Q. Yang, C.L. Xiang, J. McBreen, *J. Electrochem. Soc.*, 145 (1998) 2813; H.S. Lee, X.Q. Yang, X. Sun, J. McBreen, *J. Power Sources*, 89 (2000) 163; M. Marcinek, G.Z. Żukowska, W. Wiczorek, *Electrochim. Acta*, 50 (2005) 3934; H.S. Lee, X.Q. Yang, X. Sun, J. McBreen, *J. Power Sources*, 97-98 (2001) 566; H.S. Lee, X.Q. Yang, X. Sun, J. McBreen, *J. Electrochem. Soc.*, 149 (2002) A1460; H.S. Lee, Z.F. Ma, X.Q. Yang, X. Sun, J. McBreen, *J. Electrochem. Soc.*, 151 (2004) A1429; X.Q. Yang, H.S. Lee, W.S. Yoon, J. McBreen, S. Hossain, Y.-K. Kim, *Meet. Abstr. – Electrochem. Soc.*, 701 (2007) 30.
28. G.J.P. Britovsek, J. Ugolotti, A.J.P. White, *Organometallics*, 24 (2005) 1685.
29. C.R. Wade, A.E.J. Broomsgrove, S. Aldridge, F. P. Gabbai, *Chem. Rev.*, 110 (2010) 3958.
30. A. Adamczyk-Woźniak, M. Jakubczyk, A. Sporzyński, G. Żukowska, *Inorg. Chem. Commun.*, 14 (2011) 1753.
31. M.A. Beckett, D.S. Brassington, S.J. Coles, M.B. Hursthouse, *Inorg. Chem. Commun.*, 3 (2000) 530.
32. M.A. Beckett, G.C. Strickland, J.R. Holland, K.S. Varma, *Polymer Commun.*, 37 (1996) 4629.
33. A. Sporzyński, M. Lewandowski, B. Zarychta, J. Zaleski, *Pol. J. Chem.*, 79 (2005) 1099.
34. M.A. Beckett, D.S. Brassington, P. Owen, M.B. Hursthouse, M.E. Light, K.M.A. Malik, K.S. Varma, *J. Organomet. Chem.*, 585 (1999) 7.
35. M.A. Beckett, D.E. Hibbs, M.B. Hursthouse, K.M.A. Malik, P. Owen, K.S. Varma, *J. Organomet. Chem.*, 595 (2000) 241.
36. M.A. Beckett, P. Owen, K.S. Varma, *J. Organomet. Chem.*, 588 (1999) 107.
37. P.G.M. Wuts, T.W. Greene, *Greene's Protective Groups in Organic Chemistry*, IV ed., Wiley-Interscience, Hoboken NJ, 2007, p. 643-645.

Chapter 5

Sulfur-containing molecules in phenylboronic acids chemistry

Krzysztof M. Borys, Agnieszka Adamczyk-Woźniak
and Andrzej Sporzyński

*Warsaw University of Technology, Faculty of Chemistry,
Noakowskiego 3, 00-664 Warsaw, Poland*

Introduction

Boronic acids constitute a class of chemical compounds that have been attracting sustained scientific interest not only in the classical areas of chemistry such as organic synthesis, catalysis or supramolecular chemistry, but also on the border with biological and physical sciences, e.g. in biochemistry, medicinal chemistry and material engineering.[1] Rapid expansion of the boronic acids chemistry gave rise to compounds characteristic of gradually more complex structures, with a wide variety of substituents and functional groups included. This work is focused on sulfur in the context of phenylboronic acids chemistry. Incorporation of sulfur groups into the phenylboronic acids scaffold can result in exceptionally useful properties. Due to the incompatibility of the SH group with standard metalation – borylation procedure however, the synthesis of sulfur containing phenylboronic acids is not an easy task. Therefore, the number of so-far obtained chemicals containing both phenylboronic and sulfur units is very small. Another important issue is the compatibility of sulfur containing molecules with the Suzuki-Miyaura coupling conditions, which requires adoption of the appropriate S-protective groups.

This review covers the synthesis, properties and application of sulfur-containing molecules in phenylboronic acids' chemistry. It should be helpful for scientists working on discovery of new functional materials as well as synthetic chemists utilizing Suzuki coupling of phenylboronic compounds.

1. Structurally simplest sulfur-containing phenylboronic acid

4-Mercaptophenylboronic acid (MPBA) **1** was first synthesized by Brikh and Morin in 1999 (Figure 1).[2] The authors suggested that **1** could present similar *in vivo* interaction to borocaptate (mercaptoundecahydro-*closo*-dodecaborate anion, BSH), a thiol-bearing boron cluster successfully used in boron neutron

capture therapy (BNCT).[3] Moreover, **1** posed a convenient substrate for the synthesis of boronated analogues of aromatic thioethers, which had been already known to have melanocytotoxic properties desirable in melanoma chemotherapy. [4]

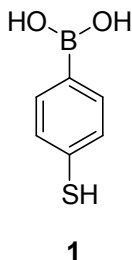
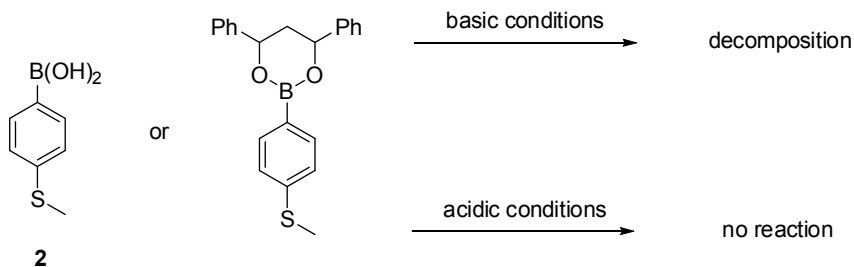


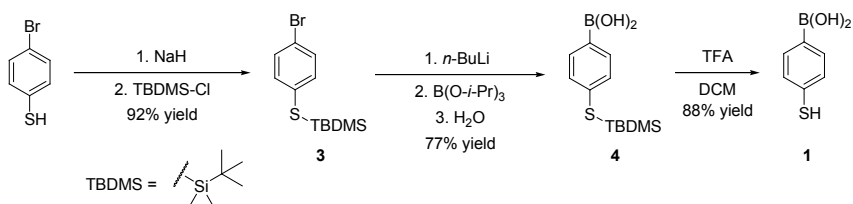
Figure 1. Structure of 4-mercaptophenylboronic acid **1**.

Initial attempts to introduce a boronic acid group into the thiophenol scaffold by using a standard metallation/boration procedure on the corresponding aryl halide failed. Treating 4-bromothiophenol with two equivalents of *n*-, *sec*- or *tert*-butyllithium at -78°C and subsequent quenching with trimethyl borate resulted in a complicated reaction mixture, without any evidence of the formation of **1**. Hence, application of protecting groups for the thiol and/or boronic acid moieties was considered. Two strategies were taken into account: deprotection of a readily available *p*-methylthiophenylboronic acid **2** (Scheme 1) as well as searching for a thiol protecting group that would be compatible with metallation/boration of an aryl halide. The first concept was based on a potential possibility of obtaining **1** via demethylation of the boronic acid **2**. However, cleavage of the methyl group (in the case of both boronic acid **2** and boronate derived from *d,l*-1,3-diphenylpropane-1,3-diol) proved a considerable difficulty: basic conditions were incompatible with the base-sensitive boronic moiety, and under acidic conditions the starting material was recovered.

The second strategy, i.e. evaluation of the applicability of *S*-protected aryl halides, turned out to be successful, *tert*-butyldimethylsilyl (TBDMS) being the most appropriate *S*-protecting group.[2]



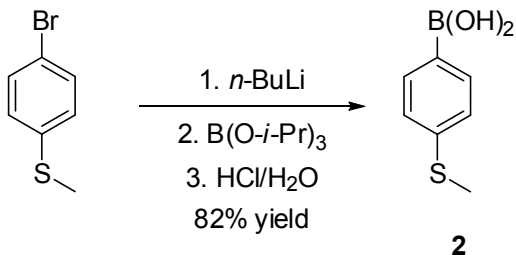
Scheme 1. Unsuccessful attempts at the preparation of boronic acid 1.



Scheme 2. Synthesis of 4-mercaptophenylboronic acid 1.

TBDMSC thioether **3** was obtained from 4-bromothiophenol *via* deprotonation and silylation with *tert*-butyldimethylsilyl chloride (Scheme 2). Lithiation of **3** with *n*-butyllithium at -78°C, followed by reaction with an excess of triisopropyl borate, afforded the *S*-protected boronic acid **5**. Deprotection of the thiol group was achieved by treating **4** with an excess of trifluoroacetic acid, resulting in the synthesis of 4-mercaptophenylboronic acid **1** in more than 60% overall yield.

The aforementioned 4-(methylthio)phenylboronic acid **2** can be synthesized from commercially available 4-bromothiophenol (Scheme 3).^[5]



Scheme 3. Synthesis of 4-(methylthio)phenylboronic acid 2.

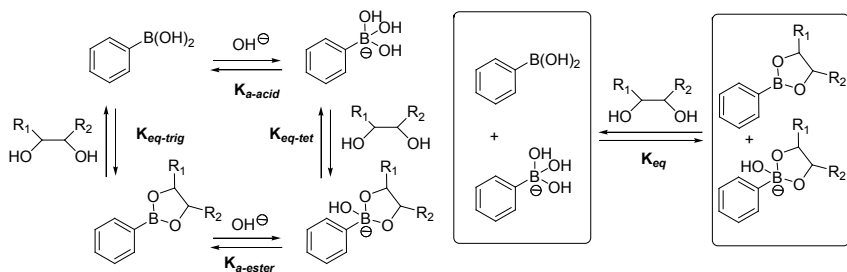
Reaction of 4-bromothioanisole with *n*-butyllithium, further boronation with triisopropylborate and hydrolysis with aqueous solution of hydrochloric acid afforded **2** in 82% yield. Alternatively, tri-*n*-butylboronate can be applied for boronation.[6]

2. Self-Assembled Monolayers: starting materials, investigations and applications

The presence of sulfur atoms in the discussed phenylboronic acids determines their main application as self-assembled monolayers (commonly abbreviated as SAMs). Thiols (including boronated ones) are frequently utilized in the formation of SAMs mainly on gold surfaces, gold itself being commonly referred to as „thiophilic“.

In general terms, self-assembled monolayer can be regarded as a spontaneously formed molecular modification of a surface. In most of the cases, three structural features of SAM forming molecules can be distinguished: terminal group having high affinity for the surface, chain- or ring-based scaffold affecting packing and organization of the monolayer, and a head moiety determining the SAM's functionality. The topic of SAMs has been comprehensively reviewed in many publications and book chapters.[7] As this work is inclined to focus on sulfur-containing boronic acids chemistry, only SAMs formed by such molecules will be discussed.

Boronic acids demonstrate an ability of reversible pH-sensitive ester formation with 1,2- and 1,3-diols (Scheme 4).[1a,1c,8]



Scheme 4. Detailed[8a] and overall[8b] equilibrium in the boronic acid-diol system.

This unique property has been extensively used for diols receptors and sensors design.[1a,9] By combining it with the advantages of SAMs, powerful tools for molecular recognition can be developed.

SAMs derived from the adsorption of the aforesaid 4-mercaptophenylboronic

acid (1) on gold are the most commonly researched sulfur-containing boronic acids-based SAMs. The most cited work on this topic was published in 2007 by Lee et al.[10] It presents a comparison of structures and properties of SAMs derived from 1, as well as from structurally related thiophenol, 4-mercaptophenol and 4-mercaptobenzoic acid (Figure 2). All of the studied compounds possess a thiol group, which chemisorbs onto gold surface to form a gold-thiolate bond. [10]

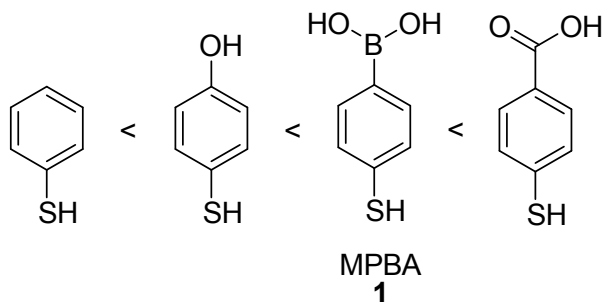


Figure 2. Thiol-containing compounds, in the order of increasing surface coverage.[10]

Evaluation of the obtained SAMs was carried out using a set of standard surface investigation techniques: ellipsometry (assessment of monolayer formation), contact-angle goniometry (surface hydrophilicity and homogeneity), polarization-modulation infrared reflection-absorption spectroscopy PM-IRRAS (molecular composition and orientation, intermolecular hydrogen bonding) and X-ray photoelectron spectroscopy XPS (monolayer film composition and surface coverage/packing density). Noteworthy, stability studies of MPBA-derived SAMs in solutions revealed that boronic acid moiety is sensitive to high pH and presence of strong amine nucleophiles, undergoing boron-carbon bond cleavage.[10]

Surfaces functionalized with 4-mercaptophenylboronic acid were *inter alia* applied in: piezoresistive microcantilevers responsive to cis-diol analytes[11] and carbohydrates-sensitive electrodes for voltammetric detection of sugars (MPBA SAMs on gold),[12] magnetic microspheres for selective enrichment of glycopeptides and glycoproteins (MPBA-functionalized core-shell structure Fe₃O₄@C@Au),[13] investigations of surface enhanced Raman scattering (SERS) (MPBA-functionalized silver nanoparticles),[14] as well as nanoscopic caps for gate-like pH- and photo-switched systems for releasing guest molecules from mesoporous silica[15] and nanoparticle systems for selective enrichment

(MPBA-functionalized gold nanoparticles).[16]

Due to the same functional groups, 3-mercaptophenylboronic acid found applications similar to its position isomer, MPBA. As an example, 3-mercaptophenylboronic acid was incorporated in boronic acid-protected silver nanoclusters utilized to investigate induced optical activity by their reversible complexation with enantiomerically pure fructose.[17]

Another group of thiol-containing phenylboronic acids are *N*-(3-dihydroxyborylphenyl)-5-mercaptoalkanamides **5** (Figure 3), varied in the number of methylene groups in the aliphatic chain.

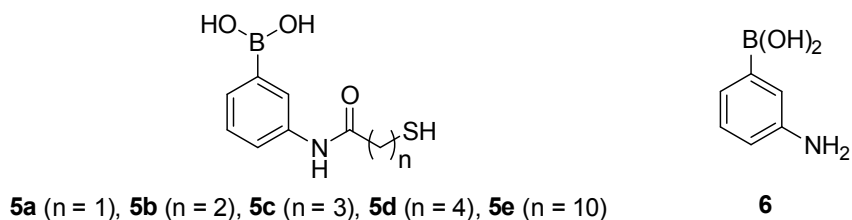
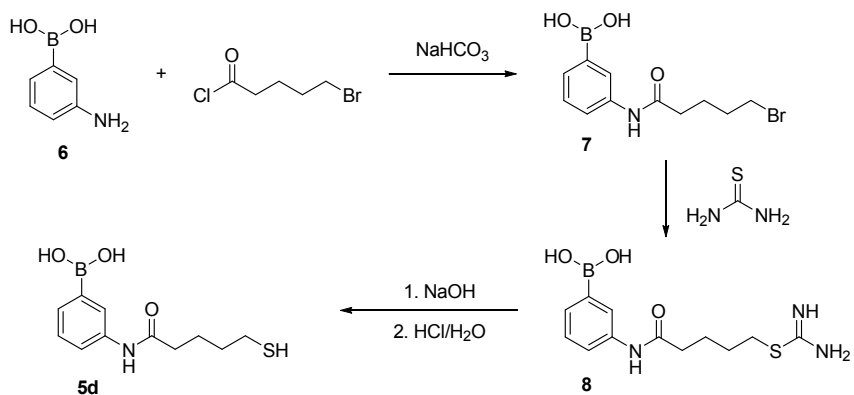


Figure 3. Structures of the reported *N*-(3-dihydroxyborylphenyl)-5-mercaptoalkanamides and their precursor, 3-aminophenylboronic acid.

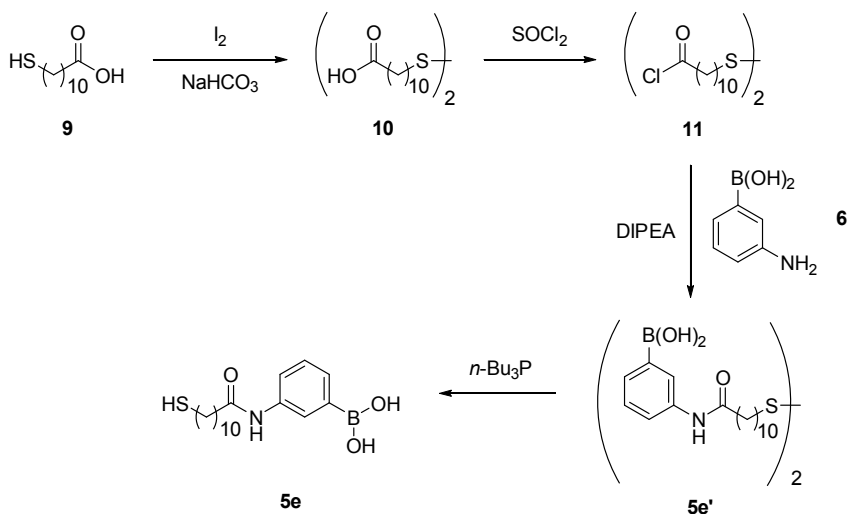
All the above boronated phenylmercaptoalkanamides are derived from a common precursor, 3-aminophenylboronic acid **6**. Their syntheses are the examples of functionalizing molecules that already possess a boronic acid moiety. The first one to be synthesized was the pentanamide **5d** (Scheme 5).[18]



Scheme 5. Synthesis of boronated phenylmercaptoalkanamide **5d**.

Reaction of 3-aminophenylboronic acid **6** with 6-bromopentanoyl chloride gave 3-(5-bromopentanoylamino)phenylboronic acid **7**, which was further reacted with thiourea. Treatment of the obtained thioamidine **8** with sodium hydroxide, followed by acidification with hydrochloric acid, produced the thiol-containing boronic acid **5d** (yields not given). Self-assembly characteristics of **5d** were investigated, showing its potential application as a self-assembling vicinal diol receptor.[18]

The synthesis and application of a long chain mercaptoundecanamide **5e** was researched by Franzen *et al.* in 2004 (Scheme 6).[19]

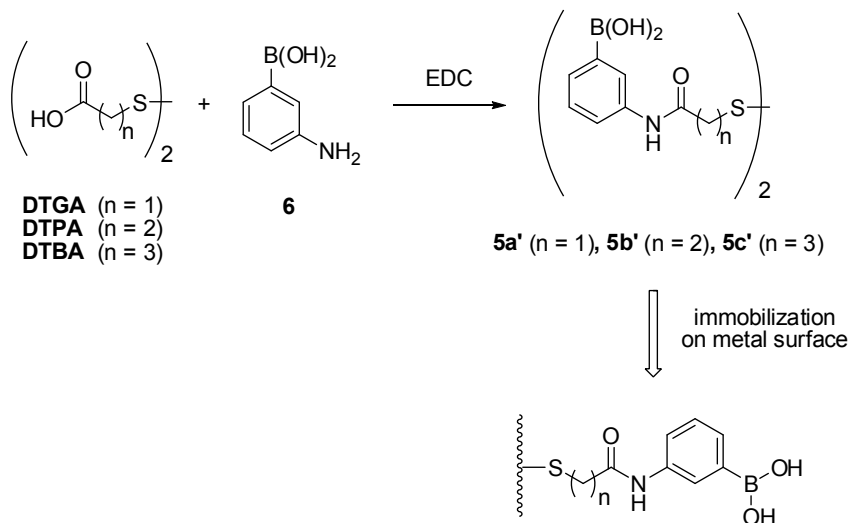


Scheme 6. Synthesis of boronated phenylmercaptoalkanamide **5e**.

Commercially available 11-mercaptoundecanoic acid **9** served as the starting material for disulfide **10** preparation. Treatment of **9** with ca 0.5 equivalent of molecular iodine in the presence of sodium bicarbonate afforded the product **10**, subsequently converted with thionyl chloride into bis-(acid chloride) disulfide **11**. Amide formation from **11** and 3-aminophenylboronic acid **6** was carried out with Hünig's base (*N,N*-diisopropylethylamine, DIPEA). Finally, bis-amide disulfide **5e'** was transformed into the target mercaptoalkanamide **5e** by reduction with tri-*n*-butylphosphine (overall yield was not given).[19]

Metal-thiolate bond, responsible for the deposition of sulfur-terminated compounds on a metal's surface, can be derived not only from thiols but from disulfides as well.[20] In 2000, Kanayama and Kitano prepared and examined

gold SAMs obtained by the deposition of disulfides **5a'**, **5b'** and **5c'** corresponding to the boronated mercaptoalkanamides **5a**, **5b** and **5c**, respectively (Scheme 7).[21] The resulting monolayers were capable of binding of monosaccharides, polysaccharides and a sugar-carrying protein (ovalbumin).



Scheme 7. Synthesis of disulfides **5a'-c'** and their deposition on metal surface.

The disulfides **5a'-5c'** were obtained from 3-aminophenylboronic acid **6** and the appropriate dithiodialiphatic acids: dithiobisglycolic acid (DTGA), 3,3'-dithiodipropionic acid (DTPA) and 4,4'-dithiodibutyric acid (DTBA). The synthesis was performed using 1-ethyl-3-(3-dimethylaminopropyl)carbodiimide hydrochloride (EDC), a carboxyl activating coupling agent well established e.g. in peptide chemistry.

The **5a'-5c'**-derived SAMs were reinvestigated by Koh *et al.* in 2007.[22] The authors followed the synthetic route for disulfides preparation developed by Kanayama and Kitano. Extensive surface characterization by atomic force microscopy (AFM), Fourier transform infrared reflection absorption spectroscopy (FTIR-RAS), surface enhanced Raman spectroscopy (SERS) and cyclic voltammetry was provided. In addition, the obtained SAMs were evaluated for saccharide detection, using surface plasmon resonance (SPR) spectroscopy as a signal amplification method.

Moreover, a comparison of saccharide-sensitive gold electrodes

modified with SAMs derived from MPBA as well as DTBA conjugated with 3-aminophenylboronic acid was reported.[12]

3. Other examples of phenylboronic acid thio compounds

An interesting example of a structurally relevant non-SAM analytical system for saccharide recognition was the phenylboronic acid-functionalized tetrathiafulvalene-anthracene dyad **12** (Figure 4), developed by Zhu *et al.*[23]

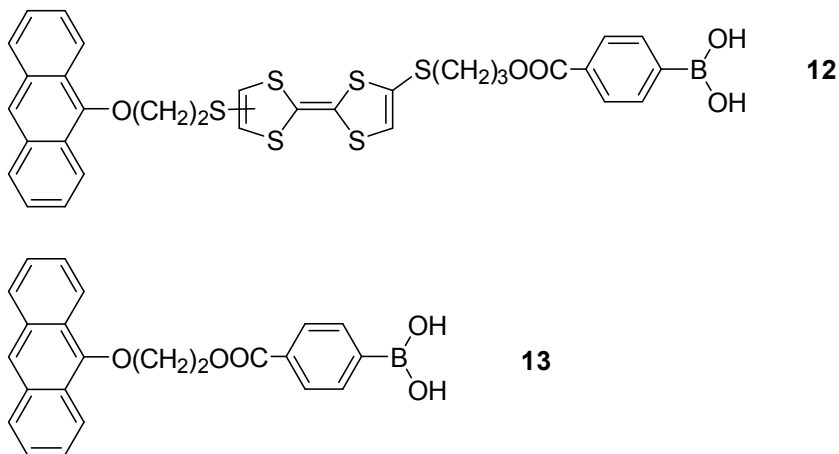
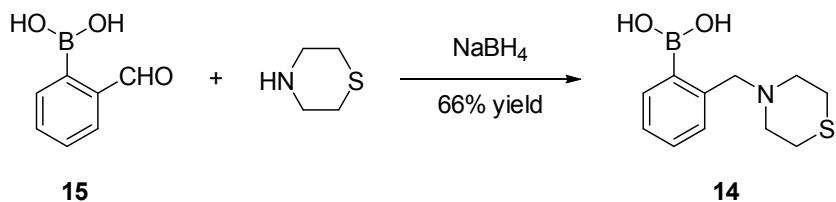


Figure 4. Structures of phenylboronic acid-functionalized anthracene dyads **12** and **13**.

The sensing properties of **12** are based on the photoinduced electron-transfer (PET) mechanism. The tetrathiafulvalene (TTF) unit, often encountered in the molecules of organic conductors, acts as a strong electron donor. On complexation of the boronic acid group with a sugar, a fluorescence response is produced. Comparative studies with compound **13** showed that the presence of the TTF group is important for the observed fluorescence enhancement after reaction with saccharides (in case of **13**, smaller fluorescence increase was achieved).

Sugar receptor activity was also studied for a sulfur-containing *ortho*-(aminomethyl)phenylboronic acid **14** (Scheme 8).[1c] The determined values of equilibrium constants with ARS (alizarin red S), glucose, fructose as well as galactose have been lower than those of the oxygen analogue. Thiomorpholine derivative **14** was obtained by reductive amination of *ortho*-formylphenylboronic **15** with thiomorpholine.

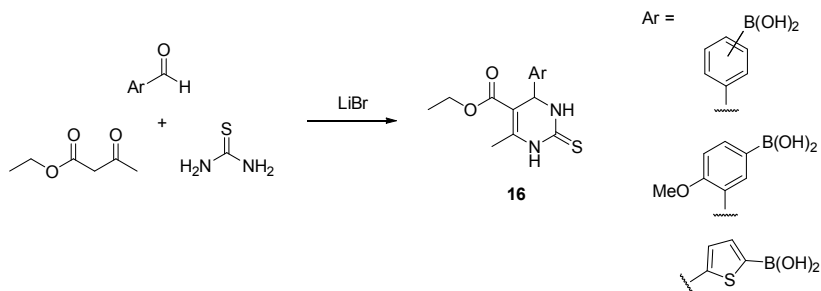


Scheme 8. Synthesis of *ortho*-(thiomorpholinemethyl)phenylboronic acid.

Other relevant sulfur-containing groups are sulfones and sulfonamides. Phenylboronic acids featuring these moieties are primarily utilized in sugar-binding solid phases. Electron-withdrawing effect of both the sulfonyl and sulfonamide groups results in decreased pK_a of the boronic acid, which in turn induces an enhanced affinity for *cis*-diols (as compared with unsubstituted phenylboronic acids). Reported examples of such solid phase systems are: sulfonamide- and sulfonyl-phenylboronic acid-modified porous silica gel for boronate affinity chromatography,[24] resin-immobilized dansylphenylboronic acid for fructose recognition,[25] and monolithic capillary for specific capture of *cis*-diol biomolecules.[26] The last one *nota bene* exhibits a highly desirable capability of two-dimensional separation: initial resolution of *cis*-diols from non-*cis*-diol compounds with subsequent separation of *cis*-diols according to differential hydrogen bonding interactions within the monolith.

Apart from BNCT mentioned in the first chapter, boronic acids (including the phenyl-substituted ones) were investigated as potential pharmaceuticals in many other areas of pharmacological therapy.[27] As far as sulfur-containing phenylboronic acids are concerned, at least two published examples should be noted.

The series of boron-containing 3,4-dihydropyrimidin-2(1H)-(thio)ones **16** (Scheme 9) was synthesized in order to test their antifungal activity.[28]



Scheme 9. Synthesis of boron-containing DHMPs **16**.

The principal idea of the research was to combine two moieties known to display considerable biological activity: dihydropyrimidinones (DHMPs) (incorporated in anticancer and antimicrobial agents) and boron compounds (introducing potential antifungal activity). The synthesis was performed using Biginelli reaction, an acid-catalyzed three-component condensation of an aldehyde, a β -ketoester and urea, yielding dihydropyrimidone derivatives. In this case, formylphenylboronic acid derivatives were reacted with thiourea and ethyl acetoacetate in the presence of a Lewis acid (lithium bromide) to give the target products **16** in moderate yields. It is interesting to note that the attempts of utilizing this synthetic route to thiopheneboronic acid derivatives ended up with the cleavage of the boron-carbon bond, along with the side formation of boric acid. However, the corresponding pinacol thiopheneboronates were obtained successfully without observation of the degradation products.

Recently, a phenylboronic acid-based sulfur-containing inhibitor of autotaxin (ATX, nucleotide pyrophosphatase/phosphodiesterase involved in signalling pathway implicated in such pathologies as chronic inflammation, fibrotic diseases and tumor progression) was developed as a promising drug candidate (Figure 5).[29]

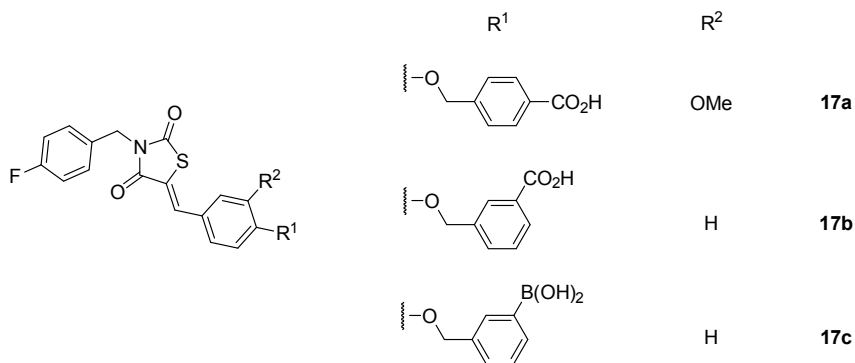


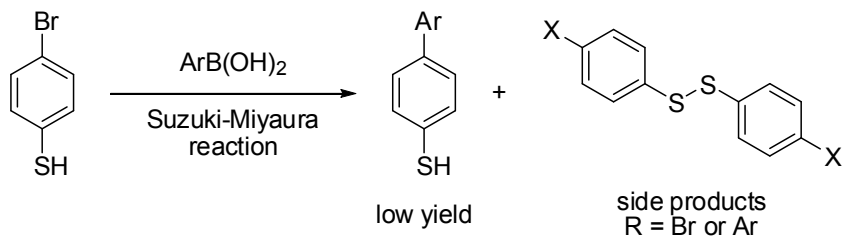
Figure 5. Structures of thiazolidinedione derivatives **17**.

In comparison with concurrently devised carboxylic acid-terminated thiazolidinediones **17a** and **17b**, phenylboronic acid-functionalized agent **17c** showed nearly one hundred times higher potency for ATX inhibition.[29]

4. Thiol group in Suzuki-Miyaura cross-coupling

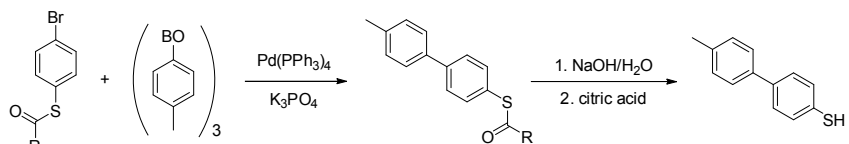
The issue of protecting the thiol group emerged also in the context of Suzuki-Miyaura palladium-catalyzed cross-coupling, the reaction that boronic

acids are most commonly associated with in organic synthesis.[30] Unprotected thiol group is not tolerated in Suzuki coupling reactions because of its high affinity for certain transition metals, including palladium. This phenomenon, called catalyst poisoning, is the reason that more than stoichiometric amounts of palladium would be necessary to run an efficient cross-coupling involving a mercaptan substrate. Typical Suzuki-Miyaura conditions (with catalytic amounts of palladium) result in low yields of the cross-coupling product, along with the formation of side products. As an example, coupling of 4-bromothiophenol with arylboronic acids afforded disulfide by-products (Scheme 10).[31]



Scheme 10. Outcome of Suzuki-Miyaura cross-coupling of unprotected aromatic thiols.

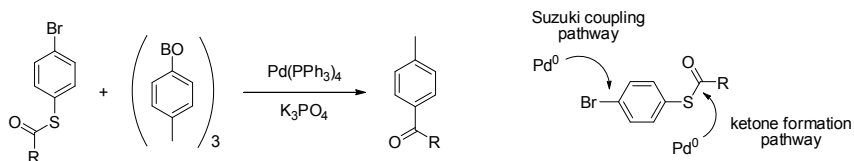
Although there are many thiol protecting groups known,[32] only a few are suitable for the conditions of Suzuki reaction. In the year 2000, Terfort *et al.* examined the Pd-catalyzed coupling of 4-tolylboronic acid anhydride with a range of 4-(thioacyl)bromobenzenes (Scheme 11).[33]



Scheme 11. Model reaction for the examination of acyl-based protective groups for thiol moiety.

Thioesters tend to cleave easily under basic conditions, making the thiol deprotection facile. Based on the yields of biaryl product (determined by gas chromatography), 2-methoxyisobutyryl group appeared to be the promising one.

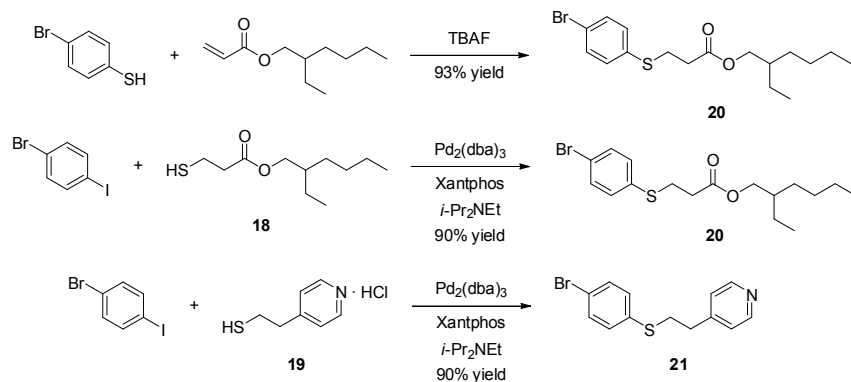
Remarkable feature of the majority of tested reactions was the full conversion of thioesters, regardless of the yield of biaryl product. This observation led to their closer examination by means of GC/MS, resulting in identification of the main by-products as 4-tolyl ketones (Scheme 12).



Scheme 12. Cross-coupling side product and different mechanistic pathways of the reaction.

In case of 4-(thioacetyl)bromobenzene, the yield of the side reaction product reached ca 40% under conditions optimized for biaryl coupling. The authors suggested that ketone formation predominates when the formal insertion of palladium between the sulfur atom and the carbonyl group is faster than the oxidative addition into the carbon-bromine bond.

In 2006, Itoh and Mase proposed another approach to the issue of thiol protection in Suzuki coupling: the use of thiol surrogates, namely 2-ethylhexyl-3-mercaptopropionate **18** and 4-(2'-mercaptoethyl)pyridine hydrochloride **19** (Scheme 13).[31] Synthesis of the corresponding aryl thioethers **20** and **21** was carried out, as they could prove useful substrates for preparation of biaryl scaffolds.

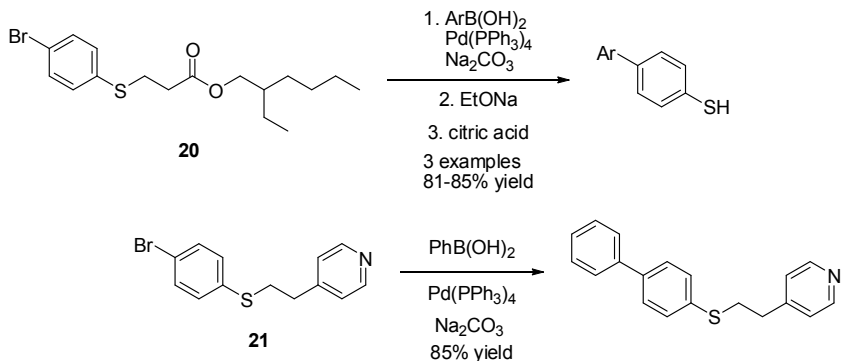


Scheme 13. Use of thiol surrogates **18** and **19** for the preparation of thioethers **20** and **21**.

Thioether **20** was obtained using two different methods. The first one was based on 1,4-conjugate addition of 4-bromothiophenol to isooctyl acrylate in the presence of tetra-*n*-butylammonium fluoride. The second method featured a Pd-catalyzed coupling of 1-bromo-4-iodobenzene with compound **18**, achieved under conditions previously reported also by Itoh and Mase.[34] The same

coupling protocol turned out to be applicable in the synthesis of thioether **21** as well.

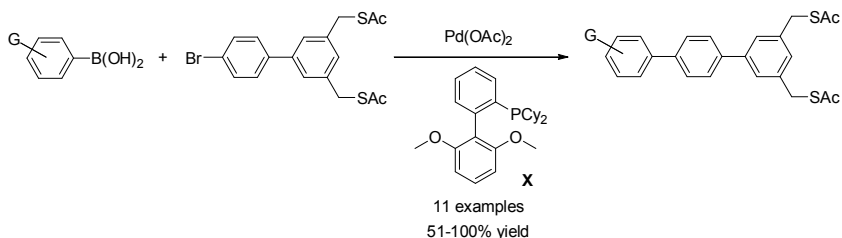
Stability of the developed thiol protective groups was investigated in several Pd-catalyzed cross-coupling reactions, including Suzuki-Miyaura (Scheme 14).



Scheme 14. Suzuki cross-couplings with thiol protected thioethers **20** and **21**.

Both thioethers **20** and **21** were tolerated under the reaction conditions, giving high yields of the desired products. Deprotection of thiols obtained using compound **20** was achieved via a β -elimination mechanism using sodium ethoxide in ethanol, with subsequent acidification with aqueous citric acid.

Suzuki-Miyaura cross-coupling of thiol protected substrates was also the key step in the synthesis of oligoarylenedithiols (Scheme 15).[35]



Scheme 15. Acetyl as the protective group for thiols in the synthesis of oligoarylenedithiols.

Notwithstanding the problems posed by side reactions, Naso *et al.* decided to employ *S*-acetyl protection. In order to make it compatible with coupling process, a range of different catalyst/solvent/base systems and reaction conditions was examined. The best results were obtained using catalytic system

of palladium(II) acetate together with sterically hindered, electron rich biaryl phosphine belonging to the group of Buchwald's ligands, tripotassium phosphate as a base and toluene as a solvent.

The choice of *S*-acetyl protection instead of other thioesters or thiol surrogates is particularly noteworthy. The primary reason was the possibility of its straightforward *in situ* removal during the deposition of target oligoarylenedithiols from solution on gold, just by adding a few drops of aqueous ammonia (a method developed by Whitesides et al.).[36]

Acknowledgement

The authors acknowledge financial support by the Ministry of Science and Higher Education (Grant N N204 135639).

References

1. (a) Hall, D. G., Ed. *Boronic Acids: Preparation And Applications in Organic Chemistry and Medicine*; Wiley-VCH: Weinheim, 2005. (b) Petasis, N. A. *Aust. J. Chem.* 2007, *60*, 795-798, and references therein. (c) Adamczyk-Woźniak, A.; Brzózka, Z.; Cyrański, M. K.; Filipowicz-Szymańska, A.; Klimentowska, P.; Żubrowska, A.; Żukowski, K.; Sporzyński, A. *Appl. Organometal. Chem.* 2008, *22*, 427-432, and references therein.
2. Brikh, A.; Morin, C. *J. Organomet. Chem.* 1999, *581*, 82-86.
3. (a) Soloway, A. H.; Tjarks, W.; Barnum, B. A.; Rong, F.-G.; Barth, R. F.; Codogni, I. M.; Wilson, G. J. *Chem. Rev.* 1998, *98*, 1515-1562. (b) Issa, F.; Kassiou, M.; Rendina, L. M. *Chem. Rev.* 2011, *111*, 5701-5722.
4. Jimbow, K.; Iwashina, T.; Alena, F.; Yamada, K.; Pankovich, J.; Umemura, T. *J. Invest. Dermatol.* 1993, *100*, 231S-238S.
5. Norman, M. H.; Smith, H. D.; Andrews, C. W.; Tang, F. L. M.; Cowan, C. L.; Steffen, R. P. *J. Med. Chem.* 1995, *38*, 4670-4678.
6. Santucci, L.; Gilman, H. *J. Am. Chem. Soc.* 1958, *80*, 193-196.
7. (a) Ulman, A. *Chem. Rev.* 1996, *96*, 1533-1554. (b) Wink, Th.; van Zuilen, S. J.; Bult, A.; van Bennekom, W. P. *Analyst* 1997, *122*, 43R-50R. (c) Gooding, J. J.; Ciampi, S. *Chem. Soc. Rev.* 2011, *40*, 2704-2718. (d) Schroeder, G., Ed. *Chemiczna funkcjonalizacja powierzchni dla potrzeb nanotechnologii*; Cursiva: Kostrzyn, 2005; specifically Chapters 2 and 3; book issued in Polish. (e) Schreiber, F. *J. Phys.: Condens. Matter* 2004, *16*, R881-R900. (f) Love, J. C.; Estroff, L. A.; Kriebel, J. K.; Nuzzo, R. G.; Whitesides, G. M. *Chem. Rev.* 2005, *105*, 1103-1169. (g) Kind, M.; Wöll, C. *Progress in Surface Science* 2009, *84*, 230-278. (h)

- Samanta, D.; Sarkar, A. *Chem. Soc. Rev.* 2011, 40, 2567-2592.
8. (a) Kuivila, H. G.; Keough, A. H.; Soboczenski, E. J. *J. Org. Chem.* 1954, 19, 780-783. (b) Springsteen, G.; Wang, B. *Tetrahedron* 2002, 58, 5291-5300.
 9. (a) James, T. D.; Philips, M. D.; Shinkai, S. *Boronic Acids in Saccharide Recognition*; RSC Publishing: Cambridge, 2006. (b) James, T. D.; Sandanayake, K. R. A. S.; Shinkai, S. *Angew. Chem. Int. Ed.* 1996, 35, 1910-1922. (c) Hartley, J. H.; James, T. D.; Ward, C. J. *J. Chem. Soc., Perkin Trans. 1* 2000, 3155, (d) Sporzyński, A.; Żubrowska, A.; Adamczyk-Woźniak, A., *Synthesis of boronic acids – molecular receptors for sugars*, in *Synthetic receptors in molecular recognition*, Rybachenko V. I. (Ed.), Publishing House „Schidnyj wydawnyczyj dim”, Donetsk, Ukraine, 2007, 51-88. (e) Sporzyński, A.; Adamczyk-Woźniak, A.; Żubrowska, A., *Intramolecular interactions in ortho-(aminomethyl)phenylboronic acids – potent saccharide receptors*, in *From concept to molecular receptor*, Rybachenko V. I. (Ed.), Publishing House „Schidnyj wydawnyczyj dim”, Donetsk, Ukraine, 2008, 77-92. (f) Adamczyk-Woźniak, A. *Phenylboronic compounds as molecular recognition and self-assembling agents*, in *Application of molecular receptors*, Rybachenko V. I. (Ed.), Publishing House „Schidnyj wydawnyczyj dim”, Donetsk, Ukraine, 2009, 9-24.
 10. Barriet, D.; Yam, C. M.; Shmakova, O. E.; Jamison, A. C.; Lee, T. R. *Langmuir* 2007, 23, 8866-8875.
 11. Baker, G. A.; Desikan, R.; Thundat, T. *Anal. Chem.* 2008, 80, 4860-4865.
 12. Takahashi, S.; Anzai, J. *Langmuir* 2005, 21, 5102-5107.
 13. Qi, D.; Zhang, H.; Tang, J.; Deng, C.; Zhang, X. *J. Phys. Chem. C* 2010, 114, 9221-9226.
 14. Kinnan, M. K.; Chumanov, G. *J. Phys. Chem. C* 2007, 111, 18010-18017.
 15. Aznar, E.; Marcos, M. D.; Martínez-Mañez, R.; Sancenón, F.; Soto, J.; Amorós, P.; Guillem, C. *J. Am. Chem. Soc.* 2009, 131, 6833-6843.
 16. Yao, G.; Zhang, H.; Deng, C.; Lu, H.; Zhang, X.; Yang, P. *Rapid Commun. Mass. Spectrom.* 2009, 23, 3493-3500.
 17. Yao, H.; Saeki, M.; Kimura, K. *J. Phys. Chem. C* 2010, 114, 15909-15915.
 18. Pavey, K. D.; Olliff, C. J.; Baker, J.; Paul, F. *Chem. Commun.* 1999, 2223-2224.
 19. Brewer, S. H.; Allen, A. M.; Lappi, S. E.; Chasse, T. L.; Briggman, K.

- A.; Gorman, C. B.; Franzen, S. *Langmuir* 2004, 20, 5512-5520.
20. Bain, C. D.; Biebuyck, H. A.; Whitesides, G. M. *Langmuir* 1989, 5, 723-727.
 21. Kanayama, N.; Kitano, H. *Langmuir* 2000, 16, 577-583.
 22. Chen, H.; Lee, M.; Lee, J.; Kim, J.-H.; Gal, Y.-S.; Hwang, Y.-H.; An, W. G.; Koh, K. *Sensors* 2007, 7, 1480-1495.
 23. Wang, Z.; Zhang, D.; Zhu, D. *J. Org. Chem.* 2005, 70, 5729-5732.
 24. Li, X.; Pennington, J.; Stobaugh, J. F.; Schöneich, C. *Anal. Biochem.* 2008, 372, 227-236.
 25. Vélez López, E.; Pina Luis, G.; Suárez-Rodríguez, J. L.; Rivero, I. A.; Díaz-García, M. E. *Sensors and Actuators B* 2003, 90, 256-263.
 26. Liu, Y.; Ren, L.; Liu, Z. *Chem. Commun.* 2011, 47, 5067-5069.
 27. Yang, W.; Gao, X.; Wang, B. *Med. Res. Rev.* 2003, 23, 346-368.
 28. Duguay, D. R.; Zamora, M. T.; Blacquiére, J. M.; Appoh, F. E.; Vogels, C. M.; Wheaton, S. L.; Baerlocher, F. J.; Decken, A.; Westcott, S. A. *Cent. Eur. J. Chem.* 2008, 6, 562-568.
 29. Albers, H. M. H. G.; Dong, A.; van Meeteren, L. A.; Egan, D. A.; Sunkara, M.; van Tilburg, E. W.; Schuurman, K.; van Tellingen, O.; Morris, A. J.; Smyth, S. S.; Moolenaar, W. H.; Ovaa, H. *Proc. Natl. Acad. Sci.* 2010, 107, 7257-7262.
 30. For a review article on Suzuki-Miyaura cross-coupling reactions, see: Miyaura, N.; Suzuki, A. *Chem. Rev.* 1995, 95, 2457-2483.
 31. Itoh, T.; Mase, T. *J. Org. Chem.* 2006, 71, 2203-2206.
 32. Greene, T. W.; Wuts, P. G. *Protective Groups in Organic Synthesis*; John Wiley & Sons: New York, 1999; Chapter 6.
 33. Zeysing, B.; Gosch, C.; Terfort, A. *Org. Lett.* 2000, 2, 1843-1845.
 34. Itoh, T.; Mase, T. *Org. Lett.* 2004, 6, 4587-4590.
 35. Operamolla, A.; Omar, O. H.; Babudri, F.; Farinola, G. M.; Naso, F. J. *Org. Chem.* 2007, 72, 10272-10275.
 36. Tour, J. M.; Jones, L. R., II; Pearson, D. L.; Lamba, J. J. S.; Burgin, T. P.; Whitesides, G. M.; Allara, D. L.; Parikh, A. N.; Atre, S. V. *J. Am. Chem. Soc.* 1995, 117, 9529-9534.

Chapter 6

The application of the energy-resolved in-source collision-induced dissociation method for examination of ion fragmentation pathways

Natalia Mańkowska and Grzegorz Schroeder
*Adam Mickiewicz University, Faculty of Chemistry,
Grunwaldzka 6, 60-780 Poznań, Poland*

Mass spectrometry confirms continuously its effectiveness as an instrument for the studies of the structure and the stability of different complexity molecules. The collision- induced dissociation (CID) is commonly used method for this purpose and it is carried out both in the ion source and in the collision chamber. This technique has been studied various systems of biologically active compounds [1,2] as well as peptides [3] and glycopeptides [4]. The information about the intrinsic reactivity of the short-lived intermediates of oxidation processes was obtained [5]. The absolute stability of the gas phase ion by means on the threshold of collision- induced dissociation (TCID) [6-17] and the relative stability of the gas phase ions by means of energy-resolved (also called *energy-dependent* or *energy-variable*) mass spectrometry (ERMS) [11,18-24] were determined.

Previously, we presented the studies results in concerning method of the relative stability evaluation of ions studied in the ion source [24], based on the dependence of ion signal intensity on cone voltage (V_c). This method which uses the V_c value can be applied in a wider area than previously described. The study the fragmentation of ions can be made with the use of systematic research in a wide range of values cone voltage [24-26]. The curve applies to research ways of fragmentation ions in mass spectrometry based on the analysis functions $I/I_{\max} = f(V_c)$.

In the present paper we discuss the bell-like curve fragment corresponding to the range of V_c values less than $V_{c,\max}$ (Fig. 1) and introduce a general method for the interpretation of these results. The discussed fragment of the bell-like curve fragment consists of three distinctive cone voltage values. The first one corresponds to on the threshold of ion signal observing at the breakdown curve

($V_{c,0}$). The second one corresponds to the beginning of the slowdown of the ion signal intensity growth. As we assume the ion decomposition starts at this cone voltage value and is called $V_{c,dec}$. The third $V_{c,Imax}$ value is such as cone voltage value, is characteristic for decomposition of ions.

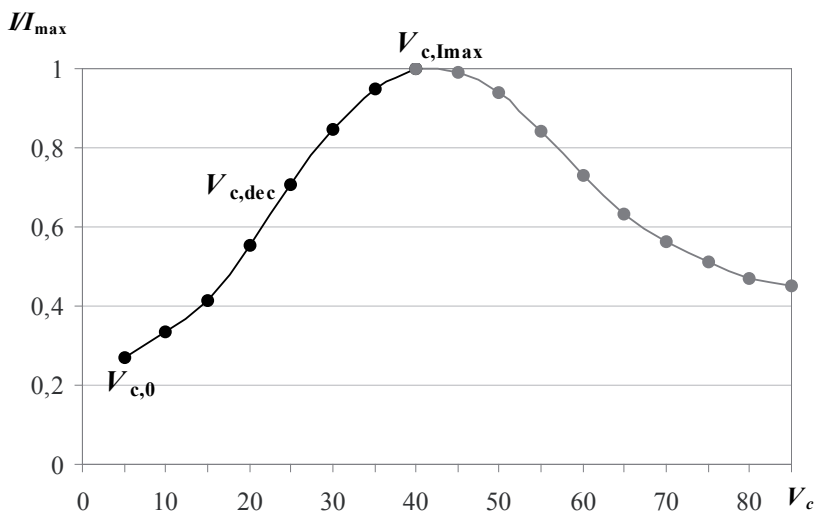
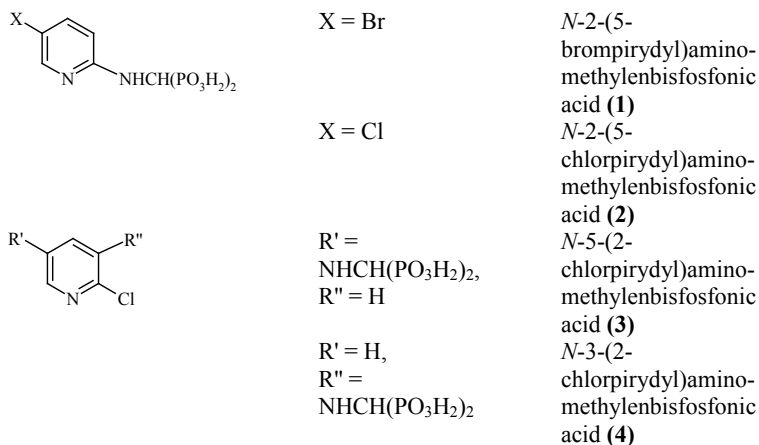


Figure 1. Exemplary breakdown curve

This paper assumes that in view of obvious correlation between the precursor ion decomposition and the fragment ion formation, there should exist a correlation between two cone voltage values: the $V_{c,dec}$ value for precursor ion and the $V_{c,0}$ value for fragment ion. It could allow the separation of the fragmentation pathways with the lowest collision activation energy, and thus the determination of the subtlest details of fragmentation process (the sequence of decomposition reaction) and ion structure using ESIMS.

Structures of the compounds used as model to interpretation of mass spectra are shown in Scheme 1. This compounds were synthesised by Burzyńska methods [27].

Fig. 2 presents the exemplary dependence of the normalized intensities (I/I_{max}) of precursor ion signals ($[M+H]^+$) and fragment ions on cone voltage value for compounds (1) and (2).



Scheme 1. The compounds studied

The breakdown curves of the fragment ions, just as the breakdown curves of the precursor ions, are also characterized by bell-like shape but the bell-like curve of the fragment ions is preceded, in the lowest cone voltage values range, by more or less significant segment characterized by extremely low intensity values. The presence of such a segment is caused by the phenomena of the mass spectrum noising by random signals with m/z ratio equal to one of the considered ion, for which the dependence $I/I_{\max} = f(V_c)$ is created. In that case, there exist the background line, which describes noise level with the same m/z ratio as ion in the range of cone voltage values below the appearance threshold of considered ion. Moreover, it is also obvious that the intensity increase of fragment ion signals as the cone voltage increases is related not only to the improvement in the ion transmission through the mass analyzer region, but first of all to the augmentation of those ion amount due to the precursor ion decomposition.

The maxima of ion decomposition curves (Fig. 2) with lower m/z ratio are located at higher values of cone voltage, which corresponds to the general direction of the fragmentation process – from more complexed molecules to simpler ones. However, the analysis of presented set of the decomposition curves based only on $V_{c, \text{Imax}}$ values consideration hinders interchangeable statement whether, for instance ion having m/z 174 (Fig. 2, a) is formed during the direct fragmentation of the precursor ion or in the result of many further reaction of the precursor ion fragmentation. In order to determine the fragmentation pathways, taking place in a given system, the ion(1)-ion(2) pair whose $V_{c, \text{dec}}(\text{ion}1) \approx V_{c,0}(\text{ion}2)$ should be found. The $V_{c, \text{dec}}$ value was calculated as zeroing point of second derivative of

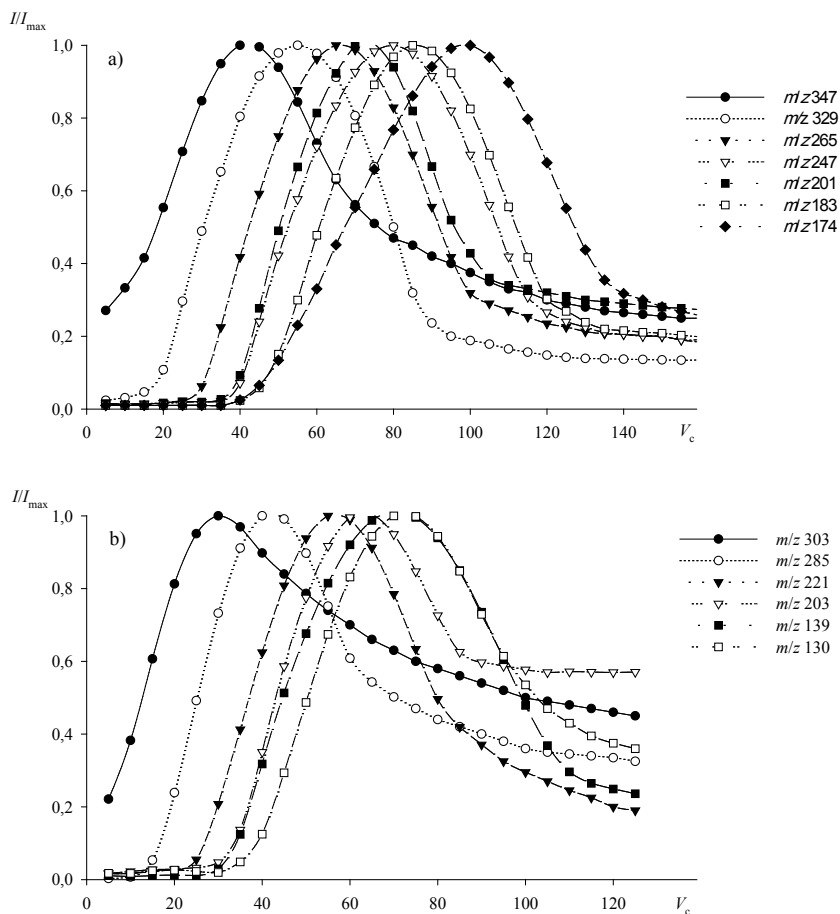


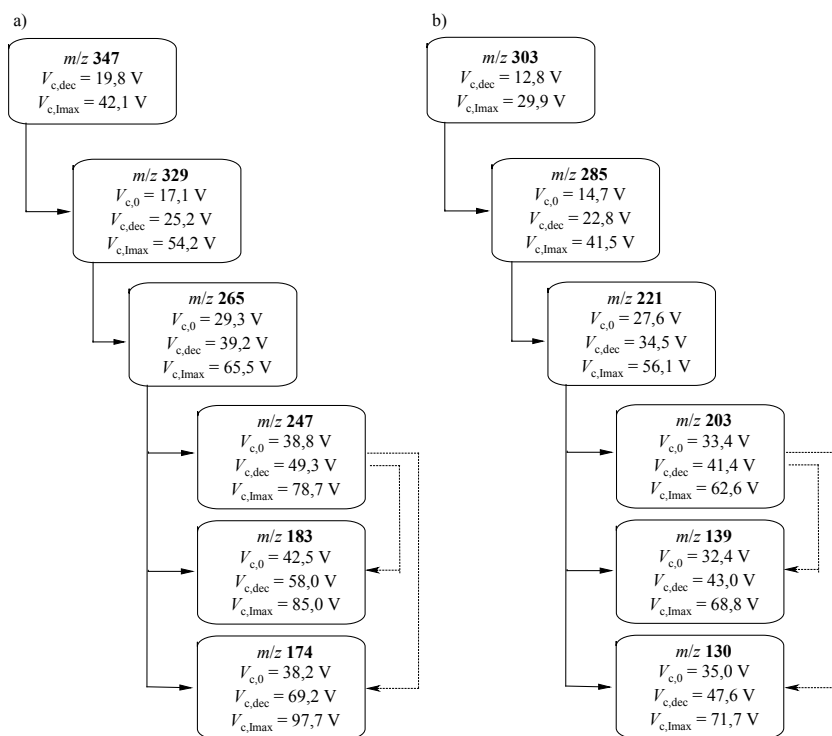
Figure 2. Cone voltage dependences of normalized (I/I_{\max}) signal intensities for protonated ions of *N*-2-(5-bromopyridyl)aminomethylenbisfosfonic (a) and *N*-2-(5-chloropyridyl)aminomethylenbisfosfonic (b) acids

function, describing the dependence of the ion signal intensity on cone voltage, while $V_{c,0}$ – as intersection point of tangent to breakdown curve in $V_{c,\text{dec}}$ point with noise line corresponding to m/z ratio of the considered ion. The sequence verification of the fragmentation reaction, obtained by calculation of $V_{c,\text{dec}}$ and $V_{c,0}$ cone voltage values, was achieved on the basis of MS/MS studies in the ion trap. Both, the fragmentation in the ion source and the one in the ion trap

are soft methods, when ion collisions with gas molecules cause the induction of the vibrational level of the fragmented ion and lead to the decomposition of the weakest bonding in the molecule. It suggests significant similarity of the fragmentation pathways taking place in both instruments.

The fragmentation studies of N-2-(5-bromopyridyl)aminomethylenbisfosfonic (1) and N-2-(5-chloropyridyl)aminomethylenbisfosfonic (2) acids

Scheme 2 presents calculated $V_{c,fr}$ i $V_{c,0}$ values for [(1) + H]⁺, [(2) + H]⁺ and for its fragment ions.



Scheme 2. Distinctive cone voltage values for protonated ions of N-2-(5-bromopyridyl)aminomethylenbisfosfonic (a) and N-2-(5-chloropyridyl)aminomethylen-bisfosfonic (b) acids

The great conformity of distinctive cone voltage values for particular ions were observed. It enables the arrangement of fragmentation pathways of

protonated ions in the mass spectrometer ion source (Fig. 3). Mass spectra from MS/MS experiment are shown in Fig. 4. The precise data analysis presents unusually high conformity and mutual data complementing from both methods. The test with ion trap confirmed that the ions formed at the lowest collision activation energies of the precursor ions are the ions with m/z 329 (**1**) and m/z 285 (**2**), for which the decompositions with the lowest collision activation energies lead to the formation of the ions with m/z 265 (**1**) and m/z 221 (**2**). For compound (**1**), ion with m/z 265 ratio decomposition at the lowest possible fragmentation energy proceeds accordingly to three parallel pathways: creating ions with m/z 247, 183 and 174 ratios; for compound (**2**), ion with m/z 221 ratio dissociates at the lowest possible fragmentation energy accordingly to parallel formation of ions with m/z 203, 139 and 130 ratios. Unfortunately, both the experiment conditions in the ion source and in the ion trap forbid the precise distinction of these parallel decomposition reactions by its collision activation energies. In the case of compound (**1**) the fine fragmentation of ion with m/z 247 leads to the formation of ions with m/z 183 and 174. Nevertheless, it seems to be a secondary process. The calculated values of distinctive cone voltage evidence that $V_{c,0}$ values for ions with m/z 183 and 174 (42.5 and 38.2 V respectively) are more close to $V_{c,fr}$ values for m/z 265 ion ($V_{c,fr} = 39,2$ V) than the m/z 247 one ($V_{c,fr} = 49,3$ V). It suggests that m/z 183 and 174 ions are rather formed not from m/z 247 ion but directly from m/z 265 one in the chain of decomposition reaction of the protonated ion (**1**). Analogously in the case of compound (**2**) decomposition of m/z 203 ion with two ions formation (m/z 139 and 130) is a secondary fragmentation reaction. $V_{c,0}$ values for m/z 139 and 130 ions (32.4 V and 35.0 V respectively) are more close to $V_{c,fr}$ value for m/z 221 ion ($V_{c,fr} = 34.5$ V) than to m/z 203 ($V_{c,fr} = 41.4$ V). It suggests that m/z 139 and 130 ions are formed directly not from m/z 203 ion, but from m/z 221 one in the chain of decomposition reaction of the protonated ion. The mass spectra obtained both in the ion source ESIMS and in the ion trap, included also rich signals at m/z 201 value (for (**1**)) and at m/z 157 value (for (**2**)), which origin is discussed below.

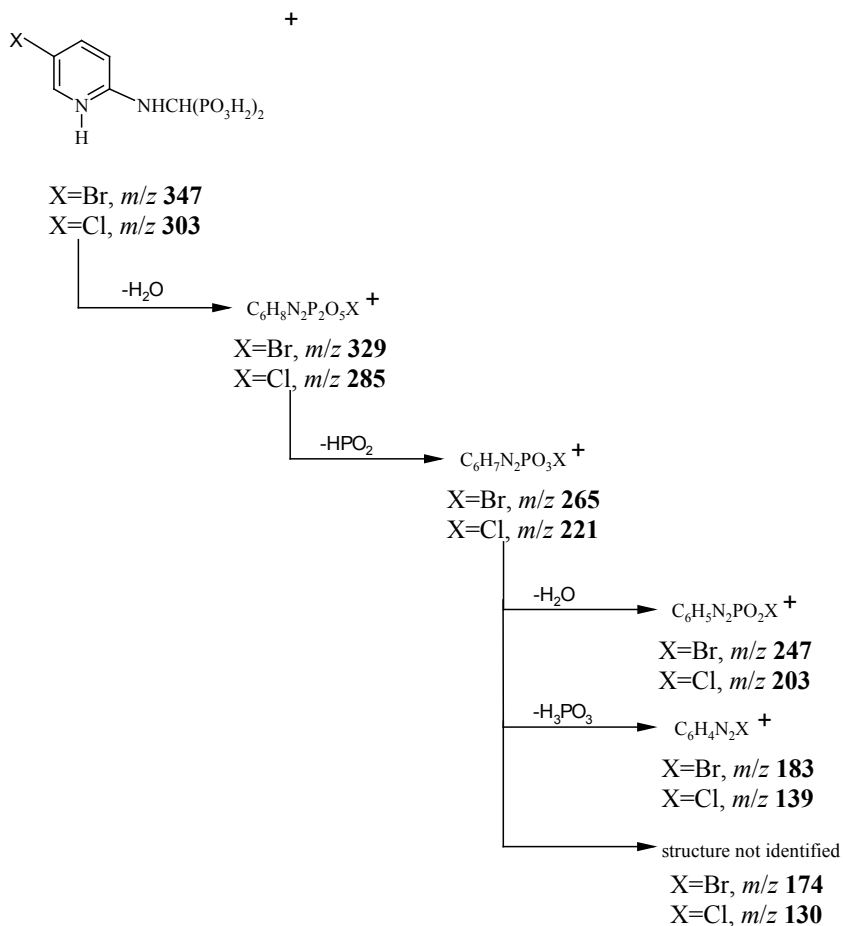


Figure 3. Fragmentation pathways of protonated ions of *N*-2-(5-bromopyridyl) aminomethylenbisfosfonic (a) and *N*-2-(5-chloropyridyl)aminomethylen-bisfosfonic (b) acids

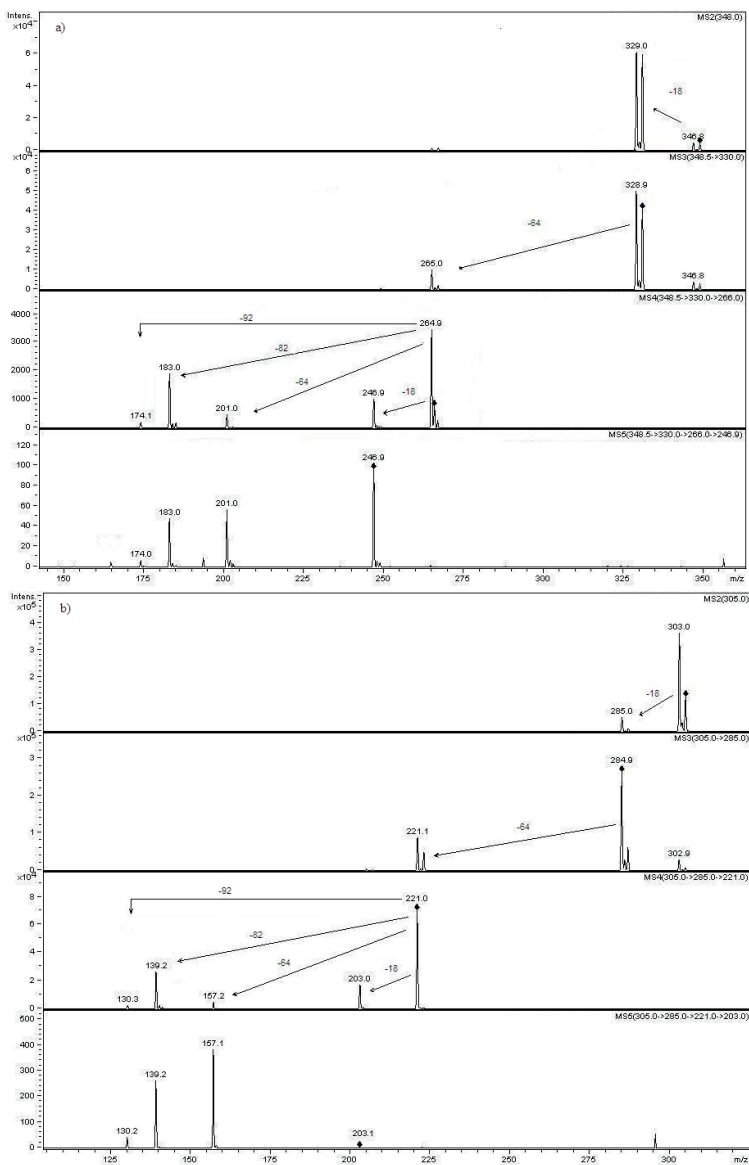


Figure 4. Ion trap mass spectra of protonated ions of *N*-2-(5-bromopyridyl) aminomethylenbisfosfonic (a) and *N*-2-(5-chloropyridyl)aminomethylen-bisfosfonic (b) acids

The fragmentation studies of N-5-(2-chlorpirydy)aminomethylenbisfosfonic acid (**3**)

The calculation of distinctive cone voltage values from ion source mass studies as well as mass spectra of protonated ion (**3**), obtained from the ion trap studies (Fig. 5, Scheme 3), suggest that different substitution position of molecule (**3**) in comparison with compound (**2**) causes slight modification in the decomposition. The formation of m/z 285 and 221 ions happens in the one step – directly from the precursor ion. The reaction m/z 285 \rightarrow 221 has marginal meaning in the chain of decomposition reaction [**3**] + H⁺ (as opposed to decomposition reaction of [(**2**) + H]⁺) since $V_{c,0}$ value of m/z 221 ion (20.5 V) is more approximate to $V_{c,fr}$ value of m/z 303 ion than m/z 285 one (17.0 V and 27.8 V respectively). In the follow-up of the fragmentation the m/z 130 ion is not formed. The proposed decomposition scheme [(**3**) + H]⁺ is presented at Fig. 6. The origin of m/z 157 ion is discussed below.

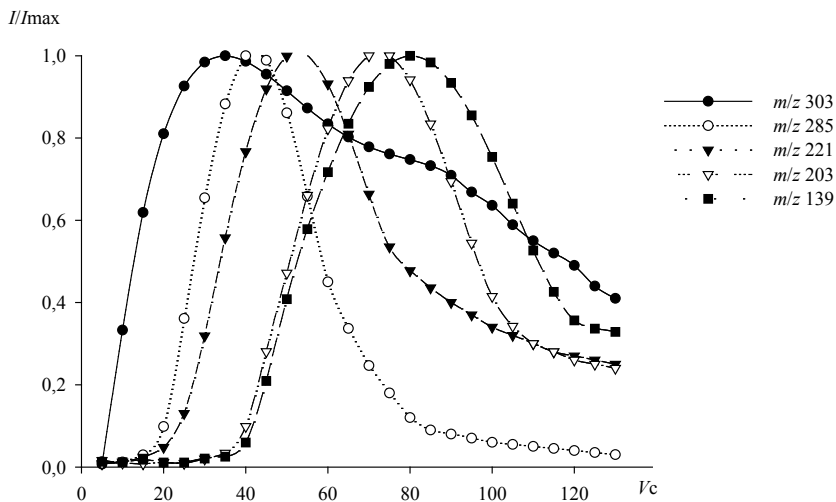
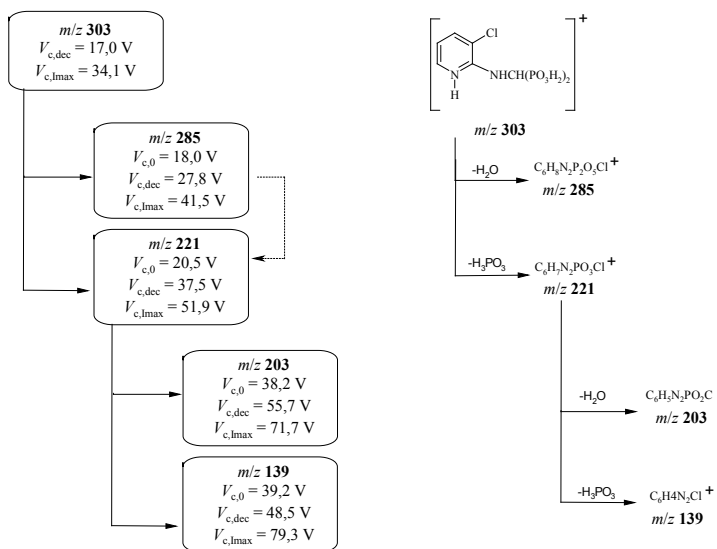


Figure 5. Cone voltage dependences of normalized (I/I_{max}) signal intensities for protonated ions N-5-(2-chlorpirydy)aminomethylenbisfosfonic acid



Scheme 3. Distinctive cone voltage values and fragmentation pathway for *N*-5-(2-chloropyridyl)aminomethylenbisfosonic acid

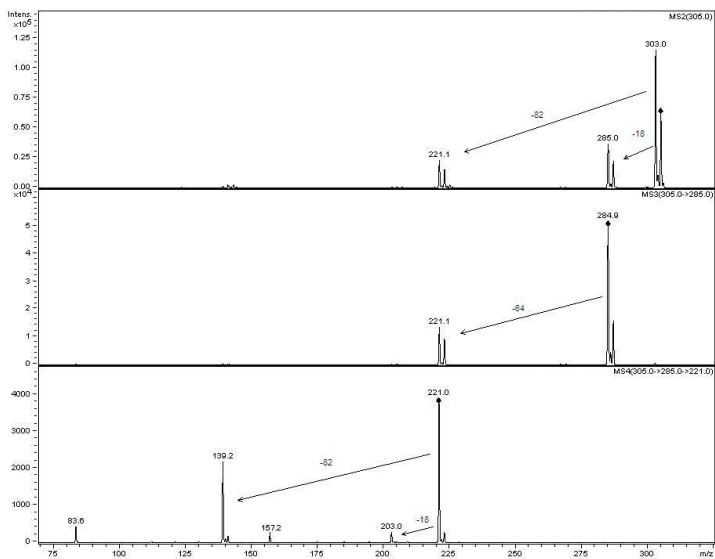


Figure 6. Ion trap mass spectra of monoprotonated ions of *N*-5-(2-chloropyridyl)aminomethylenbisfosonic acid

The fragmentation studies of N-3-(2-chloropyridyl)aminomethylenbisfosfonic acid (4)

The compound (4), with is isomer of compounds (2) and (3), has radically different structure: in relation to the piridyne nitrogen atom, the *N*-alkyl substituent is in the *meta* position, and the halogen substituent is in the *ortho* position. The breakdown curves of the [(4) + H]⁺ decomposition, as well as mass spectra obtained in MS/MS studies are pictured on Figs. 7 and 8. These data show that together with fragment ions described earlier for ions [(2) + H]⁺ and [(3) + H]⁺, an additional fragment ion with *m/z* 267 is formed. Doubtless, this ion formation indicates the HCl elimination *via* the intramolecular nucleophilic substitution (Fig. 9). The fragmentation pathway consisting on HCl elimination proceeds parallel to earlier described pathways, and is similar to H₂O elimination in respect of distinctive cone voltage values (Scheme 4 and Fig. 10).

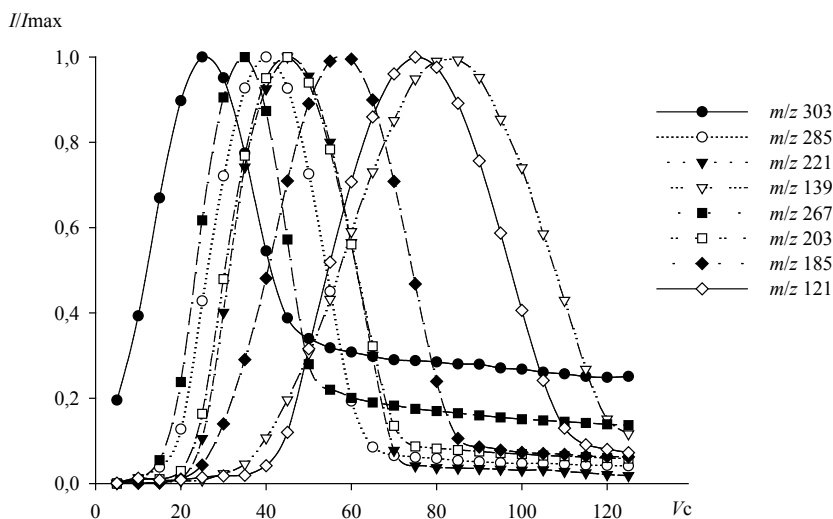


Figure 7. Cone voltage dependences of normalized (I/I_{max}) signal intensities for monoprotonated ions of N-3-(2-chloropyridyl)aminomethylenbisfosfonic acid

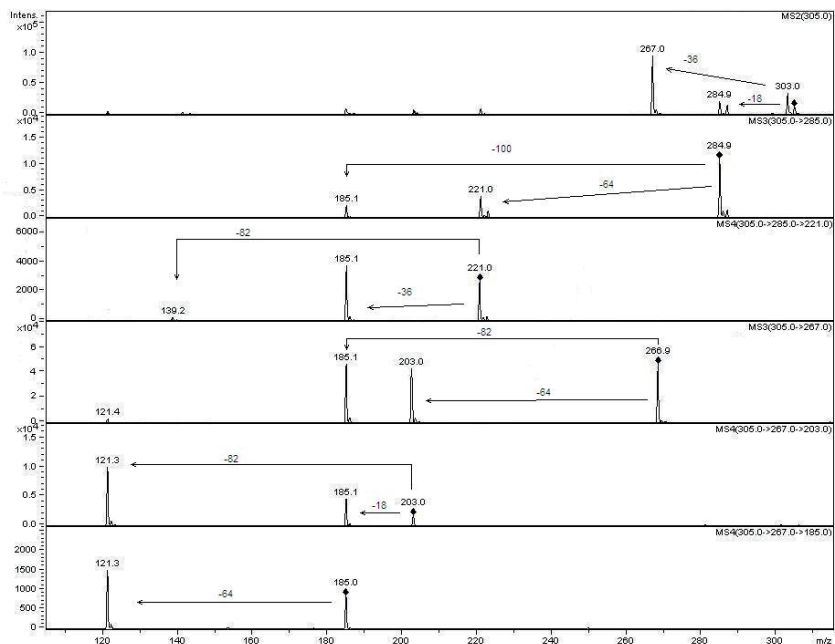
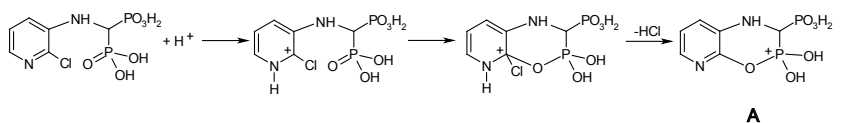
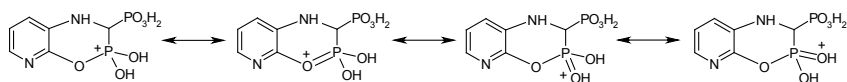


Figure 8. Ion trap mass spectra of protonated ion of *N*-3-(2-chloropyridyl) aminomethylenbisfosfonic acid



resonance stabilization of product **A**



tautomeric stabilization of product **A**

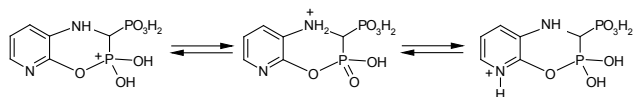
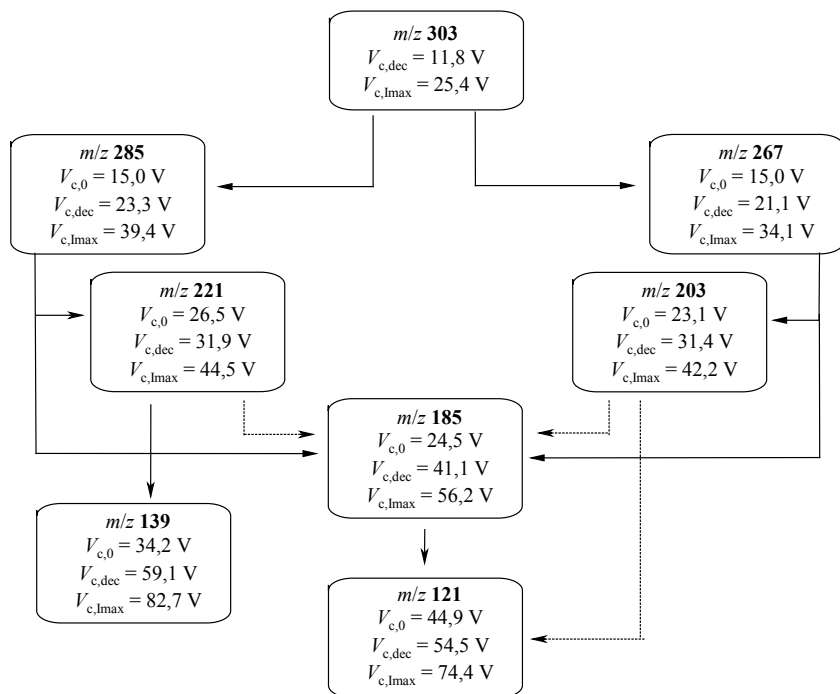


Figure 9. Interamolecular nucleophilic substitution during fragmentation of protonated ion of *N*-3-(2-chloropyridyl) aminomethylenbisfosfonic acid



Scheme 4. Distinctive cone voltage values for protonated ions of *N*-3-(2-chloropyridyl) aminomethylenbisfosfonic acid

The dependence of $V_{c,0}$ value for the fragment ion on $V_{c,dec}$ value for the precursor ion is pictured in Fig.11. It is clearly seen good linear correlation ($r^2 = 0,94$) $V_{c,0} - V_{c,dec}$ for all ion described above. It confirms our hypothesis of close relation between the cone voltage value corresponding to the beginning of slowdown of the precursor-ion signal intensity growth at the breakdown curve ($V_{c,dec}$ value for precursor ion) and the second one corresponding to the threshold of fragment ion signal observing at the breakdown curve ($V_{c,0}$ for fragment ion). The r^2 value suggests the dependence of fragment ion $V_{c,0}$ value on precursor ion $V_{c,dec}$ value only.

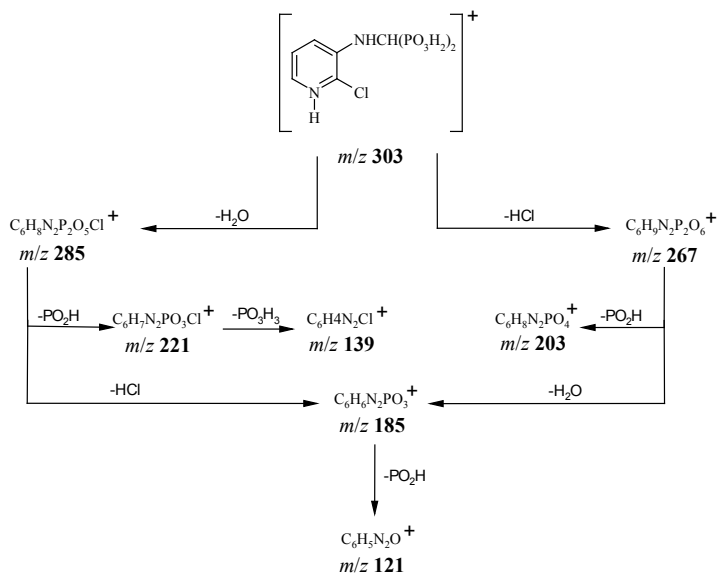


Figure 10. Fragmentation pathways of protonated ion *N*-3-(2-chloropyridyl) aminomethylenbisfosonic acid

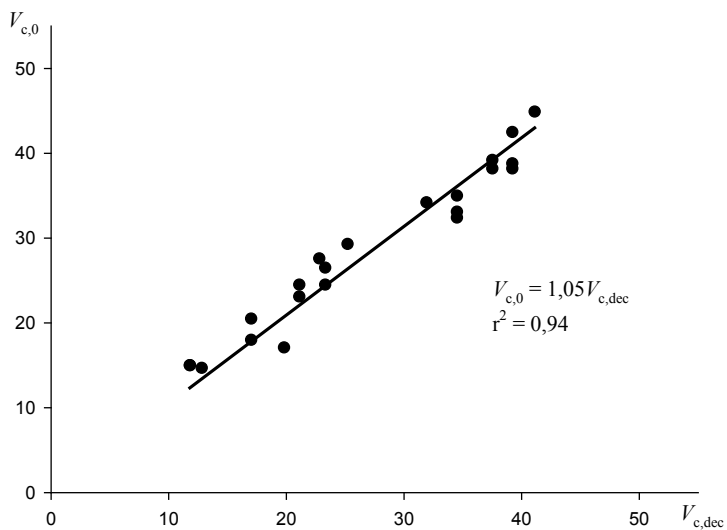


Figure 11. Dependence of $V_{c,0}$ value for the fragment ion on $V_{c,dec}$ value for the precursor ion for all ions studied. Data are shown at schemes 2-4.

The origin of ions with m/z 201 (for (1)) and m/z 157 (for (2), (3)) ratios

The origin of m/z 201 ion (for compound (1)), m/z 157 ion (for compounds (2) and (3)) may be caused by two reasons. First, it may be due to recombination according to the schema shown on Fig. 12, which ensures additional ion stability due to formamid derivatives formation with conjugated systems extended in comparison to precursor ions. In MS/MS experiments, the mass spectra of isolated ions with m/z 183 (compound (1)) and m/z 139 (compound (2)) clearly show signals shifted by 18 units above m/z ratios of isolated ions (Fig. 13). The signals of m/z 201 (1) and m/z 157 ions (2) were observed both in MS and MS/MS spectra. However those ions signal intensity in the MS/MS spectra from ion trap experiments are relatively lower compared to ion abundances in MS spectra obtained in ion source studies. It is definitely related to smaller amount of water, available in the ion trap, as well as to the specific character of measurements in both cases. In case of MS studies in the ion source, the precursor and fragment ions, as well as solvent vapors are in the same space, while ions in the ion trap are separated and only trace amount of solvent vapor are available. In the case of compound (3), sterical restrictions forbid ion with m/z 139 recombination with formamid derivative formation, so any signal with m/z ratio above this one of isolated ion were observed on MS/MS spectra of isolated m/z 139 ion. Secondly, another reasons of the discussed ions presence could be the hydrogen bonding formation in the precursor ion, oxygen atom sharing in phosphorite groups between phosphorus and hydrogen atoms bounded with pyridine nitrogen atom. It may cause parallel cracking of O-H and O-P bonds followed by complex mixture of the fragmentation products formation. This interpretation is confirmed by a fact that in case of acid (4), which structure make impossible hydrogen bonding formation between hydrogen atom bounded with pyridine nitrogen atom and oxygen atom of phosphoric group, the signal of m/z 157 ion was not observed.

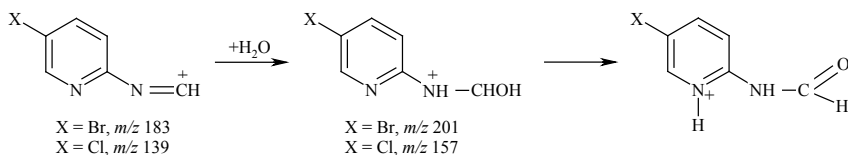


Figure 12. Possible way of recombination reaction for ions with m/z 183 (for N-2-(5-bromopyridyl)aminomethylenbisfosfonic) and m/z 139 (for N-2-(5-chloropyridyl)aminomethylenbisfosfonic)

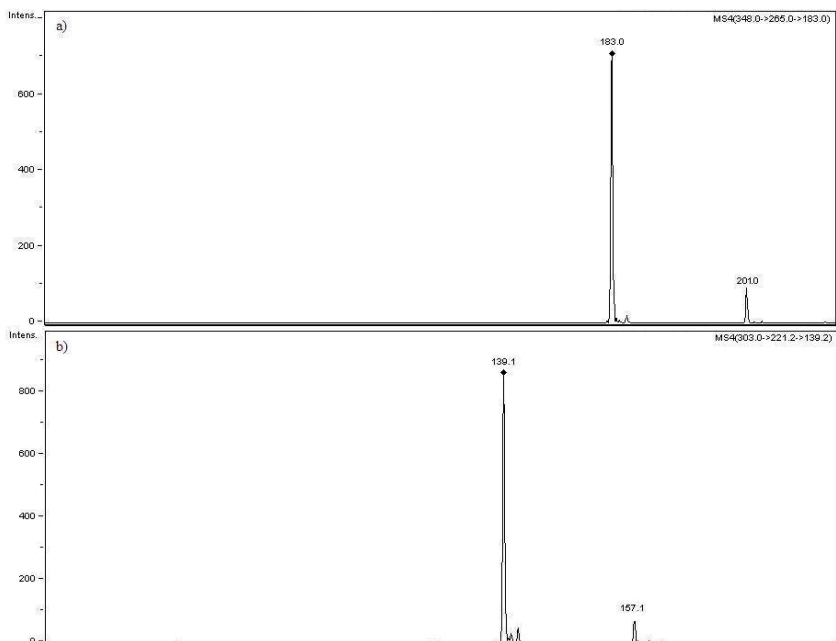


Figure 13. The mass spectra of isolated ions with m/z 183 (for *N*-2-(5-bromopyridyl)aminomethylenbisfosfonic) and m/z 139 (for *N*-2-(5-chloropyridyl)aminomethylenbisfosfonic) obtained by experiments in the ion trap

The data and the dependences obtained in the present study extend the application of the breakdown curves of ions beyond the evaluation of gas-phase ion relative stability. It has been shown very good correlation between the cone voltage value corresponding to the beginning of slowdown of the precursor ion signal intensity growth at the breakdown curve ($V_{c,fr}$ value for precursor ion) and the second one corresponding to the threshold of fragment ion signal observing at the breakdown curve ($V_{c,0}$ for fragment ion). It enables to use the techniques of distinctive cone voltage analysis to precise determination of fragmentation reactions sequence in a chain of fragmentation pathway using in-source collision-induced dissociation.

References

1. Hong J., Miao R., Zhao C., Jiang J., Tang H., Guo Z., Zhu L., *J. Mass. Spectrom.* 2006; **41**: 1061.
2. Will J., Kyas A., Sheldrick W.S., Wolters D., *J. Biol. Inorg. Chem.*

- 2007; 12: 883.
3. Wang F., Fu H., Jiang Y., Zhao Y., *J. Am. Soc. Mass. Spectrom.* 2006; 17: 995.
 4. Irungu J., Dalpathado D. S., Go E. P., Jiang H., Ha H. V., Bousfield G.R., Desaire H., *Anal. Chem.* 2006; 78: 1181.
 5. Bortolini O., Conte V., *Mass. Spectrom. Rev.* 2006; 25: 724.
 6. More M. B., Ray D., Armentrout P. B., *J. Am. Chem. Soc.* 1999; 121: 417.
 7. Parks E. K., Wexler S., *J. Phys. Chem.* 1984; 88: 4492.
 8. Rodgers M. T., Armentrout P. B., *J. Am. Chem. Soc.* 2000; 122: 8548.
 9. Ruan C., Rodgers M. T., *J. Am. Chem. Soc.* 2004; 126: 14600.
 10. Rodgers M. T., Armentrout P.B., *J. Am. Chem. Soc.* 2002; 124: 2678.
 11. Harrison A.G., *Rapid Commun. Mass Spectrom.* 1999; 13: 1663.
 12. Rodgers M. T. *J. Phys. Chem. A* 2001; 105: 2374;
 13. Armentrout P. B., Rodgers M. T. *J. Phys. Chem. A* 2000; 104: 2238;
 14. Amicangelo J. C., Armentrout P.B., *J. Phys. Chem. A* 2000; 104: 11420;
 15. Rodgers M. T., Stanley J.R., Amunugama R. *J. Am. Chem. Soc.* 2000; 122: 10969;
 16. Rodgers M. T., Armentrout P.B., *J. Phys. Chem. A* 1999; 103: 4955.
 17. Rodgers M.T., Armentrout P. B., *Mass Spectrom. Rev.* 2000; 19: 215.
 18. Brodbelt J. S., Dearden D.V., *Mass spectrometry*. In *Comprehensive supramolecular chemistry*, Lehn J-M. (ed). Pergamon/Elsevier: Oxford, 1996; Vol. 8: 567.
 19. Crowe M. C., Brodbelt J. S., *J. Am. Soc. Mass Spectrom.* 2003; 14: 1148.
 20. Satterfield M., Brodbelt J. S., *Inorg. Chem.* 2001; 40: 5393.
 21. Sjöberg P. J. R., Markides K. E., *J. Mass Spectrom.* 1998; 33: 872.
 22. Dyson P.J, Hearley A. K., Johnson B. F. G, McIndoe J. S., Langridge-Smith PRR, Whyte C. *Rapid Commun. Mass Spectrom.* 2001; 15: 895.
 23. Dyson P. J., Johnson B. G., McIndoe J. S., Langridge-Smith P. R.R., *Rapid Commun. Mass Spectrom.* 2000; 14: 311.
 24. Lyapchenko N., Schroeder G., *Rapid Commun. Mass Spectrom.* 2005; 19: 3517.
 25. Mäkinen M., Holopainen S., Rissanen K., Vainiotalo P., *Rapid Commun. Mass Spectrom.* 2006; 20: 1082.
 26. Schneider B. B., Chen D. D. Y., *Anal. Chem.* 2000; 72: 791.
 27. Burzyńska A., *Synthesis of bisfosfonic acids and its analogues*. PhD Thesis. Institute of Organic Chemistry, Biochemistry and Biotechnology, Technical University of Wrocław. Wrocław, 2003.

Chapter 7

Application of noble gas NMR in fullerene chemistry

Błażej Gierczyk

*Adam Mickiewicz University, Faculty of Chemistry,
Grunwaldzka 6, 60-780 Poznań, Poland*

1. Introduction

Fullerenes make a large, unique and diverse group of molecules. Since their discovery in 1990, fullerenes have been studied in various fields of chemistry, biochemistry, material sciences and nanotechnology. Wide range of their potential applications has stimulated development in fullerene synthetic chemistry and methods of their analysis. Although, contrary to the prognosis announced by fullerene chemists until now fullerenes have not been applicable in any branch of technology, their unique chemistry and amazing shapes make them still interesting for many scientific groups.

One of the great problems in fullerene chemistry is finding an easy and fast analytical method for studying and monitoring of the fullerene reactions and determination of the product structures. The absence of hydrogen atoms in the fullerene moiety make the ^1H NMR spectroscopy inapplicable for the purpose. The ^{13}C NMR spectra of fullerene derivatives are usually very complex because of the presence of signals from many inequivalent fullerene core's carbon atoms. Additionally, the absence of nOe enhancement means that this signal has a rather low intensity. An interesting and promising technique is the nuclear magnetic resonance spectroscopy of the noble gas atoms, incarcerated inside the fullerene cage. Spectral parameters of these signals (especially chemical shifts) are very sensitive to changes in the electronic properties of the host molecules and may be used for studying fullerene transformations.

This paper presents a review of the experimental studies on the application of noble gas NMR in fullerene chemistry. Theoretical studies are not included unless they have been used to solve experimental problems.

2. Nuclear magnetic resonance of noble gases

Four non-radioactive noble gases have isotopes suitable for NMR measurements. These are ^3He , ^{21}Ne , ^{83}Kr and two xenon isotopes: ^{129}Xe and

^{131}Xe . The fifth stable noble gas, argon, is one of three known elements, whose all stable isotopes have the spin number equal to 0. Basic properties of NMR-active nuclei of noble gases are summarized in Table 1.

Table 1. Basic nuclear properties of NMR-suitable noble gases isotopes

Nuclei	Spin	Natural abundance (%)	Receptivity ($^{13}\text{C} = 1.00$)	Quadrupole moment (10^{-30} m^2)	Resonant frequency (MHz) at 2.348T	Chemical shift standard
^3He	1/2	0.00014	0.00326	-	76.178	
^{21}Ne	3/2	0.27	0.0036	9	7.894	
^{83}Kr	9/2	11.50	1.23	15	3.847	
^{129}Xe	1/2	26.4	31.8	-	27.660	XeOF_4 Xe^a
^{131}Xe	3/2	21.2	3.31	-12	8.199	XeOF_4 Xe^a

^a *infinitely dilute Xe gas*

As it could be seen, two of the above mentioned isotopes are not quadrupolar nuclei, therefore their spectra may be recorded without any disturbances due to quadrupolar interactions. Both of them have been widely studied in the field of fullerene chemistry. However xenon atom encapsulated by fullerene has modified reactivity, so helium is much more widely used.

No NMR data for the fullerene-encapsulated neon or krypton atoms have been published until now.

3. Encapsulation of noble gas atoms inside fullerenes

The energy barrier for passing of helium atoms through hexagonal C_6 holes of fullerene molecules was estimated to be ca. 200 kcal mol⁻¹, therefore the encapsulation of noble gas atoms inside fullerenes requires the cage rupturing and its further reformation. In spite of this fact, incarceration of noble gas atom inside the fullerene molecule needs application of extreme conditions. It is carried out at high temperature (600-650°C) and high pressure (1700-3000 atm) in sealed cooper tubes over 8-64 h. The addition of potassium cyanide increases the fraction of gas contained within the fullerene molecules in final product. After extraction, about 50% of the fullerene used for the reaction may be successfully recovered, the rest is lost during the synthesis. The fraction of the labelled molecules is only 0.1% for He and 0.008% for Xe, therefore the labelling process is usually repeated two to four times to increase the content

of noble gas containing cages in the sample. Because of small differences in retention times between “empty” and labelled fullerenes, purification of the material by HPLC may increase the amount of the expected complexes.¹⁻⁷

4. NMR studies of noble gases incarcerated by the fullerenes

The first example of the ³He spectrum of the helium complex with C₆₀ and C₇₀ (Fig. 1A & 1B) was presented by Saunders et al.⁷ After heating of the above fullerene mixture under high helium pressure they obtained the material whose ³He spectrum exhibited two sharp resonance lines at -6.36 ppm (He@C₆₀) and -28.81 ppm (He@C₇₀) in a 4:1 mixture of 1-methylnaphthalene with dichloromethane, with respect to dissolved helium as a reference. The same authors have shown the non-sensitivity of the chemical shift of endohedral helium to changing of solvent or temperature variation. In the subsequent paper these authors have presented the sensitivity of the ³He chemical shift of the encapsulated helium to the chemical modification of the fullerene ball.² A mixture of both above mentioned helium-containing fullerenes has been reacted with the azomethine ylide to form N-methylpyrrolidines (1,3-dipolar cycloaddition; Fig. 2A). The ³He NMR spectrum of the obtained product shows additional peaks, originating from C₆₀ monoadduct (-9.4 ppm), two isomeric C₇₀ monoadducts (-23.8 and -27.9 ppm) as well as C₆₀ bis-adducts (-10.9 and -12.3 ppm). It shows the excellent sensitivity of ³He chemical shift to modification of the host molecule. The authors have not discussed which of the other isomeric adducts are formed.

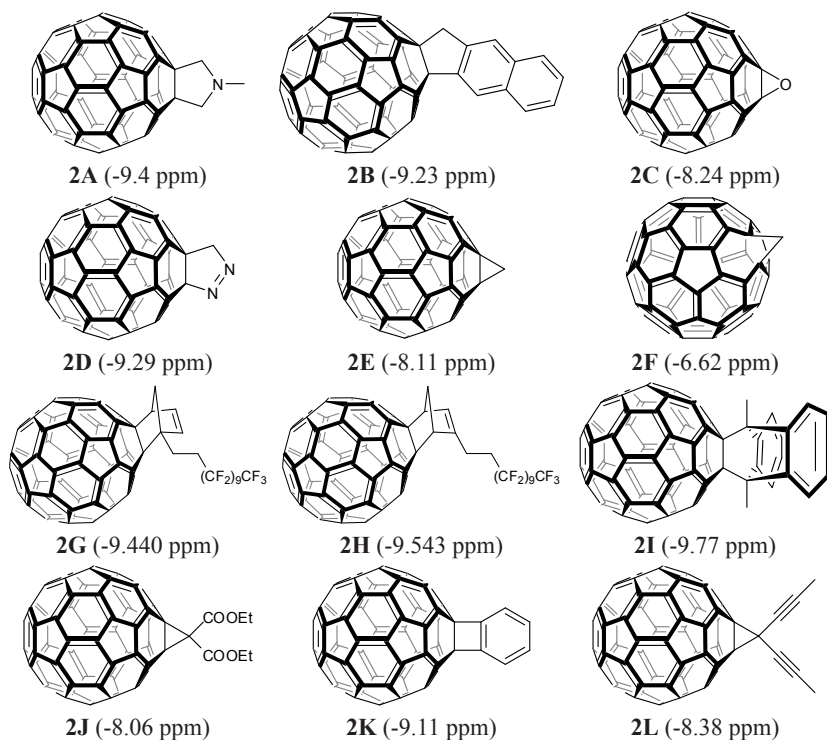


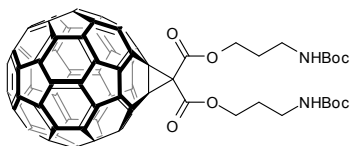
Figure 1. Structures of fullerenes: A – C₆₀ (symmetry I_h); B – C₇₀ (symmetry D_{5h})

Saunders et al. have reported the studies of addition of 1,3-biradical, obtained in thermolysis of cyclopropa[b]naphthalene, to a mixture of [60]- and [70]fullerene.⁸ They have shown that only C₆₀ undergoes the reaction. The ³He NMR spectrum of 6,6-adduct (Fig. 2B) consists of one signal at -9.23 ppm. The observed chemical shift indicates higher value of the ring current (in comparison with that of C₆₀ molecule), caused by the breaking of one of the double bonds of the parent molecule.

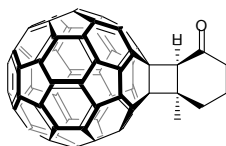
The work of Smith III et al. presents the ^3He NMR results for a group of monosubstituted C_{60} and C_{70} derivatives.⁹ The following C_{60} analogues were obtained: monoepoxide **2C** (at 6,6 ring junction; -8.24 ppm), 6,6-monopyrazolidine **2D** (-9.29 ppm), 6,6-bridged cyclopropane **2E** (methanofullerene; -8.11 ppm) and 6,5-bridged annulene **2F** (homofullerene; -6.62 ppm). The C_{70} derivatives are isomeric compounds of the formula C_{71}H_2 : cyclopropanes **3A** and **3B** (-28.14 and -25.56 ppm, respectively) and annulenes **3C** and **3D** (-27.46 and -27.82 ppm, respectively). The authors explain the values obtained as a results of large net diamagnetic ring current for C_{70} , which is slightly diminished in derivatives, and the modest aromaticity of C_{60} .

Saunders et al. have shown some examples of ^3He NMR applications in fullerene chemistry in a short review published in 1996.¹⁰ Besides the previously published data,^{2,8,9,11,12} they have presented chemical shifts for some unpublished monoadducts: **2K**, **2L**, **2U** and **2W**.

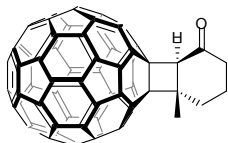




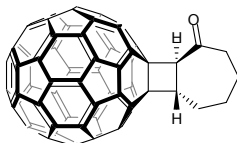
2M (-8.045 ppm)



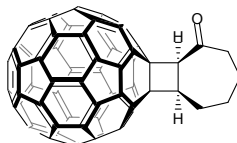
2N (-9.34 ppm)



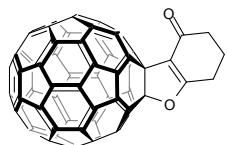
2O (-9.28 ppm)



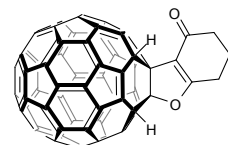
2P (-9.21 ppm)



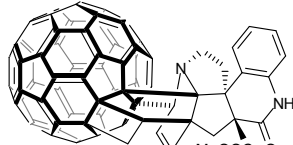
2Q (-9.29 ppm)



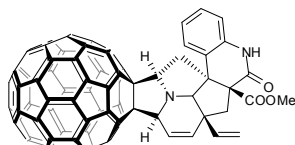
2R (-9.37 ppm)



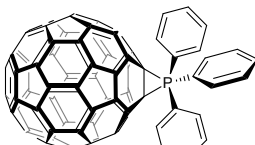
2S (-11.56 ppm)



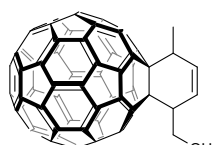
2T (-11.09 ppm)



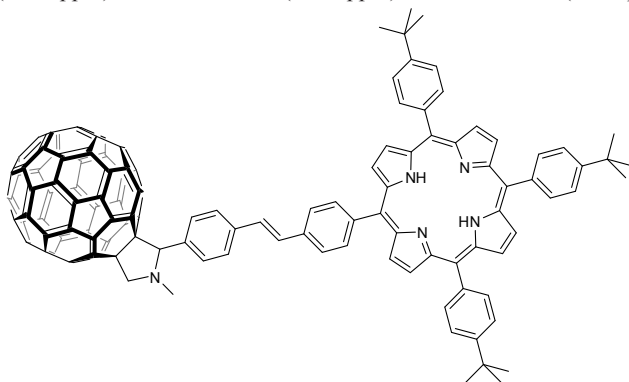
2U (-9.09 ppm)



2W (-7.20 ppm)



2X (-9.71 ppm)



2Y (-9.7 ppm)

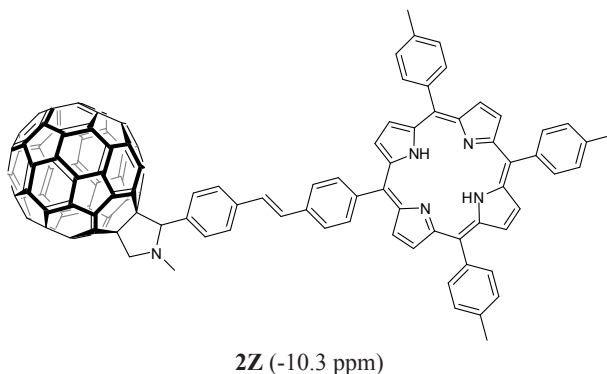


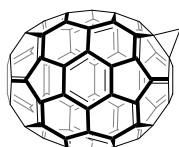
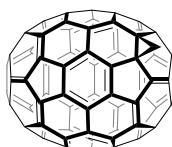
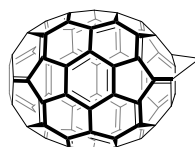
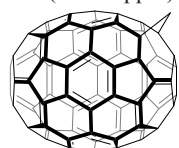
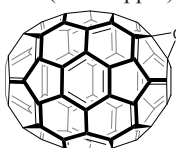
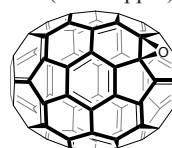
Figure 2. Structures and ^3He NMR chemical shifts of [60]fullerene monoadducts

Also Diels-Alder adducts of fullerene have been intensely studied by ^3He NMR method. Wilson et al. have studied the fluorinated compounds obtained in the reaction of C_{60} with a mixture of 1- and 2-(1*H*,1*H*,2*H*,2*H*-perfluorodecyl)-1,3-cyclopentadiene.¹³ The obtained mixture of isomeric adducts (Fig. 2G & 2H) has been characterized by helium-3 NMR spectroscopy. The spectrum shows two signals, at -9.44 and -9.54 ppm, respectively. The authors have tried to obtain multiple Diels-Alder adducts, but the ^3He NMR spectrum of such a reaction mixture shows no signal of a product or unreacted C_{60} . It is probably caused by the formation of complex mixture of many products and, in consequence it is responsible for the absence of a distinct NMR signal. Other Diels-Alder adducts studied have been prepared in the reaction of 9,10-dimethylantracene (DMA) with [60]fullerene.¹⁴ The authors show that in the above reaction a mixture of mono-, bis-, tris- and tetrakis-adducts has been obtained. The reaction studied is a reversible process. On the basis of ^3He NMR spectra the authors determine the fractional concentrations of the above products at different temperatures. They have identified 29 different species (see Table 2) and proved that higher (penta-, hexakis- etc.) adducts are not formed in this reaction. On the basis of integrals of ^3He NMR peaks, the distribution of C_{60} and $\text{C}_{60}(\text{DMA})_n$ as a function of C_{60}/DMA ratio was plotted and the equilibrium constants were determined. Having performed measurements at different temperatures, the authors calculated the free energy values of the processes studied. Similar experiments were conducted for C_{70} . Only formation of mono- and bis-adducts was confirmed. Also for this system, stability constants and ΔG values were determined. The authors have proposed the structure of C_{60} -DMA monoadduct (Fig. 2I), but they have not determined the structures of multiple adducts.

Table 2. ^3He NMR chemical shifts of 9,10-dimethylantracene/fullerene Diels-Alder multiple adducts

Adduct	^3He NMR chemical shift		Adduct	^3He NMR chemical shift	
	C_{60}	C_{70}		C_{60}	C_{70}
Mono	-9.77	-26.93	Tris-8	-13.65	-
Bis-1	-8.95	-24.73	Tris-9	-14.21	-
Bis-2	-10.44	-24.67	Tris-10	-15.44	-
Bis-3	-10.66	-24.59	Tris-11	-16.14	-
Bis-4	-11.29	-	Tetrakis-1	-11.08	-
Bis-5	-12.83	-	Tetrakis-2	-12.77	-
Bis-6	-12.84	-	Tetrakis-3	-13.70	-
Tris-1	-10.93	-	Tetrakis-4	-14.52	-
Tris-2	-11.42	-	Tetrakis-5	-14.47	-
Tris-3	-11.43	-	Tetrakis-6	-14.60	-
Tris-4	-11.54	-	Tetrakis-7	-14.79	-
Tris-5	-12.08	-	Tetrakis-8	-15.26	-
Tris-6	-13.42	-	Tetrakis-9	-15.30	-
Tris-7	-13.42	-	Tetrakis-10	-15.47	-

The epoxide of C_{70} was first obtained by the Smith III group.¹⁵ They have reported the ^3He NMR values for both obtained isomeric epoxides (**3E** and **3F**), which are -27.8 and -25.8 ppm, respectively. The ratio of ^3He signals is the same as that of ^{13}C signals obtained for helium-free C_{70} materials. This indicates that the presence of endohedral helium does not influence the regioselectivity of epoxide formation.

**3A** (-28.14 ppm)**3B** (-25.56 ppm)**3C** (-27.46 ppm)**3D** (-28.82 ppm)**3E** (-28.7 ppm)**3F** (-25.8 ppm)

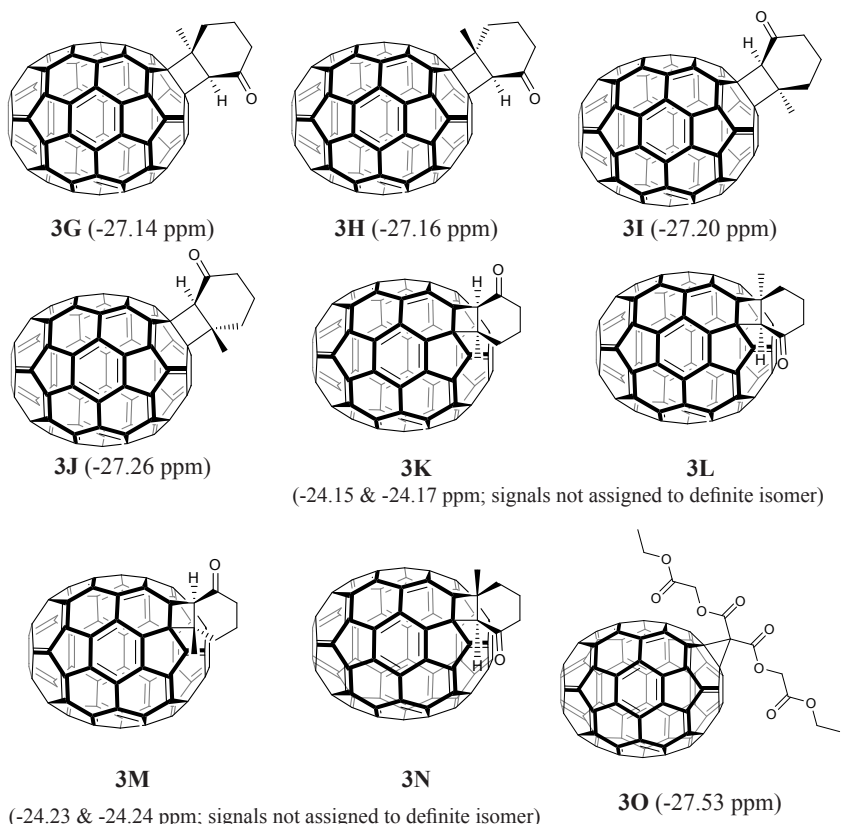
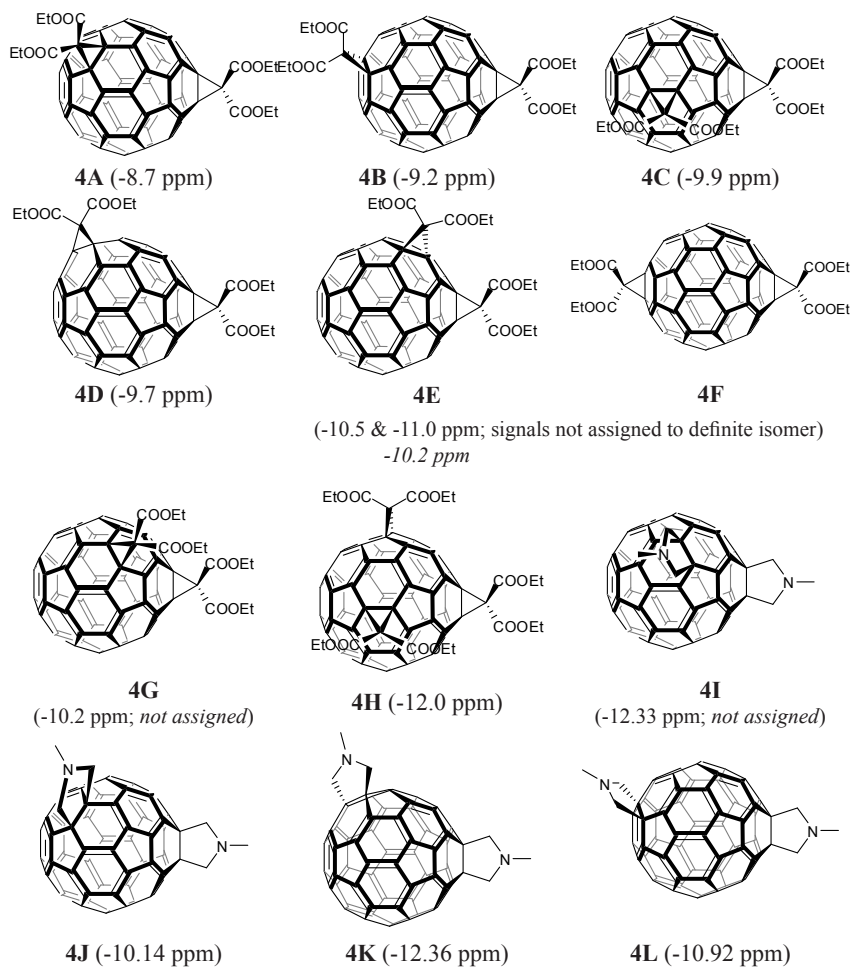


Figure 3. Structures and ^3He NMR chemical shifts of [70]fullerene monoadducts

The multiple adduct formation in the reaction of C_{60} with carbenes and ylides has been intensively studied by ^3He NMR.¹⁶ The cyclopropanation with diethylmalonate gives seven isomeric bis-adducts, one monoadduct and one tris-adduct (Bingel-Hirsch reaction). Each of them shows a separate signal in ^3He NMR spectrum. Also the four major azomethine ylide bis-adducts (Prato adducts) have been characterized by this method, together with previously known monoadduct. The assignments were made on the basis of ^1H and ^{13}C NMR spectra analysis. The results for these two groups of bis-adducts (and one tris-adduct) are summarized in Fig 4. The data for monoadducts are given in Fig. 2A & 2J. As shown, the cyclopropane derivatives are more similar to unperturbed C_{60} because of the considerable double bond character of cyclopropane bonds. The authors

pointed out the applicability of the ^3He NMR for rapid determination of relative yields and isomers ratio in fullerene chemistry. Further DFT studies by Wang et al. have forced a reassignment of some signals and permitted elucidation of the structure of some other Prato adducts.¹⁷ Also the assignment of Bingel adduct has been partially changed.



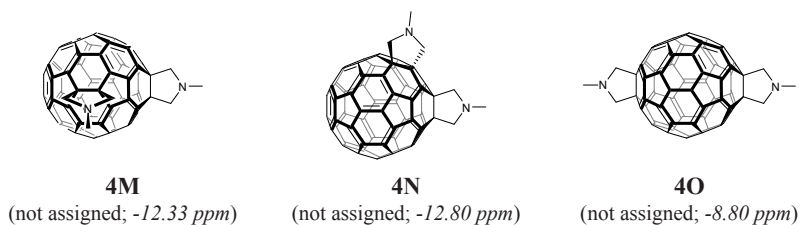


Figure 4. Structures and ^3He chemical shifts of Prato and Bingel-Hirsch bis-adducts as well as one Bingel-Hirsch triadduct; normal font – assignments of Cross *et al.*,¹⁶ italic – assignments of Wang *et al.*¹⁷

Another example of multiple substituted cyclopropane derivatives of C_{60} are the water soluble amino-substituted fullerenes, obtained by Richardson *et al.*¹⁸ These authors use the ^3He spectra for identification of products synthesized: a monoadduct **2M** (-8.045 ppm) and tris-adduct **5** (-11.966 ppm). The structures are presented in Fig. 2M & 5.

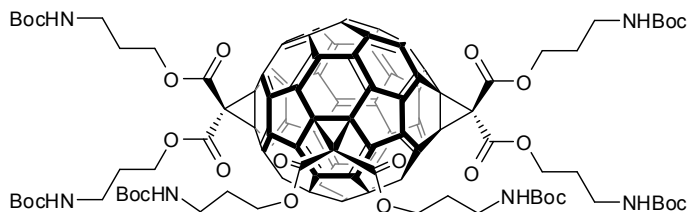


Figure 5. Structure of water soluble triadduct **5**

Also the polyether fullerene multiple adducts were characterized by ^3He NMR spectra.¹⁹ At first selective formation of *e,e,e* tris-adduct (Fig. 6A) in the reaction of C_{60} with macrocyclic malonate, consisting three malonyl units, was confirmed on the basis of ^3He measurements. The addition of cyclic malonate ester of triethylene glycol [2+2] to C_{60} gives only one, *cis*-bis-adduct (Fig. 6B). For the reaction mixture of buckminsterfullerene with macrocyclic malonate ester of triethylene glycol [3+3] only one signal of tris-adduct (Fig. 6C) was observed in ^3He spectrum. Unfortunately, the UV spectrum of this compound does not match to that of the previously obtained and characterized tris-adducts, so the structure of the compound **6C** is not known. The mono-adducts formed in these reactions have not been identified.

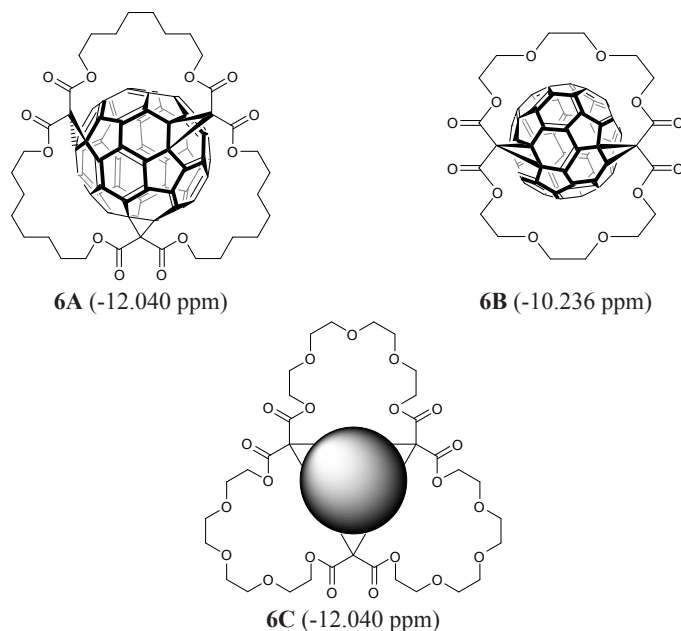


Figure 6. Structures and ^3He NMR chemical shifts for the [60]fullerene/macrocyclic malonates adducts

^3He NMR technique has been widely used for studying of the [2+2] photocycloadditions of enones to fullerenes. Schuster et al. have reported the NMR results obtained for photoadducts of C_{60} and 3-methyl-2-cyclohexenone and 2-cycloheptenone.¹¹ In both cases two peaks corresponding to products were observed in helium-3 spectra. This effect was explained by the formation of a mixture of *cis*- and *trans*-fused cycloadducts. The ^3He chemical shifts of these products (about -9.3 ppm) indicate the addition to [6,6] bonds. The structures of adducts and the helium NMR data are collected in Fig. 2N-Q. The reaction between 3-methyl-2-cyclohexenone and C_{70} has been studied by Rosental et al.²⁰ In this reaction 14 different regioisomers and diastereoisomers of monoadduct may be formed. The HPLC analysis confirms the formation of 8 products (4 *cis*- and 4 *trans*-fused adducts). The ^3He NMR spectrum of the reaction mixture shows four pairs of peaks, two at -24 ppm and two at -27 ppm. This indicates the addition to [6,6] bonds only. The assignments of the *cis/trans* isomers signals were made after acid-catalyzed epimerization of less stable *trans* isomers to *cis*-adducts. The structures and δ ^3He values are presented in Fig. 3G-N.

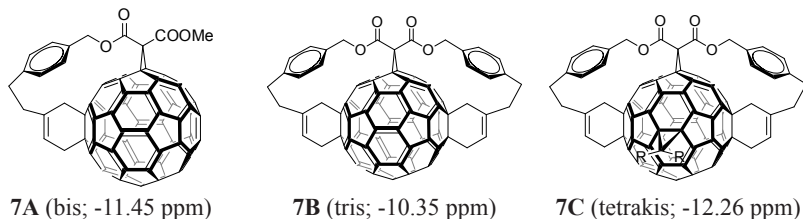
Nuclear magnetic resonance of endohedral helium atoms was used as a tool

for determination of the structures of photoadducts of 1,3-dione trimethylsilyl monoethers with fullerenes.²¹ The cycloadducts were obtained in the reaction of 1-trimethylsilyloxy-5,5-dimethyl-1-cyclohexene-3-one with C₆₀. Two isomeric compounds were isolated after UV-Vis irradiation. One of them was characterized by the ³He NMR signal at -9.37 ppm – the value typical of adducts to [6,6] bond. The second minor component was characterized by the chemical shift value of -11.56 ppm. This frequency was not typical of any previously known C₆₀ fullerene derivatives. The structures proposed for the products obtained are presented in Fig. 2R & 2S.

Also more complex molecules have been used as substrates for cycloaddition to fullerenes reaction. Guo et al. have studied the reaction between some alkaloids and C₆₀.²² The structures of two adducts obtained for scandine were determined with support of ³He NMR. The δ ³He values of one of the isolated compounds are typical of [6,6] adducts (-9.09 ppm; Fig. 2U), while the value of the other one is -11.09 ppm, which is outside of the range typical of the [6,6] as well as [6,5] adducts. For this compound a new type of structure was proposed, described as a bis-[6,6] closed junction (Fig. 2T).

Schuster et al. have used the ³He NMR technique in studies of the fullerene-porphyrin dyades.²³ This method was used for confirmation of the formation of 1:1 pyrrolidine adducts (Fig. 2Y & 2Z). For the synthesized compounds only a peak at about -9.7 to -10.0 ppm, typical of such structures, was observed. Small, downfield shifted signal, obtained after prolonged accumulation (at -9.3 to -9.5 ppm) was assigned to a decomposition product, formed due to instability of the diazo group.

A wide range of various multiple adducts has been studied by Rüttimann et al. to evaluate the relation between the structure and π -electron ring-current.²⁴ They have obtained a series of [60]fullerene bis- to hexa-adducts (Fig. 7) and a series of mono- to tetra-adducts of C₇₀ (Fig. 8 & 3O), labelled by helium-3 isotope. The helium-3 chemical shifts are presented in Fig. 6, 7 and 3O.



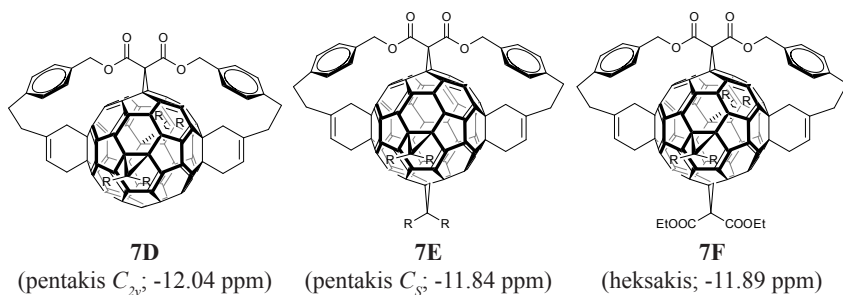
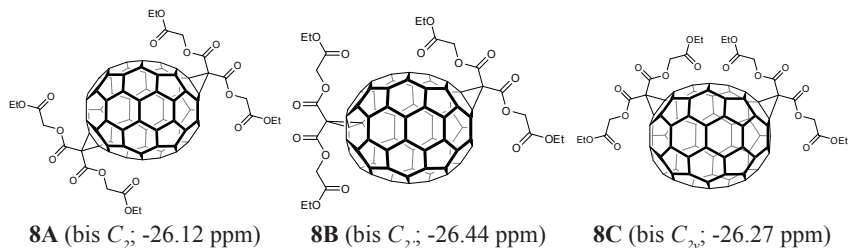


Figure 7. Structures and incarcerated ^3He atom chemical shifts of the multiple-adducts of [60]fullerene; $R = \text{CH}_2\text{COOCH}_2\text{COOEt}$

Although the general tendency observed for C_{60} series indicates the upfield shift upon increasing number of substituents in the range 1-4, the shielding of He atom is not enhanced by further functionalization. This observation was surprising, because it was expected that in higher adducts the paramagnetic ring currents of pentagons would vanish and localized benzoid rings with strong diamagnetic currents would develop. These authors have rationalized that in higher adducts the deshielding due to a reduction in diamagnetic ring currents balances out the shielding caused by decreasing pentagonal ring currents and increased number of localized benzoid rings. A comparison of two tris-adducts: **7B** and **4H** indicates that the benzoid substructure of **4H**, which is absent in **7B**, causes diamagnetical shielding and upfield shift of the endohedral helium signal. For adducts of C_{70} a monotonic increase in the ^3He chemical shift (deshielding) upon increasing functionalization degree has been observed. Because in [70] fullerene the addends are located mainly on the poles, functionalization destroys the paramagnetic ring currents of the pentagonal rings on the poles (on pyracyclene subunits) but leaves the diamagnetic current of biphenyl subunits in the equatorial belt. Functionalization destroys also the diamagnetic ring currents of corannulene subunits localized in the pole regions, which are expected to have substantial contribution to total magnetic susceptibility of the C_{70} molecule.



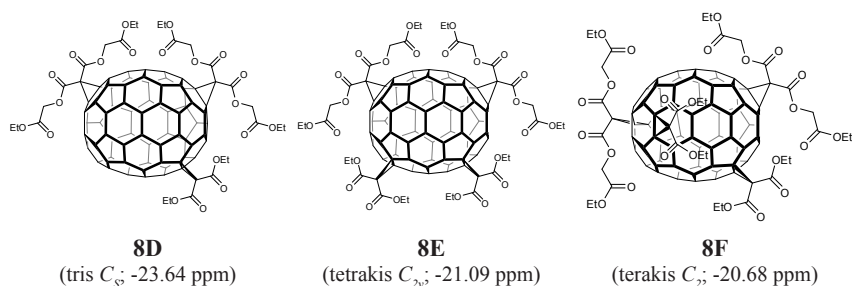


Figure 8. Structures and incarcerated ^3He atom chemical shifts of the multiple-adducts of [70]fullerene

^3He NMR of endohedral helium was used as a tool for studying isomers of higher fullerenes. As follows from topological considerations, two C_{76} isomers, 5 isomers of C_{78} and 23 isomers of C_{84} can exist. The first studies of ^3He nuclear magnetic resonance of those molecules have been carried out by Saunders and coworkers.¹² After labelling the sample of higher fullerenes with helium-3, it was separated into two fractions, the first enriched in C_{78} and the second one containing mainly C_{84} isomers. The helium-3 NMR spectrum obtained for the first of the fractions showed 7 signals: -18.72 (i), -18.58 (ii), -17.59 (iii), -16.90 (iv), -16.78 (v), -11.84 (vi) and -11.93 ppm (vii) (in 1-methylnaphthalene/ CD_2Cl_2 4:1 mixture). The peaks were assigned on the basis of the sample composition, established by MALDI MS and ^{13}C NMR experiments as well as ^3He chemical shifts calculated by Haddon & Pasquarello and Bühl & Thiel.^{25,26} The authors have assigned the signal (i) to C_{76} fullerene. Because for C_{76} only the isomer of D_2 :1 symmetry is known to be stable (Fig. 9) and it has a closed-shell structure, the authors recognize it as a C_{76} component of the studied mixture (the isomer numbers are given according to Fowler et al.²⁷). Three major peaks observed in the spectrum (iv, v and vii) were assigned to the isomers of C_{78} of the symmetry C_{2v} :2, C_{2v} :3 and D_3 :1, respectively (see Fig. 9). Three other signals (ii, iii and vi) were not assigned to definite fullerenes. The authors speculate that the signals at -11.84 and -17.59 may come from the other two C_{78} isomers, which are expected to be higher in energy. On the basis of DFT calculations, Bühl and Wüllen have assigned these three signals to C_{76} :2 D_{2d} (-11.84 ppm), C_{78} :4 D_{3h} (-17.59) and C_{78} :5 D_{3h} (-18.58 ppm) respectively, but they have stressed that it is uncertain.²⁸ The structures of the isomers discussed are summarized in Fig. 9. The C_{84} fraction shows eight peaks in the ^3He NMR spectrum: -8.96, -7.51/-7.55, -8.41/-8.37, -9.61/-9.65, -10.50, -11.12 and -24.35 ppm (six signals form pairs of one intense and one minor line). The most intense signal in this spectrum have been assigned

to the major C_{84} isomer of the symmetry D_{2d} (-8.96 ppm). Unfortunately, the other signals have remained unidentified. The signal of the second major isomer $C_{84}:4 D_{2d}$ has been assigned by Bühl and Wüllen as the line at -24.35 ppm on the basis of DFT calculations.²⁸

The same system has been further investigated by Wang et al.²⁹ They have changed the assignments of some signals of C_{78} fraction. They have also remeasured $\delta^3\text{He}$ values for this system as well as C_{84} fraction. One signal not given by Schuster et al.¹² has been found in this study (-10.00 ppm). The signal at -11.93 ppm, previously recognized as $C_{78}:1 D_3$ was now interpreted as $C_{78}:3 C_{2v}$. Contrary, the chemical shift of $C_{78}:1 D_3$ was given to be -17.59 ppm. They have also left the isomers $C_{78}:4 D_{3h}$ and $C_{78}:5 D_{3h}$ unassigned. Moreover, these authors have claimed that $C_{76}:2 D_{2d}$ isomer is not formed in experimental conditions. They have identified six different isomers of C_{84} but they have not assigned them to definite structures, except the previously recognized signal of $C_{84}:22 D_2$ isomer. The signal pair at -10.495/-10.577 was assigned to unidentified isomer of C_{86} , while the peak at -13.05 ppm, present in one fraction, to C_{82} . Authors have also proposed the explanation of the existence of pairs of the close signals as evidence of formation of dihelium species (two He atoms inside one fullerene capsule).

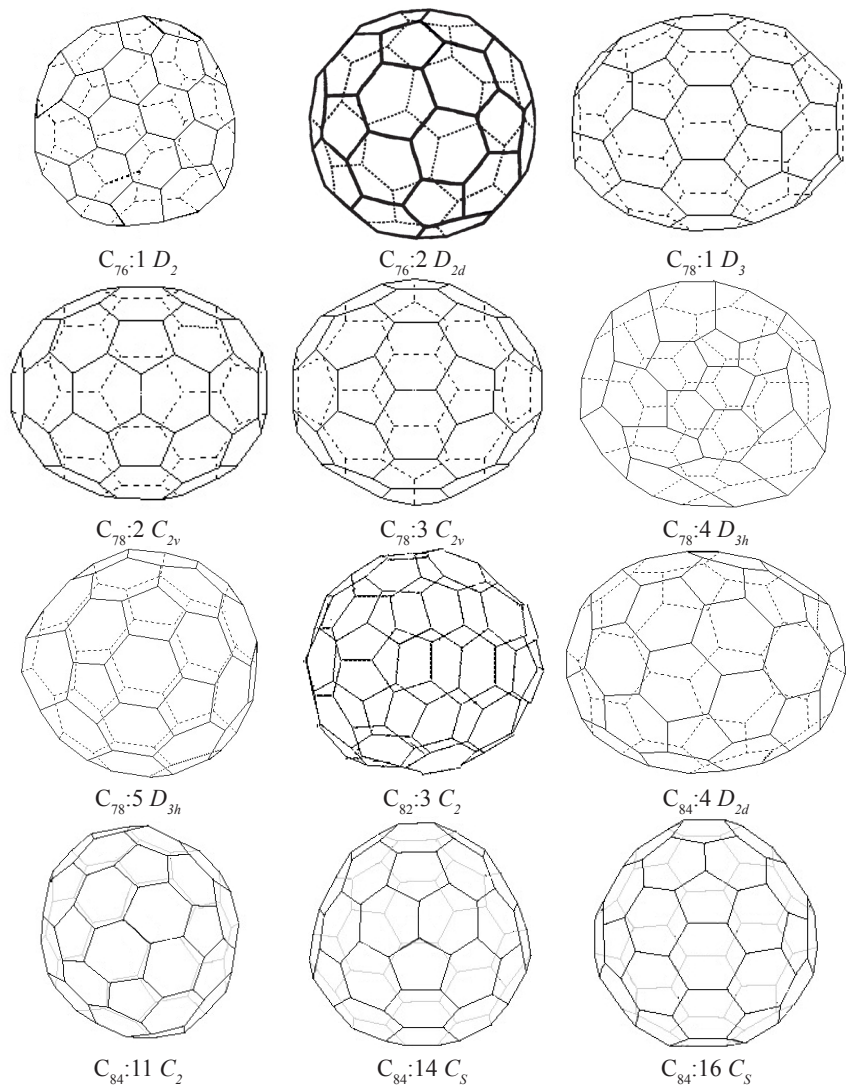
Chen et al.³⁰ have calculated the endohedral chemical shifts for C_{72} - C_{86} fullerene isomers on the basis of DFT theory and have proposed some assignments of the signals reported previously.^{12,29} They have assigned the signal at -13.05 ppm to $C_{82}:3 C_2$ isomer, while the one at -10.58 ppm to $C_{86}:17 C_2$.

Wang and Wu have continued their theoretical studies on endohedral helium-3 chemical shifts and have proposed further assignments of C_{84} fraction signals.³¹ The existence of the following isomers was proposed (the underlined chemical shift values have not been reported by Schuster et al.¹² and come from Wang et al.²⁹ paper): $C_{84}:4 D_{2d}$ (-24.35 ppm), $C_{84}:11 C_2$ (-7.50 ppm), $C_{84}:14 C_5$ (-11.11 ppm), $C_{84}:16 C_5$ (-9.61 ppm), $C_{84}:18 C_{2v}$ (-10.01 ppm), $C_{84}:22 D_2$ (-8.96 ppm), $C_{84}:23 D_{2d}$ (-8.40 ppm), $C_{84}:24 D_{6h}$ (-13.05 ppm). They also assigned the signal at -10.50 ppm to the $\text{He}@C_{82}:3 C_2$ isomer (in the previous paper of Chen et al.³⁰ the value of -13.05 ppm was assigned to the same species). The signals at -10.58 and -14.15, found by Wang et al.²⁹ were correlated with $C_{86}:17 C_2$ and $C_{86}:16 C_5$ isomers, respectively, the only two stable C_{86} fullerenes. See Fig. 9 for structures.

The $\text{He}@C_{84}$ system was also studied by Štěpánek and coworkers.³² They have used DFT method to calculate chemical shifts of incarcerated helium atom in various fullerenes and have compared the obtained values with experimental ones. The computations well reproduced the shifts and confirmed the previous

assignments. The minor components of the pairs of the signals (-7.55, -8.37 and -9.65 ppm) were interpreted as corresponding to two helium atom containing complexes.

Assignments made by different authors are summarized in Table 3.



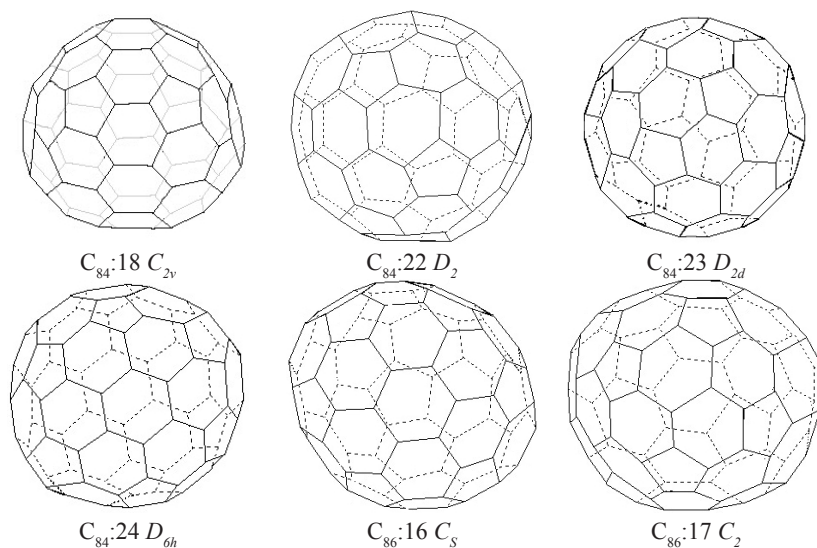


Figure 9. Structures of higher fullerenes

Table 3. Chemical shifts of helium-3 atom incarcerated by fullerenes

Fullerene	Assignments of ^3He NMR chemical shifts					
	Saunders et al. ¹²	Bühl & Wüllen ²⁸	Wang et al. ²⁹	Chen et al. ³⁰	Wang & Wu ³¹	Štěpánek et al. ³²
$C_{76}:1 D_2$	-18.718	-18.7	-18.703	-15.0	-18.703 -18.565	-
$C_{76}:2 D_{2d}$	n.s.	-11.8	n.s.	n.a.	n.s.	-
$C_{78}:1 D_3$	-11.928	-	-17.575	-11.9	-11.914 -11.821	-
$C_{78}:2 C_{2v}$	-16.904	-16.9	-16.868	-16.9	-16.888 -16.766	-
$C_{78}:3 C_{2v}$	-16.778	-16.8	-11.914	-16.8	-17.575	-
$C_{78}:4 D_{3h}$	-	-18.6	n.a.	-	-	-
$C_{78}:5 D_{3h}$	-	-17.6	n.a.	-	-	-
$C_{82}:3 C_2$	-	-	-	-13.05	-10.495	-
$C_{84}:4 D_{2d}$	-	-24.4	n.o.	-24.35	-24.35	-24.354

$C_{84} \cdot 11 C_2$	-	-	-	-	-7.502	-7.502
					-7.539	
$C_{84} \cdot 14 C_S$	-	-	-	-	-11.114	-11.114
$C_{84} \cdot 16 C_S$	-	-	-	-	-9.605	-9.605
					-9.647	
$C_{84} \cdot 18 C_{2v}$	-	-	-	-	-10.006	-10.006
$C_{84} \cdot 22 D_2$	-8.962	-9.0	-8.957	-8.96	-8.957	-8.957
$C_{84} \cdot 23 D_{2d}$	-	-	-	-	-8.404	-8.404
					-8.369	
$C_{84} \cdot 24 D_{6h}$	-	-	-	-	-13.046	-
$C_{86} \cdot 16 C_S$	-	-	-	-	-14.149	-
$C_{86} \cdot 17 C_2$	-	-	-	-10.58	-10.577	-

n.s. – mentioned as not stable isomer and not present in the sample; *n.a.* – not assigned; *n.o.* – signal not observed by authors; *italic* – ^3He NMR chemical shifts for $\text{He}_2@C_n$ species

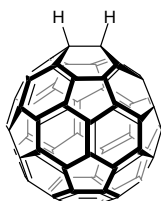
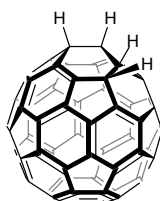
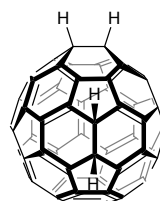
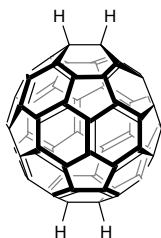
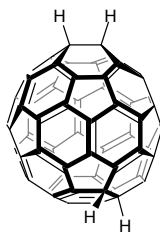
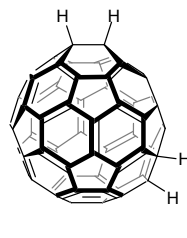
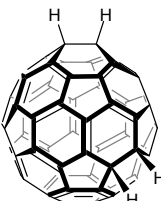
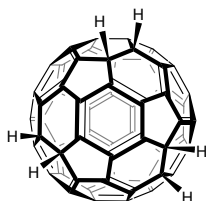
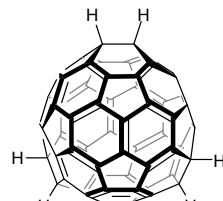
The incarceration of two helium atoms inside the fullerene cage has been first reported by Khong et al.³³ after the publication by Laskin et al. on two neon atoms encapsulation inside the cage of C_{70} .³⁴ The procedure of formation of 2:1 complex between noble gas and fullerene was similar to that of formation of 1:1 incarcerand, but the procedure of the helium (or neon) labelling was repeated four times. The formation of such species was first confirmed by mass spectrometry. The ^3He NMR spectrum of the $\text{He}_2@C_{70}$ containing sample consists of two signals, one of chemical shift typical of $\text{He}@C_{70}$ (-28.716 ppm) and the second one, downfield shifted (-28.702 ppm). The intensity of the second signal was about 10% of the parent one. The signal of the dihelium species had been observed earlier, but it remained unassigned until Khong's publication. The small difference between the major and minor signals (0.014 ppm) eliminates the possibility of the deshielded signal origin from the C_{70} derivative, because the chemical modifications of the fullerene cage cause more pronounced changes in δ values. For the helium- C_{70} complexes, a very small gradient of the magnetic field along the 5-fold axis of fullerene capsule is responsible for a petite difference in chemical shifts between monohelium and dihelium species. The authors have also shown the NMR results for modified (cyclopropanated) C_{70} -dihelium complex. Because the functionalization of the C_{70} molecule on one end on the cage alters the pi-ring current to produce a higher gradient inside the C_{70} capsule, the difference between mono- and dihelium ^3He chemical shifts

for cyclopropanated C_{70} complexes should be higher. For the C_{70} malonate diethyl ester adduct (undefined isomer) the difference between these two helium containing species was 0.11 ppm. For C_{60} the presence of dihelium species was not observed by NMR spectroscopy. It is probably due to fast dislocation of helium atoms within ca. 0.75 Å from the centre of the cage. Since the C_{60} molecule has net low aromatic character, the magnetic field over most of the cage volume is uniform, so it could be expected that $He@C_{60}$ and $He_2@C_{60}$ may have very similar and undistinguishable chemical shifts. The existence of C_{60} -dihelium complex was confirmed for polyanion of C_{60} (see below).³⁵ Dihelium complexes of higher fullerenes has been mentioned by Wang et al.²⁹ (see above).

Helium-3 NMR was employed in the studies of hydrogenated fullerenes. The first samples studied were $C_{60}H_2$ and $C_{60}H_4$.^{10,16} The first of them, obtained from C_{60} by hydroboration shows the 3He signal at -9.663 ppm. Its structure was determined on the basis of 1H and ^{13}C NMR measurements as 1,2- $C_{60}H_2$ (**Fig. 10A**). The further reduction produces a number of isomeric $C_{60}H_4$ species, which show at least six signals between -10.3 and -12.8 ppm. Unfortunately, the authors have not assigned them to the definite structures. Further studies by Billups et al. have proved the existence of six $C_{60}H_4$ isomers (δ 3He : -9.3, -10.0, -10.9, -11.21, -12.42, -12.48 ppm), obtained by reduction of C_{60} with anhydrous hydrazine.³⁶ One signal (-11.21 ppm) has been assigned to *cis-1* isomer (1,2,16,17- $C_{60}H_4$). The DFT calculations made by Wang et al. permitted the assignment to the other signals of tetrahydro[60]fullerene (see Fig. 10B-F).¹⁷

Wang et al. have obtained partially reduced C_{60} and C_{70} molecules and assigned the major signals in 3He NMR spectra to definite isomers.³⁷ The hydrogenation of C_{60} with Zn(Cu)/ H_2O system yields a mixture of $C_{60}H_6$ species. After HPLC separation the authors have obtained 1,2,18,22,23,36- $C_{60}H_6$ isomer (δ 3He -16.35 ppm) and a fraction containing a mixture of three compounds. Repeated chromatography gives two products, one identified as 1,2,33,50- $C_{60}H_4$ (-12.73 ppm) and a mixture of two hexahydrofullerenes: 1,2,33,41,42,50- $C_{60}H_6$ (-15.31 ppm) and unidentified compounds of δ 3He equal to -14.24 ppm. The same reduction procedure employed for helium labelled C_{70} fullerene gives a mixture of $He@C_{70}H_2$, $He@C_{70}H_4$ and $He@C_{70}H_8$. After HPLC separation, the fractions obtained were studied with 3He NMR. The only one formed isomer of dihydro[70]fullerene – 1,2- $C_{70}H_2$ shows the helium resonance at -27.18 ppm. The major $C_{70}H_4$ isomer, characterized by δ 3He of -25.33 ppm was recognized as 1,2,56,57- $C_{70}H_4$. The tetrahydro[70]fullerene fraction contained also two minor components, with helium-3 chemical shifts equal to -24.77 and -23.76 ppm. The authors claim that one of them probably corresponds to 1,2,67,68- $C_{70}H_4$. The 3He signal of only one octahydroderivative formed, 7,19,23,27,33,37,44,53- $C_{70}H_8$ is

distinctly downfield shifted (-17.84 ppm) in comparison with those of the other hydrogenated C_{70} fullerenes. It is the effect of different mode of hydrogen atoms arrangement around the fullerene molecule – all hydrogen atoms are added near the equatorial line in 1,4 pattern, while for di- and tetrahydro ones they were bonded near poles in 1,2 pattern. $C_{70}H_{10}$ was also obtained. The major isomer was 7,8,19,26,33,37,45,49,53,63- $C_{70}H_{10}$ (δ ^3He -17.17 ppm). The similarity of the chemical shift to that of 7,19,23,27,33,37,44,53- $C_{70}H_8$ is the effect of similarity of their structures (see Fig. 10 for details).

1,2- $C_{60}H_2$ (-9.66 ppm)1,2,16,17- $C_{60}H_4$
(*cis-I*; -11.21 ppm)1,2,18,36- $C_{60}H_4$
(*e*; -12.42 ppm)1,2,55,60- $C_{60}H_4$
(*trans-I*; -9.30 ppm)1,2,51,52- $C_{60}H_4$
(*trans-2*; -10.90 ppm)1,2,33,50- $C_{60}H_4$
(*trans-3*; -12.48 ppm)1,2,34,35- $C_{60}H_4$
(*trans-4*; -10.00 ppm)1,2,18,22,23,36- $C_{60}H_6$
(-16.35 ppm)1,2,33,41,42,50- $C_{60}H_6$
(-15.31 ppm)

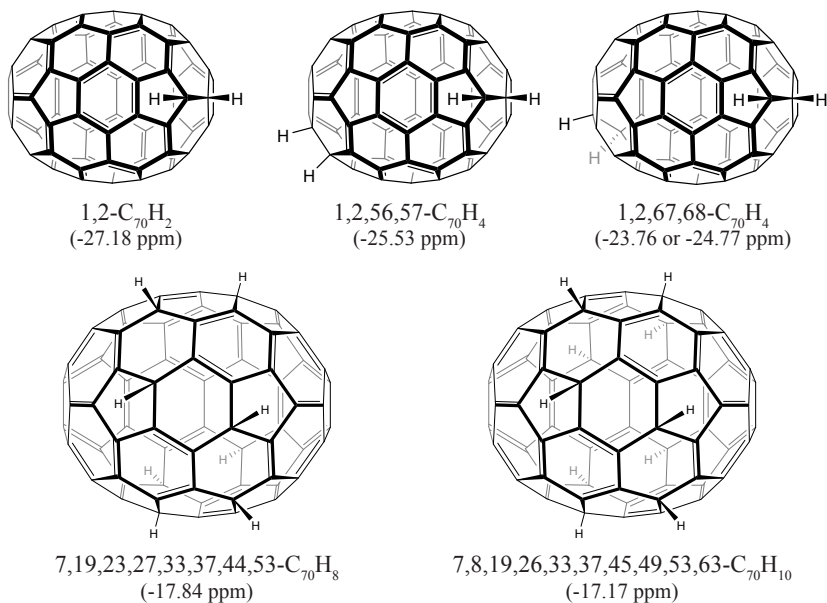


Figure 10. Structures of C_{60}H_n and C_{70}H_n ($n = 2\text{-}10$) studied by ^3He NMR method together with endohedral helium NMR chemical shifts

The highly reduced fullerenes have been for the first time studied by Billups et al.³⁸ These authors obtained a mixture of $\text{He}@C_{60}\text{H}_{18}$ and $\text{He}@C_{60}\text{H}_{36}$ by Birch reduction of $\text{He}@C_{60}$ material and reported the ^3He NMR chemical shifts. The spectrum of the first compound obtained shows the signal at -16.45 ppm, while the second one gives two close peaks at -7.7 and -7.8 ppm. The higher signal (-7.7 ppm) probably represents the isomer of D_{3d} symmetry (Fig. 11). The second one has not been assigned yet.

A detailed study of $\text{C}_{60}\text{H}_{36}$ isomers has been conducted by Nossal et al.³⁹ The authors have obtained a mixture of isomers and identified the major components by ^1H , ^{13}C and ^3He NMR spectroscopy. After HPLC separation of the Birch reduction product four fractions were collected: (i) $\text{C}_{60}\text{H}_{38}$ & $\text{C}_{60}\text{H}_{40}$ mixture (broad signal in ^3He NMR between -3.20 and -4.0 ppm); (ii) $\text{C}_{60}\text{H}_{36}$ (broad signal between -4.6 and -5.8 ppm); (iii) $\text{C}_{60}\text{H}_{36}$ (broad signal between -6.0 and -6.8 ppm); (iv) $\text{C}_{60}\text{H}_{32}$ & $\text{C}_{60}\text{H}_{36}$ mixture (broad signal between -7.6 and -8.4 ppm). The authors claim that all fractions are the mixtures of isomers. Separation of these products is practically impossible because of the products instability and fast degradation in solution. After computation (DFT method) of chemical shifts

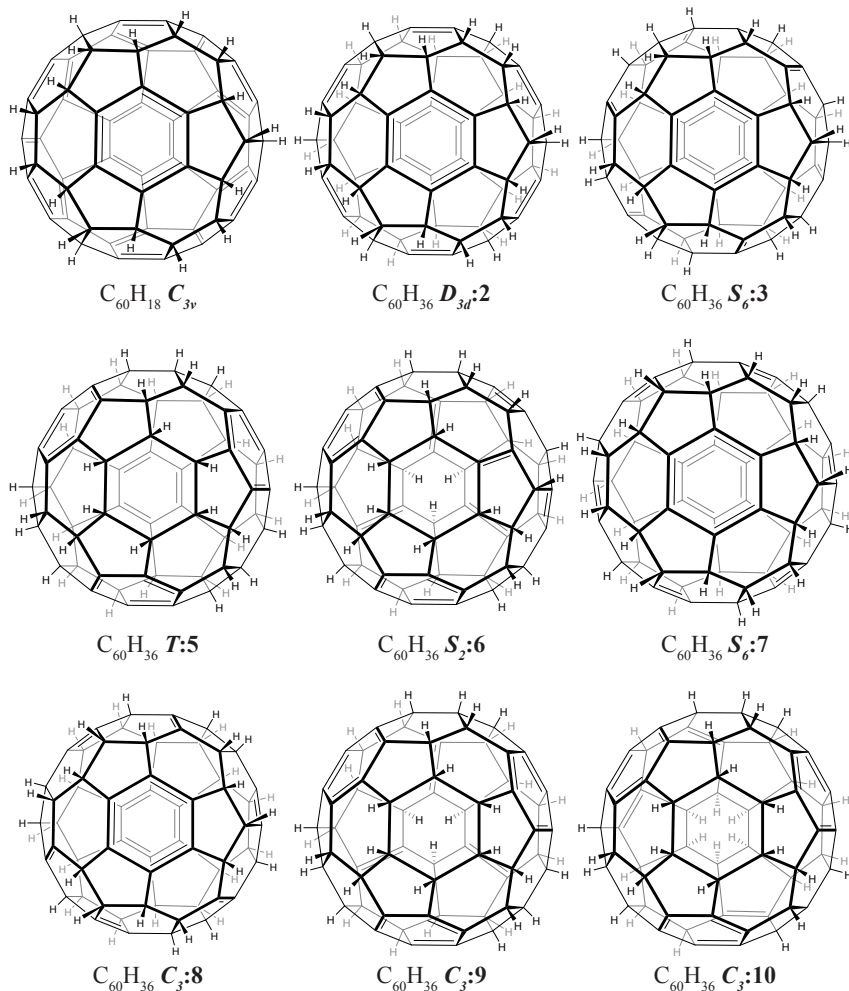
of endohedral helium atoms for different possible isomers, the authors have tried to propose the composition of each fraction. The chemical shifts in the region -4.6 to -5.8 ppm are obtained for isomers of symmetry $S_6:3$ (-4.7 ppm), $C_2:6$ (-5.1 ppm), $S_6:7$ (-5.0 ppm) and $C_3:8$ (-4.9 ppm) therefore these isomers are proposed as components of fraction (ii). The band (iii) includes of at least two isomers on the basis of HPLC evidence. These isomers may be compounds of symmetry $D_{3d}:2$ (-6.1 ppm), $C_3:9$ (-6.8 ppm) and $C_3:11$ (-6.3 ppm). The fourth band (iv) major component is probably $T:5$ isomer of $C_{60}H_{36}$ (computed ^3He NMR chemical shifts -8.8; see Fig. 13 for structures) or $C_3:10$ (-6.9 ppm). When dihydroanthracene was used as reducing agent, three components were isolated from the reaction mixture. The major fraction (II) was composed of two products, giving sharp signals in the ^3He NMR spectrum (-8.014 and -8.139 ppm). They are probably the same $C_{60}H_{36}$ isomers as obtained by Billups et al.³⁸ On the basis of proton and carbon NMR spectra, the authors eliminate some of the possible isomers (among them the one of D_{3d} , symmetry, postulated by Billups), but they conclude that the elucidation of final structure needs additional data. The third isolated fraction (III) gives the ^3He NMR signal at -8.149 ppm but, because of a small amount of the sample it was not studied by other methods.

Peera and co-workers have presented some ^3He NMR data for isomeric hydrogenated [60]fullerene.⁴⁰ The high hydrogenated fullerene material was prepared from $C_{60}H_{36}$ by Bankeser reduction. The HPLC analysis of the obtained mixture has shown that it contains $C_{60}H_{36}$, $C_{60}H_{38}$, $C_{60}H_{40}$, $C_{60}H_{42}$ and $C_{60}H_{44}$. After fraction separation (i-v; v has been a mixture of two isomeric $C_{60}H_{36}$), each of them was analyzed by ^3He NMR spectroscopy. The authors have mentioned three clusters of signals, near -6.4 ppm, -4.8 ppm and -3.0 ppm, respectively, each composed of a few lines. The authors have attributed the first of them to the isomers of $C_{60}H_{36}$ and $C_{60}H_{38}$, the second one to $C_{60}H_{38}$ and $C_{60}H_{40}$ and the third one to $C_{60}H_{40}$, $C_{60}H_{42}$ and $C_{60}H_{44}$. Unfortunately, none of the signals observed has been assigned to a definite structure.

An excellent review on ^1H , ^{13}C and ^3He NMR spectroscopy of hydrogenated fullerenes has been written by Hedenström et al.⁴¹, while a general review on synthetic and analytical aspects of fullerene hydrides has been prepared by Nossal et al.⁴²

Boltalina's group has studied the fluorinated [60]fullerene by ^3He NMR spectra.⁴³ The samples of fluorinated $\text{He}@C_{60}$ were prepared by fluorination with K_2PtF_6 and MnF_3 and their ^3He spectra were recorded. The helium-3 spectrum of $C_{60}F_{18}$ consists of an intense signal at -16.66 ppm and a small one at -16.76 ppm. The latter one is probably present due to some impurities, e.g. higher fluorinated fullerenes or their oxides. The major component has been recognized

as the isomer of C_{3v} symmetry (Fig. 11). The authors have pointed to a similarity of the chemical shift of $C_{60}F_{18}$ to that of the hydrogenated analogue, published earlier.^{38,44} The ^3He NMR spectrum of $C_{60}F_{36}$ sample consists of two signals: -10.492 and -10.521 ppm. The products were identified on the basis of 2D ^{19}F NMR spectroscopy as the isomers of T and C_3 symmetry (Fig. 11).



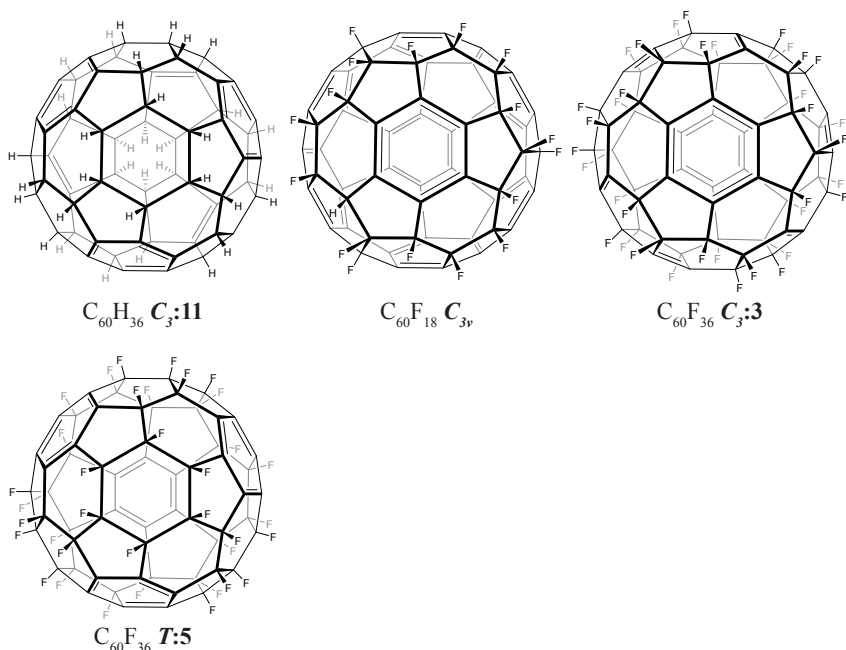
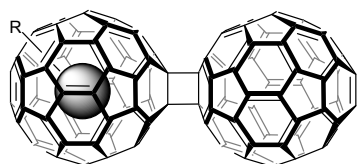
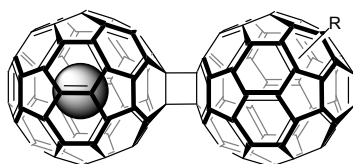
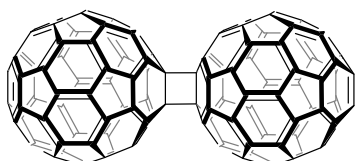
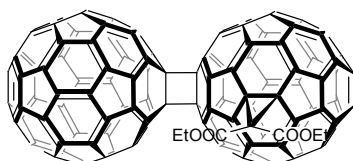
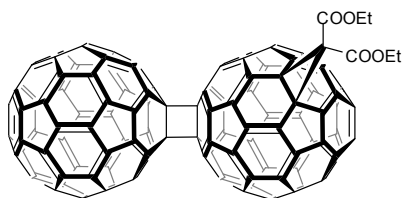
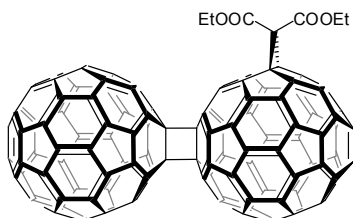
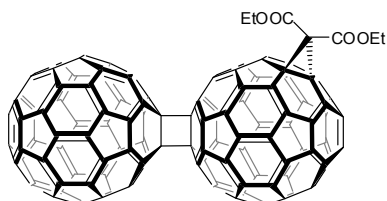
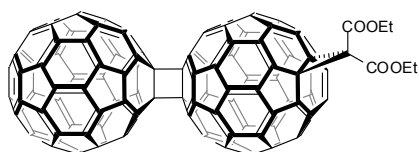
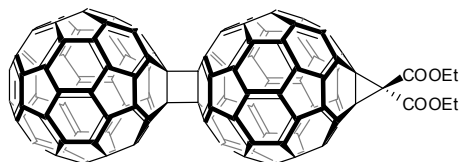


Figure 11. Structures of highly hydrogenated and highly fluorinated [60]fullerene (isomer numbers given according to Nossal et al.³⁹ and Boltalina et al.⁴³)

Helium-3 NMR spectroscopy has also been used for characterization of [60]fullerene dimer (Fig. 12A) obtained by mechanochemical synthesis.⁴⁵ The spectrum of this dimer shows, besides the signal corresponding to unreacted He@C₆₀, an upfield shifted one (-8.81 ppm), which was attributed to the C₆₀ dimer, containing helium atom in one cage, only. The authors compare the observed shift with those obtained for other C₆₀ adducts. They use also the helium-3 NMR spectroscopy to prove the existence of equilibrium between C₁₂₀ and C₆₀ under mechanochemical conditions (if the labelled C₁₂₀ and unlabelled C₆₀ were mixed together in high-speed vibration milling apparatus, the presence of labelled C₆₀ was confirmed in final sample). Further study on these dimers reported by Fujiwara et al. has concerned the application of ³He NMR method for studying chemical modifications of C₆₀ dimer.⁴⁶ They have obtained a series of monoadducts of diethyl bromomalonate to C₆₀ dimer (C₁₂₀). Six fractions were isolated and characterized by ³He NMR spectra. Each of them contained two isomers – one with the cyclopropane ring added to the cage containing helium atom (Type A), and the other with a modification on “empty” capsule (Type B).

The structures and chemical shifts are collected in Fig. 12. The authors have clearly shown that the chemical changes in the “empty” part of the molecule cause significant shifts of the helium atom encapsulated in second part of the dimer. The variation in the chemical shifts of compounds of Type A is 1.8 ppm, while that of Type B compounds is 0.14 ppm only. They prove also that the reactivity of both, He-containing and empty capsules of the dimer have the same reactivity (intensities of the ^3He signals of both isomers are the same).

**Type A adducts****Type B adducts****11A** (-8.81 ppm)**11B** (A: -10.61 ppm; B: -8.79 ppm)**11C** (A: -8.96 ppm; B: -8.73 ppm)**11D** (A: -10.48 ppm; B: -8.79 ppm)**11E** (A: -10.41 ppm; B: -8.72 ppm)**11F** (A: -9.50 ppm; B: -8.65 ppm)



11G (A: -8.79 ppm; B: -8.66 ppm)

Figure 12. [60]Fullerene dimer and its isomeric Bingel-Hirsch monoadducts' structures and ^3He NMR chemical shifts of endohedral helium atom

Another intensely explored field of ^3He NMR application is the study of ionic form of the fullerene ball. The first report of Shabtai⁴⁷ has concerned the chemical shifts of hexaanions of $\text{He}@C_{60}$ and $\text{He}@C_{70}$, obtained in the reaction of labelled fullerene with lithium in THF containing corannulene. The experimental results were compared with calculated ones. The spectrum of $\text{He}@C_{60}^{6-}$ showed a signal at -48.7 ppm has been found, while $\text{He}@C_{70}^{6-}$ - a signal at 8.3 ppm. The reduction of C_{60} converts it into the strongest shielding fullerene for endohedral helium. This huge effect is related to strong diatropic ring currents in the pentagons and hexagons of the C_{60}^{6-} cage⁴⁸ and it proves the ability of electron delocalization over the surface of a spheroid fullerene molecule. Contrary, the anion generation of C_{70} causes a strong deshielding, which indicates the reduction of aromaticity.

The same systems have also been studied by Sternfeld et al.³⁵ As mentioned above, the [60] or [70]fullerene molecules may incarcerate two helium atoms. The authors studied the effects observed in ^3He NMR spectra of such species upon hexaanion generation. For C_{70} the difference in the ^3He NMR chemical shifts between $\text{He}@C_{70}$ and $\text{He}_2@C_{70}$ was 10 times larger for anion than for the neutral molecule and had the opposite sign (the $\text{He}_2@C_{70}^{6-}$ was found at 8.044, while $\text{He}@C_{70}^{6-}$ at 8.198 ppm). Also for C_{60}^{6-} two signals were recorded, at -49.173 (He_2 species) and -49.403 ppm (He species). For the neutral C_{60} molecule, signals of both complexes had the same chemical shifts (see discussion above). The reduction of C_{60} to hexaanion decreases strongly the internal magnetic field at the centre of the cage, but this effect is less pronounced at sites between the centre and the sphere surface. Therefore, the changes in the magnetic field "filled" by one helium atom (located at the centre of the capsule) are different from these for complexes containing two He atoms (which could not be located at the centre and are closer to the surface). The C_{70}^{6-} is probably anti-aromatic in character. In consequence, the magnetic field gradient inside the cavity is reversed to that in C_{70} , so the changes observed upon ionisation of $\text{He}@C_{70}$ and $\text{He}_2@C_{70}$ are different.

Another paper of Sternfeld group concerns the aromaticity of different

fullerenes studied on the basis of changes in the helium-3 chemical shifts upon reduction to polyanions.⁴⁹ Since the aromaticity of fullerene systems cannot be deduced from resonance energies, the only way to get such information is by measurements of magnetic properties. The magnetic field inside the fullerene cage originates from its diamagnetism and it is related to ring currents in molecular orbitals of fullerenes. The authors have decided to study changes in aromaticity upon anion formation for higher fullerenes and to examine the shifts of mono- and dihelium complexes anions. The results are summarized in Table 4. The authors conclude that the reduction increases the aromaticity of $C_{78} D_3$, C_{84} and C_{76} , while it decreases the aromatic character of two isomers of $C_{76} C_{2v}$. Analysis of the signals of $He_2@C_n$ and $He_2@C_n^{6-}$ enables concluding that in the majority of high-aromatic fullerene anions the magnetic field is the highest near the centre, while for less-aromatic anions the opposite effect occurs. The signals of C_{84} hexaanions have not been assigned.

Table 4. Effect of hexaanion generation on the 3He NMR chemical shifts of $He@C_n$ and $He_2@C_n$ complexes (after Sternfeld et al.⁴⁹)

Fullerene	Encapsulated helium atom 3He NMR chemical shift [ppm]			
	$He@C_n$	$He@C_n^{6-}$	$He_2@C_n$	$He_2@C_n^{6-}$
C_{60}	-6.40	-49.27	-6.40	-49.17
C_{70}	-28.82	8.20	-28.81	8.04
$C_{76}:1 D_2$	-18.75	-20.62	-18.61	-20.55
$C_{78}:2 C_{2v}$	-16.91	-10.02	-16.79	-
$C_{78}:1 D_3$	-11.94	-32.39	-	-32.54
$C_{78}:3 C_{2v}$	-17.60	-13.50	-17.45	-22.06
C_{84} (isomers mixture)	-7.53; -8.40; -8.99; -9.64	-22.12; -22.80	-7.57; -8.43; -9.68	-22.06; -22.76

The fullerene carbocations have been studied by Birkett et al.⁵⁰ The authors report the shifts of helium labelled $C_{60}(4-FC_6H_4)_5Cl$ and carbocation derived from it: $C_{60}(4-FC_6H_4)_5^+$ as well as model compounds: 1,4- $C_{60}Ph_2$, 1,3,11,30- $C_{60}Ph_4$, 1,2,4,11,15,30- $C_{60}Cl_6$ and $C_{60}Ph_5Cl$, used for determination of the effects of chloro and aryl group on δ 3He values. The compound structures and chemical shifts are presented in Fig. 13. The authors claim that a substituent (both Cl- as well as Ar-) decreases the fullerene aromaticity because of formation of sp^3 centres in fullerene sphere upon substitution. Chlorine groups decrease the aromaticity (and helium-3 chemical shifts) because of reduction of p -character

of adjacent carbon. The cation formed from $C_{60}(4-FC_6H_4)_5Cl$ in the reaction with $AlCl_3$ is less aromatic than the parent molecule. It has been explained by increasing sp^3 character of carbon atoms of one of the pentagon rings.

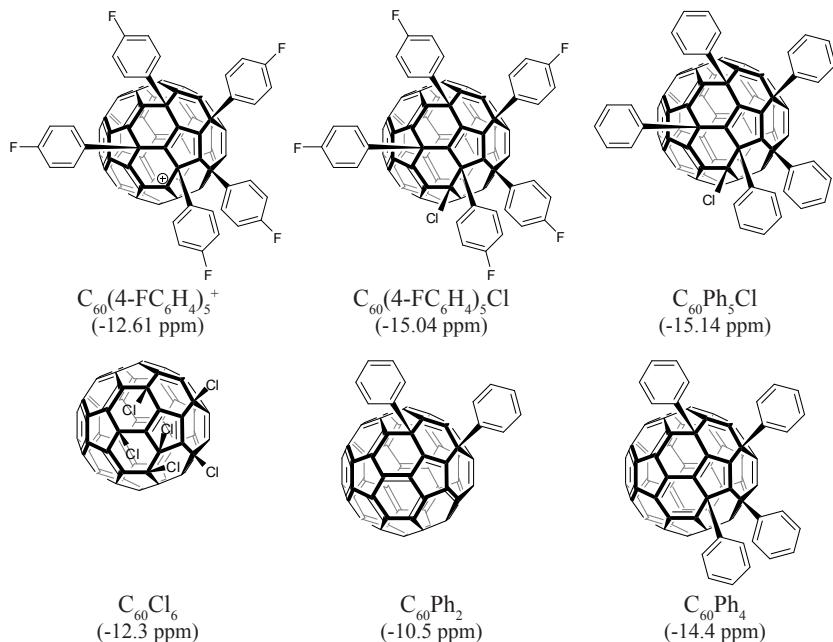


Figure 13. Endohedral 3He chemical shifts and structures of fullerene carbocation, its parent compound and model molecules

Another class of molecules, studied by 3He NMR spectroscopy, are the open-cage fullerenes. These molecules have the hole in the fullerene wall, formed by chemical modification (the so-called “chemical surgery”). The first example of 3He NMR studies of these hosts has been published by Rubin et al.⁵¹ The molecule studied by this group was obtained in the reaction of C_{60} with 1,4-bis(2-diazophenyl)-1,4-butadiene (Fig. 14A). The obtained modified fullerene had a 14-membered orifice in the wall. The authors have obtained the complex with helium under mild conditions (4 atm, 100°C). The signal of endohedral helium occurs at -10.10 ppm. By measuring of the intensity of 3He NMR signal at different temperatures it was possible to determine the activation barrier of the process of helium escape from the capsule.

Stanisky and co-workers have studied the so-called Komatsu’s open-cage

fullerene (KOCF; Fig. 14B).⁵² It is the C_{60} molecule opened by the reaction with substituted 1,2,4-triazine. The KOCF molecule has a 13-membered ring orifice on the [60]fullerene capsule.^{53,54} At 2 atm and after heating in 80°C overnight, it incarcerates helium to produce a mixture of free KOCF and He@KOCF, with the fraction of “filled” molecules of over 0.01%. Higher incorporation can be achieved at elevated pressure. The chemical shift measured for He@KOCF was -11.86 ppm. The authors determined the rate of helium escape using ^3He NMR spectroscopy, by integration of helium signal at constant time intervals and upon sample heating. The equilibrium constant of the process was determined by integration of ^3He signals of He@KOCF and He@ C_{60} , which was used as a standard at a known concentration. The authors have presented the equilibrium constants for helium incorporation and rate constants for helium escape at different temperatures as well as Arrhenius activation parameters for the escape process. The calculations of endohedral helium-3 chemical shifts of opened fullerenes (Rubin’s and Komatsu’s hosts) have been reported by Wang and Wu.³¹

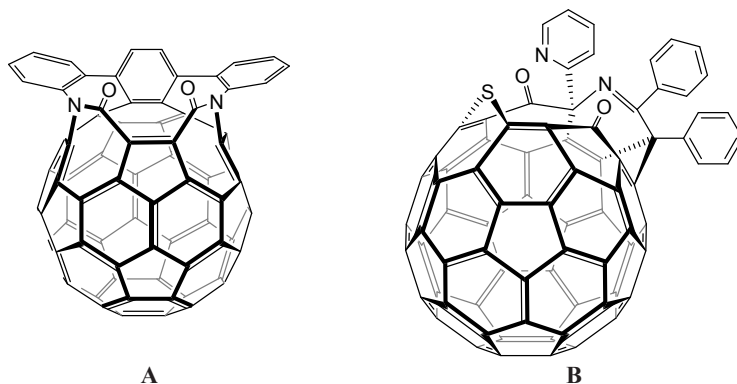


Figure 14. Structures of “opened” [60]fullerene molecules

Khong et al. have used ^3He NMR for controlling of the cyclopropanation process of $^3\text{He}@C_{60}$ and $^3\text{H}@C_{60}$ mixture by bromomalonic acid diethyl ester (Fig. 2J).¹ They have shown that tritium labelled fullerene is significantly less reactive than helium labelled one. When over 90% of He@ C_{60} was converted to products, most of tritium containing capsules remained unreacted. The conversion of $^3\text{He}@C_{60}$ was determined from helium-3 NMR spectra. Also Frunzi et al. have used ^3He NMR for determination of conversion of helium labelled C_{60} during studies of the reactivity differences between helium and hydrogen containing fullerenes in reaction with 9,10-dimethylantracene.⁵⁵

The first example of ^{129}Xe NMR spectrum of incarcerated xenon has been published by Syamala et al.³ The signal of endohedral xenon has been found at -8.89 ppm relative to xenon dissolved in benzene (i.e. 174.24 ppm in the IUPC scale). The authors pointed out the high difference between the calculated and experimental ^{129}Xe NMR chemical shifts, contrary to the values for ^3He , which were well reproduced by computation. This effect was explained by strong interactions of $5p$ orbitals of xenon atom with π -electrons of fullerene. This could be very effective for large Xe atom, while interactions of small helium atom orbitals with π -system was very weak.

The interaction of xenon atom with delocalized electrons of fullerene capsule should modify the C_{60} reactivity. It has been confirmed by Frunzi et al.⁵⁶ They have compared the activation parameters of formation of Diels-Alder monoadduct of $\text{NG}@C_{60}$ (NG – noble gas atom) and 9,10-dimethylantracene (DMA), determined from equilibrium constants of this process, measured by ^3He and ^{129}Xe NMR spectroscopy. The differences in ΔH and ΔS were -0.5 (kJ mol^{-1}) and -1.6 (J $\text{mol}^{-1} \text{K}^{-1}$), respectively. Additionally, the authors reported that no multiple adducts of $\text{Xe}@C_{60}$ and DMA were formed, even when the excess of DMA was used, while for $\text{He}@C_{60}$ they found bis-, tris- and tetrakis-adducts. The value of $\text{Xe}@C_{60}:\text{DMA}$ adduct ^{129}Xe chemical shift is -5.6 ppm relative to that of Xe dissolved in C_6D_6 .

5. Experimental aspects of noble-gases NMR of fullerene complexes

Practically all common solvents are suitable for ^3He NMR spectroscopy. Non-substituted fullerenes were usually measured in 1-methylnaphthalene/ CD_2Cl_2 mixture (3:1 or 4:1), because of good solubility of these materials in this solvent. Most data for substituted fullerene analogues have been obtained in 1-methylnaphthalene/ CD_2Cl_2 , CDCl_3 , *o*-dichlorobenzene- d_4 , $\text{CS}_2/\text{CDCl}_3$ or $\text{CS}_2/\text{acetone-}d_6$. All authors have pointed out the non-sensitivity of the chemical shift of endohedral helium to solvent variation. An addition of 0.5-1 mg of chromium(III) acetylacetonate ($\text{Cr}(\text{acac})_3$) per 1 ml of solvent as relaxation agent is recommended. The spectra are usually referred to the signal of helium dissolved in a solvent, saturated before spectra recording by bubbling of helium-3 gas (0.00 ppm). For the samples containing a few milligrams of the material studied (with 0.1 % labelling ratio) usually 20 000 – 40 000 scans (20 – 40 h of acquisition) are required to obtain a satisfactory signal to noise ratio.

6. Conclusion

Nuclear magnetic resonance of the noble gas atom incarcerated inside fullerene molecule is an excellent tool for fullerene chemistry. The high sensitivity

of helium-3 chemical shift to chemical modification of fullerene capsule makes ^3He NMR one of the best method for studying fullerene reactions. Despite some experimental difficulties, it could be expected that this spectroscopic method will become a routine tool in the chemistry of carbon clusters.

Acknowledgements

This work was partially supported from the funds of National Science Centre (grant No. N N204 155840).

References

1. A. Khong, R.J. Cross, M. Saunders; From $^3\text{He}@C_{60}$ to $^3\text{H}@C_{60}$: Hot-atom incorporation of tritium in C_{60} . *J. Phys. Chem. A* 2000, *104*, 3940-3943.
2. M. Saunders, H.A. Jimenez-Vazquez, B.B. W., R.J. Cross; ^3He NMR: A powerful new tool for following fullerene chemistry. *J. Am. Chem. Soc.* 1994, *116*, 3621-3622.
3. M.S. Syamala, R.J. Cross, M. Saunders; ^{129}Xe NMR spectrum of xenon inside C_{60} . *J. Am. Chem. Soc.* 2002, *124*, 6216-6219.
4. R. Taylor, G.A. Burley, in *Fullerenes. Principles and Applications*. (Eds: F. Langa, J.-F. Nierengarten), RSC, Cambridge, UK, 2007, pp. 1-9.
5. M. Saunders, H. A. Jimenez-Vazquez, R. J. Cross, R. J. Poreda; Stable compounds of helium and neon: $\text{He}@C_{60}$ and $\text{Ne}@C_{60}$. *Science* 1993, *259*, 1428.
6. M. Saunders, H.A. Jimenez-Vazquez, R.J. Cross, S. Mroczkowski, M.L. Gross, D.E. Giblin, R.J. Poreda; Incorporation of helium, neon, argon, krypton, and xenon into fullerenes using high pressure *J. Am. Chem. Soc.* 1994, *116*, 2193-2194.
7. M. Saunders, H.A. Jimenez-Vazquez, R.J. Cross, S. Mroczkowski, D.I. Freedberg, F.A. Anet; Probing of interior of fullerenes by ^3He NMR spectroscopy of endohedral $^3\text{He}@C_{60}$ and $^3\text{He}@C_{70}$. *Nature* 1994, *367*, 256.
8. M. Saunders, H.A. Jimenez-Vazquez, R.J. Cross, W.E. Billups, C. Gesenberg, D.J. McCord; Reaction of cyclopropa[b]naphthalene with $^3\text{He}@C_{60}$. *Tetrahedron Lett.* 1994, *35*, 1869-1872.
9. A.B. Smith III, R.M. Strongin, L. Brard, W.J. Romanow; Synthesis and ^3He NMR studies of C_{60} and C_{70} epoxide, cyclopropane and annulene derivatives containing endohedral helium. *J. Am. Chem. Soc.* 1994, *116*, 10831-10832.

10. M. Saunders, R.J. Cross, H.A. Jimenez-Vazquez, R. Shimshi, A. Khong; Noble gas atoms inside fullerenes. *Science* 1996, 271, 1693.
11. D.I. Schuster, J. Cao, N. Kaprinidis, Y. Wu, A.W. Jensen, Q. Lu, H. Wang, S.R. Wilson; [2 + 2] Photocycloaddition of cyclic enones to C₆₀. *J. Am. Chem. Soc.* 1996, 118, 5639-5647.
12. M. Saunders, H.A. Jimenez-Vazquez, R.J. Cross, W.E. Billups, C. Gesenberg, A. Gonzales, W. Luo, R.C. Haddon, F. Diederich, A. Herrmann; Analysis of isomers of the higher fullerenes by ³He NMR spectroscopy. *J. Am. Chem. Soc.* 1995, 117, 9305-9308.
13. S.R. Wilson, M.E. Yurchenko, D.I. Schuster; Synthesis of fluorinated fullerene adducts: Reversible solubilization of fullerenes in perfluorinated solvents. *J. Org. Chem.* 2000, 65, 2619-2623.
14. G.-W. Wang, M. Saunders, R.J. Cross; Reversible Diels-Alder additions to fullerenes: A study of equilibria using ³He NMR spectroscopy. *J. Am. Chem. Soc.* 2001, 123, 256-259.
15. A.B. Smith III, R.M. Strongin, L. Brard, G.T. Furst, J.H. Atkins, W.J. Romanow; Synthesis and ³He NMR studies of C₆₀ and C₇₀ epoxide, cyclopropane and annulene derivatives containing endohedral helium. *J. Org. Chem.* 1996, 61, 1904-1905.
16. R.J. Cross, H.A. Jimenez-Vazquez, Q. Lu, M. Saunders, D.I. Schuster, S.R. Wilson, H. Zhao; Differentiation of isomers resulting from bisaddition to C₆₀ using ³He NMR spectrometry. *J. Am. Chem. Soc.* 1996, 118, 11454-11459.
17. G.-W. Wang, X.-H. Zhang, H. Zhan, Q.-X. Guo, Y.-D. Wu; Accurate calculation, prediction, and assignment of ³He NMR chemical shifts of helium-3-encapsulated fullerenes and fullerene derivatives. *J. Org. Chem.* 2003, 68, 6732-6738.
18. C.F. Richardson, D.I. Schuster, S.R. Wilson; Synthesis and characterization of water-soluble amino fullerene derivatives. *Org. Lett.* 2000, 2, 1011-1014.
19. Z. Zhiguo, D.I. Schuster, S.R. Wilson; Selective synthesis of novel polyether fullerene multiple adducts. *J. Org. Chem.* 2003, 68, 7612-7617.
20. J. Rosenthal, D.I. Schuster, R.J. Cross, A.M. Khong; ³He NMR as a sensitive probe of fullerene reactivity: [2 + 2] photocycloaddition of 3-methyl-2-cyclohexenone to C₇₀. *J. Org. Chem.* 2006, 71, 1191-1199.
21. A.W. Jensen, A. Khong, M. Saunders, S.R. Wilson, D.I. Schuster; Photocycloaddition of cyclic 1,3-diones to C₆₀. *J. Am. Chem. Soc.* 1997, 119, 7303-7307.

22. L.-W. Guo, X. Gao, D.-W. Zhang, S.-H. Wu, H.-M. Wu, Y.-J. Li; Alkaloid-fullerene systems through photocycloaddition reactions. *J. Org. Chem.* 2000, *65*, 3804-3810.
23. D.I. Schuster, K. Li, D.M. Guldi, A. Palkar, L. Echegoyen, C. Stanisky, R.J. Cross, M. Niemi, N.V. Tkachenko, H. Lemmetyinen; Azobenzene-linked porphyrin-fullerene dyads. *J. Am. Chem. Soc.* 2007, *129*, 15973-15982.
24. M. Rüttimann, R.F. Haldimann, L. Isaacs, F. Diederich, A. Khong, H.A. Jimenez-Vazquez, R.J. Cross, M. Saunders; π -Electron ring-current effects in multiple adducts of $^3\text{He}@C_{60}$ and $^3\text{He}@C_{70}$: A ^3He NMR study. *Chem. Eur. J.* 1997, *3*, 1071-1076.
25. M. Bühl, W. Thiel; Ab initio helium NMR chemical shifts of endohedral fullerene compounds $\text{He}@C_n$ ($n = 32-180$). *Chem. Phys. Lett.* 1995, *233*, 585-589.
26. R.C. Haddon, A. Pasquarello; Magnetism of carbon clusters. *Phys. Rev. B: Condens. Matter* 1994, *50*, 16459-16463.
27. P.W. Fowler, D.E. Manolopoulos; *An atlas of fullerenes*, Clarendon Press: London, UK, 1995.
28. M. Bühl, C. van Wüllen; Computational evidence for new C_{84} isomer. *Chem. Phys. Lett.* 1995, *247*, 63-65.
29. G.W. Wang, M. Saunders, A. Khong, R.J. Cross; New method for separating the isomeric C_{84} fullerenes. *J. Am. Chem. Soc.* 2000, *122*, 3216.
30. Z. Chen, J. Ciosłowski, N. Rao, D. Moncrieff, M. Bühl, A. Hirsch, W. Thiel; Endohedral chemical shifts in higher fullerenes with 72-86 carbon atoms. *Theor. Chem. Acc.* 2001, *106*, 364-368.
31. G.W. Wang, P. Wu; Calculations and assignments of endohedral helium-3 chemical shifts of open-cage fullerenes and higher fullerenes. *Theor. Chem. Acc.* 2009, *123*, 375-381.
32. P. Štěpánek, P. Bour, M. Straka; Assignment of the $\text{He}@C_{84}$ isomers in experimental NMR spectra using density functional calculations. *Chem. Phys. Lett.* 2010, *500*, 54-58.
33. A. Khong, H.A. Jimenez-Vazquez, M. Saunders, R.J. Cross, J. Laskin, T. Peres, C. Lifshitz, R. Strongin, A.B. Smith III; An NMR study of He_2 inside C_{70} . *J. Am. Chem. Soc.* 1998, *120*, 6380-6383.
34. J. Laskin, T. Peres, C. Lifshitz, M. Saunders, R.J. Cross, A. Khong; An artificial of Ne_2 inside C_{70} . *Chem. Phys. Lett.* 1994, *285*, 7-9.
35. T. Sternfeld, R.E. Hoffman, M. Saunders, R.J. Cross, M.S. Syamala, M. Rabinovitz; Two helium atoms inside fullerenes: Probing the internal

- magnetic field in C_{60}^{6-} and C_{70}^{6-} . *J. Am. Chem. Soc.* 2002, *124*, 8786-8787.
36. W.E. Billups, W. Luo, A. Gonzales, D. Arguello, L.B. Alemany, T. Marrlott, M. Saunders, H.A. Jimenez-Vazquez, A. Khong; Reduction of C_{60} using anhydrous hydrazine. *Tetrahedron Lett.* 1997, *38*, 171-174.
 37. G.-W. Wang, W. B.R., M.S. Meier, M. Saunders, R.J. Cross; ^3He NMR study of $^3\text{He}@C_{60}H_6$ and $^3\text{He}@C_{70}H_{2-10}$. *Org. Lett.* 2000, *2*, 2241-2243.
 38. W.E. Billups, A. Gonzales, C. Gesenberg, W. Luo, T. Marrlott, L.B. Alemany; ^3He NMR spectra of highly reduced C_{60} . *Tetrahedron Lett.* 1997, *38*, 175-178.
 39. J. Nossal, R.K. Saini, A.K. Sadans, H.F. Bettinger, L.B. Alemany, G.E. Scuseria, W.E. Billups, M. Saunders, A. Khong, R. Weisemann; Formation, isolation, spectroscopic properties, and calculated properties of some isomers of $C_{60}H_{36}$. *J. Am. Chem. Soc.* 2001, *123*, 8482-8495.
 40. A. Peera, R.K. Saini, L.B. Alemany, W.E. Billups, M. Saunders, A. Khong, M.S. Syamala, R.J. Cross; Formation, isolation, and spectroscopic properties of some isomers of $C_{60}H_{38}$, $C_{60}H_{40}$, $C_{60}H_{42}$ and $C_{60}H_{44}$ - Analysis of effect of the different shapes of various helium-containing hydrogenated fullerenes on their ^3He chemical shifts *Eur. J. Org. Chem.* 2003, 4140-4145.
 41. M. Hedenström, T. Wågberg, D. Johnels, in *Fullerenes: The Hydrogenated Fullerenes* (Eds: F. Cataldo, S. Iglesias-Groth), Springer Science+Business Media B.V., New York, USA, 2010, pp. 171-202,
 42. J. Nossal, R.K. Saini, L.B. Alemany, M.S. Meier, W.E. Billups; The synthesis and characterization of fullerene hydrides. *Eur. J. Org. Chem.* 2001, 4167-4180.
 43. O.V. Boltalina, M. Bühl, A. Khong, M. Saunders, J.M. Street, R. Taylor; The ^3He NMR spectra of $C_{60}F_{18}$ and $C_{60}F_{36}$: the parallel between hydrogenation and fluorination. *J. Chem. Soc. Perk. Trans. 2* 1999, 1475-1479.
 44. A.D. Darwish, A.G. Avent, R. Taylor, D.R.M. Walton; Structural characterization of $C_{60}H_{18}$; a C_3 symmetry crown. *J. Chem. Soc. Perk. Trans. 2* 1996, 2051.
 45. K. Komatsu, G.-W. Wang, Y. Murata, T. Tanaka, K. Fujiwara; Mechanochemical synthesis and characterization of the fullerene dimer C_{120} . *J. Org. Chem.* 1998, *63*, 9358-9366.
 46. K. Fujiwara, K. Komatsu, G.-W. Wang, T. Tanaka, K. Hirata, K. Yamamoto, M. Saunders; Derivatization of fullerene dimer C_{120} by the Bingel reaction and a ^3He NMR study of $^3\text{He}@C_{120}$ monoadducts. *J.*

- Am. Chem. Soc.* 2001, *125*, 10715-10720.
47. E. Shabtai, A. Weitz, R.C. Haddon, R.E. Hoffman, M. Rabinovitz, A. Khong, R.J. Cross, M. Saunders, P.-C. Cheng, L.T. Scott; ^3He NMR of $\text{He}@C_{60}^{6-}$ and $\text{He}@C_{70}^{6-}$. New records for the most shielded and the most deshielded ^3He inside a fullerene. *J. Am. Chem. Soc.* 1998, *120*, 6389-6393.
 48. M. Bühl; NMR properties of polyolithied C_{60} . *Z. Anorg. Allg. Chem.* 2000, *626*, 332-337.
 49. T. Sternfeld, M. Saunders, R.J. Cross, M. Rabinovitz; The inside story of fullerene anions: A ^3He NMR aromaticity probe. *Angew. Chem. Int. Ed.* 2003, *42*, 3136-3139.
 50. P.R. Birkett, M. Bühl, A. Khong, M. Saunders, R. Taylor; The ^3He NMR spectra of a [60]fullerene cation and some arylated [60]fullerenes. *J. Chem. Soc. Perk. Trans. 2* 1999, 2037-2039.
 51. Y. Rubin, T. Jarrosson, G.W. Wang, M.D. Bartberget, K.N. Houk, G. Schick, M. Saunders, R.J. Cross; Insertion of helium and molecular hydrogen through the orifice of open fullerene. *Angew. Chem. Int. Ed.* 2001, *40*, 1543-1546.
 52. C.M. Stanisky, R.J. Cross, M. Saunders, M. Murata, Y. Murata, K. Komatsu; Helium entry and escape through a chemically opened window in a fullerene. *J. Am. Chem. Soc.* 2005, *127*, 299-302.
 53. Y. Murata, M. Murata, K. Komatsu; Synthesis, structure, and properties of novel open-cage fullerenes having heteroatom(s) on the rim of the orifice. *Chem. Eur. J.* 2003, *9*, 1600-1609.
 54. Y. Murata, M. Murata, K. Komatsu; 100% Encapsulation of a hydrogen molecule into an open-cage fullerene derivative and gas-phase generation of $\text{H}_2@C_{60}$. *J. Am. Chem. Soc.* 2003, *125*, 7152-7153.
 55. M. Frunzi, H. Xu, R.J. Cross, M. Saunders; NMR temperature-jump method for measuring reaction rates: Reaction of dimethylantracene with $\text{H}_2@C_{60}$. *J. Phys. Chem. A* 2009, *113*, 4996-4999.
 56. M. Frunzi, R.J. Cross, M. Saunders; Effect of xenon on fullerene reactions. *J. Am. Chem. Soc.* 2007, *129*, 13343-13346.

Chapter 8

Mass spectral analysis of synthetic polymers end groups by MALDI MS (matrix-assisted laser desorption/ionization mass spectrometry)

Grażyna Bartkowiak and Grzegorz Schroeder
*Adam Mickiewicz University, Faculty of Chemistry,
Grunwaldzka 6, 60-780 Poznań, Poland*

Mass spectrometry is a powerful tool for the analysis and structural characterization of chemical compounds. However, its utility to the macromolecules, including polymers, has been limited due to the low volatility of these compounds and their low ability to be ionized. More extreme ionization conditions lead to the destruction of the molecule so that the molecular mass is impossible to estimate. The introduction of matrix-assisted laser desorption/ionization (MALDI), as a gentle ionization technique, has enabled the ionization and detection of intact large polymer molecules. Due to this technique it became possible to obtain molecular ions of masses in the range of kiloDaltons (kDa) and more. The first successful attempt has been made by Tanaka and co-workers¹, who used fine metal powder (Co) suspended in glycerol as a matrix and obtained molecular ions of poly(ethylene glycol) i.e. PEG with molecular mass about 20 000 Da.

Another barrier in the macromolecule's molecular mass determination was a low mass range accessible for the mass analyzers. This problem has been overcome through development of time-of-flight (ToF) analyzer.²

The further progress in polymer analysis by MALDI MS has been made by Karas, Hillenkamp and co-workers,³ who obtained MALDI mass spectra of poly(ethylene glycol)s PEGs and poly(propylene glycol)s PPGs with well resolved peaks of oligomers and achieved the highest mass range at that time, i.e. over 80 000 Da for polystyrene PS70000.

The development in the area of polymer analysis by mass spectrometry is very fast and the continuous improvement of instruments, progress in their resolution ability and reduction of their cost at the same time make mass spectral methods common and irreplaceable tool for analytic chemists. In contrast to other

methods, which enable polymer molar mass determination and mass distribution estimation very roughly, MALDI-TOF MS allows detailed mass characteristic of the polymer sample investigated, even if the amount of substance available is very small.⁴

The structure of polymer end group is very important subject in polymer chemistry. The end-group type is often crucial for the polymer properties and its change through the chemical modification implies change of the reactivity and solubility of the compound⁵, its miscibility with other chemicals and acidic or basic character, therefore reliable methods of end-group determination are desirable. At an earlier time the polymer end-group determination has been performed mainly by means of NMR and IR spectroscopy. These methods, however, have one big disadvantage: the end-group signal is there proportional to the end-group contribution in the entire mass of the molecule studied. It means that as the molecular weight is getting higher, the end-group signal decreases and becomes very low. Practically, for polymers with MW above a few kiloDaltons, the recognition and analysis of end groups via NMR or IR turns to be impossible. On the contrary, in MALDI-TOF all the signals noticeable in the spectrum bear information about the masses of the end groups present. As the polymerization degree increases, the intensity of the mass spectral signal attributed to the end group is even enhanced. Moreover, mass spectral detectors display high sensitivity and the sample amount needed for the analysis is very small, sub-nanomolar. Thanks to these features the MALDI-TOF and MALDI-CID (MALDI combined with collision-induced dissociation) mass spectra often allow determination of type and structures of the end-groups present in the polymer sample. These facts make MALDI-TOF mass spectrometry rapidly developing and preferred, if not the standard method for polymer end-group analysis.

The first applications of MALDI MS to the polymers with different end groups appeared in 1996^{6,7,8}. Very interesting work considering polymer end group analysis in Nylon6 (Figure 1) presented Montaudo et al.^{9,10}. The authors designed and prepared samples of Nylon6 with various end groups and analyzed their MALDI-TOF mass spectra.

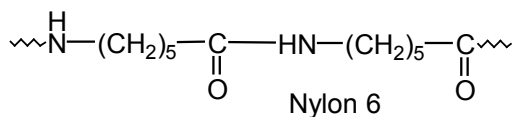
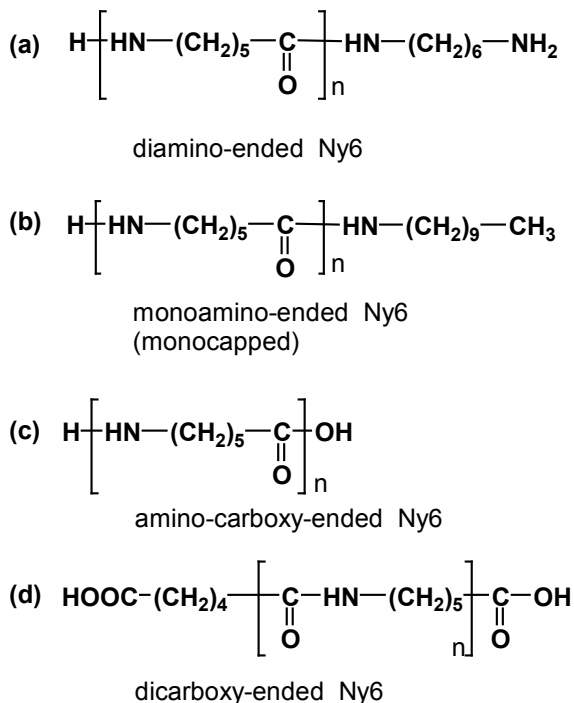


Figure 1. Structure of Nylon 6

They synthesized four samples of modified Nylon6, each terminated by different end groups, i.e. diamino terminated (a), monoamino terminated (monocapped) (b), amino-carboxy- terminated (c) and dicarboxy terminated (d) oligomers. The measurements were made on MALI-TOF Bruker Reflex mass spectrometer, equipped with nitrogen laser, using 2-(4-hydroxyphenylazo) benzoic acid (HABA) as a matrix and trifluoroethanol (TFE) as a solvent. The structures of end groups obtained are presented in the Scheme 1.



Scheme 1. Structures of end groups obtained in Nylon6.

Respective MALDI-TOF mass spectra^{9,10} of resulting polymers are given in Figure 2 as representative examples.

Nylon6 in reaction with diamino-hexamethylene $\text{H}_2\text{N} - (\text{CH}_2)_6 - \text{NH}_2$ yielded oligomers bearing NH_2 groups at both chain ends. The structure of created oligomers describes formula $\text{H} - [\text{NH}(\text{CH}_2)_5\text{CO}]_n \text{NH}(\text{CH}_2)_6\text{NH}_2$ with the repeat unit $[\text{NH}(\text{CH}_2)_5\text{CO}]_n$ i.e. $\text{C}_6\text{H}_{11}\text{NO}$, which have the mass 113,1 Da. The MALDI-TOF mass spectrum of the diamino-terminated Ny6 displays sets of three intense

peaks, marked as **A**, **B** and **C** (see inset in Fig. 2a), corresponding to protonated (**A**), sodiated (**B**) and potassiated (**C**) species. The most intense peaks in the mass spectrum (Fig. 2a) should be assigned to the sodiated species **B**:

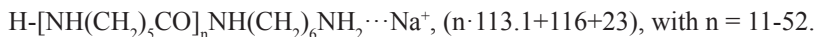
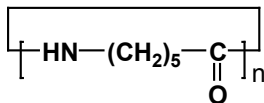


Figure 2b displays mass spectrum of Ny6 submitted to the action of decylamine $\text{C}_{10}\text{H}_{21}\text{NH}_2$, which gave amino-terminated at one end oligomers with general formula:



The MALDI spectrum (see inset in Fig. 2b) shows intense sodiated ions **D** and less intense protonated ions **C**. The species marked as **1** and **2** correspond to sodiated and potassiated ions of Ny6 cyclic oligomers, which can be consider as oligomers without end group.



The cyclic oligomers of Ny6 can be isolated from the original polymer used through the extraction with hot methanol, giving the yield about 3%. The MALDI mass spectrum of this fraction has been shown in Figure 3 (matrix HABA, matrix signals in the spectrum indicated with a cross). The main peaks in this spectrum correspond to the sodiated cyclic oligomers with $n = 5$, m/z 588.5 ($5 \times 113.1 + 23$); $n = 6$, m/z 701.6; $n = 7$, m/z 814.7 and $n = 8$, m/z 927.8. The difference of m/z value between these peaks is 113.1, which corresponds to the repeat unit mass.

The problem of polymer end groups analysis was thoroughly examined by Jackson et al.¹¹, who tested several samples of polymers with the end groups structure confirmed by NMR techniques.

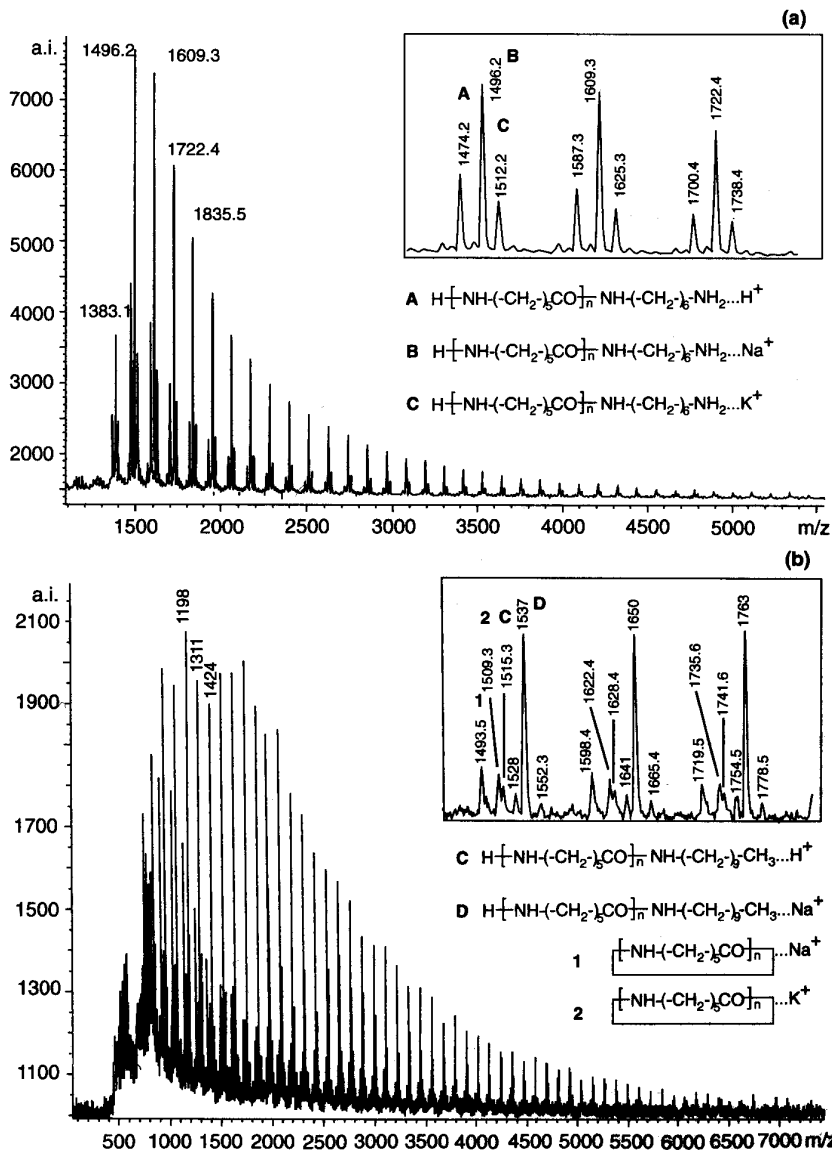


Figure 2. MALDI-TOF mass spectrum of Nylon6 reacted with diaminohexamethylene (a) and decylamine (b)

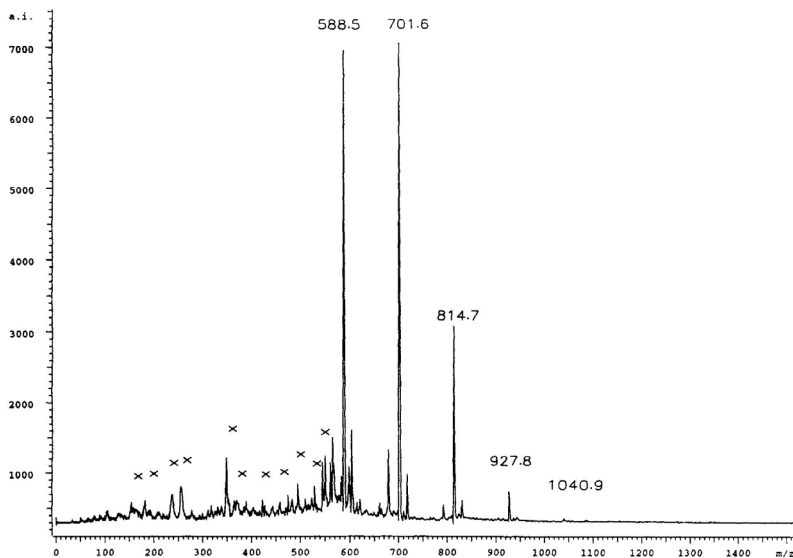
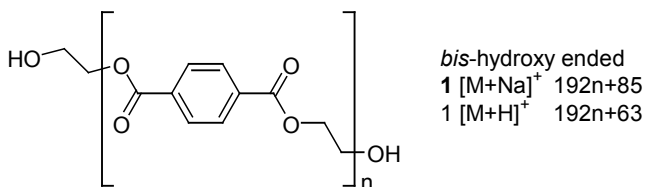
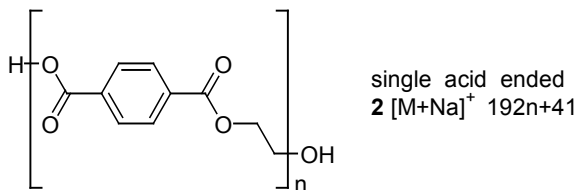


Figure 3. MALDI-TOF mass spectrum of Ny6 cyclic oligomers (fraction soluble in methanol, matrix: HABA). Matrix signals indicated as x.

The authors have observed in the MALDI MS spectrum of poly(ethylene terephthalate) fraction from the reaction vessel (Figure 4) that main intense ion peaks $[1+\text{Na}^+]$ are accompanied by the set of analogous minor peaks labeled **1**, **2** and **3** in the Fig.4. and the distance of these peaks from the main peaks is constant. The main peaks $[1+\text{Na}^+]$ differ one from another of 192u, which is consistent with the mass of repeat unit of polymer (PET) i.e. $-\text{[CO-C}_6\text{H}_4\text{-CO-OCH}_2\text{CH}_2\text{O]-}$, $\text{C}_{10}\text{H}_8\text{O}_4$, 192 Da. The respective protonated ion **1** appears at the m/z values 22u (M-Na+H) lower than $[1+\text{Na}^+]$.



The minor satellite ions are attributed to the oligomers with other end groups, namely ions **2** are consistent with sodiated oligomers, containing acid end on the one side of polymer chain, and are seen 44u lower than $[1+\text{Na}^+]$.



Ions **3** can be assigned as sodiated oligomers ions which possess di(ethylene glycol) end group and therefore can be seen at m/z 44u higher than $1+Na^+$.

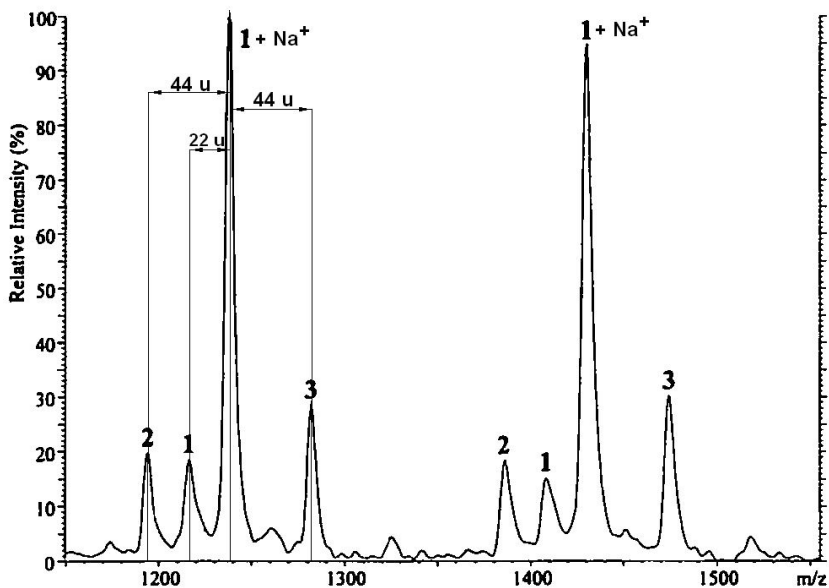
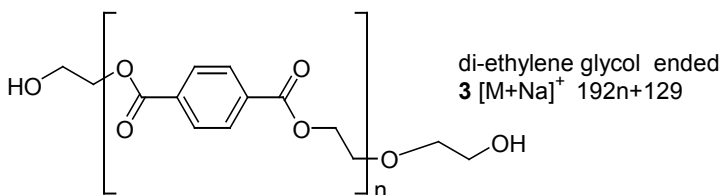


Figure 4. UV-MALDI MS spectrum (expanded part in the m/z range 1150 – 1550) of the final aliquot of PET (extract 6) from the reaction vessel. Ion peaks **1**, **2** and **3** represent the variety of end groups.

Interesting observation has been made that different polymers give various responses in MALDI mass spectra, i.e. some of them yield very intense signal and the other show very low ion abundances. The first possible explanation was that the detector is not ideal and the problem will be solved with the introducing of the new, more reliable detector, which will give a response independent of mass value and molar mass distribution. The more detailed study has been made to examine the MALDI mass spectral behavior of equimolar polymer mixtures, containing Nylon 6 (Ny6) and hydroxyl-terminated polybutyleneterephthalate (PBT) with comparable average molar masses and polydispersity. The authors suspected that chemical nature of the polymer end group may have strong influence on the ionization efficiency and therefore on the response observed. Positive and negative ion MALDI-TOF mass spectra of the variety of polymer mixtures with different end groups were recorded and analyzed.¹² The representative example can be an equimolar blend of Ph-Ny6-COOH (Nylon 6 with phenyl and carboxyl end groups) and HO-PBT-OH (PBT with hydroxyl groups on both ends), which shows strong imbalance between these two components in the MALDI mass spectra (Fig. 5). Figure 5 presents positive MALDI-TOF spectrum (enlarged region 2250-2700 m/z) of Ph-Ny6-COOH (M_v 2500) and HO-PBT-OH (M_v 2300), mixture 1:1. All peaks denoted NA, NB and NB' correspond to the Nylon 6 (NA – cyclic oligomers, NB = Ph-CO-[NH-(CH₂)₅CO]_n-OH, NB' – sodium salt), only THC corresponds to HO-PBT-OH. The most intense peaks observed in the spectrum are due to sodiated carboxyl-terminated Ny6 chains (NB species), whereas PBT chains terminated with hydroxyl groups (THC species) appear with very low intensity.

The study revealed that ionization efficiency in MALDI spectra of polymers is strictly dependent of the end groups structure. The results obtained confirmed the relevance of end groups in MALDI ion desorption mechanism.

Scrivens group¹³ applied orthogonal acceleration MALDI-ToF MS combined with collision-induced dissociation (CID) to the analysis of commercially available synthetic polymers: PMMAA, B, C, D and E - poly(methylmetacrylate), PET - poly(ethylene terephthalate) and PEG - poly(ethylene glycol) with the oligomers mass range 500-4500 Da. Most of the polymer samples had *peak average molecular weight* Mp established by manufacturer through gel-permeation chromatography (GPC). Among the PMMA samples there were ones denoted as PMMA C, D and E, containing various end groups with structures determined by means of nuclear magnetic resonance spectroscopy. Structural and end-group information were obtained using LSIMS-MS/MS and MALDI-CID and the results were compared in favor of MALDI, which gave much better signal-to-noise ratios in the spectrum (higher sensitivity). In the MALDI-CID

mass spectra of PMMA B 45-mer precursor ions $[M+Na]^+$ (Fig. 6) a series of low-mass fragment ions (A, B and C) is clearly seen.

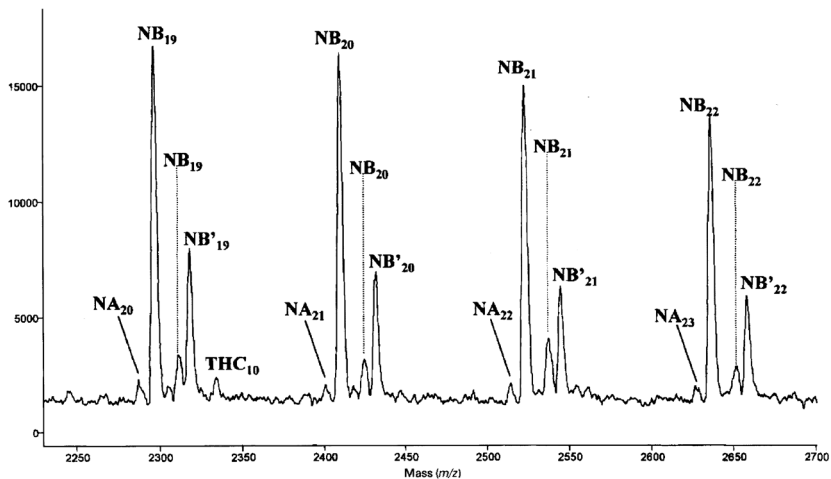
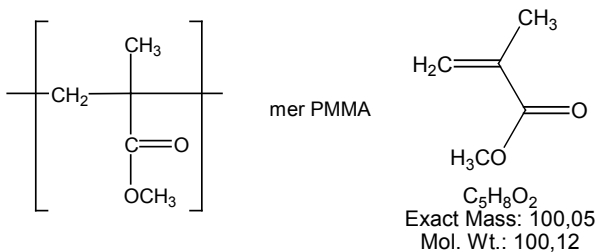


Figure 5. Enlarged region of the MALDI-TOF mass spectrum of an equimolar mixture of *Ph-Ny6-COOH* (M_v 2500) and *HO-PBT-OH* (M_v 2300), positive mode.



These ions are generated by the homolytic cleavage of the polymer chain with Na^+ retention. The m/z values of the A ($110+100n$) and B (m/z $124+100n$) ions obtained are in the agreement with the polymer end groups masses.

Ions C (m/z $164+100n$) are probably created from ions B (m/z $124+100n$) through the neutral loss of CO and CH_3OH molecules.

Figure 7 a-c shows MALDI-CID spectra of the sodiated ion $[M+Na]^+$ of the 14-mer of PMMA C, D and E samples with different end groups. In the spectra prevail peaks of low even m/z values. Series of ions A in all the spectra 7a, 7b and 7c are identical with the A ions in the Fig. 6 for PMMA B and correlate

with the m/z values $(110+100n)$, where 100 is a repeat unit mass of poly(methyl methacrylate) ($C_5H_8O_2$). The end groups of PMMA B are $-H$ (on both ends), so the peaks A suit the hydrogen end groups. The other ion series – C (Fig. 7a), D (Fig. 7b) and E (Fig. 7c) are created through the homolytic cleavage on the opposite polymer chain end and indicate that PMMA C, D and E have three different end groups. The fragmentation routes leading to these peaks are shown in Scheme 1 for all three PMMA (C, D and E) types.

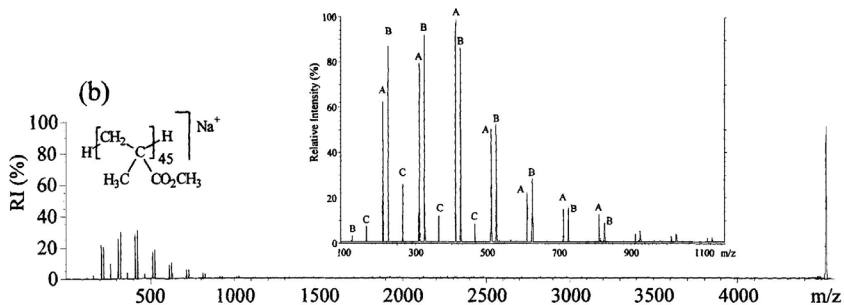


Figure 6. MALDI-CID spectrum of the $[M+Na]^+$ ion of the 45-mer of PMMA B.

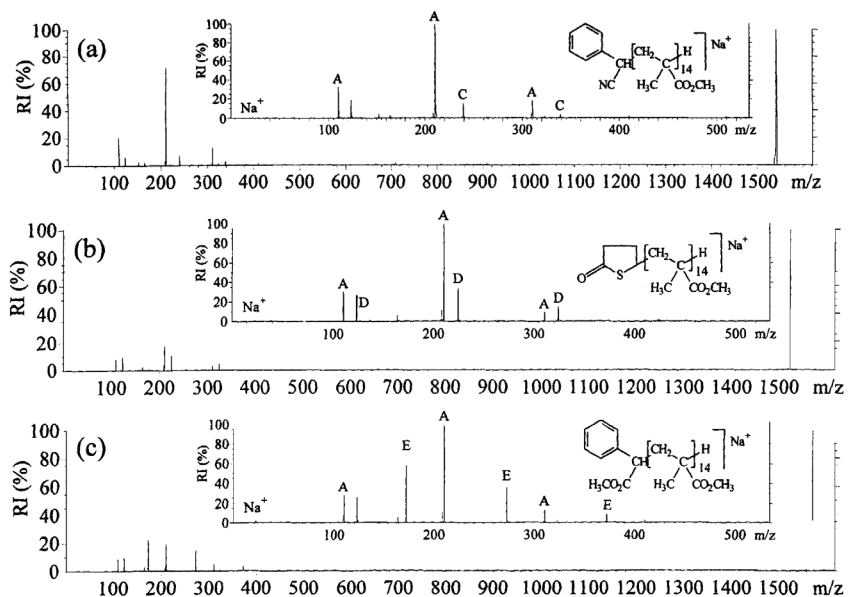
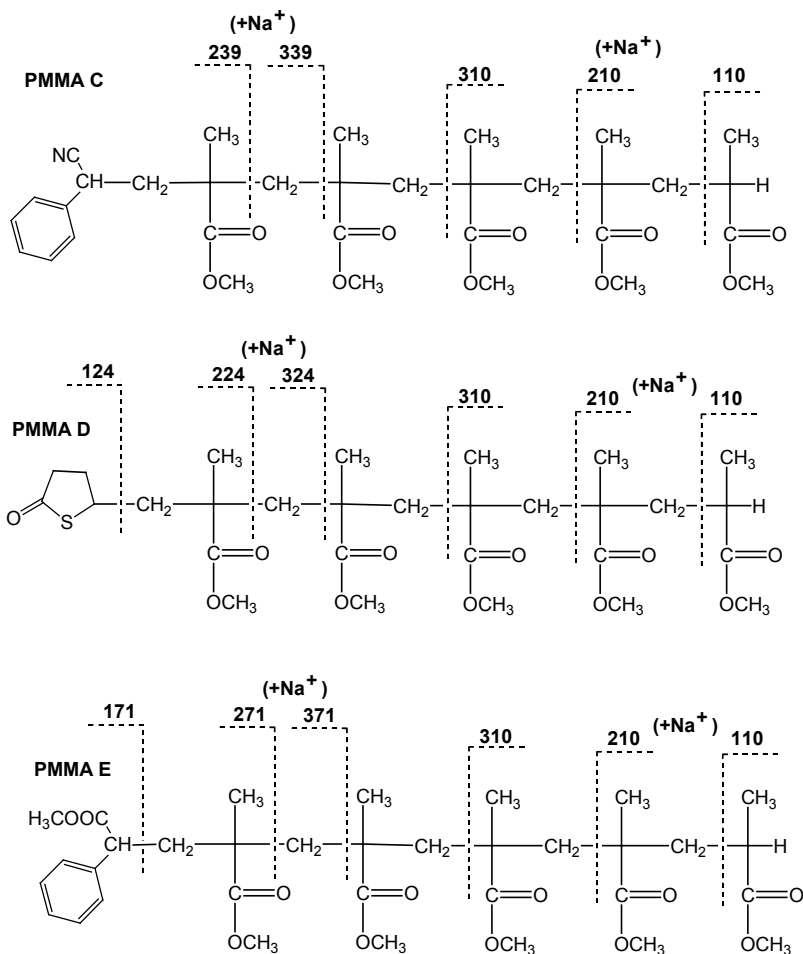


Figure 7. (a-c). MALDI-CID spectra of the $[M+Na]^+$ ion of the 14-mer of (a) PMMA C, (b) PMMA D, (c) PMMA E.

Fragment ions resulting from polymer chain cleavage at the site adjacent to the end group (Scheme 2) are observed as peaks at m/z 124 for PMMA D and 171 for PMMA E, respectively. However, the respective fragment ion at m/z 139 for PMMA C is not present in the spectrum (Fig. 7a), probably due to the weaker interaction of the corresponding end group with sodium cation.



Scheme 2. CID fragmentation pathways of the $[M+Na]^+$ ions of the 14-mers of PMMA C, D and E.

Jackson et al.¹³ analyzed also PET i.e. poly(ethylene terephthalate) oligomers using MALDI-ToF MS and submitted sodiated molecular ion $[M+Na]^+$ of the 6-mer of PET to MALDI-CID fragmentation. The spectrum obtained is presented in Figure 8. The main series of fragment ions denoted as α is attributed to the composition $(237+192n)$, where 192 is a repeat unit mass and 237 is $HOCH_2CH_2CO\Phi COOCH_2CH_2$ mass (Φ = phenyl).

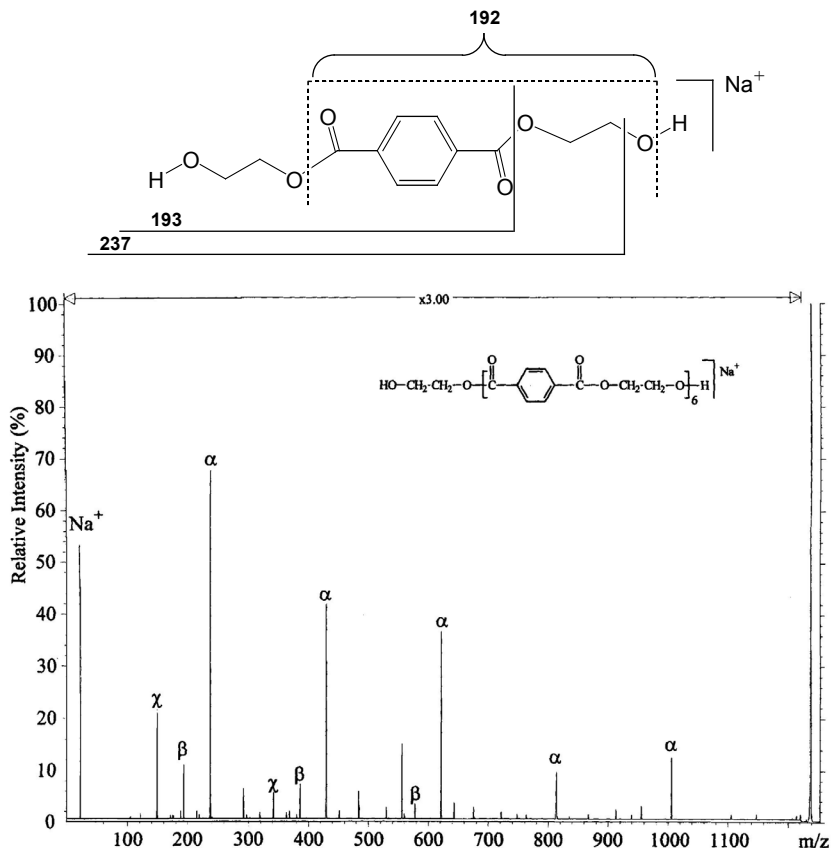


Figure 8. MALDI-CID spectrum of the $[M+Na]^+$ ion of the 6-mer of PET A.

Another series of ions – β – is observed at m/z values $(193+192n)$, which is also consistent with the polymer structure presented in the spectrum Fig. 8. A third series of ions, represented by peaks at m/z 149 and 341, differing by 192u (repeat unit) as well and labeled as χ , seems to be originated from a different end

group (another structure of precursor ion).

The authors prognosed that the MALDI ionization technique may provide useful data for determination of unknown end groups in more complex polymer arrangements.

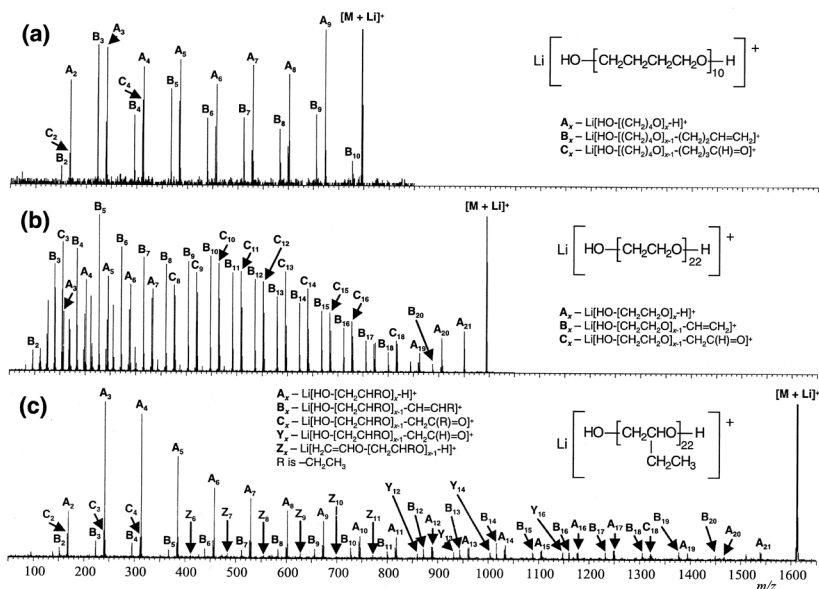


Figure 9. MALDI-CID spectra of $[\text{M}+\text{Li}]^+$ precursor ions from (a) decamer (m/z 745) of dihydroxyl end-capped PTMeG, (b) 22-mer (m/z 993) of dihydroxyl end-capped PEG, (c) 22-mer (m/z 1609) of dihydroxyl end-capped PBG and proposed structures of product ions (A, B, C, Y, Z series).

The matrix-assisted laser desorption/ionization collision-induced mass spectrometry were also used to obtain information about end groups of a series of polyethers¹⁴, i. e. poly(ethylene glycol) (PEG), poly(butylene glycol) (PBG) and poly(tetramethylene glycol) (PTMeG) as well as to gain insight in the influence of initiating groups on these polymers mass spectra. The authors took advantage of the high affinity of Li^+ ions to the polyethers and used lithiated molecular ions $[\text{M}+\text{Li}]^+$ as precursor ions for collision-induced dissociation in order to investigate the fragmentation routes of these ions and generate data concerning the end groups. The $[\text{M}+\text{Li}]^+$ ions appeared the best precursors for MS/MS experiments, because sodiated $[\text{M}+\text{Na}]^+$ ions generated daughter ions of minor abundance and mainly bare Na^+ cations were seen in the MALDI-

CID spectrum. The authors analyzed polyethers with hydroxyl groups at both ends and compared the data obtained with those from previous work^{15,16,17}. The MALDI-CID mass spectra for PEG and PTMeG [M+Li]⁺ precursor ions were dominated by the three main series of ions: A_x , B_x and C_x , where x – number of monomer units in the product ions (see Figure 9 for the corresponding spectra and proposed structures of precursor and daughter ions). The data are in agreement with previously obtained by means of a quadrupole ion trap TOF mass spectrometer¹⁶.

As can be deduced from the spectra in Figure 9, three series of product ions with the retained lithium cation are dominating in all the spectra (PTMeG, PEG and PBG): A_x , alcohol ended; B_x , vinyl mono-capped; and C_x , aldehyde mono-capped. Only the spectrum of PBG differs from the others and displays additionally Y_x and Z_x series of daughter ions due to the ethyl side chain present in the PBG molecules. The conclusion is that the presence of Y_x and/or Z_x ion series may be applied to the differentiation between a PBG and PTMeG polymers.

Another problem analyzed by using MALDI-CID spectrometry was checking the ability of this spectral method for end-group identification of commonly used ethoxylates, initiated with alcohols containing alkyl groups of various lengths, namely nonyl, decyl, undecyl, tridecyl and pentadecyl. The oligomers chosen had the same number of moles (12) of ethylene oxide (EO) and different end-group chain length on the initiating ends. (Figure 10). All the oligomers have been ionized through Li complexation. As displayed in Figure 10, the [M+Li]⁺ ions and the corresponding fragment ions are shifted by multiples of 14 Th (multiples of CH₂) depending on the alcohol used as an initiator. The difference in mass-to-charge ratios of ions from the A_x ' series allow differentiation of the alkyl chain length of the initiator.

The detailed methodology of the identification and analysis of homopolymer end groups has been elaborated⁴ using MALDI-TOF instrument of good resolving power and examples of its applications to the linear polymers, polycaprolactone and polystyrene have been given, concerning the polydisperse character of polymers, the possibility of different end groups presence and different ionization modes (different cations used to ionization of polymers). The relation between observed masses in the spectrum, number of repeat units and summed masses of end groups can be described by the equation [1]:

$$M_{obs} = n(M_{ru}) + M_{end} + M_{ion} \quad [1]$$

where

M_{obs} – function describing each discrete mass within the polymer distribution,

M_{ru} – mass of the polymer repeat unit,

n – number of polymer repeat units for each discrete signal observed,

M_{end} – mass of the both end groups summed together,

M_{ion} – mass of the cationizing ion, for example H^+ , Na^+ , K^+ or Ag^+ .

The graphical depiction of this relationship is displayed in Figure 11. The drawing can be interpreted as a graph of a linear function with the number of repeat units, n , as the abscissa; the mass of observed signal [D] as the ordinate; mass of repeat unit, M_{ru} , as the slope and the value ($M_{end} + M_{ion}$) as the intercept.

The main problem in determining an exact polymer's end-group mass from its mass spectrum is that we do not know the absolute number of repeat units, n , corresponding to a given mass peak; therefore the abscissa are presented as relative values (x rather than n). This makes the position of the intercept (the ordinate value for $n = 0$) is not certain and a series of possible values should be considered. However, the knowledge about synthetic conditions and parameters, catalyst and initiators as well as ionizing agents used can narrow the possibilities to a single, most probable, solution. In order to calculate the end-group mass M_{end} correctly, it is necessary to determine the other variables from Equation [1], i.e. the mass of repeat unit M_{ru} (from the distance between peaks in the mass spectrum), the mass change due to the ionization process M_{ion} (deduced examining several differing counterions) and the value of n (although it cannot be determined from the mass spectral data with absolute certainty, it can be deduced through the elimination, on the basis of known polymerization procedures).

The mass spectral data analysis, however, must involve two mass regimes: isotopically resolved and isotopically unresolved. The first one is applied to the lower molecular weights, when isotopic signals are narrow and mass spectra measured are in good agreement with theoretical ones (Figure 12 a and c). At higher molecular weights the isotopic peaks are broadened (due to the natural abundance of heavier isotopes, like ^{13}C and ^{18}O) and (at the sufficiently high molecular weight) they merge into one broad peak, differing from the well-resolved peaks in the simulated MALDI spectrum (Figure 12 b and d). In this case, for the masses above 7500 Da, mass spectra are isotopically unresolved and the average mass values are used for calculations.

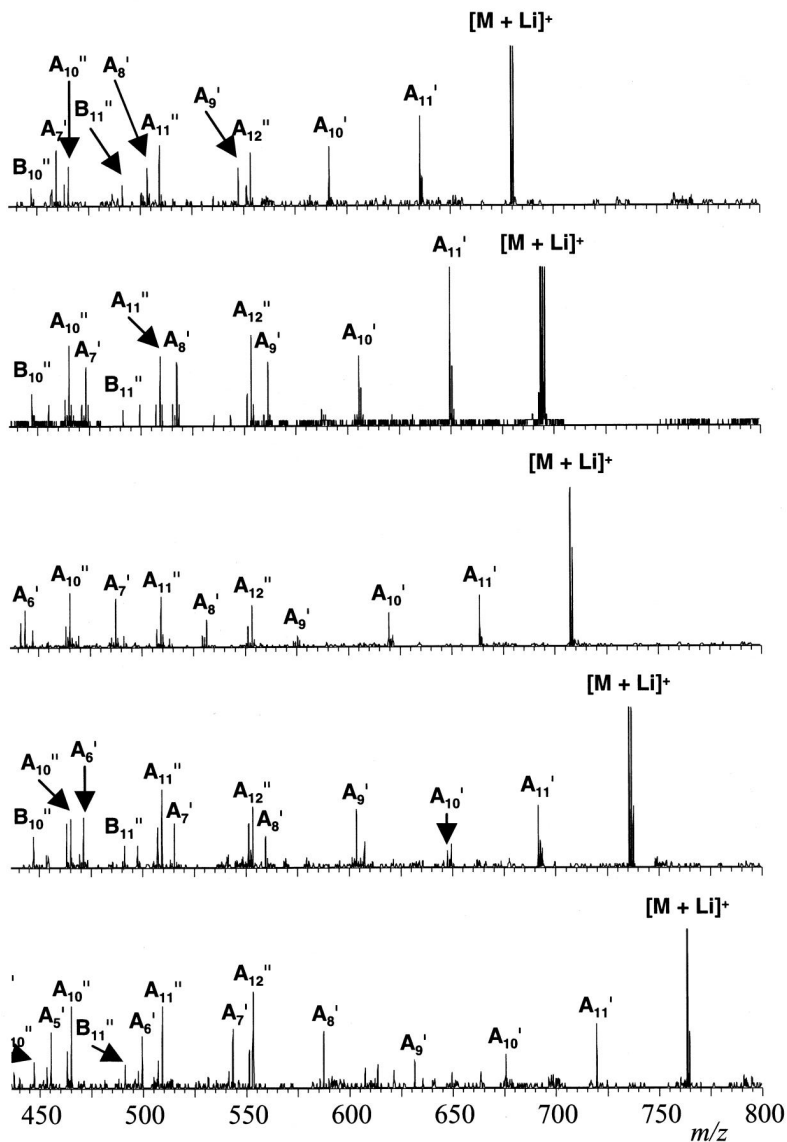


Figure 10. MALDI-CID spectra of $[M+Li]^+$ ions from 12-mers of PEG, initiated by: a) nonyl alcohol, b) decyl alcohol, c) undecyl alcohol, d) tridecyl alcohol, e) pentadecyl alcohol (m/z range 450-800).

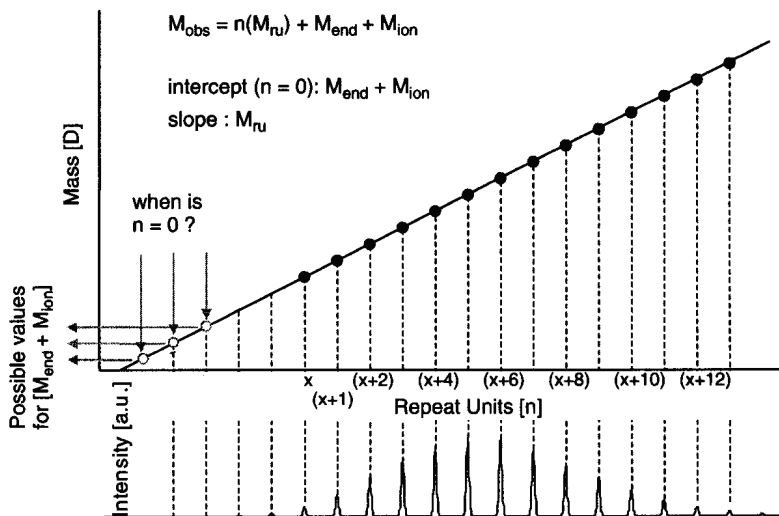


Figure 11. Graphical illustration of the relationship between the observed mass spectrum and Equation [1].⁴

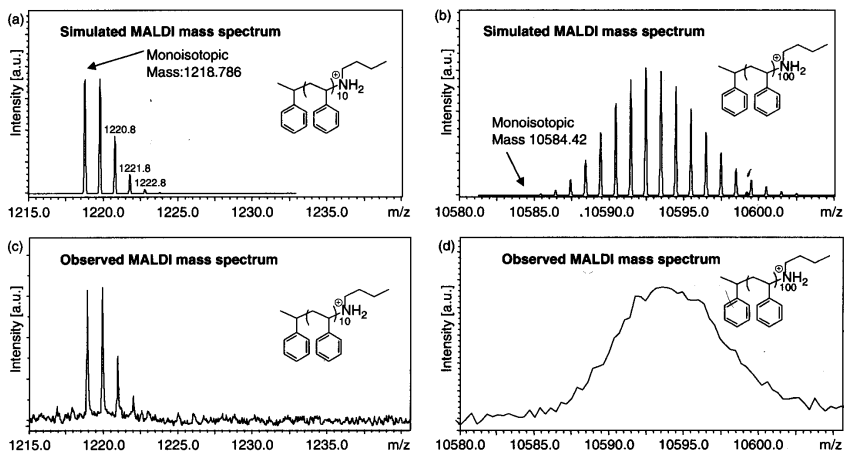


Figure 12. Simulated isotope distribution for (a) a polystyrene 10-mer and (b) a polystyrene 100-mer in comparison with observed data for (c) the PS 10-mer and (d) the PS 100-mer.⁴

One of the important problems is the determination of ionization mode. Most of polymers are ionized through the complexation with cation (hydrogen or metal), so the M_{ion} value is equal to the mass of the cation added. Some polymers, however, are prone to the elimination or fragmentation reactions during the ionization. As an example may serve polystyrene (PS) obtained in atom transfer radical polymerization, where the terminal repeat unit contains a benzylic bromide. This polymer undergoes elimination of HBr to create a styryl end group during the cationization with Ag^+ , yielding the $[M+Ag-HBr]^+$ species observed¹⁸. Therefore, the ionization mode should be first elucidated to establish the M_{ion} value which would be used in Equation [1]. This problem can be clarified by examining the mass spectra generated by using different cationizing salts. For example, the mass spectra of polycaprolactone samples, prepared with use of different trifluoroacetate salts (Na^+ , K^+ and Ag^+) display that the polymer ionize via the cation complexation (Figure 13).

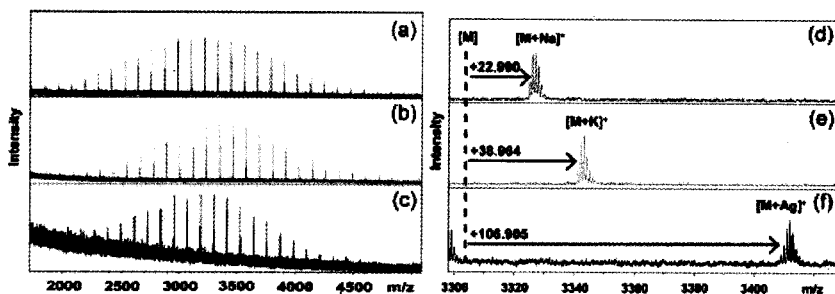


Figure 13. MALDI-TOF mass spectra of polycaprolactone using Na^+ , K^+ and Ag^+ cations to yield the macromolecular ions.⁴

Only when we know M_{ion} , we can correct the series of masses observed in the mass spectrum, M_{obs} , for the mass associated with the ionization process and calculate the masses of neutral, un-ionized polymer “n-mers” as:

$$M_{n-mer} = M_{obs} - M_{ion}$$

which will transform Equation [1] to:

$$M_{n-mer} = n(M_{rt}) + M_{end} \quad [2]$$

(The graphical representation of the correction is shown in Figure 14.)

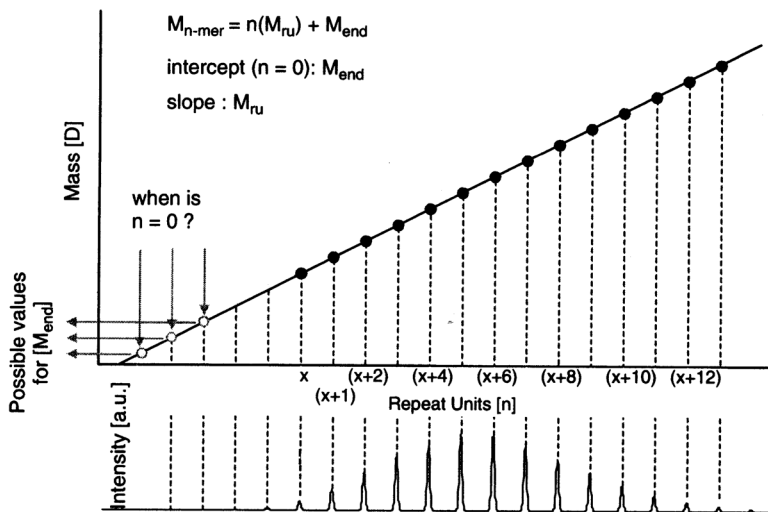


Figure 14. Correction of polymer distribution, taking into account the mode of ionization. The line intercept represents the end-group mass.⁴

Further mathematical analysis performed using various methods allows precise and accurate determination of the repeat unit mass, M_{ru} , as a slope of linear function graph to the abscissa. The approaches applied involve three techniques:

- [1] the 'arbitrary segment slope', taking into account the mass difference between two arbitrary, consecutive data points;
- [2] the 'average slope', calculating the average mass difference across the entire distribution;
- [3] the linear regression (LR) slope, showing the linear trend through the data set.

These three methods are depicted in Figure 15.

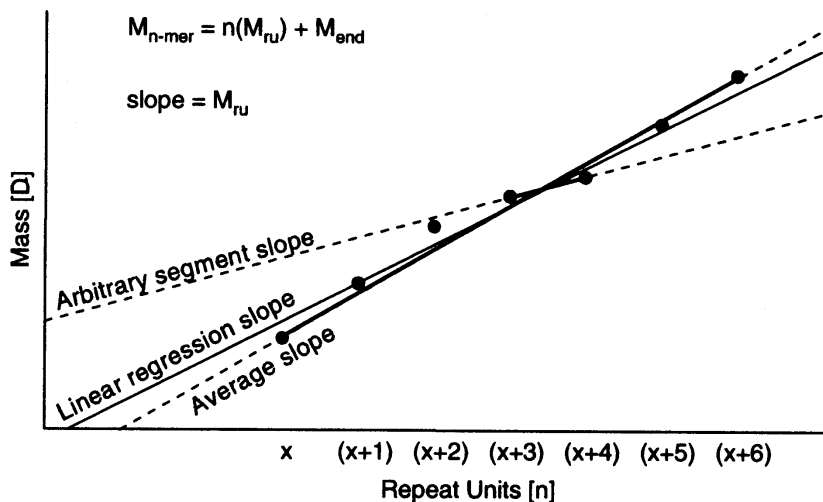


Figure 15. Graphical depiction of the three described approaches for calculating the repeat unit mass.⁴

The best method of the presented above seems to be the linear regression model [3], which defines the general linear trend rather than the value based on two data points only.

Once we finally know the values of variables M_{ion} and M_{ru} , we can calculate the residual mass, M_{res} , in order to determine the mass of the end group. However, because the absolute number of repeat units n for each data set remains still unknown, multiple solutions are possible, i.e.:

$$\begin{aligned}
 M_{end} &= M_{res}, \text{ or} \\
 M_{res} &+ M_{ru}, \text{ or} \\
 M_{res} &+ 2(M_{ru}), \text{ or} \\
 M_{res} &+ 3(M_{ru}), \text{ or} \\
 &(\dots)
 \end{aligned}$$

Now the general knowledge of the reaction conditions will allow us to find the correct solution, i.e. deduce the single end-group mass. It has been demonstrated that this approach allows to calculate the mass of end groups with an accuracy of 0.3 Da for polymers with molecular mass up to 7500 Da. Above this molecular weight, when peaks are isotopically unresolved, the resolution drops rapidly (to

within ~3 Da), making it difficult to identify the unknown end groups, but in this case MALDI mass spectrometry still provides valuable information to study the transformation of known end groups.

Summary

Synthetic polymers show various kinds of heterogeneity. Aside from different types of molar mass distribution they can possess various structures (linear, branched, cyclic, grafted), monomer sequence and different functional end-groups. These features of synthetic polymers construction are not easy to understand or solve. The MALDI-TOF mass spectra often allow to determine the type and structure of the end-groups present in the polymer sample.

The polymer end-group identification by means of MALDI mass spectrometry has been a subject of many papers¹⁹⁻²⁷. All these studies confirm that MALDI mass spectral technique offers a great capability for the determination of end groups and tracking their synthetic modification.

Acknowledgements

The authors thank the Polish Ministry of Science and Higher Education for financial support in years 2009-2012 as scientific grant No. N 204 028636.

References

1. K. Tanaka, H. Wak, Y. Ido, S. Akita, Y. Yoshida, T. Yoshida; Protein and polymer analysis up to m/z 100 000 by laser ionization time-of-flight mass spectrometry; *Rapid. Commun. Mass Spectrom.* 1988, 2, 151-153.
2. I.V. Bletsos, D.M. Hercules, D. van Leyen, B. Hagenhoff, E. Niehuis, A. Benninghoven; Molecular weight distribution of polymers using time-of-flight secondary-ion mass spectrometry; *Anal. Chem.* 1991, 63(18), 1953-1960.
3. U. Bahr, A. Deppe, M. Karas, F. Hillenkamp, U. Giessmann; Mass spectrometry of synthetic polymers by UV-matrix-assisted laser desorption/ionization; *Anal. Chem.*, 1992, 64(22), 2866-2869.
4. Li Y., Hoskins J.N., Sreerama S.G., Grayson M.A., Grayson S.M.; The identification of synthetic homopolymer end groups and verification of their transformations using MALDI-TOF mass spectrometry; *J. Mass Spectrom.* 2010, 45, 587-611.
5. Li L.; MALDI-MS for polymer characterization; in: "MALDI-MS, A practical guide to instrumentation, methods and applications", edited by: Hillenkamp F and Peter-Katalinic J; Wiley-VCH 2007, ISBN 978-

- 3-527-31440-9.
6. Whittal R.M.; Li L.; Lee S.; Winnik M.A.; Characterization of pyrene end-labeled poly(ethylene glycol) by high resolution MALDI time-of-flight mass spectrometry; *Macromol. Rapid Commun.* 1996, 17, 59-64.
 7. Lee S., Winnik M.A., Whittal R.M., Li L.; Synthesis of symmetric fluorescently labeled poly (ethylene glycols) using phosphoramidites of pyrenebutanol and their characterization by MALDI Mass Spectrometry; *Macromolecules*, 1996, 29, 3060-3072.
 8. Pasch H.; Functionality analysis of polymers by MALDI-MS; American Chemical Society, Polymer Preprints, Division of Polymer Chemistry 1996, 37 (1), 319-320.
 9. Montaudo G., Montaudo M.S., Puglisi C., Samperi F.; Characterization of end-groups in Nylon 6 by MALDI-TOF mass spectrometry; *J. Polym. Sci. A, Polym. Chem.* 1996, 34, 439-447.
 10. Montaudo G., Lattimer R.; in: "Mass Spectrometry of Polymers", CRC Press: Boca Raton, 2002, 584, ISBN 0-8493-3127-7.
 11. Jackson A.T., Yates H.T., MacDonald W.A., Scrivens J.H., Critchley G., Brown J., Deery M.J., Jennings K.R., Brookes C.; Time-lag focusing and cation attachment in the analysis of synthetic polymers by matrix-assisted laser desorption/ionization-time-of-flight-mass spectrometry; *J. Am. Soc. Mass Spectrom.* 1997, 8(2), 132-139.
 12. Alicata R., Montaudo G., Puglisi C., Samperi F.; Influence of chain end groups on the matrix-assisted laser desorption/ionization spectra of polymer blends; *Rapid Commun. Mass Spectrom.* 2002, 16, 248-260.
 13. Jackson A.T., Yates H.T., Scrivens J.H., Critchley G., Brown J., Green M.R., Bateman R.H.; The application of matrix-assisted laser desorption/ionization combined with collision-induced dissociation to the analysis of synthetic polymers; *Rapid Commun. Mass Spectrom.* 1996, 10,1668-1674.
 14. Jackson A.T., Green M.R., Bateman R.H.; Generation of end-group information from polyethers by matrix-assisted laser desorption/ionization collision-induced mass spectrometry; *Rapid Commun. Mass Spectrom.* 2006, 20, 3542-3550.
 15. Lattimer R.P., Tandem mass spectrometry of lithium-attachment ions from polyglycols, *J. Am. Soc. Mass Spectrom.* 1992, 3, 225-234.
 16. Lattimer R.P., Tandem mass spectrometry of poly(ethylene glycol) lithium- attachment ions, *J. Am. Soc. Mass Spectrom.*1994, 5, 1072-1080.
 17. Okuno S., Kiuchi M., Arakawa R.; Structural characterization of

- polyethers using matrix-assisted laser desorption/ionization quadrupole ion trap time-of-flight mass spectrometry, *Eur. J. Mass Spectrom.* 2006, 12, 181-187.
18. Ladavière C., Lacroix-Desmazes P., Deloime F.; First systematic MALDI/ESI mass spectrometry comparison to characterize polystyrene synthesized by different controlled radical polymerizations; *Macromolecules* 2009, 42, 70-84.
 19. Pasch H., Ghahary R.; Analysis of complex polymers by MALDI-TOF mass spectrometry; *Macromol. Symp.* 2000, 152, 267-278.
 20. Montaudo G., Montaudo M.S., Puglisi C., Samperi F., Sepulchre M.; End-group characterization of poly(methylphenylsilane) by alkali metal salts doped MALDI-TOF mass spectra, *Macromol. Chem. Phys.* 1996, 197, 2615-2625.
 21. Skelton R., Dubois F., Zenobi R.; A MALDI sample preparation method suitable for insoluble polymers; *Anal. Chem.* 2000, 72, 1707-1710.
 22. Jackson A.T., Yates H.T., Lindsay C.I., Didier Y., Segal J.A., Scrivens J.H., Brown J.; Utilizing time-lag focusing matrix-assisted laser desorption/ionization mass spectrometry for the end-group analysis of synthetic polymers; *Rapid Commun. Mass Spectrom.* 1997, 11, 520-526.
 23. De Koster C.G., Duursma M.C., van Rooji G.J., Heeren R.M.A., Boon J.J.; Endgroup analysis of polyethylene glycol polymers by matrix-assisted laser desorption/ionization Fourier-transform ion cyclotron resonance mass spectrometry; *Rapid Commun. Mass Spectrom.* 1995, 9, 957-962.
 24. Montaudo G., Montaudo M.S., Puglisi C., Samperi F.; Characterization of polymers by matrix-assisted laser desorption/ionization- time of flight mass spectrometry. End-group determination and molecular weight estimates of poly(ethylene glycols), *Macromolecules* 1995, 28, 4562-4569.
 25. Yamanaka K., Kimura Y., Aoki T., Kudo T.; End-group analysis of bacterially produced poly(3-hydroxybutyrate): discovery of succinate as the polymerization starter; *Macromolecules*, 2009, 42 (12), 4038-4046.
 26. Weidner S.M., Falkenhagen J., Knop K., Thünemann A.; Structure and end-group analysis of complex hexanediol-neopentylglycol-adipic acid copolyesters by matrix-assisted laser desorption/ionization collision-induced dissociation tandem mass spectrometry, *Rapid Commun. Mass Spectrom.* 2009, 23, 2768-2774.

27. Chen H., He M., Pei J., Liu B.; End-group analysis of blue light-emitting polymers using matrix-assisted laser desorption/ionization time-of-flight mass spectrometry; *Anal. Chem.* 2002, 74(24), 6252-6258.

Chapter 9

Selected tripodal receptors for halide anions

Bogusława Łęska

*Adam Mickiewicz University, Faculty of Chemistry,
Grunwaldzka 6, 60-780 Poznań, Poland*

Introduction

Since many years the molecular recognition of anions by synthetic receptors has been a rapidly expanding field of research. The mostly synthetic anion receptors contain in their composition: macrocyclic polyamines, guanidines, pyrroles [1-7], Lewis acids [8-11], calixarenes [12-14], amides [10, 15-20], urea (or thiourea) molecules [10, 17-19, 21] in various combinations. When designing a selective anion receptor must be taken into account the geometry and basicity of the anion, and the type of solvent.

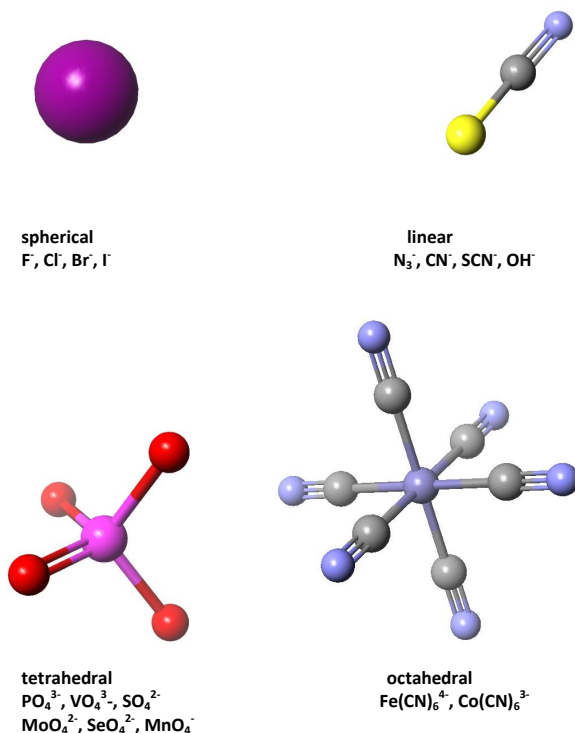
The topology of receptor is important in determining the overall receptor-ion interactions. Tripodal receptors are a special class of acyclic ionophores, which consist of multiarmed ligands with each arm bearing a functional group that can coordinate with the target ion. Designing podand receptor (host) having the possibility of complexation of anions (guests), subject to the same rules as set out the synthesis of supramolecular podand compounds, which can form complexes with cations or neutral molecules. The durability of host-guest connections depends on complementarity, adjustment to the spatial receptor and the guest interactions, ligand selectivity, etc. However, because the properties of anions due to their spatial structure, ionic radius size, sensitivity to the environment (pH), etc., it is a much harder task.

Tripodal receptors for anions. Why?

Anions are relatively large and therefore require a much larger receptors than cations. The size of the smallest ionic radius of anions, fluoride ion (1.33 Å) is comparable to the radius of the cation of potassium ion (1.38 Å). Chloride ion (1.81 Å) is larger than the cation cesium (1.70 Å). Anions are characterized by a variety of spatial structure, and therefore require especially designed receptor, acting more selectively and selectively than the cationic receptor. Even the relatively simple inorganic anions (NO_3^- , PO_4^{3-} , PF_6^- , SCN^- , or N_3^-) have very

different shapes have different geometry, from linear, flat with tetrahedral or octahedral, up to even more complex structures present in the biological systems.

Furthermore, compared with cations, “in a similar size,” anions have higher values of solvation free energy, which is why the receptors complexing anions must overcome a significant energy barrier resulting from the interaction of the reaction (Scheme 1). The anions are also more sensitive to the environment (pH) in which they are located. Even a small change in pH of the system in which there are anions, can cause loss of charge by anions, by joining the proton.



Scheme 1. Structural diversity of anions [23]

Why the use of tripodal receptors in anion complex chemistry is so important? The answer is not so easy, but the main features of tripodal receptors for anions are:

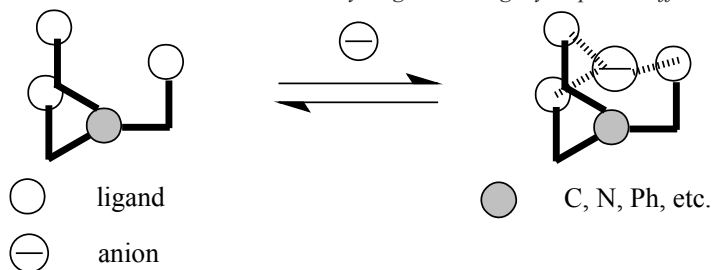
- sufficient number of positively charged or neutral electron-deficient groups in the ligand to serve as a place of interaction;

- receptors with a flexible tripodal structure have a strong affinity for the trigonal oxoanions, such as carbonate, phosphate and chlorate, because the geometry and orientation of the molecules of the host to create a stable host-guest complex;
- the classical mechanism of complexation can also be used. The interactions are based on non-covalent interactions, which include electrostatic interactions, hydrogen bonding, hydrophobicity, coordination to metal ions, and the combination of these interactions [16, 24].

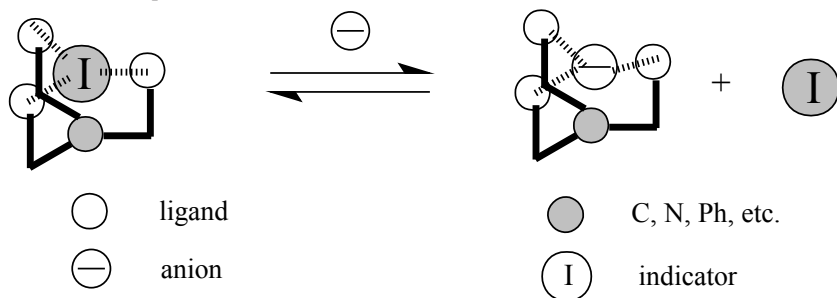
Scheme 2 shows different types of tripodal receptor interaction modes toward anions.

One of the most interesting group of tripodal receptors are ligands for halide anions. The first redox active anion receptors based on the rest of the cobalt was proposed in 1989 [25]. Cyclic voltammetry results showed that the receptor 1 (Fig.1) [26] complexes anion very good. Complexes of anionic guest effectively stabilizes the positively charged cobalt center, making it difficult to reduce. The complexation process of chloride ions by receptor 1 induced a cathodic shift of 30 mV.

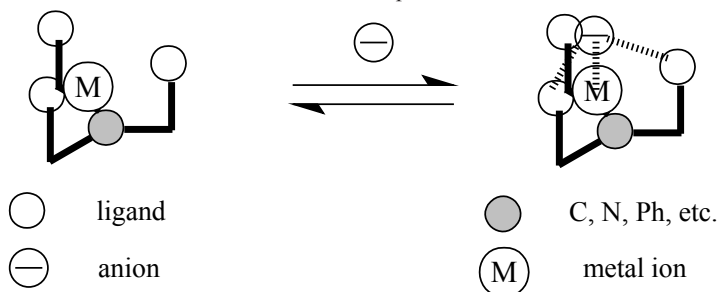
A - the direct interactions - non-covalent: hydrogen bonding, hydrophobic effect:



B - indicator displacement:



C - electrostatic interactions with the metal complex:



Scheme 2. Different types of the interaction of tripodal receptors with anions: directly using noncovalent interaction, viz. hydrogen bonds or hydrophobic effect (a) or indicator displacement (b) or electrostatic interaction with metal complex (c) [24].

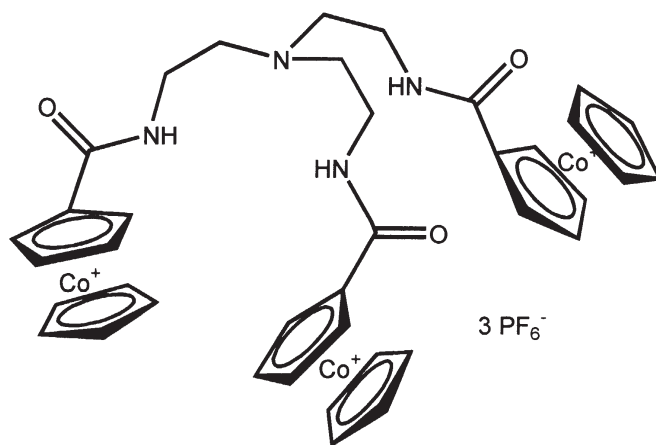


Figure 1. Receptor 1 [24, 26]

These preliminary anion coordination studies have revealed that relatively simple, easily prepared, acyclic cobalt derivatives containing amide N-H groups can coordinate and electrochemically recognize anionic guest species *via* the cooperative binding forces of mutual electrostatic attraction between the positively charged host and anionic guest, and favorable amide N-H anion hydrogen bonding interactions [26].

The group of Japanese researchers [27] received a tripodal receptor

2, containing three imidazolium groups that coordinate anions through a combination of hydrogen bonds and electrostatic interactions (Fig. 2).

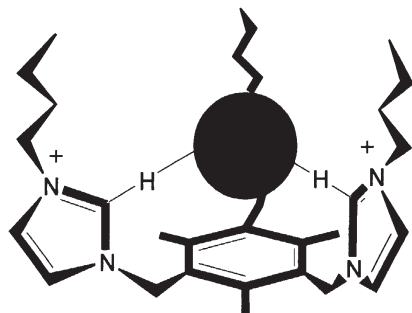


Figure 2. Receptor 2

Tripodal receptor 2 preorganized is more than for halide coordination compounds model (receptors 3 or 4, Fig 3.) resulting in more permanent stability in acetonitrile- d_3 .

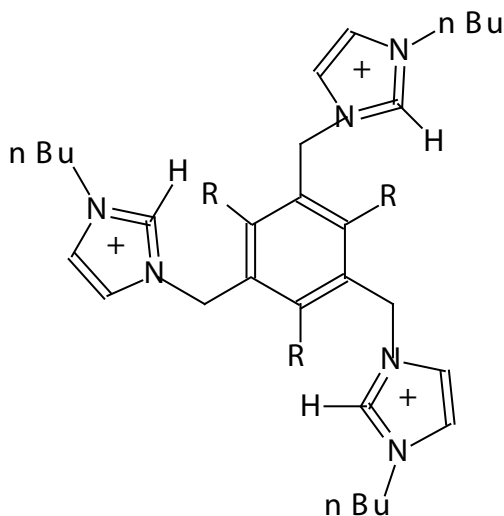


Figure 3. The receptors 3 ($R=CH_3$) and 4 ($R=H$)

These results agree with those Anslyn and co-workers [28], who studied the

number of similarly preorganized tripodal anion receptors containing different anion coordination group Fig. 4.

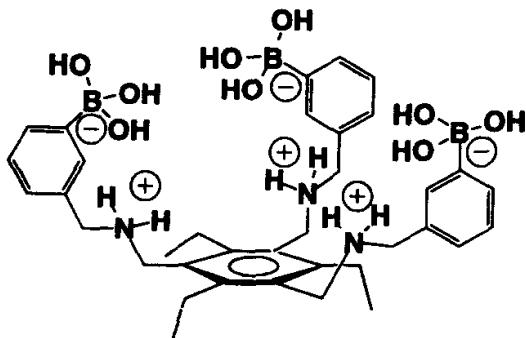


Figure 4. Analogue receptor to receptor 3 [28]

At the paper Beer and co-workers [29] presented a synthesis of his work and studies on the receptor 5 (tren-based), which is characterized by the amide-containing anion-binding cavity linked to three cation binding benzo-15-crown-5 (Fig. 5).

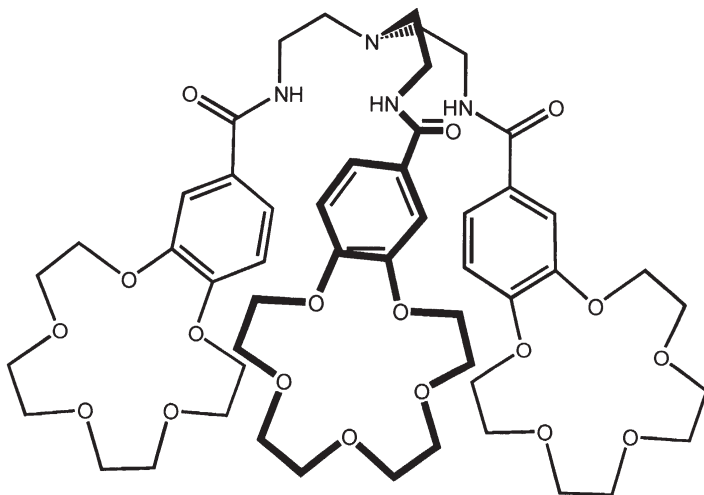


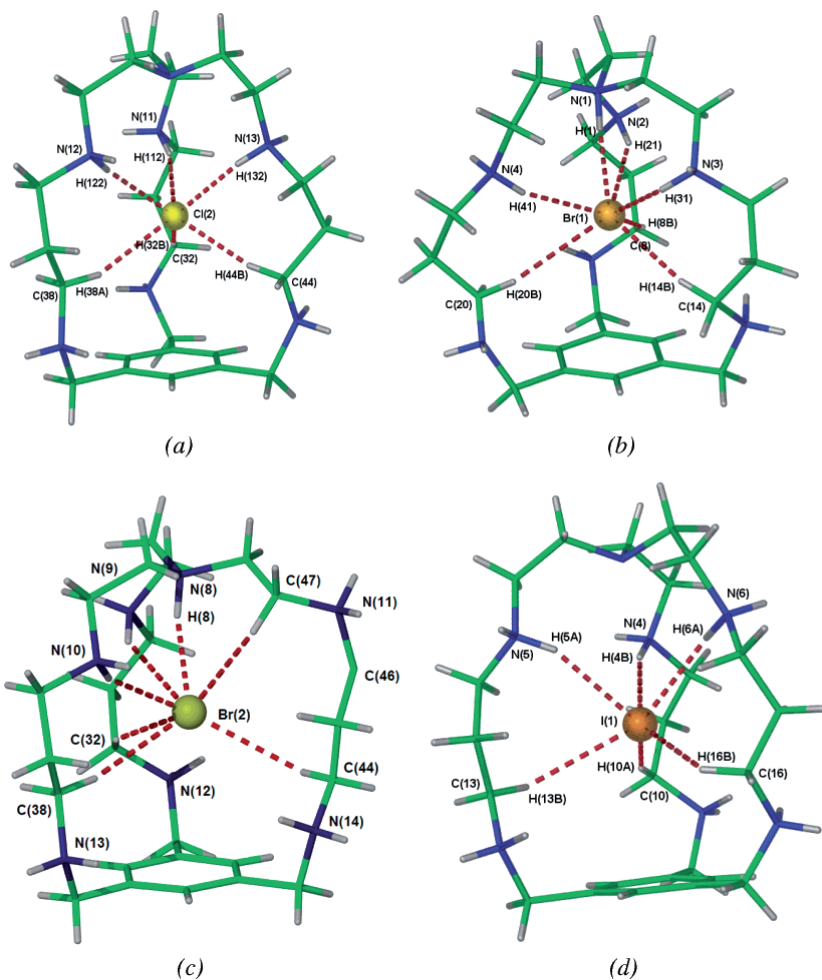
Figure 5. Receptor 5 [29]

This receptor is highly effective extracts of sodium pertechnetate from simulated aqueous nuclear waste streams. In the absence of cobound cations, the anion affinity for the receptor was significantly reduced. In this case, pertechnetate anions are probably related to both hydrogen bonds and electrostatic interactions.

Another example of a tripodal ligands binding halide anions are described macrobicyclic azaphanes (receptors 6 and 7) exhibit remarkable strong, selective fluoridebinding capacity, comparable with the most effective bis (tren) cryptands, although the anion is bound only via only three NH groups coupled with three CH hydrogen bond donors. Lower internal affinity CH donors is compensated by a high degree of preorganization exhibited by azacyclophane (receptor 6). Receptor 6 is prepared via a tripod-tripod cyclization reaction between 1,3,5-tris-bromomethyl-benzene and an aliphatic tripodal hexatosylated polyamine, followed by the reduction of the resulting bicyclic tosylamine. The tosylamine crystals structures (receptor 7) and four macrobicyclic polyammonium halides of receptor 6 are reported. X-ray studies showed the formation of 1:1 complexes, including fluoride, chloride, bromide and iodide. In Scheme 3 the encapsulation of (a) a chloride anion in the crystal structure of receptor 6 $6\text{HCl}\cdot 4.5\text{H}_2\text{O}$ and (b, c) bromide in receptor 6 $7\text{HBr}\cdot 3\text{H}_2\text{O}$, two conformationally different independent molecules is presented. An additional $\text{NH}^+ \cdots \text{Br}$ hydrogen bond in each case is formed because the cryptand is heptaprotonated with $\text{N}_{\text{apical}} \cdots \text{Br}$ distances of 3.169(12) Å and 3.187(14) Å. Disordered H atoms on C46 not shown. (d) Iodide anion in the crystal structure of receptor 6 $2\text{HI}\cdot 4\text{HI}_3$. Smaller “bite” angles are observed as a result of the positioning of the encapsulated iodide further away from the apical nitrogen atom [30]. (Scheme 3).

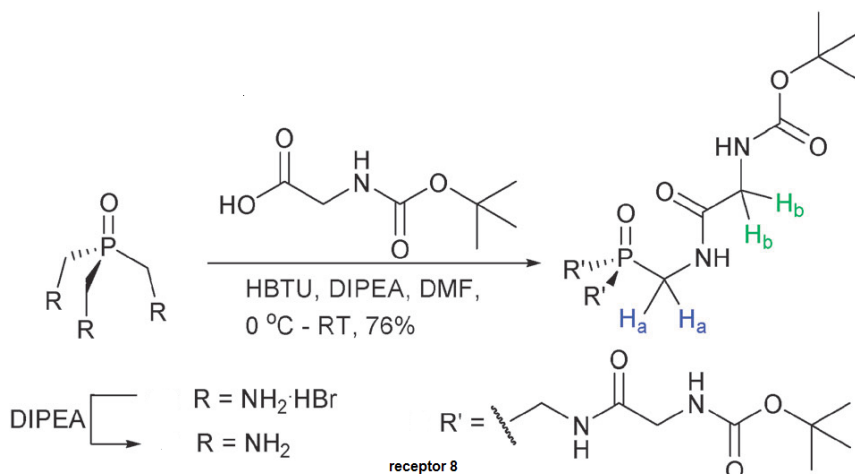
Potentiometric titration showed very high binding constants for fluoride and chloride F-/Cl- selectivity of more than five log units. The final geometry of the anion cryptates largely depends on the optimization of NH and CH ... anion interactions coupled with unfavorable anion-D repulsion for larger anions.

Anion binding by synthetic receptors are widely attention due to emerging applications in the remediation of waste and research aimed at understanding biological structure and function [31-33]. Some of these are triamines, such as 1,3,5-tris(aminomethyl)benzene [34-38] and tris (2-aminoethyl)-amine (TREN) [39] proved to be workhorse scaffolds to drudge tripodal anion receptors. The popularity of these scaffolds due to simple, modular synthetic modification of their primary amino groups in the strong hydrogen bond donors such as secondary amines, amides [40-44], ureas [45,46] and thioureas [47].



Scheme 3. The encapsulation of (a) a chloride anion in the crystal structure of receptor 6 ($6\text{HCl}\cdot 4.5\text{H}_2\text{O}$) and (b, c) bromide in receptor 6 ($7\text{HBr}\cdot 3\text{H}_2\text{O}$), two conformational different independent molecules [30]

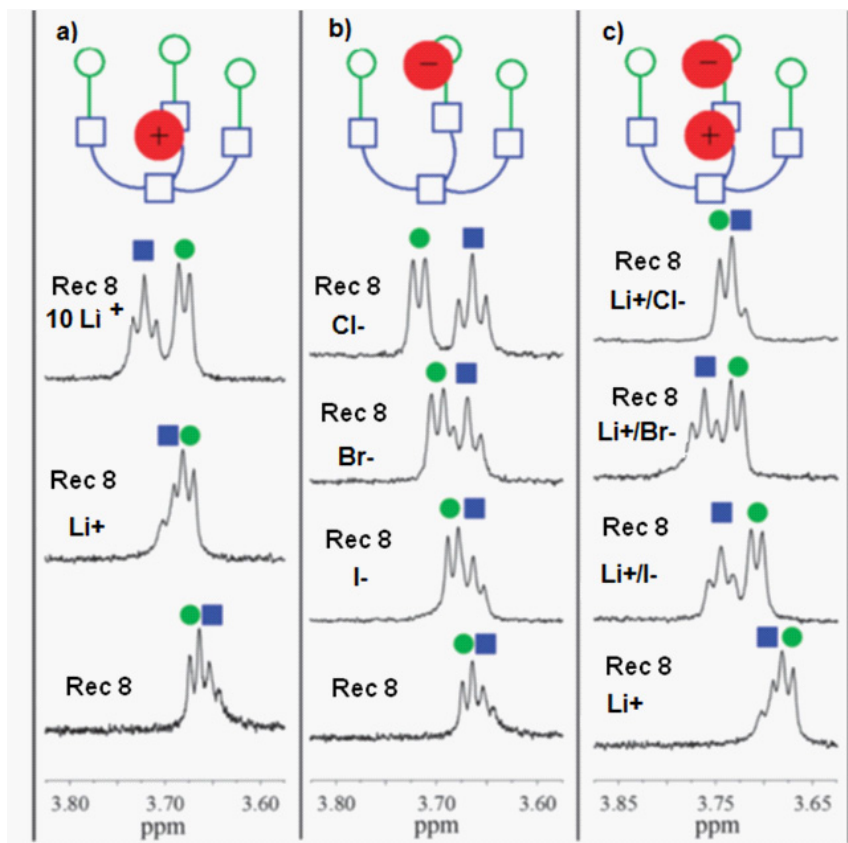
Gavette and co-workers [33] have presented the use of a tris-(aminomethyl) phosphine oxide as a scaffold for the neutral ditopic tripodal receptor 8 (Scheme 4). This synthesised receptor 8 shows a greater enhancement in the binding of bromide over chloride and iodide in the presence of ca. 1 equiv. of a lithium source, while sodium has little to no effect on anion association.



Scheme 4. Synthesis of ditopic receptor 8 using as starting material *O*-(benzotriazole-1-yl)-*N,N,N',N'*-tetramethyluronium hexafluorophosphate (HBTU) and Hunig's base (DIPEA) [34].

Determination of association constants of lithium and sodium by receptor 8 $\cdot \text{X}^-$ are currently underway as are investigations into possible cooperative effects of other positively charged species on anion binding. ^1H NMR spectra of methylene resonances of receptor 8 with 0.1 and 10 equiv. of Li^+ ; receptor 8 with excess iodide, bromide and chloride; and complex receptor 8 $\cdot \text{Li}^+$ with excess iodide, bromide and chloride are presented (Scheme 5).

The example of the others use of tripodal colorimetric anion is receptor 9 (Fig. 6), that shows a good selective recognition ability and color change for F^- by multiple hydrogen-bonding interactions, with an obvious change in the absorption spectra, while it shows no recognition ability for Cl^- , Br^- or I^- [48]. The association constants for these anions follow the order: $\text{F}^- \gg \text{AcO}^- \gg \text{Cl}^-$, Br^- , I^- . Since the complexation of F^- by ligand 9 induces a visible colour change, it is promising as a component in optode membranes for colorimetric detection of fluoride ions.



Scheme 5. ^1H NMR spectra of methylene resonances of (a) receptor 8 (Rec 8) with 0.1 and 10 equiv. of Li^+ ; (b) receptor 8 (Rec 8) with excess iodide, bromide and chloride; (c) complex receptor 8 (Rec 8) Li^+ with excess iodide, bromide and chloride [33].

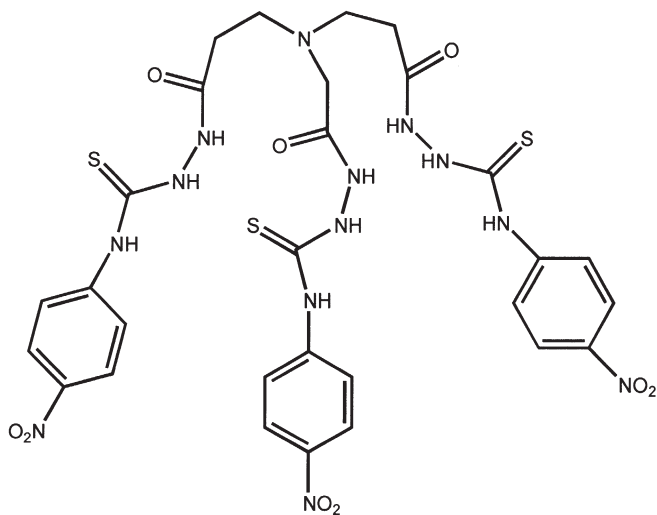


Figure 6. Receptor 9 [48]

The next presented receptor 10 (Fig. 7) is characterized by analogue structure to the receptor 9 (Fig. 6).

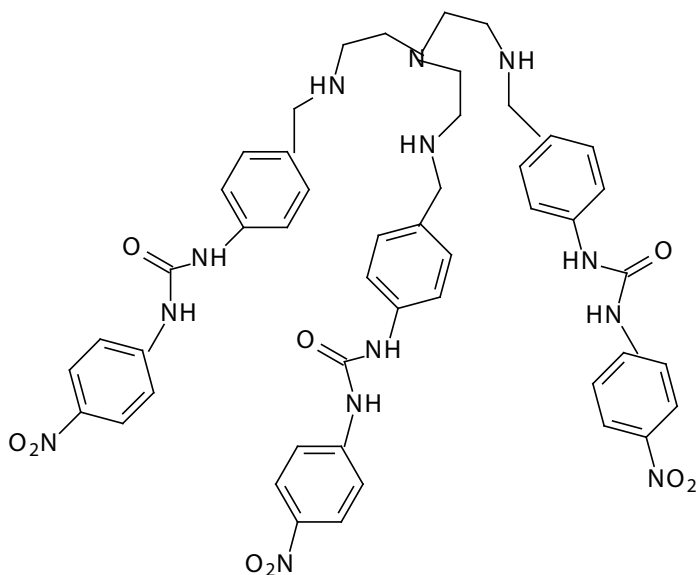


Figure 7. Receptor 10 [49, 50]

The its tripodal Cu(II) complex with has intriguing optical anion sensing properties [49]. This receptor has a cavity with two distinct anion binding sites—the vacant site on the Lewis acidic Cu(II) centre, and the three favourably arranged nitrophenylurea fragments. On titration with up to one equivalent of azide or dihydrogen phosphate in DMSO solution the Cu(II) d–d bands in the region 600–900 nm increased markedly in intensity. This indicates that the anion is binding at the metal centre. On their own halide anions were found to give only 1:1 complexes (with the halide bound at the Cu(II) centre) [49, 50]. In recent years the use of tripodal receptors as the off–on signalling chemical sensor for halide anions was observed. The receptor 11 is a good example of fluorescent sensor (Fig.8), that its structure was developed by incorporating a naphthalene ring into the preorganised benzene-based tripodal receptor with arms comprising benzoimidazolium hydrogen bonding moieties [51].

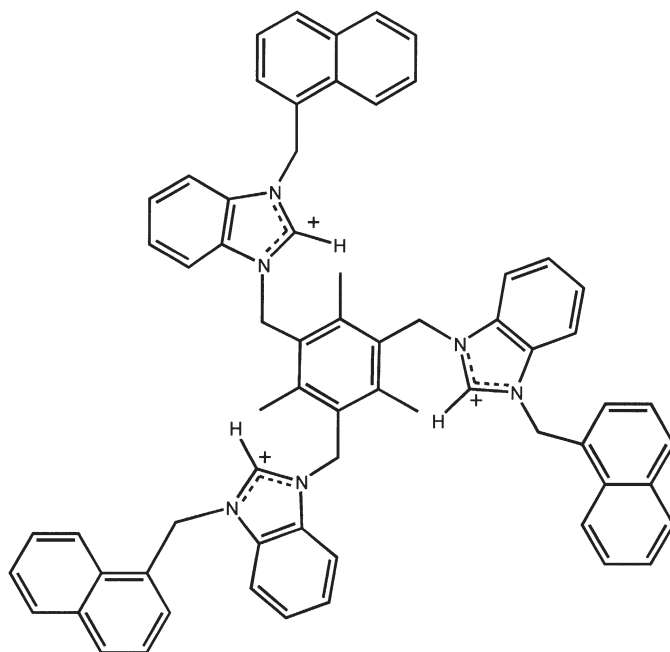
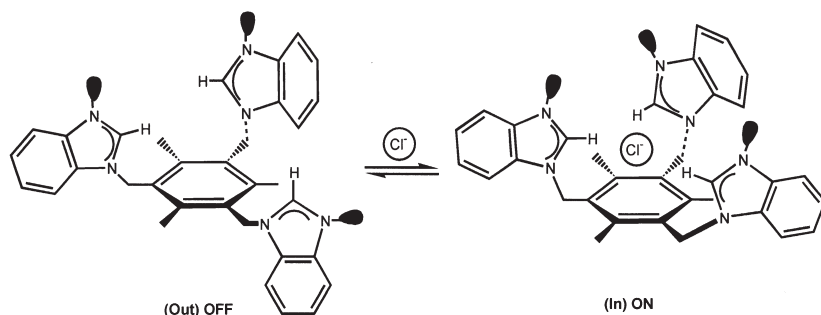


Figure 8. Receptor 11 [51]

A new fluorescent “off–on” signaling chemical sensor with high selectivity for chloride anion through a guest-induced conformational switching process

was achieved by using a positively charged tripodal receptor with naphthyl groups attached to the benzoimidazolium arms. This new type of hydrogen bonding between a halide anion and the benzoimidazolium is very intriguing in comparison with many other types of hydrogen bonding [51-53]. The host falls into the category of the fluorophore–spacer–receptor model and could act as a simple PET sensor. The presence of more than one naphthyl group allows the excited naphthyl unit to associate with the ground state of a second fluorophore to produce an intramolecular excimer through the anion-bonding induced conformational changes (Scheme 6) [51].



Scheme 6. The receptor 11 as fluorescent sensor [51]

In the presence of a specific anion conformational template, the hydrogen bonds between the arms and the anion induce the tripodal receptor 11 to display a cone conformation with all three positively charged arms oriented in the same direction (in) bringing the three naphthalene lumophores into close proximity with one another, leading to excimer fluorescence (on state). In the absence of the template anion, the electrostatic interactions between the benzoimidazolium groups of receptor 11 destabilise the cone conformation of the podand and lead to the spread out conformation (out), in which the three naphthyl lumophores are separated from each other and no excimer fluorescence will be observed (off state). This receptor is promising for the development of a luminescence sensor for chloride ions.

Conclusion

In the years 2001-2011 there were over 5000 publications on cyclic anion receptors, while only about 80 papers relate to the tripodal receptors complexing anions (Scopus Database).

In recent years, a definite increase in interest in these tripodal receptors, not only as sensors for halides. The presented work has sought to provide an overview of current progress in the design and evaluation of synthetic receptors based on a tripodal platform for halide ions. New methods of synthesis are constantly introduced and improved electrochemical and optical sensors are being explored. Interest to many chemists of organic compounds in the tripodal host has led to the development of many new receptors interesting, I hope that they will occur more and more new examples.

Acknowledgements

Author thanks the Polish Ministry of Science and Higher Education for financial support under Grants No. NN 204 338237 and N 204 005536 in the years 2009–2013.

References

1. K. Niikura, A. Metzger, E.V. Anslyn, *J. Am. Chem. Soc.* 1998, 120, 8533-8534;
2. P.A. Gale, J.L. Sessler, V. Kral, V. Lynch, *J. Am. Chem. Soc.* 1996, 118, 5140-5141;
3. I Alfonso, *Mini-Rev. Org. Chem.* 2008, 5, 33-46;
4. C. Bazzicalupi, A. Bencini, S. Biagini, E. Faggi, S. Meini, C. Giorgi, A. Spepi, B. Valtancoli, *J. Org. Chem.* 2009, 74, 7349-7363;
5. P. Ballester, *Chem. Soc. Rev.*, **2010**, 39, 3810-3830;
6. P. Mateus, R. Delgado, P. Brandão, V. Félix, *Chem.- Eur. J.* 2011, 17, 7020-7031;
7. M.T. Reetz, C.M. Niemeyer, K. Harms, *Angew. Chem., Int. Ed. Engl.* 1991, 30, 1472-1474;
8. N.-S. Choi, S.-W. Ryu, J.-K. Park, *Electrochim. Acta* **2008**, 3, 6575-6579;
9. M.E. Amato, F.P. Ballistreri, S. Gentile, A. Pappalardo, G.A. Tomaselli, R.M. Toscano, *J. Org. Chem.* 2010 75, 1437-1443;
10. P.A. Gale, *Chem. Soc. Rev.* **2010**, 39 3746-3771;
11. A. Dalla Cort, G. Forte, L. Schiaffino, *J. Org. Chem.* 2011, 76, 7569-7572;
12. Y. Morzherin, D.M. Rudkevich, W. Verboom, D.N. Reinhoudt, *J. Org. Chem.* 1993, 58, 7602-7605;
13. A. Casnati, M. Fochi, P. Minari, A. Pochini, M. Reggiani, R. Ungaro, D.N. Reinhoudt, *Gazz. Chim. Ital.* 1996, 99-106;
14. H. Galán, M.T. Murillo, R. Quesada, E.C. Escudero-Adán, J. Benet-

- Buchholz, J. De Mendoza, *Chem. Commun.* 2010, 46, 1044-1046;
15. P.D. Beer, C. Hazlewood, D. Heseck, J. Hodacova, S.E. Stokes, *J. Chem. Soc., Dalton. Trans.* 1993, 1327-1332;
 16. B. Cameron, S.J. Loeb, *Chem. Commun.* 1997, 573-574;
 17. R.M. Duke, E.B. Veale, F.M. Pfeffer, P.E. Kruger, T. Gunnlaugsson, *Chem. Soc. Rev.* 2010, 39, 3936-3953;
 18. I. Ravikumar, P.S. Lakshminarayanan, P. Ghosh, *Inorg. Chim. Acta*, 2010, 363, 2886-2895;
 19. J. Hao, K. Hiratani, N. Kameta, T. Oba, *Supramol. Chem.* 2011, 23, 319-328;
 20. S.K. Lee, H. Kim, S. Jang, J. Kang, *Tetrahedron Lett.* 2011, 52, 1977-1980;
 21. C. Raposo, N. Perez, M. Almaraz, M. Luisa Mussons, M. Cruz Cabarello, J.R. Moran, *Tetrahedron Lett.* 1995, 36, 7-12;
 22. L. Fabbrizzi, M. Licchelli, L. Mosca, A. Poggi, *Coordin. Chem. Rev.* 2010, 254, 1628-1636;
 23. J.W. Steed, D.R. Turner, K.J. Wallace, "Core Concepts in Supramolecular Chemistry and Nanochemistry", John Wiley&Sons (2007);
 24. B. Kuswandi, Nuriman, W. Verboom, D.N. Reinhoudt, *Sensors* 2006, 6, 978-1017;
 25. P.D Beer, A.D. Keefe, *J. Organomet. Chem.* 1989, 375, C40-C42;
 26. P.D. Beer, D. Heseck, J. Hodacova, S.E. Stokes, *J. Chem. Soc., Chem. Commun.* 1992, 270-272;
 27. K. Sato, S. Arail, T. Yamagishi, *Tetrahedron Lett.* 1999, 40, 5219-5222
 28. L.A. Cabell, M.-K. Monahan, E.V. Anslyn, *Tetrahedron Lett.* 1999, 40, 7753-7756;
 29. P.D. Beer, P.A. Gale, G.Z. Chen, *Coord. Chem. Rev.* 1999, 3, 185-186;
 30. C.A. Ilioudis, D.A. Tocher, J.W. Steed, *J. Am. Chem. Soc.* 2004, 126, 12395-12402;
 31. J. W. Steed, J. L. Atwood, *Supramolecular Chemistry*, John Wiley and Sons, Ltd, West Sussex, 2009;
 32. J. L. Sessler, P.A. Gale, W.-S. Cho, *Anion Receptor Chemistry*, Royal and Society of Chemistry, Cambridge, 2006;
 33. J.V. Gavette, J. Lara, O.B. Berryman, L.N. Zakharov, M.M. Haley, D.W. Johnson *Chem. Commun.* 2011, 47, 7653-7655;
 34. K. J. Wallace, R. Hanes, E. Anslyn, J. Morey, K. V. Kilway, J. Siegel, *Synthesis* 2005, 2080-2083;
 35. G. Henrich, E. V. Anslyn, *Chem.-Eur. J.* **2002**, 8, 2219-2224;
 36. D. M. Perreault, L.A. Cabell, E.V. Anslyn, *Bioorg. Med.Chem.* 1997,

- 5, 1209–1220;
37. T. D. P. Stack, Z. G. Hou, K.N. Raymond, *J. Am. Chem. Soc.* 1993, 115, 6466–6467
38. T. Benzing, T. Tjivikua, J. Wolfe, J. Rebek, *Science* 1988, 242, 266–268;
39. S. Valiyayeettil, J.F.J.Engbersen, W. Verboom, D.N. Reinhoudt, *Angew. Chem., Int. Ed. Engl.* 1993, 32, 900–901;
40. M. Mazik, M. Kuschel, *Chem.–Eur. J.* 2008, 14, 2405–2419;
41. M. Mazik, C. Sonnenberg, *J. Org. Chem.* 2010, 75, 6416–6423;
42. F. Fernandez-Trillo, E. Fernandez-Megia, R. Riguera, *J. Org. Chem.* 2010, 75, 3878–3881;
43. K.J. Winstanley, S.J. Allen, D.K. Smith, *Chem. Commun.* 2009, 4299–4301;
44. J.V. Gavette, J.M. McGrath, A.M. Spuches, A.L. Sargent, W.E. Allen, *J. Org. Chem.* 2009, 74, 3706–3710;
45. I. Ravikumar, P.S. Lakshminarayanan, M. Arunachalam, E. Suresh, P. Ghosh, *Dalton Trans.* 2009, 4160–4168;
46. C. Jia, B. Wu, S. Li, X. Huang, Q. Zhao, Q.-S. Li, X.-J. Yang, *Angew. Chem., Int. Ed.* 2011, 50, 486–490;
47. N. Busschaert, P.A. Gale, C.J.E. Haynes, M.E. Light, S. J. Moore, C.C. Tong, J.T. Davis, W.A. Harrell, *Chem. Commun.* 2010, 46, 6252–6254;
48. L. H. Wei, Y.B. He, J.L. Wu, H.J. Qin, K.X. Xu, L.Z. Meng, *Chin. J. Chem.* 2005, 23, 608–612;
49. M. Allevi, M. Bonizzoni, L. Fabbrizzi, *Chem.- Eur. J.* 2007, 13, :3787-3798;
50. R. Vilar, *Recognition of Anions*, 2008, Springer-Verlag, Berlin, Heidelberg;
51. Y. Bai, B.-G. Zhang, J. Xu, C.-Y. Duan, D.-B. Dang, C.-J. Liu, Q.-J. Meng, *New J. Chem.* 2005, 29, 777-779;
52. S.K. Kim, N.J. Singh, S.J.; Kim, H.G. Kim, J.K. Kim, J.W. Lee, K.S. Kim, J. Yoon, *Org. Lett.* 2003, 5, 2083-2086;
53. J. Yoon, S.K. Kim, N.J. Singh, J. Lee, Y.J. Yang, K. Chellappan, K.S. Kim, *J. Org. Chem.* 2004, 69, 581-584.

Chapter 10

Biological and chemical properties of semduramicin

Radosław Pankiewicz and Bogusława Łęska

Adam Mickiewicz University, Faculty of Chemistry,

Grunwaldzka 6, 60-780 Poznań, Poland

Ionophorous antibiotics are a wide class of natural and artificial metal cation carrier bioactive molecules. The most interesting feature of this group is the ability to complex ions and transport them through the natural and artificial membranes. Ionophores are host molecules that bind ionic guests and transport them across a membrane, such as a bulk organic phase or phospholipid bilayer [1]. These antibiotics can transport and regulate the concentrations of the main biological cations such as lithium, sodium, potassium, calcium [2] and some anions (Cl^-) or neutral molecules (NH_3). The molecule of ionophore contains a lipophilic skeleton and hydrophilic groups ($-\text{OH}$, $\text{C}=\text{O}$, $\text{C}-\text{O}-\text{C}$). Thanks to this structure, the ionophore can induce conformational changes upon complex formation that involve the ion capture in a hydrophilic. The ionophore molecule is soluble in a hydrophobic or membrane phase. Ionophore can release (or dissolve) a charged ion inside the lipid membrane. The ionophore as a host compound captures the guest ion at the aqueous – hydrophobic phase interface. The mechanism of the ion transportation is as follows. The host (ionophore) molecule dissolved in the hydrophobic phase captures the ion at the interface and then the complex diffuses in the lipid membrane. When the complex reaches the other side of the membrane, the host opens and the ion is released into the water phase. The empty host diffuses back to the other side of the membrane and the cycle is repeated until reaching equilibrium. Many classification systems of the ionophores have been proposed, but the most appropriate is that dividing this group into two subclasses of cyclic and noncyclic ionophores. Many of them show preferences in forming complexes, e.g. lasalocid forms complexes with Na^+ ions four orders of magnitude more stable than with K^+ cations. These features are useful for molecular recognition and make basis for development of ion receptors and ion-selective electrodes.

1. Structure and chemical properties of semduramicin

Semduramicin is a noncyclic, polyether ionophore. In its structure we can distinguish four six-membered pyrane rings and three five-membered furan rings (Fig.1). Its chemical properties is determined by one carboxylic group and four hydroxyl group. Carbon atom No. 13 is a spiro atom.

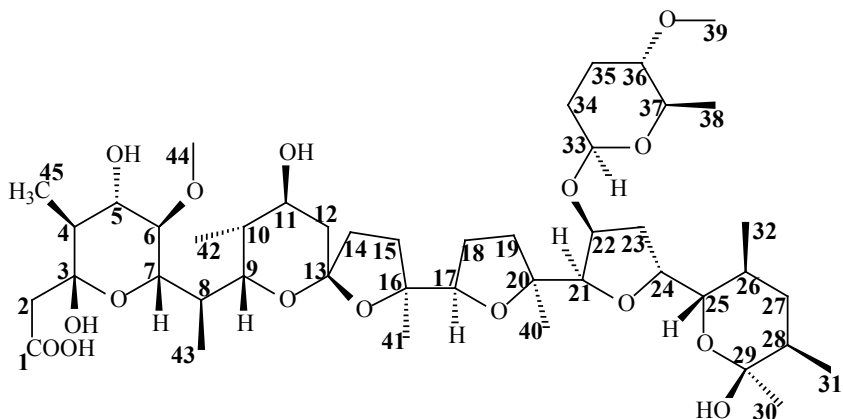


Figure 1. Structure of semduramicin

Thanks to this properties semduramicin is able to dynamically adjust to the cation to form a complex. The obtained structure, like in many other polyether ionophores, is a pseudo-ring. This structure is formed thanks to the formation of hydrogen bond of head-to-tail type between the carboxyl group and the hydroxyl group attached to the last pyrane ring. Study of this structure is difficult because of problems with getting the crystalline form of semduramicin. Only quantum-mechanical simulations enable visualization of the structures of the complexes (Fig.2) and determine their structural parameters. This is characteristics ionophore structure, hydrophilic groups are directed inside to the cation. Hydrophobic alkyl groups are directed outside, creating lipophilic “surface” of the molecule.

Semduramicin is naturally occurred from *Actinomadura roseorufa* as sodium salt [3]. It is crystalline, non-volatile, white solid, m.p. 170°C. Molecular weight: 895 Da.

Semi-empirical calculations (PM5) and the geometric optimization were performed using the Scigress 2.1.0 program [4].

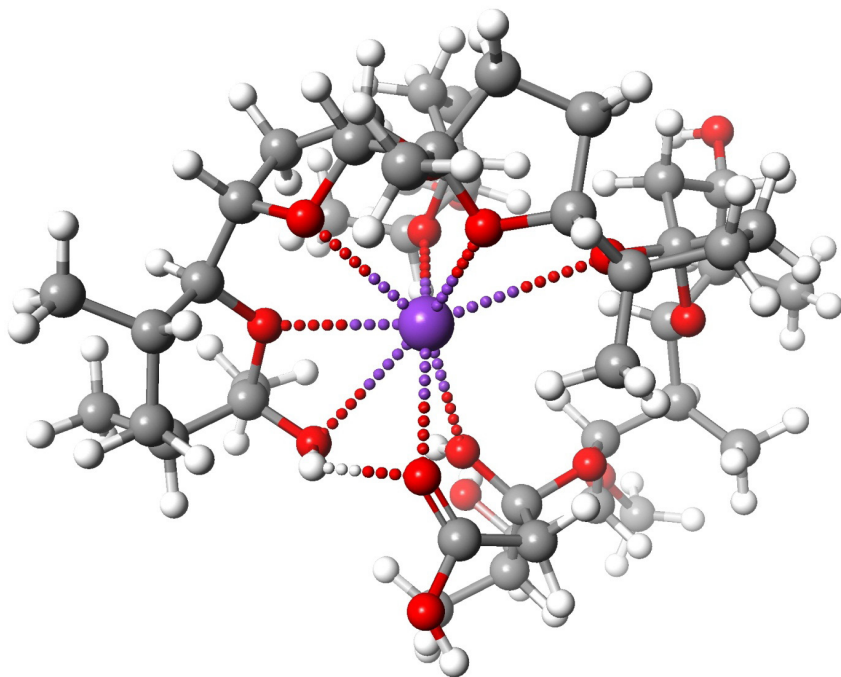


Figure 2. Calculated by PM5 method complex semduramicin with potassium cation [5]

The DFT calculations were performed using the GAUSSIAN 03 package [6]. The geometries were optimized according to Becke's three parameters hybrid method with the Lee, Yang and Parr correlation functional (B3LYP) [7]. The ^{13}C NMR chemical shifts was calculated using GIAO method using the same base set [5]. The ^{13}C NMR data was collected in Table 1. The theoretical values are in good correlation with the experimental data obtained by Sharp and coworkers [8]. In known literature there are no complete ^{13}C NMR data of semduramicin.

Hydrolysis of semduramicin in water solutions was determined in pH 5, 6, 7, 8 and 9 aqueous buffers [9]. Semduramicin sodium hydrolyses under acidic conditions with a half-life of 11-36 days, reaction is faster at lower pH. In neutral conditions, it is moderately stable, half-life 90 days. Half-life is prolonged to 77-115 days in alkaline conditions. Sharp obtained additional evidence of hydrolysis from control samples (dark) from photolysis experiments where the only degradation path is via hydrolysis. Data were obtained at 34°C and were

13.7 days (pH=6), 31.2 days (pH=7) and 17.4 days (pH=9).

Table 1. ^{13}C NMR chemical shifts [δ_c (ppm)]

Atom No.	Theoretical data	Experimental data	Atom No.	Theoretical data	Experimental data
1	157.48		24	82.29	
2	47.19		25	77.77	
3	94.82		26	35.44	
4	51.37		27	36.43	
5	75.61	74.9	28	40.61	
6	81.58	82.1	29	94.41	
7	70.64	66.9	30	27.26	
8	40.33		31	21.25	
9	65.52		32	26.02	
10	37.12		33	97.41	
11	70.04		34	34.17	
12	38.72		35	26.98	27.0
13	103.46		36	78.22	80.0
14	42.87		37	72.50	74.7
15	39.19		38	23.57	
16	86.34		39	52.66	56.9
17	83.75		40	29.05	
18	35.23		41	25.77	
19	39.10		42	17.39	
20	84.92		43	17.02	
21	91.10		44	57.80	59.1
22	78.22		45	18.29	
23	39.30				

2. Biological properties

2.1. Coccidiosis

Coccidiosis is a parasitic disease of animals (cattle, poultry, rabbits, pigeons), caused by protozoa living in the intestinal epithelium. This disease

occurs wherever animals are kept in small areas, contaminated by coccidial oocysts. Coccidiosis are in the form of intestinal and liver. They are caused by *Coccidia* - parasite that lives in the intestinal epithelium. Coccidiosis exacerbated the poor conditions in the industrial farming and animal husbandry. Pathogen are protozoa belonging to the order *Coccidia*, *Eimeria*. There are seven main affecting poultry species (*E. acervulina*, *brunetti*, *mitis*, *necatrix*, *praecox*, *tenella* and *maxima*), five other species specific to turkeys (such as *E. meleagrimitis*) and six to rabbits (eg, *E. stiedae*) [10].

Historically, the poultry showed the greatest susceptibility to coccidiosis due to the intensive nature of most of the poultry industry. In poultry, coccidiosis is caused by *Eimeria* spp oocysts., of which eight species are causing serious clinical illness. Further 22 species cause less severe clinical effects. Symptoms of coccidiosis in poultry may be one or more of the following: bloody diarrhea, high mortality, reduced feed and water consumption, emaciation and loss of egg production. Most of the economic loss that is associated with coccidiosis is incurred prior to diagnosis. This makes prevention more important than treatment [11].

Coccidiostats are an important group of chemotherapeutic agents used in animal production, especially poultry. They are used in the prevention of coccidiosis, a disease which is the major health and economic problem. Currently, the administration considered the most effective way of coccidiostats for combating this disease. Wide range of available drugs is to prevent and treat coccidiosis. The first drugs used to treat coccidiosis were sulphonamides. Then replace them such as: clopidol, bacitracin and methylbenzoquate, nicarbazin, toltrazuril and diclazuril, robenidine, halofuginone, amprolium and ethopabate. Currently, the most commonly used compounds are carboxylic acid ionophores [10-12].

Over the last 40 years coccidiosis in farmed animals has been controlled by adding substances to feed and since 1970 the Community regulates and authorizes coccidiostats as feed additives under Directive 70/524/EEC of 23 November 1970 concerning additives in feeding-stuffs. The Directive was fully reviewed in 2003 and Regulation (EC) No 1831/2003 represented a major overhaul of the existing EU legislation on feed additives [12].

In animals, in whom prophylactic coccidiostats used, they are delivered in the form of feed additives. Broilers get them through the whole period of fattening before slaughter subject to a grace period. For chickens reared for laying coccidiostats used to produce the time of natural immunity against coccidiosis - usually for 12 - 16 weeks of age.

Currently there are 11 different coccidiostats which have been granted 28

different authorizations for different species and under certain conditions the application. The products are currently authorized for chickens, turkeys and rabbits. These coccidiostats can be divided into two main types. In the first group are ionophores, that should be the following six substances: monensin sodium, lasalocid sodium, maduramicin ammonium, narasin, salinomycin sodium and semduramicin sodium. The second group are four other synthetic products, which do not have ionophoric properties: decoquinate (a compound belonging to the chemical group quinolones), robenidine hydrochloride (chemical group guanidines), halofuginone (chemical group quinazolinones) and diclazuril (chemical group benzene acetonitriles) and nicarbazin. At present, none of the EU histomonostats are not admitted or used as feed additives. All coccidiostats have been subjected to safety assessment carried out by EFSA or by the Scientific Committee on Animal Nutrition [10-12].

The use of coccidiostats as feed additives is associated with lower than for the control of veterinary drugs during their manufacture and distribution. Feed additives in the form of prefixes containing a large (of the order g / kg) concentrations of coccidiostat can be bought by farmers and their own mixed with feed.

The commercial production index is a method of controlling coccidiosis in addition of coccidiostats to the feed at the authorized level and to compliance with recommended hygiene requirements. In general, coccidiostats should be administered lifelong animal (for chickens for fattening) in order to protection against re-infection, that is pervasive effect coccidiosis in the oocyst stag [12].

Availability and continued use of prophylactic coccidiostats contributed significantly to the development of poultry production with a high level of health and welfare. The introduction of the first ionophore coccidiostat (monensin) in the seventies of the twentieth century was a significant achievement in the control of coccidiosis. Earlier outbreaks were common, and its treatment or prevention more difficult, since were available only to non-ionophoric coccidiostats, much less effective due to the rapid development of parasite resistance.

Semduramicin, this is one of ionophores used successfully as veterinary premix used against coccidiosis, that disrupts the function of cell membranes and as a consequence of this action adversely affects, this action has a negative effect on the development of coccidiosis. The product is registered as commercial name AVIAX contains semduramicin (mycelial) at 50 g/kg, is to be used for the control of coccidiosis (the disease caused by coccidia) in broiler chickens. The premix (AVIAX, AVIAX II) is used in two forms, crystalline and mycelial. The crystalline semduramicin has been purified from the mycelial form, which remains associated with the mycelium mass of fungi, from that

is produced. Semduramicin is currently registered for use as an anticoccidial in Peru, Argentina, Brazil, Mexico, Malaysia, Singapore, Venezuela, Saudi Arabia, Algeria, Chile, Uruguay, Ecuador, Colombia, Korea, Poland, Bolivia, Guatemala, Nicaragua, El Salvador, Panama, USA, Dominican Republic, Costa Rica, Kenya, Japan, Turkey, Indonesia, Canada, South Africa, New Zealand and Honduras [9].

2.2. Assessment of semduramicin toxicology

Semduramicin characterized by a large, acute oral and inhalation toxicity, slightly irritating to eyes and damaged skin, but it does not irritate the skin intact and does not cause skin sensitization. In studies conducted in dogs and rats after administration of multiple semduramicin found that muscle degeneration occurring after the diet is secondary to its effect on cell membranes. Although the dosage of semduramicin caused damage the peripheral nervous system and affects the sight of dogs, similar effects were not reported in rodents. And in the case of rats it was found that semduramicin may induce cancer or have an impact on birth defects. Metabolism studies indicate that semduramicin is absorbed after oral dosing and metabolized to a small extent [9-12].

Four weeks and 3 - month studies in rats and dogs, and studies of reproduction and fertility in rats with mycelial semduramicin, showed no significant differences in toxicity between the mycelial and crystalline forms semduramicin. Based on the evaluation of toxicity and probable residue levels, it was concluded that no adverse effects on human health.

Toxicological database for semduramicin conducted using animals, are quite extensive. When interpreting the data, it should be noted that toxicity tests were conducted generally at doses that are high in comparison with those that would cause problems in humans. The use of high doses increases the likelihood that potentially significant toxic effects will be identified. Toxicity tests should also indicate dose levels at which the specific toxic effects are unlikely.

These doses as No-Observable-Effect-Level (NOEL - the highest concentration or amount of a substance to cause no detectable alteration of morphology, functional capacity, growth development or life span of the most sensitive test organism) are used to develop acceptable limits for dietary or other approaches, in which adverse health effects in humans would be expected. Studies have been conducted for both forms semduramicin (crystalline and mycelial). Metabolism studies indicate that semduramicin is absorbed after oral dosing and accumulates in the liver. Identified metabolites in the liver, feces and bile were closely related to semduramicin. Table 2 indicates the total residue figures in the different tissues and organs during the withdrawal period for

chicken. Both studies showed that the highest residue levels were found in the liver, the total residues being about four times higher than in the fat, the next highest concentration. Therefore the liver is the target tissue [9].

Table 2. Total residues of semduramicin-¹⁴C in chicken tissues fed a 25 ppm supplemented feed for 7 days (expressed as mg equivalent semduramicin / kg tissue, mean value n= 6) [10]

Time (hrs)	Liver	Kidneys	Muscle	Fat	Skin (+ Fat)
6	0.273	0.051	0.015	0.074	0.057
12	0.112	0.027	0.007	0.027	0.022
24	0.058	0.012	0.003	0.015	0.015
48	0.031	0.006	0.002	0.011	0.011
120	0.019	0.004	0.001	0.010	0.009

In laboratory toxicity on animals were carried out in different species in various periods and with relevant endpoints. In acute toxicity studies, semduramicin been classified as toxic to rats and mice (oral) LD₅₀ values from 5 to 100 mg/kg and very toxic by inhalation (inhalation) of 67 mg/m³ LC₅₀ (rat). No evidence was found for eye irritation or skin a rabbit. In beagle dogs, toxicity tests conducted for five weeks, six months and one year, recorded data, which would indicate muscle damage, but without apparent effect on the heart. The lowest NOAEL (No-observed-adverse-effect-level) was 0.3 mg/kg/day. Studies in rats have shown a marginal and non-specific effects (reduced protein and sodium concentration) at 0.25 mg / kg / day in a two year toxicity/carcinogenicity study and there was no evidence for carcinogenicity. Thus, the overall lowest NOAEL was set at 0.125 mg/kg. Results from studies in rats and rabbits have not shown significant deleterious effects on reproduction, NOAEL is 0.5 mg/kg/day based on maternal fetal /fetotoxicity [10, 14, 15].

Are therefore need to worry about some danger for the consumer? What is the metabolic fate of semduramicin in chickens for fattening? Does this use result in the presence of residues in meat? If so, what is the qualitative and quantitative composition of these residues? In summary, these studies the lowest NOAEL of 0.125 mg/kg body weight was established in the two year rat study. Applying a safety factor of 100 this results in an ADI (the daily intake of a chemical, which, during an entire lifetime, appears to be without appreciable risk to the health of the consumer) of 1.25 µg/kg body weight (i.e. 0.075 mg/day for a 60 kg person) [10, 14, 15].

However there is a risk for the user primarily on the „ground” inhalation

because semdurmicin shows a significant inhalation toxicity (LC_{50} in rats is 67 mg/m³). Therefore, additional precautions (mask) are still recommended [10-15].

The genotoxicity studies were performed. For example, Ames/S. typhimurium tests with semduramicin and urine of semduramicin treated mice, with and without metabolic activation, respectively, were both negative, although no toxicity was seen. In a number of genotoxicity studies conducted with semduramicin sodium, or mycelial semduramicin, there was no evidence to suggest that semduramicin damages genetic material. All of these tests produced consistently negative results and therefore the compound is considered to be nongenotoxic [9-12].

2.3. Environmental assessment

Analyzing toxicity of feed additives containing semduramicin worth considering, what are the nature and the persistence of the excreted products derived from semduramicin and can these products be prejudicial to the environment? The use of semduramicin sodium is not expected to have a significant impact on the environment when used as directed. The potential exists for some adverse effects where contaminated manure is applied to very sandy soils either through leaching to groundwater or through collection of run-off water in small bodies of water.

Semduramicin sodium is rapidly hydrolyzed in acidic media, but is relatively stable under neutral and alkaline. This compound is immobile in soils with low sand content, but is more mobile, as the sand content increases. The binding semduramicin sodium is associated more strongly with the mineral fraction of soils, compared with the organic fraction. Semduramicin is slightly toxic to fish and daphnia, algae, however, is not toxic to earthworms and soil microorganisms, but moderately toxic to the growth of seedlings. The ecotoxicity of semduramicin sodium suggests that the greatest area of concern is to plants and freshwater algae. It is used as a feed additive for chickens for fattening, so it can be released into the environment. Fortunately Semduramicin expected concentration in the environment, both in soil and in water, is much lower than concentrations shown to be toxic to soil bacteria, earthworms, plants and various species of fish, daphnia and algae. Semduramicin potentially suitable for groundwater leaching in soils very sandy, especially if the water table is shallow.

Mixing producing feed, also involved in the mixing prefixes coccidiostat in feed, are not as rigorously controlled as producing medicated feed mixing. Mistakes during the production and administration of feed containing coccidiostats have a large impact on the levels of residues of these substances

in food of animal origin. The relatively high percentage of samples of eggs and poultry tissues containing coccidiostats is a serious problem in many European Union countries [10-13].

In order to protect the health of consumers introduced maximum limits for feed contaminants coccidiostats which are supposed to be free from this type of feed additives [16-18]. The principle that such a feed may not contain more than 1% or 3% of the highest concentrations permitted for use in feed for target animals (Table 3).

Table 3. Acceptable levels of coccidiostats in feed in the European Community - the declared content in feed for target animals (List of the authorised additives, 2004) and maximum limits (ML) in feed for animals other than target [16-18]

Coccidiostat	ML - equine species, turkeys, laying birds and chickens reared for laying (1% the highest concentrations permitted for use in feed for target animals) [mg/kg]	ML - other animal species (3% the highest concentrations permitted for use in feed for target animals) [mg/kg]
Decoquinat	0.4	1.2
Diclazuril	0.01	0.03
Halofuginone hydrobromide	0.03	0.09
Lasalocid sodium	1.25	3.75
Maduramicin ammonium alpha	0.05	0.15
Monensin sodium	1.25	3.75
Narasin	0.7	2.1
Nicarbazin	0.5	1.5
Robenidine hydrochloride	0.7	2.1
Salinomycin sodium	0.7	2.1
Semduramicin sodium	0.25	0.75

The introduction of these regulations is the joint responsibility of feed manufacturers for food safety in the field of residues of coccidiostats. For the first time in an official document because it was cross-contamination as a cause of residues of coccidiostats and set out clearly what level of contamination of feed will not (should not) result in illegal residues in food. Finally feed should develop procedures for assessing the degree of cross-contamination and implement remedial measures to prevent transmission of the next generation of coccidiostats

to the feed lot. Frequently the removal of active substances used in production lines are called. cleaning compound. Checking the contents of coccidiostats in compound cleaning and proper disposal is therefore necessary to meet the requirements for acceptable levels of contamination of feed coccidiostats. Both the official laboratories and quality control laboratories in the feed labels must as soon as possible to develop and validate methods for the determination of coccidiostats in feed at levels required by law [10-12].

A very important point was the development and validation of methods the determination of coccidiostats in feed at levels required by law. In the case of the most commonly used coccidiostats ionophoric not should this be a problem due to very low values of ML and the availability of relatively cheap methods using chromatography with post-column liquid chromatography with derivatization.

For some chemical coccidiostats, whose values are much lower ML, the determination as low concentrations in the feed is possible by using only a very sensitive and selective methods such as liquid chromatography coupled mass spectrometry. There are many scientific studies showing this problem [16, 19].

2.4. Methods for determining contamination of feed coccidiostats

In the case of methods for the determination of coccidiostats in feed for target animals are the most important parameters of the method accuracy and precision, allowing to obtain reliable quantitative results. When determining the most important pollutants is high sensitivity of the method, because for some coccidiostats introduced maximum limits are very low.

For some compounds, the methods described in the regulation or in national standards can be relatively easily and quickly adapted to the determination of lower concentrations. This includes coccidiostats ionophoric. Any modification of the procedure, allowing for lower detection limit, however, requires a full validation of the method.

Using a simple modification of existing methods is not always possible. In some cases it is necessary to use other, much more sensitive analytical techniques. In this case the technique of choice is liquid chromatography coupled with mass spectrometry. An additional advantage of LC-MS technique is its versatility, it allows the simultaneous determination of virtually all of coccidiostats (both chemical and ionophoric) [20-27].

An excellent example is the use of liquid chromatography single quadrupole mass spectrometry (LC-MS) as a method for the determination of the feed additive semduramicin in poultry feed (Fig. 3). This method was developed and single-laboratory validated and was selected as a real case scenario to outline the different steps that may be needed whenever the standardisation of an analytical

method in the field of methods of analysis for animal feeding stuffs is attempted. In this manuscript [27] the main achievements reached within the development and the single laboratory validation of an analytical method for the determination of semduramicin in feeding stuffs are detailed.

The method has been successfully validated for the determination of semduramicin concentrations ranging between half of the minimum authorized concentration (10mgkg^{-1}) to twice of the maximum authorized concentration (50mgkg^{-1}). A good relative standard deviation for repeatability (RSD_r) varying from 2.8 to 3.2% has been obtained whereas the relative standard deviation for intermediate precision (RSD_{Int.}) ranged from 3.7 to 7.3%.

3. Conclusion

Coccidiostats authorized for use in animal feed are not used for treating humans. Safety of the coccidiostats that are currently authorized, has been recently undergo a comprehensive evaluation, mainly by the European EN 7 EN Food Safety Authority (EFSA). This evaluation includes the lack of harm to animals, consumers and users, as well as for the environment. The fact that Regulation (EC) No 1831/2003 regulates the determination of the highest residue limits (MRLs) for residues of the additive the appropriate food of animal origin means that thanks to a specific Over the past few years, the MRLs currently exist more efficient and transparent than prior methods of controlling the use of coccidiostats in feed.

In accordance with Regulation (EC) No 183/2005 of the European Parliament and Council of 12 January 2005 laying down requirements for feed hygiene, establishments manufacturing or placing on the market coccidiostats, histomonostats, premixtures and compound feedingstuffs containing these additives are approved by the competent authority for this activity. These provisions mean in practice that, in principle, farmers wishing to use coccidiostats and histomonostats will obtain only ready-to-use mix complete or complementary feedingstuffs produced by approved manufacturers of compound feed. For example in Sweden, in force surveillance programs to detect the increase in antimicrobial resistance antimicrobial, associated with the use of coccidiostats as feed additives for which no date has not been observed signs of such an increase in resistance [12].

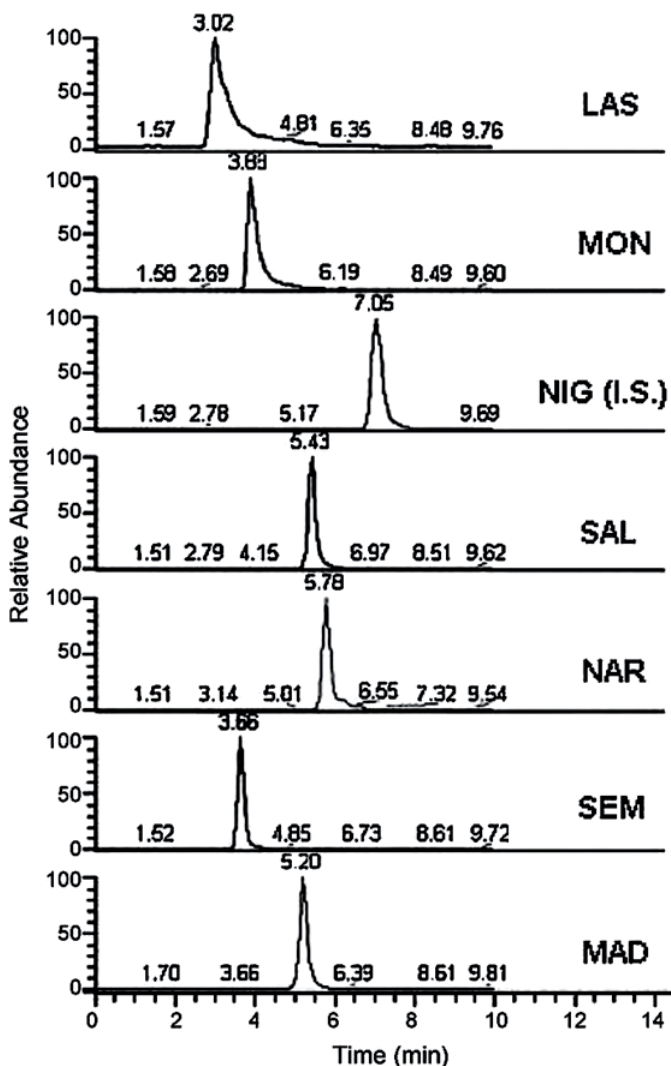


Figure 3. Chromatograms of semduramicin along with the other five ionophore coccidiostats in poultry feed plus the internal standard used for quantification (nigericin). Standard mixture of the seven compounds at equivalent concentration in acetonitrile. Selected ion monitoring (SIM) of the respective molecular ammonium adducts. Mobile phase NH_4COOH 20mM:MeOH (10:90); flow rate 0.25 ml min⁻¹; probe temperature 375°C; cone voltage 80V; needle voltage 2.7 kV [27].

Acknowledgements

This work was supported by research funds in years 2009-2013 from the Polish Ministry of Science and Higher Education as scientific grant N 204 005536.

References

1. R. Ferdani, G.W. Gokel, *Encyclopedia of Supramolecular Chemistry* 2004, DOI: 10.1081/E-ESMC 120012686, p 760.
2. D.W. Urry, "Potassium-39 NMR of K⁺ interaction with the gramicidin channel and NMR-derived conductance ratios for Na⁺, K⁺ and Rb⁺", *Top. Curr. Chem.* 128 (1985) 175.
3. "Environmental assessment of the use of semduramicin sodium premix in the feed of broiler chickens for the prevention of coccidiosis", Pfizer Inc., April 1993.
4. MO-G Version 1.1, Fujitsu Limited, Tokyo, Japan (2008).
5. R. Pankiewicz *unpublished results*.
6. Gaussian 03, Revision D.01.
7. A.D. Becke, "Density-functional thermochemistry. III. The role of exact exchange", *J. Chem. Phys.* 98 (1993) 5648.
8. T.R. Sharp, J.A. Wood, A. Grizzuti, "Semduramicin and two desmethyl analogs: ¹³C NMR and FAB mass spectral correlations", *Tetrahedron Lett.* 34 (1993) 6197-6200.
9. National Registration Authority for Agricultural and Veterinary Chemicals 2001 ISSN 1443-1335.
10. European Commission Health & Consumer Protection Directorate-general, "Report of the Scientific Committee on Animal Nutrition on the use of Semduramicin sodium in feeding stuffs for Chickens for fattening", 17 April 2002.
11. [C. T. Elliott, D. G. Kennedy and W. J. McCaughey, "Methods for the detection of polyether ionophore residues in poultry", *Analyst* 123 (1998) 45R-56R.
12. "Report from the commission to the council and the European Parliament on the use of coccidiostats and histomonostats as feed additives", Brussels, 5.5.2008COM(2008)233 final.
13. European Committee for Standardization, Animal feeding stuffs – "Determination of nicarbazin - High-performance liquid chromatographic method", Draft prEN 15782, 2008.
14. "Freedom of information summary Original new animal drug application NADA 141-281 AVIAX II Semduramicin Type A Medicated Article

- Broiler Chickens”, December 7, 2007.
15. “Environmental assessment of the use of semduramicin sodium premix in the feed of broiler chickens for the prevention of coccidiosis”, Pfizer Inc., April 1993.
 16. „Farmacja weterynaryjna– zarządzanie, monitoring, farmakoterapia, metody badań weterynaryjnych produktów leczniczych i pasz leczniczych” W. Cybulski ISBN 978-83-89946-31-7 [*polish*].
 17. “Commission Directive 2009/8/EC amending Annex I to Directive 2002/32/EC of the European Parliament and of the Council as regards maximum levels of unavoidable carry-over of coccidiostats or histomonostats in non-target feed”, OJ L 40 (2009) 19-25.
 18. Commission Regulation (EC) No. 124/2009 of 10 February 2009 “Setting maximum levels for the presence of coccidiostats or histomonostats in food resulting from the unavoidable carry-over of these substances in non-target feed”, OJ L 40 (2009) 7-11.
 19. Mortier L., Daeseleire E., Van Peteghem C.: “Liquid chromatographic tandem mass spectrometric determination of five coccidiostats in poultry eggs and feed”, J Chromatogr B 820 (2005) 261-270.
 20. M. Cronly, P. Behan, B. Foley, E. Malone, P. Shearan, L. Regan, “Determination of eleven coccidiostats in animal feed by liquid chromatography–tandem mass spectrometry at cross contamination levels” Anal Chim Acta 700 (2011) 26– 33.
 21. Olejnik M., Szprengier-Juszkiewicz T., Kozak A., Wiśniewska-Dmytrow H., Jedziniak P., Żmudzi J.: „Wnioski z realizacji Krajowego Programu Badań Kontrolnych w zakresie pozostałości kokcydiostatyków w żywności pochodzenia zwierzęcego w latach 2003-2007”, W: Kwiatek K. (red): „Bezpieczeństwo pasz dla bezpieczeństwa żywności”, Puławy 2007, pp. 148-151 [*polish*].
 22. U. Vincent, M. Chedin, S. Yasar, C. von Holst, “Determination of ionophore coccidiostats in feedingstuffs by liquid chromatography–tandem mass spectrometry Part I. Application to targeted feed”, J. Pharmaceut. Biomed. 47 (2008) 750–757.
 23. U. Vincent, Z. Ezerskis, M. Chedin, C. von Holst, “Determination of ionophore coccidiostats in feeding stuffs by liquid chromatography–tandem mass spectrometry. Part II. Application to cross-contamination levels and non-targeted feed”, J. Pharmaceut. Biomed. 54 (2011) 526–534.
 24. E. A. Glazer, D. A. Koss, J. A. Olson, A. P. Ricketts, T. K. Schaaf, and R. J. Wiscount, Jr., “Synthetic Modification of a Novel Microbial Ionophore:

- Exploration of Anticoccidial Structure-Activity Relationships”, *J. Med. Chem.* 35 (1992) 1839-1844.
25. R. P. Schneider, M. J. Lynch, J. F. Ericson, and H. G. Fouda, “Electrospray Ionization Mass Spectrometry of Semduramicin and Other Polyether Ionophores”, *Anal. Chem.* 63 (1991) 1789-1794.
 26. E. Dubreil-Chéneau, M. Bessiral, B. Roudaut, E. Verdon, P. Sanders “Validation of a multi-residue liquid chromatography–tandem mass spectrometry confirmatory method for 10 anticoccidials in eggs according to Commission Decision 2002/657/EC”, *J Chromatogr. A*, 1216 (2009) 8149–8157.
 27. M. J. González de la Huebra, U. Vincent, C. von Holst, “Determination of semduramicin in poultry feed at authorized level by liquid chromatography single quadrupole mass spectrometry”, *J. Pharmaceut. Biomed.* 53 (2010) 860–868.

Chapter 11

Humic acids as molecular receptors

Svetlana Khil'ko¹, Rimma Semenova¹, Grzegorz Schroeder²
and Volodymyr Rybachenko¹

¹*L.M. Litvinenko Institute of Physical Organic and Coal Chemistry NAS
of Ukraine, R. Luxemburg 70; 83-114 Donetsk, Ukraine*

²*Adam Mickiewicz University, Faculty of Chemistry,
Grunwaldzka 6, 60-780 Poznań, Poland*

Molecular receptors are defined as molecules or molecular complexes that are able to recognize and bind specific chemical groups or molecules and respond to these interactions, for example, by changing conformation. Protein macromolecules (cellular receptors) and other polymeric compounds (natural or synthetic nanoscale macrocyclic structures) able to covalently bind various substrates with formed complexes usually act as the molecular receptors.

In this paper, the salts of humic acid (HA) were considered as promising natural compounds having properties of molecular receptors. It has been known that these are nano-sized (4-16 nm) polymeric aromatic polyoxipolycarboxylic acids, able to come into ionic and donor-acceptor interactions, form hydrogen bonds, and participate in redox and sorption processes. The presence of both hydrophobic and hydrophilic fragments in the structure of these macromolecules forms surface-active properties of the HA salts. The Diagram of elementary units of the macromolecules of HA has been shown in Figure 1.

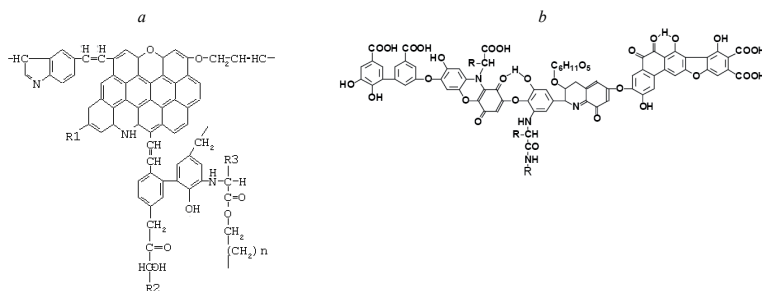


Figure 1. Diagram of elementary units of humic acids according to Orlov-Chukov (a) and Stevenson (b).

It has been known that humic acids from peat and brown coal have an expressed biological activity (hepatoprotective, antihypoxic, antitoxic properties, etc.) [1, 2]. High biological activity of humic substances is related to their signified affinity to biological membranes, the participation in ion transport, the influence on enzyme activity, and others [3-5]. Biological activity of humic acids is associated with the presence of carboxyl and hydroxyl groups in macromolecules. The high ability of low molecular weight fractions of humic acids to stimulate the ATPase activity of plasmatic membranes and induce increasing passive membrane penetrability for protons has been proven in [6].

Affinity to biological membranes of humic substances is defined by their surface activity. The adsorption isotherms of salts of native and sulfonated humic acids at the liquid-gas interface have been shown in Figure 2.

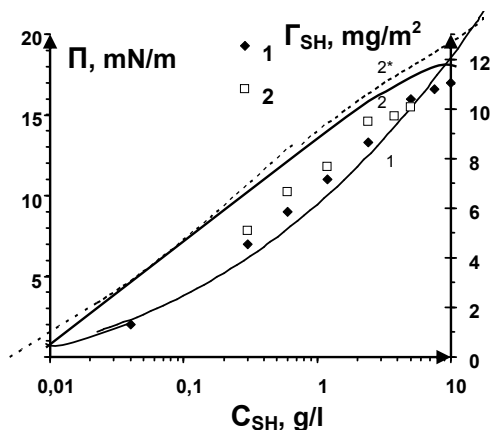


Figure 2. The dependence of the equilibrium surface pressure ($\Pi = \gamma_0 - \gamma$, γ_0 - surface tension of the solvent, γ - surface tension of the surfactant solution) of aqueous solutions of native (1) and sulfonated (2) sodium humate (SH) and calculated Π values for native SH (curve 1), Γ_{SH} adsorption for the monolayer (curve 2) and bilayer adsorption (curve 2*) on the concentration SH.

The equilibrium adsorption characteristics of humic acid salts were investigated by Du Noüy rings (Tensiometer TE-1, Lauda, Germany) at $(20.0 \pm 0.1)^\circ\text{C}$. The equilibrium surface tension was described by a model of a nonideal two-dimensional solution of the protein [7]. Experimental and calculated dependences are in good agreement.

Dilatation rheological properties of surface layers of the salts of humic acids were studied by oscillating drop shape (Tensiometer PAT 2P SINTERFACE

Technologies, Germany). Dilatation E modulus characterizes the viscoelastic properties of the surface layers of surfactants. The E module is expressed by a complex number, and includes the real and imaginary components. The real part of E_r (elasticity) reflects the accumulation of energy, and the imaginary part E_i - loss of energy in the surface layer due to the relaxation processes [8, 9].

It was shown that bilayer adsorption model better describes the experimental dependence $E=f(\Pi)$ and (in contrast to the monolayer) reflects its experimental form. This is shown by comparison of E values with the value of the limiting (high frequency) elastic modulus $E_0 = -d\gamma/d\ln\Gamma_\Sigma$ (Figure 3).

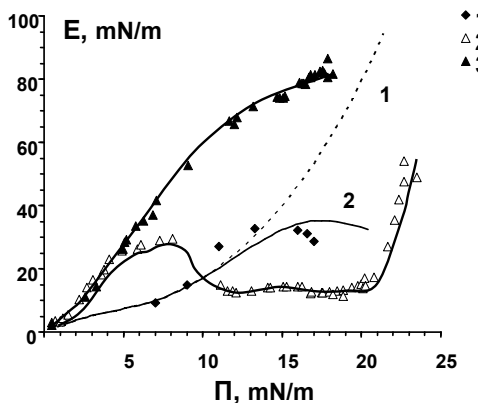


Figure 3. The E dependence on surface pressure for native sodium humates (1) and sulfonated sodium humates (2) according to data of the present work. The dependence for β -casein (3) and β -lactoglobulin (4) according to [7, 10]. Curves 1, 2 - the limit modulus of elasticity for: 1 - monolayer adsorption; 2 - bilayer adsorption.

The dependence $E=f(\Pi)$ for the SH takes an intermediate position between the globular β -lactoglobulin and flexible chain β -casein. This is consistent with the peculiarities of the molecular structure of salts of humic acids.

Such behavior of humic acids salts and proteins at the liquid-gas interface can be regarded as a possibility to apply humic compounds as cell receptors.

One of the main properties of the compounds with the receptor properties is a “molecular recognition”. It has the ability to form reversible complexes “host-guest” at the expense of intermolecular forces.

We have studied the possibility to form complexes “guest-host” between macroanions humic acid (“host”) and cationic surfactant cetyltrimethylammonium bromide (CTAB) - “guest”.

Rheological properties of the surface layers of CTAB mixtures and the SH salts at the liquid-gas interface are shown in Figure 4. High E_r values of SH/CTAB solutions indicate the formation of a highly ordered structure of the adsorbed layer that has been conditioned by the possibility to form R-COO⁻-CTA⁺ complexes. The value of E_r decreases in the CTAB concentration range from C_1 to C_2 , while E_i – increases. This might be due to the formation and collapse of the SH/CTAB aggregates of different configurations.

The possible formation of R-COO⁻-CTA⁺ complexes has been demonstrated by the potentiometric method (Figure 5), and aggregates of SH-CTAB – by the colorimetric method (at $\lambda = 430$ nm) – Figure 6.

In the potentiometric titration of an aqueous solution of sodium humate by the CTAB solution, an equilibrium pH decrease is due to the interaction of the CTA⁺ cation with the carboxyl groups of sodium humate.

As can be seen from Figure 6, mixing SH/CTAB ratio leads to the formation of soluble and insoluble aggregates. Depending on the ratio of components in a mixture of HN-CTAB soluble ($C_{CTAB} < C_2$ и $C_{CTAB} > C_3$) and insoluble aggregates ($C_2 < C_{CTAB} < C_3$) can be formed. The solubility of aggregates depends on the pH medium.

Figure 7 is an illustration of the possible configurations of the SH-CTAB complexes as a function of CTAB concentration according to the data of [11].

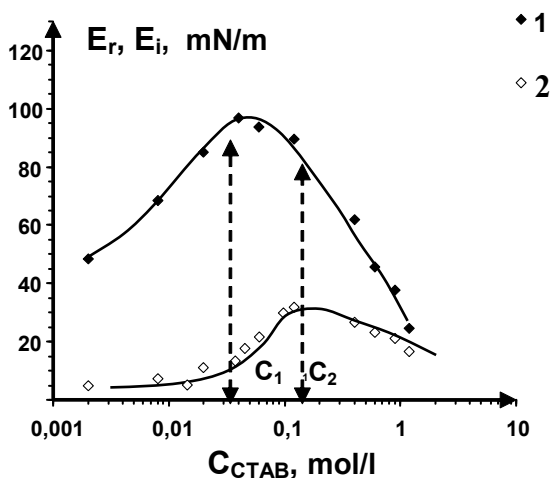


Figure 4. Elastic modulus E_r (1) and viscosity modulus E_i (2) mixtures of SH/CTAB as a function of the CTAB concentration, $C_{SH} = 0.06$ wt.%.

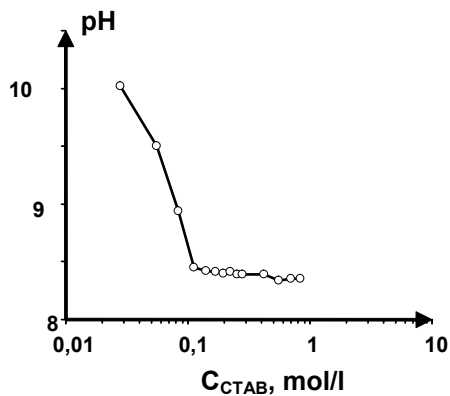


Figure 5. Curves of potentiometric titration of a sodium humate solution by the CTAB solution, $C_{SH} = 0.06\%$.

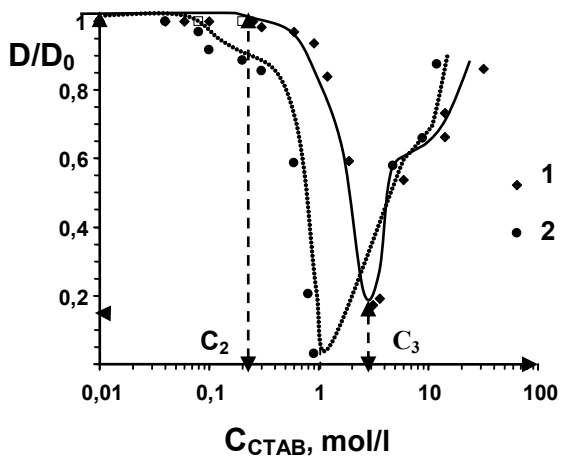


Figure 6. The ratio of the optical density of solutions of SH/CTAB and D mixtures, to an optical density of the initial solution SH, D_0 depending on the CTAB and pH concentration:

1 - pH = 11.5,

2 - pH = 4.0.

$C_{SH} = 0.6$ g/l.

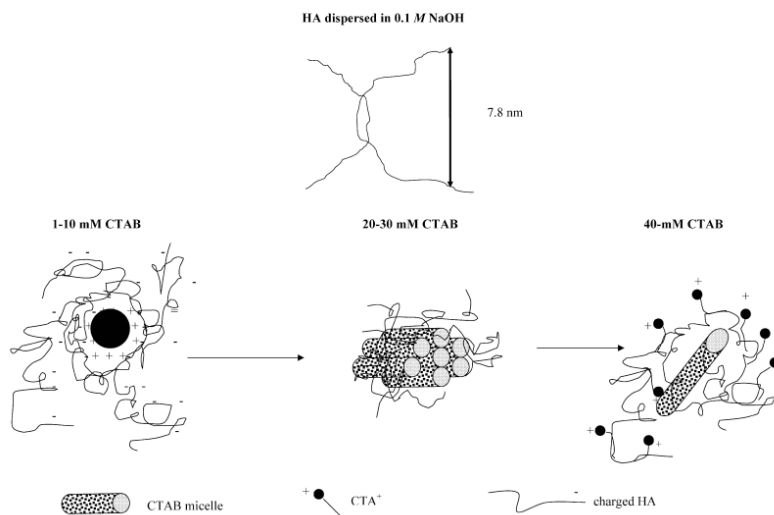


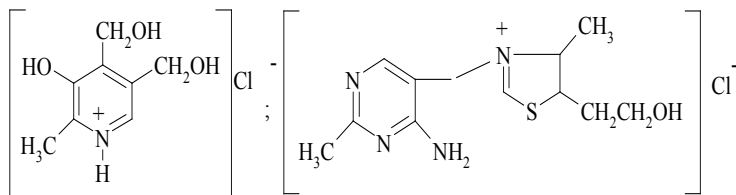
Figure 7. Illustration of possible configurations between humic acids (HA) and CTAB complexes under various experimental conditions.

It is known that the pharmacological response develops as a result of the interaction of the drug and the receptor. This interaction should be determined by the molecular entity of the drug and the receptor [12].

We considered the possibility of the interaction between humic acid macroanions (molecular receptor), and medicinal substance as an example of *B* vitamins (B_1 and B_6) by methods of calorimetric and potentiometric titration. The formation of polymer-drug complexes may be a promising fact to develop systems with a controlled release of drugs in the body [13].

Macromolecules of the humic acids contain carboxyl and hydroxyl groups capable of dissociation. Humic acids are assigned to weak polyelectrolytes. The dissociation constants of humic acids from brown coal were determined by potentiometric titration: for the carboxyl groups of $K = 1.58 \times 10^{-4}$ ($pK = 3.8$), for OH - $K = 3.16 \times 10^{-9}$ ($pK = 8.5$). The number of functional groups in mg/eq: for the COOH-groups - 2.35 and for OH-groups - 1.23. The number of groups per macromolecule of sodium humate makes: $-\text{COOH} \approx 50$, $-\text{OH} \approx 25$.

The interaction in a sodium humate – vitamin system was determined by calorimetric titration, by measuring the amount of heat (Q , J), being evolved in a cell filled with a sodium humate solution while adding a solution of vitamins [14]. The structural formula of B_1 and B_6 vitamins have been shown below.


Vitamin B₆
Vitamin B₁

Analysis of the calorimetric titration curves (Figure 8a) indicates the possibility of the interaction of one SH molecule with a large number of (n) vitamin molecules. The ratio of SH:Vitamin can reach 1:40 for B₁ vitamin and 1:25 for B₆ vitamin. The n value should be related to a number of active carboxyl groups ($-\text{COO}^-$) in the SH macromolecule. As it follows from the data of potentiometric titration, a number of functional groups capable of dissociation is:

$$-\text{COOH} \approx 50, -\text{OH} \approx 25 \text{ per SH macromolecule.}$$

Curves of potentiometric titration of 1 % solution of sodium humate by 5% solutions of B vitamins have been shown in Figure 8b. Reduction of the pH of the SH solution in relation to vitamins concentration indicates the interaction between molecules of vitamins and SH macromolecules. This interaction should take place between the charged groups of humic acid macroanions and positively charged groups of vitamins molecules.

This means that not all functional groups in the sodium humate macromolecules take part in the same reaction with the molecules of vitamins. It is known that humic substances can aggregate in solution [15]. The scheme of the association between the fragments of humic acids molecules according to Ghosh and Schnitzer has been shown in Figure 9 (according to [16]). The association of humic substances in solution may lead to the formation of large aggregates of macromolecules. This is determined by the ability of the humic substances macromolecules to structural transitions such as expanded chain \rightarrow statistical coil.

Changes in the structure and aggregation of the macromolecules of humic compounds have been associated with the degree of dissociation of their functional groups ($-\text{COOH}$ and $-\text{OH}$). As a result of aggregation, a part of functional groups is screened by fragments of SH molecules and is not sterically available for interaction.

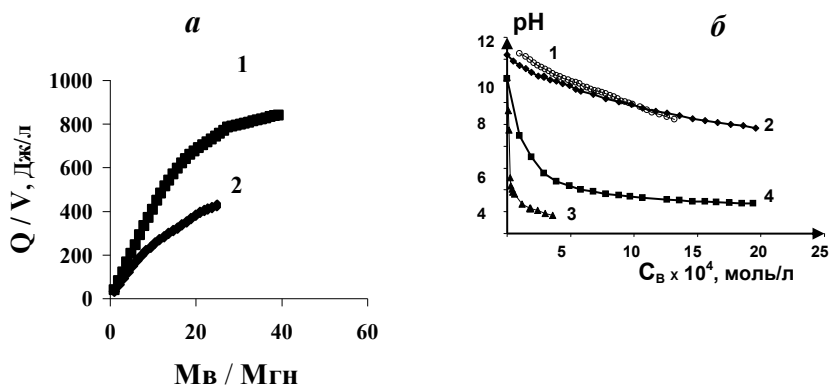


Figure 8. Calorimetric curves (a) and potentiometric curves (b) titration of 1.0 % solution of sodium humate (1, 2) and 0.0005 M NaOH (3, 4) by 5% solution of vitamins: 1, 3 - B₇, 2, 4 - B₆.

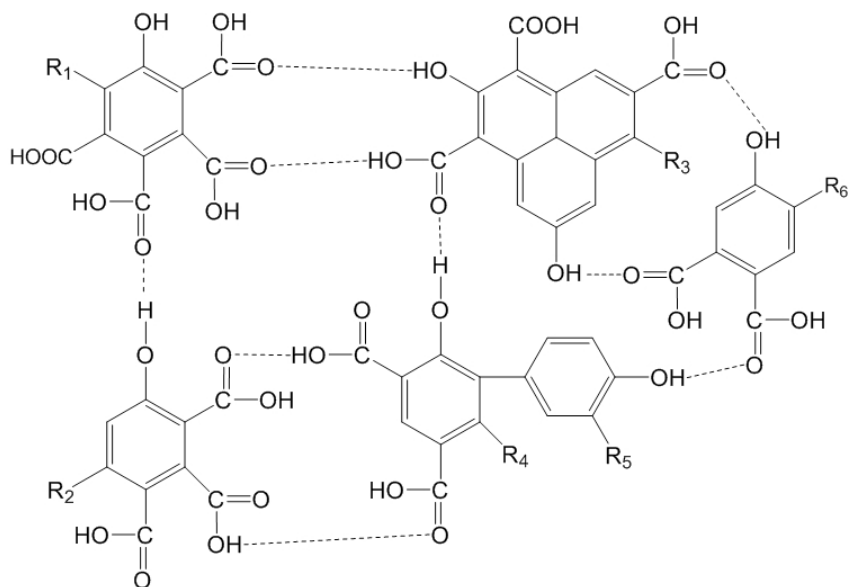


Figure 9. The scheme of the association between the fragments of the macromolecules of humic acids by Ghosh and Schnitzer [16].

References

1. Gostishcheva, M.V., Extended Abstract of Cand. Sci. (Pharm.). Dissertation, Perm, 2008.
2. Fed'ko, I.V., Gostishcheva, M.V., and Ismatova, R.R. // *Khim. Rastit. Syr'ya*. 2005. № 1. P. 49.
3. Wershaw R.L. // *Environ Health Perspect*. 1989. Vol. 83. P. 191.
4. Berkovich, A.M. // <http://www.humipharm.ru/research/prim.pdf>.
5. Pena-Mendes E.M., Havel J., Patoska J. // *J. Appl. Biomed*. 2005. № 3. P. 13.
6. Canellas L.P, Olivares F. L, Okorokova-Façanha A. L., Façanha A. R. // *Plant Physiol*. 2002. Vol. 130. P. 1951.
7. Finerman, V.B., Miller, R. // *Colloid. J*. 2005. Vol. 67, № 4. C. 437.
8. Loglio G., Pandolfini P., Miller R., Makievski A.V., Ravera F., Ferrari M. and Liggieri L. *Novel Methods to Study Interfacial Layers*. Amsterdam: Elsevier, 2001.
9. Zholob S.A., Makievski A.V., Miller R. and Fainerman V.B. // *Adv. Colloid Interface Sci*. 2007. Vol. 322. P. 134.
10. Lucassen-Reynders E.H., Fainerman V.B., Miller R. // *J. Phys. Chem. B*. 2004. Vol. 108. P. 9173.
11. Shang Ch., Rice J.A. // *J. Colloid Interface Sci*. 2007. Vol. 305. P. 57.
12. Evtyugin, G.A., Stoykova, E.E., Shamagsumova, R.V. // *Uspekhi khimii (Progress of Chemistry)*. 2010. Vol. 79. № 12. P. 1164.
13. *Sakaguchi H., Serizawa T., Akashi M.* // *J. Nanosci. Nanotechnol*. 2006. V. 6: 4: P.1124.
14. Goldstein, I.P., Guryanov E.N., Karpovich I.P. // *Russian Journal of Physical Chemistry A*. 1965. Vol. 39, № 4. P. 932.
15. Buffle J., Deloedoy M.D., Haendi L. // *Anal. Chim. Acta*. 1978. Vol. 101. P. 339.
16. Covelo E.F., Andrade M.L., Vega F.A. // *J. Colloid Interface Sci*. 2004. Vol. 280. P. 1.

Chapter 12

Synthesis and application of organic polyphosphates as drug carrier

Viktor Anischenko¹, Volodymyr Rybachenko¹, Grzegorz Schroeder²,
Constantine Chotiy¹ and Andrew Redko¹

¹*L.M. Litvinenko Institute of Physical-Organic and Coal Chemistry, National Academy of Sciences of Ukraine, Department of Spectrochemical Researches, R. Luxemburg 70; 81-134 Donetsk, Ukraine*

²*Adam Mickiewicz University, Faculty of Chemistry, Grunwaldzka 6, 60-780 Poznan, Poland*

Organic phosphates have been widely used in plastic industry as flame retardants and plasticizers, in metal industry for extraction of rare-earth metal from mineral raw materials, in nuclear industry as the extarctants in the Purex process for the recovery of uranium and plutonium from spent nuclear fuel, in medicine.

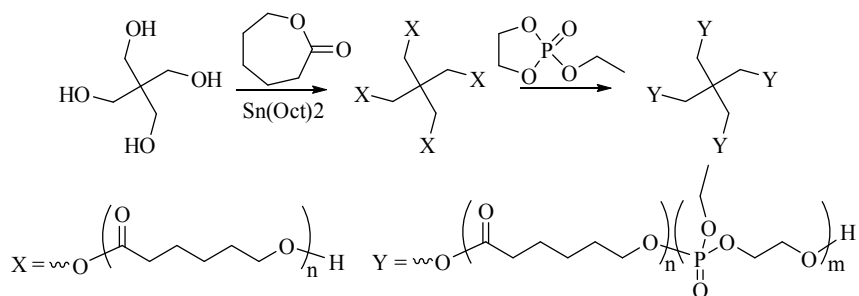
Polyphosphates as drug carrier

Though, organic phosphates cannot be used as molecular receptors by themselves, however, recently Cheng and co-workers have reported that star-shaped block copolymer of poly-(ϵ -caprolactone) (PCL) and poly(ethyl ethylene phosphate) (PEEP) can be used as receptor of drug molecule [1]. Previously was shown that biodegradable and biocompatible amphiphilic copolymers may be used as drug carriers [2-6]. This is possible as a result of self-assembling of the amphiphilic polymers into micelle in aqueous solution. The micelle core consists from aliphatic polyester which is working like reservoir for insoluble hydrophobic compounds. The hydrophilic shell is forming from ethylene glycol units and prevents the aggregations of micelles and prolongs their circulation. Such amphiphilic star-shaped polymers with linear hydrophilic arms are attractive because it may completely or partially overcome the problem of thermodynamic instability associated with micelles assembled from linear block copolymers following systemic injection. Owing to their particular architecture,

star-shaped polymers are expected to exhibit different properties compared to their linear counterparts.

Star-shaped block copolymers of poly(ϵ -caprolactone) and poly(ethyl ethylene phosphate) were obtained in two stage using the “core-first” approach (Scheme 1):

- ssPCL were prepared through ring-opening polymerization at heating of ϵ -caprolactone in bulk using pentaerythritol as an initiator and $\text{Sn}(\text{Oct})_2$ as the catalyst;
- Block copolymerization was carried out in THF at 25°C using ssPCL as macroinitiator for ring-opening polymerization of EEP and $\text{Sn}(\text{Oct})_2$ as the catalyst.



Scheme 1. Synthesis pathway of ssPCL-PEEP copolymers

The ssPCL-PEEP acceptor properties were explored in drug carrying experiments. Paclitaxel (PTX) was chosen for this researching in reasons of its hydrophobic property and high anti-cancer activity [7]. For loading PTX into the hydrophobic core of ssPCL-PEEP micelles was used a dialysis method. Experimental data is given in Table 1. The drug loading contents (DLC) were between 1.6 and 3.5%, depending on the composition of copolymers, while the drug loading efficiencies (DLE) were between 16 and 35%. The ssPCL-PEEP showed much higher DLE in comparison with analogous values for the linear counterparts (around 15%).

The drug release behavior was demonstrated by plotting the accumulative release percentages of drug versus time (Fig. 1). The observed dramatic release of drug at the beginning is explained by the diffusion of PTX located close to the surface of particles. In contrast to the linear counterpart a drug release rate is much slower in case of the copolymers and a sustained release lasting for about 2 weeks.

Polymer structure was found to be correlative to the drug release kinetics.

For example, ssPCL₃₃-PEEP₆₉ micelles gave a faster release, while PTX release from ssPCL₆₉-PEEP₅₆ micelles was slower. It is also observed that about 25-55% of loaded PTX were not released from the micelles in the test duration, which may be associated with the hydrophobic core of micelles, as observed by other groups [8].

Table 1. Effect of copolymer composition on CMC values, drug loading contents and drug loading efficiency

Sample	CMC (g·L ⁻¹)	Diameter of micelles before PTX loading (nm)	Diameter of micelles after PTX loading (nm)	DLC (%)	DLE (%)
ssPCL ₃₃ -PEEP ₂₅	1.10410 ⁻³	108.0±4.0	225.0±8.9	1.62	16.19
ssPCL ₃₃ -PEEP ₃₅	1.58410 ⁻³	45.1±2.3	114.0±3.1	2.64	26.38
ssPCL ₃₃ -PEEP ₅₃	2.38410 ⁻³	76.2±2.4	95.4±8.7	3.46	34.59
ssPCL ₃₃ -PEEP ₆₉	3.87410 ⁻³	66.8±4.0	80.6±6.0	2.09	20.88
ssPCL ₄₄ -PEEP ₃₂	6.93410 ⁻⁴	37.4±0.1	107.0±1.7	2.79	27.86
ssPCL ₆₉ -PEEP ₃₅	5.74410 ⁻⁴	61.4±0.7	119.0±0.6	2.52	25.08
ssPCL ₆₉ -PEEP ₅₆	1.03410 ⁻³	70.6±0.5	90.5±0.4	2.63	26.28

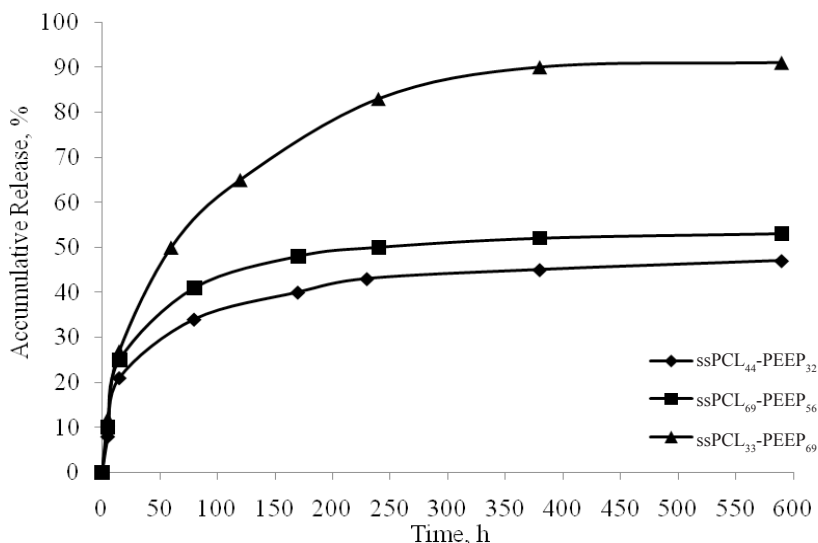
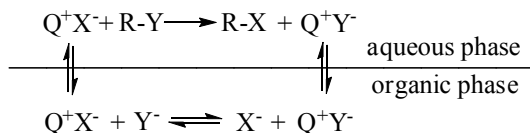


Figure 1. Release profile of PTX from ssPCL-PEEP micelles in phosphate buffer saline at 37°C

Common methods for the synthesis of phosphate (phosphonate) polyesters have a number of disadvantages and the necessity to use expensive anhydrous organic solvents, only one of them. However, there are several techniques which provide possibility of obtaining polyphosphates (polyphosphonates) in mild conditions and without using toxic solvents, such methods will be discussed further.

Phase-transfer catalysis

The most developed among them is phase transfer catalysis (PTC). This term was introduced by Starks in 1971 in order to explain the crucial role of tetraalkylammonium or phosphonium salts (Q^+X^-) in the reactions between two substances located in different immiscible phases [9]. In a PTC reaction, an added phase transfer catalyst is capable of transferring hydrophilic reactant from aqueous phase into an organic phase where it can normally encounter and react under an activated state with the hydrophobic reactant (Scheme 2).



Scheme 2. Mechanism of PTC reaction

Nowadays, PTC appears to be a prime synthetic tool, being appreciated not only in various fields of organic chemistry but also among widespread industrial applications because of its advantages:

- Elimination of dangerous, inconvenient, and expensive reactants;
- High reactivity and selectivity of the active species;
- High yield and purity of products;
- Simplicity of the procedure;
- Low investment cost;
- Low energy consumption;
- Minimization of industrial waste;
- Elimination of organic solvents (when organic reactants are liquid).

Millich and Carraher studied in details the effects of reaction time, molar ratio of the monomers, and phase transfer catalyst on the yield and viscosity of a hydroquinone (HQ)/phenylphosphonic dichloride (PPD) polymer [10-12]. Later, Millich and Imai reported about the effect of phase transfer catalyst on the interfacial polycondensation of bisphenol A (BPA) with PPD [13-14].

Richards et al. researched the factors affecting the polymerization of

BPA with other dichlorides, such as ethylphosphonic dichloride (EPD), ethyl dichlorophosphate (EOP) and phenyl dichlorophosphate (POP) [15]. Tetrabutyl ammonium bromide (TBAB), cetyl trimethyl ammonium bromide (CTMAB), cetyl trimethyl ammonium chloride (CTMAC), and 18-crown-6 ether (CE) were tested as phase-transfer catalysts (Table 2). Triethylamine (TEA), NaOH, KOH, pyridine, and 4-dimethyl-aminopyridine (DMAP) were used as acid acceptors.

Table 2. Results of PTC polycondensation of various PD with BPA

PD	B	Catalyst	Base	M_w	η_{inh}^a , dl·g ⁻¹
EOP	BPA	CE	KOH	27.000	0.0777
EP	BPA	CE	KOH	21.000	0.0954
POP	BPA	CE	KOH	24.000	0.0835
PP	BPA	CE	KOH	40.000	0.2086

^a The inherent viscosities η_{inh} were determined for solutions in chloroform, at 32°C

Results of the kinetic studies indicated that the longer chains had fully polymerized in less than 10 min. Extended reaction times had no significant effect on CE trials and were actually detrimental to polymerizations using CTMAC. Also, while all four PTC produced polymers of similar M_w averages, the molecular weight distributions differed considerably in nature. Polymers obtained with CTMAC consistently exhibited a bimodal distribution – a fraction of long polymer chains separated from a fraction consisting mainly of oligomers. Using of TBAB and CTMAB gave a much less pronounced division of the two fractions (chains of intermediate length were present in greater amounts). In addition, CTMAB was more effective than CTMAC and CE to producing long polymer chains ($M_w > 100,000$).

The efficiency of used PTC depended on the base utilized to ionize the diol and acceptor the acid. The polymer with high molecular weight wasn't obtained in the synthesis with combinations of quaternary ammonium catalysts (TBAB, CTMAC, CTMAB) and TEA (or pyridine). In contrast, both NaOH and KOH were successfully used with the quaternary ammonium PTC for obtaining long chain polymer, with the KOH yielding better results. As one would expect, the size of alkali ion have strong influence on the molecular weight in reaction catalyzed by CE.

Inverse phase transfer catalysis

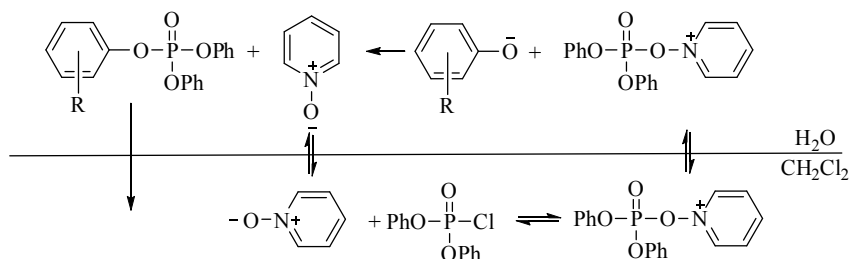
A new type of PTC was found by Mathias and Vaidya [16]. In contrast to the normal and reversed PTC methodologies, in which the chemical reaction

takes place in the organic phase, in inverse phase transfer catalysis (IPTC) the hydrophobic reactants transferring from the organic phase into the aqueous phase for reaction with a second reactant. Originally various cyclodextrins were utilized as the catalysts for providing IPTC processes. Also, the transition metal complexes, calix-[n]-arenes, surfactants, tetraalkylammonium salts and pyridine derivatives were used as catalysts in different reactions [17].

Due to complexity of interfacial polycondensation IPTC reaction of diphenyl chlorophosphate (dPOP) with various sodium phenolates (4-nitrophenolate (p-NP), 2-nitrophenolate (o-NP), 4-chlorophenolate (p-ClP), 4-propionylphenolate (p-Pr(O)P), 4-(benzyloxy)phenolate (p-BzOP)) was initially studied. Potassium carbonate was used as acid acceptor, thereby the optimal value of pH was provided and as a consequence the side reaction of hydrolysis was minimized. Pyridine derivatives (4-methylpyridine-1-oxide (MPNO), 4-methoxy-pyridine-1-oxide (MOPNO), 4-morpholinopyridine-1-oxide (MorphPNO), 4-dimethylaminopyridine-1-oxide (DMAPNO)) were chosen as catalysts, because they demonstrated high efficiency in the case of reaction between acyl halides with benzoate anions.

The general mechanism of pyridine derivatives catalyzed reaction consists of three stages (Scheme3):

- ion intermediate formation from pyridine and phosphorus compound;
- pyridinium salt transferring from organic phase to aqueous layer;
- phosphoric ester formation and pyridine (reactivation, reclaiming, reclamation, recovery, recuperation, regeneration, revivification) in result of reaction between phenolate anion and ion intermediate.



Scheme 3. Synthesis pathway of phosphate esters catalyzed by pyridinium-1-oxide in two-phase system water-dichloromethane

The phosphates were synthesized according to the following procedure: 0.03 mol of sodium phenolate was dissolved in 30 ml aqueous solution of K_2CO_3 (0.4 g) and 0.0005 mol catalyst was added. To this solution, 0.03 mol dPOP in 30 ml CH_2Cl_2 were added, maintaining the temperature at $20^\circ C$; then the

mixture was stirred (500 rpm) for 30 min at 20°C. All obtained phosphoric esters were characterized by IR, ^1H NMR and ^{31}P NMR, and the spectral data were in accordance with the proposed structures.

Kinetic studies were carried out for reaction of dPOP with p-NP. Concentration of diphenyl 4-nitrophenyl phosphate was monitored by measuring optical density of IR peak at 1340 cm^{-1} corresponding to the symmetric stretching vibration of nitro group. The result of experiments showed that reaction rate and product yield increase in the series of catalysts: MPNO < MOPNO < MorphPNO < DMAPNO (Table 3). Also was demonstrated that logarithm of the rate constant of ionic intermediates formation (k_{ef}) is linearly dependent on the pyridine-1-oxides basicity (pK_{BH^+}) (Figure 2).

Table 3. Results of IPTC reaction of dPOP with sodium 4-nitrophenolate

Catalyst	Base	T, °C	k_{ef} , $\text{l}\cdot\text{mol}^{-1}\cdot\text{s}^{-1}$	Yield, %
MPNO	K_2CO_3	20	0.0518 ± 0.012	50
MOPNO	K_2CO_3	20	0.1326 ± 0.0008	60
MorphPNO	K_2CO_3	20	1.078 ± 0.025	81
DMAPNO	K_2CO_3	20	3.62 ± 0.11	86

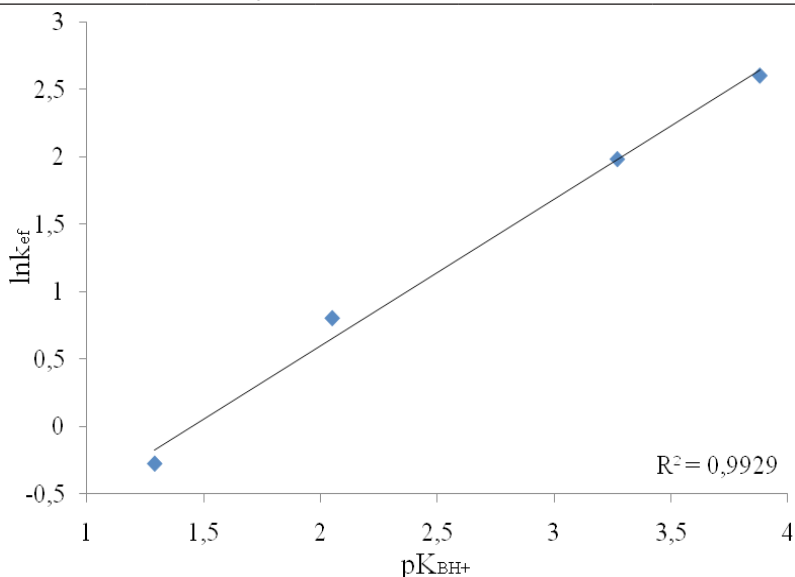


Figure 2. Relationship between logarithm of the effective rate constant and the pyridine-1-oxides basicity

IPTC polycondensation of various phosphonic(phosphoric) dichloride's (PD) with bisphenols (B) was described by Iliescu et. al. [18-21] (Table 4). Methyl dichlorophosphate (MOP), POP, p-chlorphenyl dichlorophosphate (p-CIPOP), PPD were used as phosphorus monomers. 4,4'-methylenediphenol (BHF), BPA, 4,4'-(propane-2,2-diyl) bis(2,6-dibromophenol) (BrBPA), 4,4'-(cyclohexane-1,1-diyl)diphenol (BPZ), 4,4'-(diazene-1,2-diyl)diphenol (DHB) were used as phenol monomers.

Table 4. Results of IPTC polycondensation of various phosphonic(phosphoric) dichlorides with bisphenols

PD	B	Catalyst	Base	T, °C	Yield, %	η_{inh}^a , dl·g ⁻¹
PPD	BPA	DMAP	NaOH	15	86.5	0.40 ^a
PPD	BPA	DMAP	NaOH	-12	93.1	0.63 ^a
PPD	BPA	DMAP	NaOH	-12	92.9	0.64 ^a
PPD	BPA	DMAP	NaOH	-12	92.9	0.64 ^a
PPD	BPA	DMAP	NaOH	-12	93.0	0.64 ^a
PPD	BrBPA	DMAP	NaOH	15	65.5	0.32 ^a
PPD	DHB	DMAP	NaOH	15	80.8	0.45 ^a
PPD	HPM	DMAP	NaOH	15	60.0	0.25 ^a
PPD	BPZ	PNO	NaOH	0	60.0	0.36 ^b
PPD	BPZ	PNO	Ba(OH) ₂	0	75.2	0.52 ^b
p-CIPOP	HPM	DMAP	NaOH	15	68.5	0.28 ^a
POP	BPA	DMAP	NaOH	15	78.5	0.35 ^a
POP	BrBPA	DMAP	NaOH	15	63.5	0.30 ^a
POP	DHB	DMAP	NaOH	15	80.2	0.42 ^a
MOP	BPA	DMAP	NaOH	15	92.0	0.65 ^a

^a The inherent viscosities η_{inh} were determined for solutions of 0.5 g/100 ml, in tetrachloroethane, at 30°C

^b The inherent viscosities η_{inh} were determined for solutions of 0.25 g/100 ml, in dichloroethane, at 25°C

The results of experiments with different pyridine derivatives showed that yield and polymer inherent viscosity increase in the series of catalysts: pyridine (Py) < pyridine-1-oxide (PNO) < 4-dimethylaminopyridine (DMAP).

In addition, influence of reaction conditions on yield and polymer inherent viscosity was investigated [19]. The MINITAB statistical software was used for obtaining the mathematical model of the synthesis process. Using this model the main effect of the control factors and their interactions were evaluated. Optimal values of the control factors for obtaining polymer with long chain and high yield were found:

- monomer molar ratio PD:B = 1:1;
- base concentration = 1.1M;
- reaction temperature = -12°C;

Furthermore, the advantage of using barium hydroxide compared to sodium alkali was shown [20]. Using of bases with limited solubility prevents the polymer degradation and phosphorus monomer hydrolysis. However, such bases can provide sufficient concentration of hydroxyl ions to neutralize released acid during polycondensation. Thus, IPTC method can be exploited for the synthesis different polyphosphates and polyphosphonates with high inherent viscosity and good yield. In contrast to PTC there is no need for vigorous stirring (500-1000 rpm instead of 10000 rpm) but as opposed to PTC process, where a small amount of catalyst is enough to produce a polymer, IPTC polycondensation can take place only at much higher catalyst concentration.

Vapor-liquid polycondensation

The liquid-vapor interfacial polycondensation (VLP) was exploited by Sokolov in synthesis of polyamides [22-25]. This system utilizes pairs of highly reactive reagents with one of the reagents in the vapor state and the other in solution. Iliia and co-workers have studied in detail feasibility of organophosphorus polymer synthesis by this technique [26-32].

Since PD is more volatile than B they are employed in the vapor phase mixed with nitrogen. Benefits of this method are that reaction proceeds without the using neither catalysts nor organic solvents. In the other hand, the stream of nitrogen protects the system from oxygen, provides agitation, transport of vapor of PD and controls the rate of reaction.

A series of polyphosphonates and polyphosphates were synthesized by base promoted VLP of various PD (methylphosphonic dichloride (MPD), cyclohexylphosphonic dichloride (CHPD), PPD, cyclohexyl dichlorophosphate (CHOP), POP, p-cresyl dichlorophosphate (p-CrOP), p-methoxyphenyl dichlorophosphate (p-MPOP), p-bromophenyl dichlorophosphate (p-BrPOP), p-nitrophenyl dichlorophosphate (p-NPOP), MOP, EOP and propyl dichlorophosphate (PrOP)) with different B (HQ, BPA, 4,4'-biphenol (BP), 1,5-naphthalenediol (ND), 4,4'-(naphthalene-1,5-diyl)diphenol (NBP), 4,4'-(propane-2,2-diyl)bis(2,3,5,6-tetra-chlorophenol) (ClBPA) and 4,4'-sulfonyldiphenol (BPS)). Result of these experiments showed in Table 5.

Optimal values for control factors were found:

- monomer molar ratio PD:B = 2.7:1;
- base concentration = 1.1M;
- depending on PD and B the optimum temperature of flask with PD

varies from 60 to 90°C;

- temperature of flask with aqueous solution 40-50°C;
- time of reaction \approx 60 minute, since for the reaction time over 60 minutes occurs significant degradation of the polymer.

Thus, the VLP represent a simple and green synthetic methodology for polyphosphate and polyphosphonate obtaining by the reaction in an aqueous medium, without the use of other solvents or a catalyst. The main disadvantage of this method is high consumption of PD in comparisons to PTC and IPTC techniques. However, the simplification of reaction protocols is an important concept in designing new clean methodologies.

Table 5. Results of VLP of various phosphonic(phosphoric) dichlorides with bisphenols

PD	B	T ^a , °C	Yield, %	M _n	M _w	η_{inh}^b , dl·g ⁻¹
CHPD	HQ	70	72	9.800	14.400	0.90
CHPD	BPA	70	85	9.300	13.500	0.95
CHPD	BP	70	75	19.800	35.800	1.80
CHPD	ND	70	80	29.300	56.800	2.30
CHPD	SD	70	48	8.500	12.100	0.75
MPD	HQ	65	22			0.15
MPD	BPA	65	28			0.18
MPD	BP	65	32			0.45
MPD	ND	65	44			0.48
MPD	SD	65	24			0.16
PPD	HQ	80	65	9.100	13.800	0.98
PPD	BPA	80	70	8.800	13.750	1.10
PPD	BP	80	62	25.300	41.600	1.93
PPD	ND	80	73	35.000	58.900	2.50
PPD	SD	80	54	8.650	11.940	1.02
POP	HQ	65	55	4.500	5.460	0.35
POP	BPA	65	60	4.200	4.980	0.48
POP	BPA	85	92	4.250	7.600	0.38
POP	BP	65	70	5.590	6.300	0.40
POP	BP	85	90	5.760	11.780	0.45
POP	ND	65	75	6.500	6.800	0.65
POP	SD	65	80	4.750	5.300	0.42
POP	CIBPA	85	75	3.450	6.570	0.31
CHOP	BPA	85	88	2.550	5.100	0.28
MOP	BPA	85	80	1.050	1.840	0.22
EOP	BPA	85	82	1.100	2.100	0.23
PrOP	BPA	85	85	1.150	2.200	0.24

^a Temperature of flask with PD

^b The inherent viscosities η_{inh} were determined for solutions of 0.5 g/100 ml, in tetrachloroethane, at 30°C

Conclusion

In this chapter, a review of modern methods for the synthesis of organophosphorus polymers and their use as molecular receptors is presented. The development of PTC, IPTC and VLP have followed the scientific trend that a successful application frequently stimulates further research that in turn leads to more applications and improved processes. No doubt, numerous novel ways of using these techniques wait for discovery and exploration. Already, PTC has grown to become a very important and widely applied technique not only at laboratories but also in chemical industry. IPTC and VLC also have all the necessary tools to gain further wide use.

References

1. Cheng J, Ding J. *Polymer* 2008; 49: 4784–90.
2. Chiu HC, Chern CS, Lee CK, Chang HF. *Polymer* 1998; 39:1609–16.
3. Xu JP, Ji J, Chen WD, Shen JC. *J Controlled Release* 2005; 107: 502–12.
4. Kataoka K, Harada A, Nagasaki Y. *Adv Drug Deliv Rev* 2001; 47: 113–31.
5. Rosler A, Vandermeulen GWM, Klok HA. *Adv Drug Deliv Rev* 2001; 53: 95–108.
6. Arimura H, Ohya Y, Ouchi T. *Biomacromolecules* 2005; 6: 720–5.
7. Wall ME. *Med Res Rev* 1998; 18: 299–314.
8. Zou T, Li SL, Cheng SX, Zhang XZ, Zhuo RX. *J Biomed Mater Res Part A* 2007; 83: 696–702.
9. Starks CM. *J. Am. Chem. Soc.* 1971; 93: 195–99.
10. Millich F, Carraher CE Jr. *J. Polym. Sci. Polym. Chem. Ed.* 1969; 7: 2669–2678.
11. Millich F, Carraher CE Jr. *J. Polym. Sci. Polym. Chem. Ed.* 1970; 8: 163–169.
12. Millich F, Carraher CE Jr. *Macromolecules* 1970; 3: 253–256.
13. Imai Y, Kamata H, Kakimoto MA. *J. Polym. Sci. Polym. Chem. Ed.* 1984; 22: 1259–1265.
14. Millich F, Lambing LL. *J. Polym. Sci. Polym. Chem. Ed.* 1980; 18: 2155–2162.
15. Richards M, Dahiyat BI, Arm DM, Lin S, Leong KW. *J. Polym. Sci. Part A Polym. Chem.* 1991; 29:1157–1165.
16. Mathias LJ, Vaidya RA. *J. Am. Chem. Soc.* 1986; 108: 1093–1094.
17. Volkov AG. *Interfacial Catalysis*. New-York Basel, Marcel Dekker Inc; 2002: 680.

18. Iliescu S, Ilia G, Pascariu A, Popa A, Plesu N. *Polymer*. 2006; 47: 6509–6512.
19. Iliescu S, Grozav I, Plesu N, Pascariu A, Ilia G, *Polym. Eng. Sci.* 2008; 48: 1304–1311.
20. Pascariu A, Iliescu S. *Annals of West University of Timisoara Series of Chemistry*. 2007; 16: 67–72.
21. Iliescu S, Pascariu A, Macarie L, Plesu N, Ilia G. *Polym. Bull.* 2009; 63: 485–495.
22. Sokolov LB. *J. Polym. Sci.* 1962; 58: 1253–1261
23. Sokolov LB. *Synthesis of Polymers by Polycondensation*. Jerusalem, Israel Program for Scientific Translations; 1968: 260.
24. Sokolov LB, Turetskii LV. *Vysokomol. Soedin.* 1965; 7: 1997.
25. Sokolov LB, Turetskii LV. *Vysokomol. Soedin. Ser. A.* 1970; 12: 971.
26. Iliescu S, Ilia G, Popa A, Dehelean G, Macarie L, Pacureanu L, Hurduc N. *Polym. Bull.* 2001; 46: 165–174.
27. Iliescu S, Ilia G, Plesu N, Popa A, Pascariu A. *Green Chem.* 2006; 8: 727–730.
28. Ilia G, Iliescu S, Popa A, Plesu N, Pascariu A. *Proceeding of the 8th Polymers for Advanced Technologies International Symposium*. 2005.
29. Iliescu S, Ilia G, Popa A, Dehelean G, Pascariu A, Macarie L, Plesu N. *Mol. Cryst. Liq. Cryst.* 2004; 418: 205–215.
30. Iliescu S, Ilia G, Popa A, Kurunczi L, Deheleana G. *Phosphorus, Sulfur, and Silicon*. 2003; 178: 1759–1769.
31. Iliescu S, Ilia G, Dehelean G, Popa A. *Polym. Bull.* 2002; 48: 451–456.
32. Iliescu S, Ilia G, Pascariu A, Popa A, Plesu N. *Pure Appl. Chem.* 2007; 79: 1879–1884.

Chapter 13

Products of organic wastes thermal degradation as a source of molecular adsorbents and receptors

Elena Lygina¹, Alexander Dmitruk¹, Leonid Galushko²,
Svetlana Lyubchik³, Vladimir Tret'yakov⁴ and Grzegorz Schroeder⁵

¹*Tugan-Baranovsky State University of Economy and Trade,
Zhorsa 31, 83050 Donetsk, Ukraine*

²*L.M. Litvinenko Institute of Physical Organic and Coal Chemistry
NAS of Ukraine, R. Luxemburg 70, 83-114 Donetsk, Ukraine*

³*REQUIMTE-CQFB, Faculty of Sciences and Technology,
New University Lisbon Quinta da Torre, 2829-516 Monte da Caparica,
Portugal*

⁴*Topchiev Institute of Petrochemical Synthesis, Russian Academy of
Sciences, Leninskii pr. 29, Moscow, 119991 Russia*

⁵*Adam Mickiewicz University, Faculty of Chemistry,
Grunwaldzka 6, 60-780 Poznań, Poland*

1. Introduction

Industrial processes for the manufacture of one or more kinds of commercial products from waste materials should be optimized in the context of the anthropogenic impact of organic wastes on the environment and its consequences [1–3]. The processing of organic wastes remains a problem of considerable current interest mainly because of an increase in the amount of wastes and waste accumulation, although progress was made toward the solution of this problem. The major portion of currently used methods for the processing of organic wastes resulted from a long evolution of engineering solutions and technologies, and they are characterized by relatively favorable energy and environmental characteristics [4]. First, among them are thermal methods such as pyrolysis, gasification, and combustion [5]. At the same time, certain limitations imposed on processes for the thermal treatment of organic wastes should be taken into consideration. All of these processes are characterized by relatively low selectivity: solid, gaseous, and liquid products of complex composition, which

essentially depend on the starting material, are simultaneously obtained in any versions of these processes [5, 6]. Moreover, organic wastes are often chemically heterogeneous complex multicomponent systems with various physicochemical properties. Therefore, the behavior of the organic matter of various wastes cannot be described based on the thermolysis of high-molecular-weight compounds because of the complex structure of this organic matter and various interactions occurring in the course of waste processing [7, 8]. Thermogravimetry is widely used to obtain reliable information [9–14]. In this case, the main concepts of the process mechanism of the thermolysis of carbon-containing wastes are based on simplified assumptions, which are not always consistent with a real set of complex chemical reactions that occur in the systems. However, the experimental data make it possible to compare process parameters such as the temperature, heating rate, and nature/composition of carbon-containing wastes [13–15]. Note that a theory that provides an opportunity to make reliable conclusions concerning the structure of wastes, to unambiguously predict the course of thermolysis processes, and to determine the composition of (or ratio between) by-products based on the ultimate and proximate analyses of organic wastes is currently not available. The organic matter of carbon-containing wastes consists of thermodynamically unstable formations, which undergo deep conversion on heating [16].

Table 1. Thermolysis of the sunflower husks—D coal binary system with and without alkali metal carbonate eutectic Mixture of sunflower husks + D coal

Maximum temperatures of the main peaks of individual component decomposition	Total weight loss, %								
Sunflower husks, T_{max}	-	130	-	275	305	390	-	-	-
D coal, T_{max}	101	132	-	-	-	400	429	527	-
Weight loss (WL_{theor}) for the thermolysis of individual components, %									
Sunflower husks, $WL_{.}$	-	4.24	-	18.85	4.87	4.73	-	-	32.69
D coal WL	1.65	1.21	-	-	-	1.66	2.64	0.37	7.54
Sunflower husks + D coal, $WL_{.}$	1.65	5.45	-	18.85	4.87	6.39	2.64	0.37	40.23
Maximum temperatures (T) of the main peaks of decomposition and weight loss (WL_{expt}) in the thermolysis of the sunflower husks + D coal binary system									
$T (^{\circ}C) V^1 max$	114	130	-	277	297	404	-	478	39.40
Weight loss (WL_{expt}), %	1.97	5.05	-	17.26	3.10	10.34	-	1.68	-
WL_{pt} / WL_{theo}	1.19	0.93	-	0.92	0.64	1.62	-	4.54	0.98
Mixture of sunflower husks + D coal + eutectic additives									

Maximum temperatures of the main peaks of individual component decomposition								Total weight loss, %
Maximum temperatures of the main peaks of individual component decomposition (T_{max}), °C)								
Sunflower husks + eutectic, T_{max}	-	140	-	227	275	360	425	-
D coal + eutectic, T_{max}	-	125	-	219	-	400	408	470
Weight loss (WI, K/Na) for the thermolysis of individual components, %								
Sunflower husks + eutectic, WI, K/Na	-	2.27	-	4.75	12.89	6.57	0.70	27.18
D coal + eutectic, WI Na	-	2.38	-	0.51	-	0.69	4.34	1.91 9.83
Sunflower husks + D coal + eutectic, WI, K/Na	-	4.65	-	5.26	12.89	7.26	5.04	1.91 37.01
Maximum temperatures (T_{max}) of the main peaks of decomposition and weight loss (WL _{expt} K/Na) in the thermolysis of the sunflower husks—D coal binary system+eutectic								
T (°C) V ¹ max		141	-	236	272	357	412	468 41.44
Weight loss (WL _{expt}), %		5.75		6.38	10.53	6.70	5.12	6.94
WL _{expt} K/Na/ WL _{theor} , K/Na	-	1.24	-	1.21	0.82	0.92	1.02	3.63 1.12
WL _{expt} K/Na/WL _{expt}	-	1.14	-	0.37	3.40	0.65	-	4.13 1.05
WL _{theor} K/Na/WL _{theor}	-	0.85	-	0.28	2.65	1.14	1.91	5.16 0.92
WL _{expt} K/Na/WL _{expt} / WL, K/Na/WL _{theor}	-	1.34	-	1.33	1.28	0.57	-	0.80 1.14

Therefore, in most cases, the thermolysis of each particular waste material is experimentally studied to determine the effect of process parameters on the composition and yield of products. Thus, new experimental data and knowledge of the thermolysis processes of individual kinds of organic wastes make it possible to program the behaviors of multicomponent systems in accordance with specific requirements imposed on a thermolysis process.

Table 2. Thermolysis of the AKKhZ— sunflower husks binary system with and without alkali metal carbonate eutectic Mixture of AKKhZ and sunflower husks

Maximum temperatures of the main peaks of individual component decomposition								Total weight loss, %
AKKhZ, T_{max}	-	120	145	282	-	360	-	
Sunflower husks, T_{max}	-	130	-	275	305	390	-	
Weight loss (WI) for the thermolysis of individual components, %								
AKKhZ, WL _{theor} ,	-	7.49	3.29	11.31	-	0.28	-	22.37
Sunflower husks, WE,.	-	4.24	-	18.85	4.87	4.73	-	32.69

Maximum temperatures of the main peaks of individual component decomposition							Total weight loss, %	
AKKhZ + sunflower husks, WE,	-	11.73	3.29	30.16	4.87	5.01	-	55.06
Maximum temperatures (T) of the main peaks of decomposition and weight loss (WL _{expt}) in the thermolysis of the AKKhZ—sunflower husks binary system								
$T (^{\circ}\text{C}) V^j \max$	-	120	-	246	315	365	435	51.44
Weight loss (WL _{expt}), %	-	5.37	-	27.09	4.67	8.21	6.10	
WL _{expt} /WL	-	0.46	-	0.90	0.96	1.64	-	0.93
Mixture of AKKhZ and sunflower husks + eutectic additives								
Maximum temperatures of the main peaks of individual component decomposition (T_{max}) (°C)								
AKKhZ + eutectic, T_{max}	-	110	190	260	-	-	-	
Sunflower husks + eutectic, T_{max}	-	138	-	227	275	360	425	
Weight loss (WLj. K/Na) for the thermolysis of individual components, %								
AKKhZ + eutectic, WL or K/Na	-	10.28	0.12	10.61	-	-	-	21.01
Sunflower husks + eutectic, WI K/Na	-	2.27	-	4.75	12.89	6.57	0.70	27.18
AKKhZ + sunflower husks + eutectic, WI K/Na	-	12.55	0.12	15.36	12.89	6.57	0.70	48.19
Maximum temperatures (T) of the main peaks of decomposition and weight loss (WL _{expt} K/Na) in the thermolysis of the AKKhZ—sunflower husks binary system+eutectic								
$T (^{\circ}\text{C}) V^j \max$	-	133	-	248	288	415	429	50.97
Weight loss (WL _{expt}), %	-	18.61	-	15.41	10.86	5.05	1.05	
WL _{expt} K/Na/ WL _{theo} , K/Na	-	1.48	-	1.00	0.84	0.77	1.50	1.09
WL _{expt} K/Na/WL _{expt}	-	3.47	-	0.57	2.33	0.62	0.17	0.99
WL _{theo} K/Na/WL _{theo}	-	1.07	0.04	0.51	2.65	1.31	-	0.88
WL _{expt} K/Na/WL _{expt} / WL _{theo} , K/Na/WL _{theo}	-	3.24	-	1.12	0.88	0.47	-	1.13

A choice of thermolysis process conditions (temperature, heating rate, chemical reagent additives, etc.) makes it possible to optimize the process as a whole, to make this process more economically feasible, and to utilize a wide range (in terms of chemical composition and nature) of waste materials, including nonutilizable or rejectable waste [1, 2]. Moreover, the process can be selectively directed toward the production of specified gas, liquid, or solid by-products by properly choosing the process conditions.

The aim of this work was to study the conversion of individual structural fragments as the constituents of complex multicomponent organic carbon-containing products in the course of the thermolysis of D-grade (long-flame) coal, refinery waste, coal-processing waste, and biomass. (or ratio between)

by-products based on the ultimate and proximate analyses of organic wastes is currently not available. The organic matter of carbon-containing wastes consists of thermodynamically unstable formations, which undergo deep conversion on heating [16]. Therefore, in most cases, the thermolysis of each particular waste material is experimentally studied to determine the effect of process parameters on the composition and yield of products. Thus, new experimental data and knowledge of the thermolysis processes of individual kinds of organic wastes make it possible to program the behaviors of multicomponent systems in accordance with specific requirements imposed on a thermolysis process. A choice of thermolysis process conditions (temperature, heating rate, chemical reagent additives, etc.) makes it possible to optimize the process as a whole, to make this process more economically feasible, and to utilize a wide range (in terms of chemical composition and nature) of waste materials, including nonutilizable or rejectable waste [1, 2]. Moreover, the process can be selectively directed toward the production of specified gas, liquid, or solid by-products by properly choosing the process conditions. The aim of this work was to study the conversion of individual structural fragments as the constituents of complex multicomponent organic carbon-containing products in the course of the thermolysis of D-grade (long-flame) coal, refinery waste, coal-processing waste, and biomass.

2. Experimental

The D-grade coal and particular types of solid and liquid organic wastes (biomass, refinery waste, and sludge) were used as test materials.

Long-flame coal. The D-grade coal from the L1 bed in the Lidievka coalmine (Donetsk Basin) was used in this study. The sampling and fractionation of coal were performed in accordance with DSTU (Technical Specifications) 4096-2002 requirements. To decrease the ash content of the coal samples, samples with particle sizes of 0.25–0.50 and 0.50–1.00 mm with no visible rock inclusions were taken for the experiments. Table 1 summarizes the proximate and ultimate analyses of the samples. The test samples predried at 105° were used.

Waste biomass. Sunflower husks from the AO KARGIL oil mill (Donetsk, Ukraine) were studied. The initial moisture content of the sunflower husks was ~10 wt %. The biomass samples were prepulverized and dried in a drying oven at 105° C to a moisture content of 6.1 wt %. Then, the powder was sieved to remove a fraction (about 7 wt %) with particle sizes smaller than 0.450 mm because of a high ash content of these particles. This procedure allowed us to decrease the ash content by 35%, as compared with the initial value. According to published data [17], sunflower husks contain cellulose, hemicellulose, and lignin fragments (to 27, 18, and 27 wt

% on a *daf* basis, respectively). Table 1 summarizes the proximate and ultimate analyses of the samples. The sunflower husk fractions predried at 105 °C were used. Table 2 summarizes the composition of ash according to AO KARGIL data.

Table 3. Thermolysis of the AKKhZ—D coal binary system with and without alkali metal carbonate eutectic Mixture of AKKhZ and D coal

Maximum temperatures of the main peaks of individual component decomposition										Total weight loss, %
AKKhZ, T_{max}	-	120	145	282	-	360	-	-	-	
D coal, T_{max}	101	132	-	-	-	400	429	527		
Weight loss (WL) for the thermolysis of individual components, %										
AKKhZ, WL_{theo}	-	7.49	3.29	11.31	-	0.28	-	-	-	22.37
D coal, WL_j	1.65	1.21	-	-	-	1.66	2.64	0.37	7.53	
AKKhZ + D coal, WL_{theor}	1.65	8.70	3.29	11.31	-	1.94	2.64	0.37	29.90	
Maximum temperatures (T) of the main peaks of decomposition and weight loss (WL_{expt}) in the thermolysis of the AKKhZ—D coal binary system										
T (°C) V^j max	-	124	151	291	-	404	439	530	49.42	
Weight loss (WL_{expt}), %		7.86	11.16	14.46		8.23	3.88	3.82	1.65	
Mixture of AKKhZ and D coal + eutectic additives										
Maximum temperatures of the main peaks of individual component decomposition (T_{max} °C)										
AKKhZ + eutectic, T_{max}	-	110	190	260	-	-	-	-	-	
D coal + eutectic, T_{max}	-	125	219	-	400	408	470	-		
Weight loss (WL K/Na) for the thermolysis of individual components. %										
AKKhZ + eutectic, WL_i , K/Na	-	10.28	0.12	10.61	-	-	-	-	-	21.01
D coal + eutectic, WIR K/Na	n peak	2.38	0.51	10.61	0.69	4.34	1.91	Na)	9.83	
AKKhZ + D coal + eutectic, WL K/Na	ACKhZ-	12.67	0.63	ion and system	0.69	4.34	1.91	T-expt	30.85	
Maximum temperatures (T) of the main peaks of decomposition and weight loss (WL_{expt}) in the thermolysis of the A		of decc	wnposit		weight	loss				
		D coal	binary		4-	(W				
					eutec	tic				
T (°C)	-	129	0.19	265	312	410	452	557	29.99	
V^j max		8.40		9.23	0.57	4.64	6.59	0.56	0.97	
Weight loss (WL_{expt}), %		0.66		0.87	0.83	1.07	3.45	0.15	0.61	
WL_{expt} K/Na/ WL_{theor} K/Na		1.07		0.64		0.56	1.70		1.03	
Na/WL_{expt} WL_{theor} K/Na/ WL_{theor} L		1.46		0.94		2.24	0.72		0.59	
$K/Na/L_{expt}/L_{theor}$ $K/Na/L_{theor}$		0.73		0.68		0.25	2.36			

Sludge from a sludge pond in a by-product coke plant. The sludge pond of the Avdeevka by-product coke plant (AKKhZ) is a natural dammed pit; about 15–20 000 tons of chemical waste was accumulated in this pond under a 2-m sheet of water in the course of plant operation. The chemical waste is water-bearing black mass that mainly consists of high-molecular-weight coke by-products

including fly ash and irregular suspended solids. Because of this, it is difficult to study the Analysis of liquid carbon-containing wastes (spent petroleum product mixtures and AKKhZ sludge) main characteristics of the waste in order to make recommendations for waste disposal or utilization. In this study, sludge from AKKhZ sludge ponds was used. The AKKhZ tar sample was taken from a sludge pond at a depth of 4.5 m.

Refinery waste. The oil-handling point of the Odessa port is the largest oil-loading terminal in Ukraine; this terminal with petroleum storage depots is responsible for the transshipment of all kinds of exported and imported petroleum products (the capacities of the port for petroleum, mazut, diesel fuel, and gasoline are 200000, 120000, 120000, and 25000 tons, respectively). To 1000 m³ of petroleum products is annually concentrated at the oil-handling point of the Odessa port; these petroleum products are collected upon cleaning oil and mazut tanks. According to *GOST (State Standard) 21 046-86: Spent Petroleum Products; General Specifications* [18], these petroleum products are classified as spent petroleum product mixtures. The spent petroleum product mixtures from the Odessa port are highly dispersed emulsions (heavy petroleum fractions with 5–6% Emulsol, 0.3% soda, and to 50% tap water), which are accumulated and stored in special settling reservoirs, where water is separated by gravity from the organic components of spent petroleum product mixtures, which are concentrated at the top of the reservoir. Table 1 summarizes the ultimate and proximate analyses of the liquid wastes (spent petroleum product mixtures and AKKhZ sludge) used in this work. The liquid waste samples taken from the petroleum and mazut reservoirs of the Odessa port and the AKKhZ sludge pond were analyzed without sample preparation. Table 3 summarizes the characteristics of liquid wastes, including data on the direct distillation and fractionation of bitumen by successive solvent extraction. The degrees of aromaticity of the test liquid wastes were determined by H1 NMR-spectroscopic analysis on a Bruker AS250 instrument with a working frequency of 300 MHz using deuterated chloroform as a solvent and tetramethylsilane as an internal standard. The following integration ranges were used: hydrogen at aromatic carbon (H_{ar}), 9–6 ppm; hydrogen of methyl groups bound to an aromatic ring (H_{α-2}), 4.5–3.5 ppm; hydrogen bound to α-carbon atoms (H_α), 3.5–2 ppm; hydrogen bound to β-carbon atoms (H_β), 2–1 ppm; and hydrogen bound to γ-carbon atoms (H_γ), 1–0.5 ppm. Based on the experimental data, the spent petroleum product mixtures (14% H_{ar}, 1% H_{α-2}, 56% H_α, 23% H_β, and 6% H_γ) can be tentatively ascribed to aliphatic petroleum waste. The main structure components are long unbranched (or weakly branched) hydrocarbons (to 79%) and a small fraction (to 14%) of aromatics, whereas the AKKhZ sludge can also be tentatively ascribed to aromatic tar waste

(the aromatic carbon content of this waste is as high as 26% on a total carbon basis: 26% Har, 4% H α -2, 23% H α , 28% H α , and 19% H α). *Preparation of a eutectic catalyst for thermolysis.* To study the effect of alkali metal additives on the thermolysis of particular solid and liquid organic carbon-containing products, we used an undoubted advantage of the binary eutectics of alkali metal salts—low melting points. We expected that the eutectics would occur as melts in the main temperature range of the thermolysis process, whereas pure salts would be only in a solid state, and they would not reach the same degree of dispersion on the surface of the organic matter of carbon-containing products. The eutectic catalyst was prepared as a fusion of a finely divided binary mixture of sodium and potassium carbonates containing 29% Na₂CO₃ and 71% K₂CO₃. According to the published phase diagrams, the eutectic melting temperature of this mixture is 350°C [19]. The mixture was prepared in a muffle furnace in an atmosphere of air at a temperature higher than the corresponding eutectic melting point of K/Na carbonates by approximately 100°C. After cooling, the solid mixture was crushed and thoroughly ground to fine powder in an agate mortar. The melting point of the prepared eutectic catalyst was additionally measured by differential scanning calorimetry (DSC 220°C), and it was consistent with published data [19]. To improve the dispersion of the catalyst in the pores and on the surfaces of the carbon matrices of individual waste components (to obtain a more uniform distribution), we used the impregnation method in the preparation of individual product components for the study of the process of thermolysis with catalyst additives. A sample of the finely dispersed powder of the eutectic salt (accurately weighed to within 0.0005g) was dissolved in water. Then, the solution (or a suspension, if the eutectic dissolved incompletely) was added to a solid sample component (pulverized and predried) in a proportion of ~0.5–0.6 ml per gram of the carbon-containing product; the resulting mixture was shaken on a shaker (180 rpm; 20 min) to ensure the good mixing of the solution/suspension with the component, then dried to constant weight (at 105°C for at least 12 h), and cooled to room temperature away from the atmosphere in order to exclude the adsorption of water vapor. After cooling, the impregnated mixture was crushed and thoroughly ground in an agate mortar. In the case of liquid refinery and coal-processing wastes (spent petroleum product mixtures and AKKhZ sludge), the powdered eutectic catalyst was added to the waste and the mixture with a liquid component was prepared in accordance with the above procedure. The catalyst was added in an amount of 3.3 wt % per each particular individual component of carbon-containing wastes.

Investigation techniques. The individual types of organic carbon-containing products were studied by thermogravimetry under conditions of linear

temperature programming from 20 to 950°C at a heating rate of 10 K/min in an atmosphere of flue gases in order to implement the interaction of primary solid, liquid, and gaseous products in the course of the thermolysis process. The thermogravimetric studies were performed on a Q1500D Paulik–Paulik–Erdei derivatograph under the following experimental conditions: sample weight, 0.03 g; analytical grinding; ceramic crucible with a cap 15 mm in height and 5 mm in diameter. The treatment of thermal analysis curves involved the analysis of TG, DTG, and DTA thermograms. The sample weight loss at a specified temperature was determined in accordance with the TG curve. The rate of weight loss was determined from the DTG curve, and the maximum temperatures of endo or exo effects were determined from the DTA curve in accordance with standard procedures [20]. The curves of weight loss (TG curves) and weight loss rate (DTG curves) were converted in terms of an 1-g initial sample and expressed as temperature dependences, which are illustrated by curves given in Section 3. The temperatures (T_{\max}) corresponding to the maximum rates of weight losses were determined based on the DTG curves. In this work, the weight loss was identical to the yield of volatile products, whereas the weight loss rate was equivalent to the rate of formation of volatile substances on heating. The thermogravimetric analysis of individual components (sunflower husks, AKKhZ sludge, spent petroleum product mixtures, and D-grade coal) and their mixtures with catalyst additives (binary eutectic mixtures of alkali metal carbonates) was performed.

Simulation of analytical peak groups using the SCIENTIST software. In the structural analysis of complex materials based on, for example, spectroscopic data, the deconvolution of a spectral profile into individual bands should be used because of the occurrence of a great number of broad strongly overlapping bands in the spectra. The resulting spectroscopic characteristics are used to construct/reproduce the structural models of initial materials [21]. It was noted that the correctly used deconvolution of primary spectra can be more informative for the structural analysis of complex multicomponent materials than, for example, the spectroscopy of individual structure components of the initial material [21]. In this work, we used the SCIENTIST 3.0 (Micro- Math) software [22] for the analysis of primary thermoanalytical data. This software allowed us to separate/choose a required number of deconvolution peaks in a multiplet and to optimize their parameters (deconvolution intensity, halfwidth, and T_{\max} position) until a minimum standard deviation between fit and real curves at each point. The resulting model of conversion is a set of N elementary peaks, each of them is characterized by the following four parameters: maximum position, intensity, width, and the fraction of a Lorentzian contour (band shape). The superposition of N elementary bands is a spectral function that approximates the experimental

curve. We used the uniform system of alteration (modification and combination) of base peak functions to obtain the most universal phenomenological models of analytical signals. The total number of four-parameter models can be as high as a thousand. In this work, we used a tested procedure for the discrimination of models from a system of models and the construction of the most appropriate models to describe the group of analytical peaks in thermogravimetric data (TG and DTG peaks). To solve this problem, the detailed characteristics of peak properties were taken into consideration for both a preliminary study of the shape variation range of a particular group of analytical peaks and an a priori evaluation of model parameters in the approximation of a particular experimental signal. At a preliminary stage, we compared characterization techniques for the groups of experimental signals. In this work, we used the following parameters of analytical signal series: weight loss rate, weigh loss, T_{\max} of thermal degradation, heating rate, and thermolysis temperature ranges. To evaluate signal parameters, we used the primary processing of a signal (smoothing and baseline correction). Then, the signal parameters were evaluated using the SCIENTIST software in accordance with the above procedure. The ranges of variation, the average values of parameters, and the corresponding standard deviations were found for each series of signals. Based on the range of parameter variations, a group of phenomenological models was chosen to optimally describe the range of variation of experimental peaks. Next, the individual peaks were approximated in series; based on this approximation, a final conclusion was made concerning the most adequate models for this group of peaks.

3. Results and discussion

Table 4 summarizes the initial thermogravimetric data obtained in the range of temperatures to 950 °C for the thermolysis of all of the individual components with and without eutectic alkali metal salt additives. Based on the preliminary analysis of the experimental data, we can formulate hypotheses on the character of thermolysis of the components: we can recognize individual temperature ranges of decomposition and calculate total weight losses upon decomposition for these ranges. In a number of cases, we can recognize individual decomposition peaks and calculate maximum rates of weigh losses for these peaks (Table 4). However, we cannot make a conclusion concerning the individual structural fragments (the nature and total amount of structural fragments) of initial materials and obtain quantitative data on thermal degradation (the separation of individual weight loss peaks for each individual structural component and the temperature ranges of the appearance of these peaks). Thus, the following peaks can be recognized in the thermolysis of the initial materials: two peaks of water (with T_{\max} of 100°C)

and the main decomposition of organic matter (with T_{max} of 400°C) for D coal; two peaks of water (with T_{max} of 125°C) and the main decomposition of organic matter (with T_{max} of 305°C) for sunflower husks; three peaks of water (with T_{max} of 125°C) and the main decomposition of organic matter (two peaks with T_{max} of 335 and 415°C) for spent petroleum product mixtures; and two peaks of water (with T_{max} of 120°C) and the main decomposition (with T_{max} of 280°C) for the AKKhZ sludge. Based on an analysis of initial thermogravimetric data, we cannot draw even general conclusions on the effect of carbonate additives on the thermolysis of the components (not to mention the effect of carbonates on the thermolysis of individual structural fragments in the starting materials). For the thermolysis of the starting materials in the presence of carbonates, we can recognize only particular regions of thermolysis: two peaks of water (with T_{max} of 120°C) and the main decomposition of organic matter (with T_{max} of 400°C) for D coal; two peaks of water (with T_{max} of 140°C) and the main decomposition of organic matter (with T_{max} of 385°C) for sunflower husks; two peaks of water (with T_{max} of 105°C) and the main decomposition of organic matter (with T_{max} of 410°C) for spent petroleum product mixtures; and two peaks of water (with T_{max} of 125°C) and the main decomposition (with T_{max} of 270°C) for the AKKhZ sludge. In the subsequent representation of the results, we used only the data obtained by a new methodological approach based on the following propositions: (1) the separation (based on the deconvolution of thermograms) of the thermal degradation of components into individual constituents; (2) the correlation of the resulting individual weight loss peaks (based on published data and the analysis of structural fragments by other techniques such as direct distillation, solvent extraction, and NMR spectroscopy) with the particular structural fragments of the initial carbon-containing components: sunflower husks, spent petroleum product mixtures, AKKhZ sludge, and D coal; (3) the qualitative (yield/temperature and composition/ nature) and qualitative (composition/nature) analysis of the dynamics of conversion of each individual structural fragment in the course of cothermolysis in complex solid and liquid organic carbon-containing products. On this basis, two conclusions can be made concerning (1) the composition of the individual structural fragments of the organic matter of the initial carbon-containing products and (2) the effect of alkali metal carbonates on the thermolysis of these products.

Thermolysis of sunflower husks. The results of TG–DTG analyses demonstrated that two peaks due to the main decomposition of biomass appeared in the thermolysis of sunflower husks (Table 4). Although the peaks are somewhat overlapping, they can be separated and characterized with the use of the proposed approach (Figs. 1a, 1b; Table 5). The experimental data for the thermolysis of sunflower husks are fully consistent with current concepts of

the thermolysis of biomass [23–25]. The deconvolution afforded three peaks, which were unambiguously attributed to the decomposition of cellulose, hemicellulose, and lignin as the constituents of sunflower husks at 240–290, 260–350, and 280–450°C, respectively (Fig. 1a; Table 5).

Table 4. Thermolysis of the spent petroleum product mixtures—sunflower husks binary system with and without alkali metal carbonate eutectic

Mixture of spent petroleum product mixtures and sunflower husks							
Maximum temperatures of the main peaks of individual component decomposition (T_{max} , °C)							Total weight loss, %
Spent petroleum product mixtures, T_{max}	-	125	-	283	337	-	412
Sunflower husks, T_{max}	-	130	-	275	305	390	-
Weight loss (WL_{theor}) for the thermolysis of individual components, %							
Spent petroleum product mixtures, WI	-	15.46	-	1.16	2.87	-	6.34
Sunflower husks, WI	-	4.24	-	18.85	4.87	4.73	-
Spent petroleum product mixtures + sunflower husks, WI	-	19.70	-	20.01	7.74	4.73	6.34
Maximum temperatures (T_{max}) of the main peaks of decomposition and weight loss (WL_{expt}) in the thermolysis of the spent petroleum product mixtures— sunflower husks binary system							
T (°C) V_j max	-	120	-	271	310	392	425
Weight loss (WL_{expt}), %	-	16.42	-	22.13	8.56	12.35	2.07
WL_{expt}/WL_{theor}	-	0.83	-	1.11	1.11	2.61	0.33
Mixture of spent petroleum product mixtures and sunflower husks + eutectic additives							
Maximum temperatures of the main peaks of individual component decomposition (T_{max}) °C)							
Spent petroleum product mixtures + eutectic, T_{max}	-	105	-	-	320	385	415
Sunflower husks + eutectic, T_{max}	-	140	-	227	275	360	425
Weight loss (WL_{theor} K/Na) the thermolysis of individual components, %							
Spent petroleum product mixtures + eutectic, WI, K/Na	-	21.13	-	-	5.50	7.01	6.71
Sunflower husks + eutectic, WI, K/Na	-	2.27	-	4.75	12.89	6.57	0.70
Spent petroleum product mixtures + sunflower husks + eutectic, WL_{theor} K/Na	-	23.40	-	4.75	18.39	13.58	7.41
Maximum temperatures (T_{max}) of the main peaks of decomposition and weight loss (WL_{expt} K/Na) in the thermolysis of the spent petroleum product mixtures— sunflower husks binary system + eutectic							
T (°C) V_j max	-	120	161	248	275	372	415
Weight loss (WL_{expt}), %	-	16.54	1.44	3.73	16.77	8.38	8.17
WL_{expt} K/Na/ WL_{theor} K/Na	-	0.71	-	0.79	0.91	0.62	1.10
WL_{expt} K/Na/ WL_{expt}	-	1.01	-	0.17	1.96	0.68	3.95
WL_{theor} K/Na/ WL_{theor}	-	1.19	-	0.24	2.38	2.87	1.17

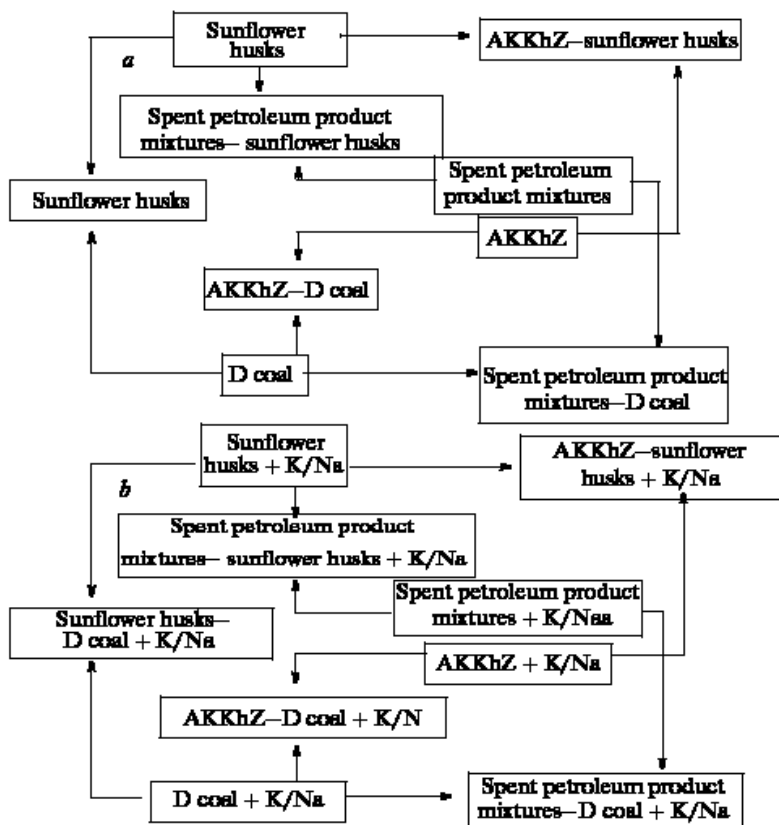


Figure 1. Thermolysis of sunflower husks (a) without additives and (b) with eutectic salt additives.

The interaction of components during the pyrolysis of biomass was not detected; the biomass components behaved independently of each other. Upon the addition of the eutectic catalyst (Fig. 1b; Table 5), the decomposition of a cellulose fragment of biomass came into play at lower temperatures (by about 50°C); however, it occurred much less intensely (the weight loss was 9.5% against 37.7% with no carbonate added). The decomposition of hemicellulose was considerably accelerated (the weight loss was 25.8% against 9.7%), although it also occurred at lower temperatures. A trend of this kind was also observed in a lignin fragment; however, the degree of decomposition increased less significantly. In general, the thermolysis of biomass with carbonate additives

was inhibited and the total weight loss was 54.4% against a weight loss of 65.4% for sunflower husks in the absence of alkali metal carbonate additives (Table 5).

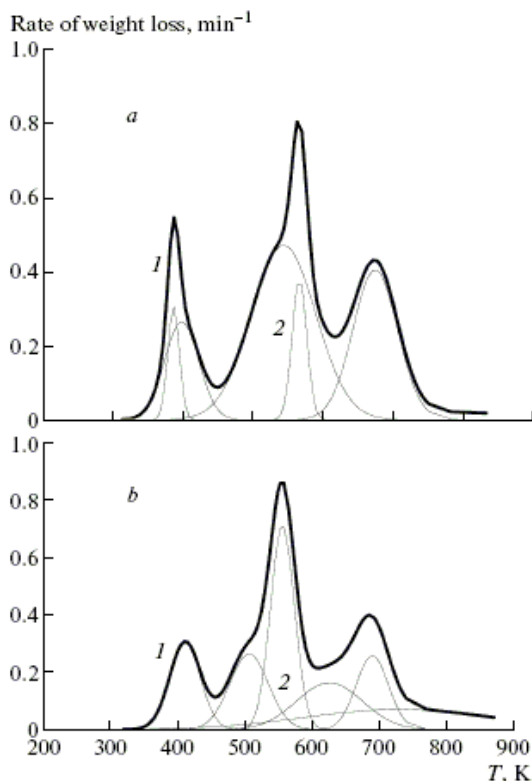


Figure 2. Thermolysis of D coal (a) without additives and (b) with eutectic salt additives.

Thermolysis of D-grade coal. The experimental data for the thermolysis of D coal are also fully consistent with the published concepts of the thermolysis of coal [7, 16, 26–28]. On heating to 120°C, physically bound water and, probably, adsorbed gases (carbon dioxide, methane, and air components [16, 26]) were released; then, water bound in the coal structure was released (a peak with T_{\max} of 125°C) (Figs. 2a, 2b). The thermal degradation of the organic matter of D coal can be tentatively subdivided into the degradation of individual structural fragments in the organic matter of coal (OMC): OMC 1 exhibited a medium-intensity peak with T_{\max} of 400°C, OMC 2 exhibited an intense peak with T_{\max}

of 425°C, and OMC 3 exhibited a low-intensity peak with T_{max} of 570°C (Fig. 2a, Table 5). In general, the thermal transformations of the OMC came into play at temperatures of about 325°C with the release of an amount of water and carbon dioxide, which resulted from the cleavage of chemical bonds at the terminal sites of coal macromolecules [7, 26]. Deep changes in the internal structure of organic matter did not occur. At temperatures higher than 350°C, the main degradation of the OMC came into play. Macromolecules decomposed to form short-lived free radicals, which underwent recombination and converted into stable systems [7, 26]. The deep decomposition of the OMC and the release of products (tars) that are liquid under ordinary conditions were complete at about 550°C. The character of OMC degradation changed upon the addition of alkali metal carbonates (Fig. 2b, Table 5): structural fragment OMC 1 decomposed less intensely, whereas the degradation of OMC 2 and OMC 3 occurred more intensely. This effect was most pronounced in OMC 3; the thermal degradation of this fragment increased by a factor of ~5 and occurred at lower temperatures (by approximately 50–60°C).

Table 5. Thermolysis of the spent petroleum product mixtures—D coal binary system with and without alkali metal carbonate eutectic

Mixture of spent petroleum product mixtures and sunflower husks									
Maximum temperatures of the main peaks of individual component decomposition ($T^{\circ}C$) V^I_{max}									Total weight loss, %
Spent petroleum product mixtures, T_{max}	-	125	-	283	337	412	-	-	
D coal, T_{max}	101	132	-	-	-	400	429	527	
Weight loss ($W_{L,i}$) for the thermolysis of individual components, %									
Spent petroleum product mixtures, WI	-	15.46	-	1.16	2.87	6.34	-	-	25.83
D coal, $W_{L,theo.}$	1.65	1.21	—	—	—	1.66	2.64	0.37	7.53
Spent petroleum product mixtures + D coal, WI	1.65	16.67	-	1.16	2.87	8.00	2.64	0.37	33.36
Maximum temperatures (T_{max}) of the main peaks of decomposition and weight loss ($W_{L_{exp}}$) in the thermolysis of the spent petroleum product mixtures—D coal binary system									
$T^{\circ}C$) V^I_{max}		125	173		357	415	490	520	39.57
Weight loss ($W_{L_{exp}}$), %		10.78	1.59		9.74	13.75	2.14	1.57	
$W_{L_{exp}}/W_{L_{theo.}}$		-	0.65	-	-	3.39	1.72	0.81	1.19
Mixture of spent petroleum product mixtures and D coal + eutectic additives									
Maximum temperatures of the main peaks of individual component decomposition (T_{max} , °C)									
Spent petroleum product mixtures + eutectic, T_{max}	-	105	-	-	320	385	415	-	
D coal + eutectic, T_{max}	-	125	219	-	-	400	408	470	

Mixture of spent petroleum product mixtures and sunflower husks									
Maximum temperatures of the main peaks of individual component decomposition (T °C) V ^j max									Total weight loss, %
Weight loss (WL _{theor} K/Na) the thermolysis of individual components, %									
Spent petroleum product mixtures + eutectic, WL K/Na	-	21.13	-	-	5.50	7.01	6.71	-	40.35
D coal + eutectic, WL ₁ K/Na	-	2.38	0.51	-	-	0.69	4.34	1.91	9.83
Spent petroleum product mixtures + D coal + eutectic, WL _{theor} K/Na	—	23.40	0.51	—	5.50	7.70	10.05	1.91	49.07
Maximum temperatures (T _{max}) of the main peaks of decomposition and weight loss (WL _{expt} K/Na) in the thermolysis of the spent petroleum product mixtures— D coal binary system + eutectic									
T (°C) V ^j max		119	151		295	400	420		51.29
Weight loss (WL _{expt}), %		11.27	5.62		5.85	19.28	9.25		
WL _{expt} K/Na/ WL _{theor} r ₁ K/Na	-	0.48	11.02	-	1.06	2.50	0.92	-	1.02
WL _{expt} K/Na/ WL _{expt}	-	1.05	3.53	-	0.60	1.40	4.32	-	1.29
WL _{theor} K/Na/ WL _{theor}	-	1.40	-	-	1.92	0.96	3.80	5.16	1.47

The character of OMC degradation also considerably changed in the region of low temperatures (150–220°C), where the initial peak of decomposition was observed in the presence of catalytic additives. For example, this peak appeared in the degradation of coalprocessing waste (AKKhZ sludge); it was likely due to the thermal decomposition of the coal structure, which mainly affected external polar groups. In general, the thermolysis of coal occurred somewhat more intensely upon the addition of the eutectic catalyst; the temperature range of decomposition changed only slightly (Fig. 2b, Table 5). The total weight loss remained almost unchanged, and it was 15.8% against 14.3% for D coal in the absence of alkali carbonate salt additives. A change in the character of water release is obvious: in the presence of carbonates, a peak due to the release of physically bound water was absent, whereas the intensity of a neighboring peak due to chemically bound water increased. In this case, the total weight loss due to the release of free and bound water remained almost unchanged in the thermolysis of D coal both with and without carbonates; it was 5–6%.

Thermolysis of AKKhZ sludge. As a result of deconvolution, the following four main regions of the thermal degradation of the AKKhZ sludge can be recognized (Fig. 3a, Table 5): a peak with T_{max} of 120°C and a total weight loss to 15%, which corresponds to the release of bound water and, probably, light hydrocarbon constituents of the AKKhZ sludge, and three peaks due to the main decomposition of the organic matter of the coalprocessing waste (a low-temperature broad peak due to the onset of decomposition with T_{max} of 145°C

and a total weight loss of 6.6%, a medium-temperature intense peak with T_{max} of $\sim 280^{\circ}\text{C}$ and a total weight loss to 22.6%, and a weakly pronounced high-temperature peak with T_{max} of 360°C and a weight loss of 0.55%). According to additional experimental data on the thermolysis of the AKKhZ sludge (Table 3), the direct distillation of this waste resulted in the removal of naphthalene (to 10.8 vol %) in the temperature range of $100\text{--}120^{\circ}\text{C}$ with an amount of light oil (to 13.9 vol %), whose density is lower than the density of water, and an amount of water (to 7.7 vol %). On further heating, an oil fraction (24–34 vol %) with a boiling temperature of $120\text{--}170^{\circ}\text{C}$ and an additional amount of water (to 16%) were boiled out. According to chromatographic analysis data, the distilled oil was a mixture of heavy hydrocarbons and their oxidation products with a predominant naphthalene content (to 50%). The chromatogram also contained signals from the derivatives of naphthalene, quinoline, biphenyl, anthracene, etc. Thus, according to the experimental data, under conditions of the direct distillation of the AKKhZ waste in the temperature range of $120\text{--}170^{\circ}\text{C}$, to 23.9 vol % water, 10.8 vol % naphthalene, 13.9 vol % light hydrocarbons, and 24–34% oil (Table 3) were released. The distillation residue was 18–26%; in principle, it can serve as a binder in various technologies, in particular, in the manufacture of activated carbon. In this case, note that, on heating the distilling tank to 300°C , the temperature of exhaust gases was no higher than 170°C , which suggests the occurrence of thermal degradation processes in the course of distillation. Upon the successive extraction of the distillation residue, a portion of the organic components of bitumen passed into solution (Table 3): a heptane-soluble fraction (mainly containing malthenes) to 42% and a toluene-soluble fraction (partially containing malthene and asphaltene tars) to 36%. The residue undissolved in toluene (to 22%) was deposited at the bottom and on the walls of a flask as a spongelike coke-like mass. After the distillation of water to a residual value of 5–7%, a homogeneous fluid mass was formed.

Upon evaporation for 30 min to remove 19 wt %, a homogeneous viscous fluid mass was formed. Upon evaporation to constant weight (weight loss of $\sim 58\%$), a brittle solid substance (heavy coal-tar products) was formed. The character of decomposition of the AKKhZ waste dramatically changed in the presence of the eutectic of alkali metal carbonates (Fig. 3b, Table 5). Apart from an individual low-temperature step (an intense peak with T_{max} of 110°C and a total weight loss of $\sim 21\%$) of the decomposition of light hydrocarbons, the release of water, and, probably, naphthalene derivatives, thermolysis in the medium-temperature region occurred in a single step with T_{max} of 260°C and a weight loss of 21.2%. In this case, the temperature range of the main decomposition shifted by $\sim 20^{\circ}\text{C}$ to the lowtemperature region. The total weight loss in the thermal degradation

of the AKKhZ sludge was almost independent of catalyst additives, and it was 42–44% (Table 4).

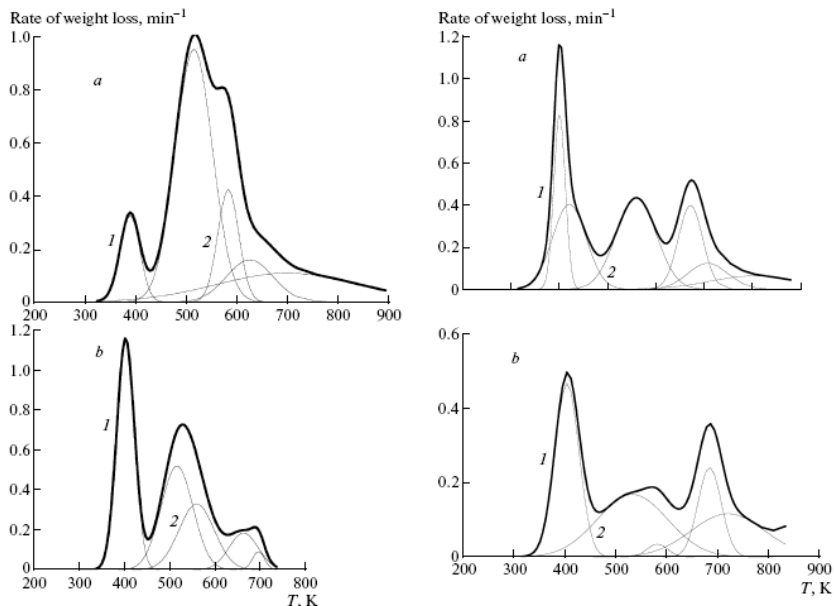


Figure 3. Thermolysis of the AKKhZ sludge (a) without additives and (b) with eutectic salt additives.

Figure 4. Thermolysis of spent petroleum product mixtures (a) without additives and (b) with eutectic salt additives.

Thermolysis of spent petroleum product mixtures. In the decomposition of spent petroleum product mixtures, two regions are also recognized: a region of the removal of water as the constituent of oily waste, where an intense peak occurs and the weight loss is greater than 30%, which is fully consistent with the nature of this waste as a suspension of petroleum products with water, and a higher temperature region (as compared with the thermal degradation of the AKKhZ sludge) of the main decomposition of the organic matter of the spent petroleum product mixture components. After deconvolution, three main peaks can be recognized (Fig. 4a, Table 5): two lower intensity peaks of the onset of decomposition in the medium temperature region (250–350°C) with the total weight loss of 8.0% and a third peak of main decomposition with a weight loss of 12.7%. On the addition of the eutectic catalyst, the thermolysis of the spent

petroleum product mixtures occurred much more intensely (Fig. 4b, Table 5). The release of water as a waste constituent occurred at a lower temperature and was more intense (the weight loss was 42.6 against 30.9% in the absence of additives). The temperature ranges of the main peaks remained almost unchanged. The medium-temperature (250–350°C) onset of decomposition occurred somewhat more intensely (the weight loss was 11.0% as compared with 8.0%); in this case, its character somewhat changed: an intense peak with T_{\max} of 320°C appeared in place of two medium-intensity peaks. The character of the hightemperature decomposition remained almost unchanged (the weight loss was 13.4% as compared with 12.7%). Considerable changes were associated with the appearance of an additional intense decomposition peak with T_{\max} of 385°C; for this structural fragment, the weight loss was 14.0%. Thus, the total weight loss considerably changed (because of the more intense separation of water and the decomposition of an additional structural constituent of spent petroleum product mixtures) and was 80.7 against 51.65% for the spent petroleum product mixture component in the absence of alkali metal carbonate additives. The experimental data on the decomposition of spent petroleum product mixtures are fully consistent with published data, according to which the thermolysis of individual fractions, such as malthenes and asphaltenes, are recognized in the thermolysis of petroleum waste [29, 30]. Saturated compounds, aromatics, and tars were chromatographically separated from the fraction of malthenes [30]. The stability of fractions increased in the order saturated hydrocarbons, aromatics, tars, and asphaltenes. According to the experimental data on direct distillation (Table 3), the first fraction (to 46.0 vol %) of water (to 33.0%) and light hydrocarbons (to 13%) can be separated in the temperature range of 63–99°C. In the thermolysis of spent petroleum product mixtures (at a heating rate of 10 K/min), the weight loss was 30.92%, which corresponds to the release of water. With potassium carbonate and sodium carbonate additives, the weight loss in this temperature range was much greater and amounted to 42.6%, which supports (along with water) the thermolysis of light hydrocarbons as the constituents of spent petroleum product mixtures. Over the temperature range of 100–250°C (according to the experimental data on direct distillation in Table 3), the second fraction (to 8.1 vol %) can be separated; this fraction consists of heavy hydrocarbons. A peak with T_{\max} of 283°C, which, probably, corresponds to the decomposition of heavy hydrocarbons (the weight loss for this structural fragment was 2.31%), was observed in the experiment on thermolysis. Then, in the course of thermolysis, the thermolysis of the direct distillation residue (42.6 vol %), which consisted of a liquid fraction (to 33.0%) with the density $d = 0.879$ g/cm³ and tars (to 9.6%), occurred.

Table 6. Generalized table of the main synergism effects in the cothermolysis of the binary mixtures of biomass, petroleum-and coal-processing wastes, and D coal

System	Effects in systems with no alkali metal carbonate additives, weight loss difference, %				<i>if</i>
	C_1	C_2	QC_2	$r, \text{''water}$	
Sunflower husks - D coal	No effect				0
AKKhZ-sunflower husks	Change in the character of AKKhZ _{OM}	+3.2 Sunflower husk _{gmin}	0	-6.3	-3.5
AKKhZ-D coal	+7.9 JvJvnZ _{joise} decomposition	+6.3 OM1 +3.5 OM3	0	No effect	+20
Spent petroleum product mixtures-sunflower husks	-4.3 Spent petroleum product mixtures _{ars}	0	+7.6 Sunflower husks Spent petroleum product mixtures _{aromatic} hydrocarbons	same	+3.0
Spent petroleum product mixtures-D coal	+6.9 Spent petroleum product mixtureSh _{cavy} hydrocarbons Spent petroleum product mixtures _{saturate} hydrocarbons	0	+5.7 Spent petroleum product mixtures _{aromatic} hydrocarbons Spent petroleum product mixtures _{ars} OMC1	-7.5	+6.0
System	Effects in systems with alkali metal carbonate additives, weight loss difference, %				dc %
Sunflower husks-D coal	No effect				0
AKKhZ-sunflower husks	The same				+6.1 +3.0
AKKhZ-Dcoal	0	+4.7 OMC2	0	-4.2	0
Spent petroleum product mixtures sunflower husks	0	0	-5.2 Sunflower husks, Spent petroleum product mixtures _{aromatics}	-5.2	-12.5
Spent petroleum product mixtures D coal	0	+5.1 Vcoal _{onset} of decomposition	+11.6 Spent petroleum product mixtures _{aromatic} hydrocarbons OMC1	-12.1 Water	+2.0

Thus, the thermolysis of spent petroleum product mixtures at 300–500°C can be simulated with a reaction scheme of three independent reactions, which correspond to the thermal degradation of three pseudomacro components of the malthe fraction of spent petroleum product mixtures (in this case, each particular pseudo-macro component is a group of compounds with close bond energies, which are responsible for such a behavior of the compounds in the course of thermal degradation): (1) saturated compounds (a broad peak with T_{max} of 320–332°C), for which the weight loss essentially depends on the additives of alkali metal carbonates and amounted to 5.73–11.01%; (2) the aromatic hydrocarbon

constituents of spent petroleum product mixtures exhibited an intense peak with T_{max} of 385°C, which appeared only in the presence of alkali metal carbonates; the weight loss was 14.01%; (3) tars exhibited a high-temperature peak with T_{max} of 415°C, for which the weight loss was ~13.01%. In this region, the interaction between asphaltenes and malthenes was observed in the course of thermolysis; the thermal degradation of asphaltene tar occurred along with the thermolysis of tar from the malthene fraction; the total weight loss for them varied from 12.58 to 13.42% (without and with carbonate additives, respectively). Thus, based on the experimental results, we can make a general conclusion on the decomposition of the test solid and liquid carbon-containing products under the specified conditions of thermolysis. In general, in the thermolysis of individual components, the following four regions of the thermal degradation of various structural fragments as the constituents of sunflower husks, AKKhZ waste, spent petroleum product mixtures, and the organic matter of D coal can be recognized: the region (105–125°C) of the release of free or bound water and the decomposition of light hydrocarbon fractions as the constituents of liquid wastes; the low-temperature region (145–220°C) of the weakly intense onset of the decomposition of coal (D) mainly involving outer polar groups and the intense onset of decomposition of heavy hydrocarbon fractions and their oxidation products (the derivatives of naphthalene, quinoline, biphenyl, anthracene, etc.) as the constituents of the coal-processing waste (AKKhZ); the medium-temperature region (250–350°C) of the intense main decomposition of the AKKhZ sludge (the pseudo-macro fragments of malthene fractions and, partially, tars of asphaltene fractions), the cellulose and hemicellulose fragments of biomass (sunflower husks), the onset of decomposition of spent petroleum product mixtures (heavy fractions of unsaturated hydrocarbons and saturated compounds from the malthene fraction); and the high-temperature region (350–450°C) of the main decomposition of the organic matter of D coal, the lignin fragment of sunflower husks, and the aromatic hydrocarbons of the malthene fraction of spent petroleum product mixtures and malthene and asphaltene tars from spent petroleum product mixtures (Table 5, Fig. 5).

The additives of alkali metal carbonates considerably affected the process of thermolysis of individual components (Table 6, Fig. 6). Thus, the temperature range of biomass decomposition considerably shifted (by ~50–60°C) to the low-temperature region; the thermolysis was slowed down, and, correspondingly, the yield of solid products increased by 11%. In this case, the character of thermolysis of the structural fragments of biomass considerably changed: the decomposition of cellulose occurred much less intensely, whereas, on the contrary, the decomposition of hemicellulose and lignin accelerated. The carbonate additives affected the character of thermolysis of the AKKhZ

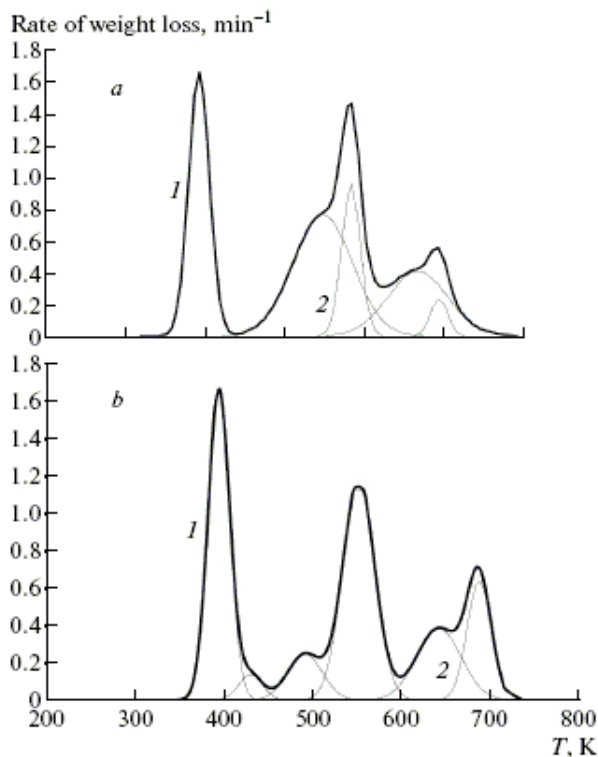


Figure 5. Schematic diagram of the main effects of the alkali metal eutectic on changes in the peak positions ($\bar{\alpha}T_{max}$, °C) and weight losses ($\bar{\alpha}m$, %) in the thermolysis of the structural constituents of carbon-containing products.

sludge: in the low-temperature region of the decomposition of light and heavy hydrocarbon fractions and their oxidation products, the process occurred much more intensely (the weight loss increased by a factor of 1.4) in almost a single step with T_{max} of 110°C. In this case, the medium-temperature decomposition of the organic matter of the AKKhZ sludge occurred at lower temperatures (by ~20°C); however, the yield of the solid product remained unchanged. The character of decomposition of spent petroleum product mixtures changed considerably: additional structural fragments aromatic hydrocarbons from the malthene fraction of spent petroleum product mixtures (an intense peak with T_{max} of 385°C), which did not underwent thermolysis in the absence of catalytic additives were involved in thermolysis. It is also evident that free and

bound water participated in thermolysis. The degree of thermal degradation of spent petroleum product mixtures in the presence of carbonates considerably increased (by about 30%) and amounted to 80.7% because of the occurrence of processes of this type. Carbonate additives resulted in an insignificant increase in the degree of thermal degradation of D coal. However, in this case, the character of OMC decomposition considerably changed: a new peak appeared in the region of low temperatures (150–220°C), which corresponds to the degradation of external polar groups. The high-temperature decomposition of the organic matter of D coal became more significant for the process of thermolysis as a whole and occurred at higher temperatures (by ~50–60°C).

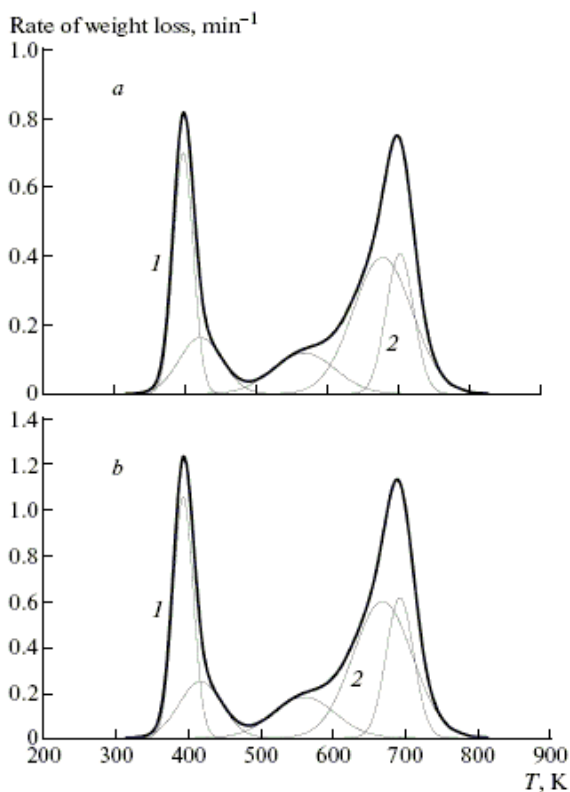


Figure 6. (a) Peak positions (T_{max} , °C) and weight losses (%) for the individual structural fragments of the initial carbon-containing products. (b) Effect of carbonate additives.

4. Conclusions

The experimental data and published concepts [23– 30] of the types of transformations that occur in the thermolysis of biomass, waste petroleum products, and coal-processing wastes provide unique theoretical prerequisites for the recognition and description of the thermal degradation of individual structural fragments in the test carbon-containing products: sunflower husks, spent petroleum product mixtures, AKKhZ sludge, and D coal. As a result of the analysis, we obtained a matrix of qualitative and quantitative data (Figs. 5, 6) for each type of the carbon-containing products used in this study with reliable information on the temperature ranges of decomposition for the particular structural fragments of biomass, petroleum or coal-processing waste, and D coal and on the quantitative degree of degradation at specified temperature and heating rate. Additionally, we found the main effects of the catalytic additives on the conversion of individual structural constituents of carbon-containing wastes (Figs. 5, 7). We intend to further develop this study in order to determine the main model reactions for the degradation of the individual structural constituents of carbon-containing products and the reactions of these products with alkali metal carbonates (and/or their conversion products) under the conditions of thermolysis.

References

1. Baikulatova, K.Sh., *Vtorichnoe syr'e—effektivnyi rezerv material'nykh resursov* (Secondary Raw Materials as Effective Material Resources), Alma-Ata: Kazakhstan, 1982.
2. Khmel'nitskii, A.G., *Munitsipal'nye i promyshlennye otkhody: sposoby obezvrezhivaniya i vtorichnoi pererabotki. Analiticheskie obzory: Ser. Ekologiya* (Municipal and Industrial Wastes: Neutralization and Utilization Processes. Analytical Reviews, Ser. Ecology), Novosibirsk, 1995.
3. Ravich, B.M., Okladnikov, P.M., Lygach, V.N., and Menkovskii, M.A., *Kompleksnoe ispol'zovanie syr'ya I otkhodov* (Multipurpose Utilization of Raw Materials and Waste), Moscow: Khimiya, 1988.
4. Maksimov, I.E., *Munitsipal'nye i promyshlennye otkhody: sposoby obezvrezhivaniya i vtorichnoi pererabotki. Analiticheskie obzory: Ser. Ekologiya* (Municipal and Industrial Wastes: Neutralization and Utilization Processes. Analytical Reviews, Ser. Ecology), Novosibirsk, 1995.
5. Bagryantsev, G.I. and Chernikov, V.E., *Munitsipal'nye I promyshlennye otkhody: sposoby obezvrezhivaniya I vtorichnoi pererabotki.*

- Analiticheskie obzory: Ser. Ekologiya* (Municipal and Industrial Wastes: Neutralization and Utilization Processes. Analytical Reviews, Ser. Ecology), Novosibirsk, 1995.
6. Bespamyatnov, G.P., Botushevskaya, K.K., and Zelenskaya, L.A., *Termicheskie metody obezvrezhvaniya otkhodov* (Thermal Methods for Waste Neutralization), Moscow: Khimiya, 1975.
 7. Gorislavets, S.P., *Piroliz uglevodorodnogo syr'ya* (Pyrolysis of Hydrocarbon Raw Materials), Kiev: Naukova Dumka, 1977.
 8. Mukhina, T.N., Barabanov, N.L., Babash, S.E., et al., *Piroliz uglevodorodnogo syr'ya* (Pyrolysis of Hydrocarbon Raw Materials), Moscow: Khimiya, 1987.
 9. Nassar, M.N., *Energy Sources*, 1999, vol. 21, p. 131.
 10. Vuthaluru, H.B., *Bioresource Technol.*, 2004, vol. 2, no. 2, p. 187.
 11. Hatakeyama, T. and Quinn, F.X., *Thermal Analysis—Fundamentals and Applications to Polymer Science*, Chichester: Wiley, 1999.
 12. Caballero, J.A., Marcilla, A., and Conesa, J.A., *J. Anal. Appl. Pyrolysis*, 1997, vol. 44, p. 75.
 13. Ahmed, S and Clements, L.D, *Research in Thermochemical Biomass Conversion*, Bridgwater, A.V. and Kuester, J.L., Eds., London: Elsevier, 1988, p. 295.
 14. Williams, R.H. and Larson, E.D, *Renewable Energy*, Johansson, T.B., Kelly, H., Reddy, A.K.N., and Williams, R.H., Eds., Washington, DC: Island, 1993, p. 729.
 15. Collot, A.G., Zhuo, Y., Dugwell, D.R., and Kandiyoti, R., *Fuel*, 1999, vol. 78, p. 667.
 16. Smith, L.H., Smoot, L.D., and Fletcher, T.H., *The Structure and Reaction Process of Coal*, New York: Plenum, 1994, p. 279.
 17. Phyllis Database for Biomass and Waste, Energy Res. Centre Netherlands: <http://www.ecn.nl/phyllis>.
 18. *Spravochnik vtorichnykh material'nykh resursov neftepererabatyvayushchei i neftekhimicheskoi promyshlennosti* (Handbook on Secondary Material Resources in Petroleum-Refining and Petrochemical Industries), Moscow: Ekonomika, 1984, p. 224.
 19. Levin, E.M., Robbins, C.R., and McMurdie, H.F., *Phase Diagrams for Ceramist*, New York: Marcel Dekker, 1964.
 20. Sestak, J., *Thermophysical Properties of Solids: Their Measurements and Theoretical Thermal Analysis*, Prague: Academia, 1984.
 21. Bazarnova, N.G., Karpova, E.V., Katrakov, I.B., et al., *Metody issledovaniya drevesiny i ee proizvodnykh* (Investigation Techniques

- for Wood and Its Derivatives), Barnaul: Altaisk. Gos. Univ., 2002.
22. *SCIENTIST* 3.0 Program, MicroMath Scientific Software, www.sstnet.com.
 23. Sharypov, V.I., Beregovtsova, N.G., Baryshnikov, S.V., and Skvortsova, G.P., Inst. Chem. Chem. Technol., Siberian Branch, Russian Academy of Sciences, Krasnoyarsk: www.shem.asu.ru/conf-2007/pdf/kniga3/sbornik_tezis-2007-kniga-III-037.pdf.
 24. Werther, J., Saenger, M., Hartge, E.U., Ogada, T., and Siagi, Z., *Progr. in Energy Combustion Sci.*, 2000, vol. 26, p. 1.
 25. Orfao, J.J.M., Antunes, F.J.A., and Figueredo, J.L., *Fuel*, 1999, vol. 78, p. 349.
 26. *Khimiya i pererabotka uglya* (Coal Chemistry and Processing) Lipovich, V.G., Ed., Moscow: Khimiya, 1988.
 27. Van Heek, K.H. and Hodek, W., *Fuel*, 1994, vol. 73, no. 6, p. 886.
 28. Dominguez, A., Blanco, C.G., Barriocanal, C., et al., *Chromatography. A*, 2001, vol. 918, no. 1, p. 135.
 29. Mildred, G., *Fundamentals of Petroleum*, Austin: Univ. Texas, 1986, p. 378.
 30. Jimhez-Mateos, J.M., Quintero, L.C., and Rial, C., *Fuel*, 1996, vol. 75, no. 15, p. 1691.

Chapter 14

Hybrid inorganic-organic mesostructured thin films

Agata Wawrzyńczak and Izabela Nowak

*Adam Mickiewicz University, Faculty of Chemistry,
Grunwaldzka 6, 60-780 Poznań, Poland*

Introduction

Considering the nature of the interactions existing between the organic and inorganic part of the hybrid mesostructured thin films, these materials can be classified into two different classes. First class corresponds to the doped systems in which organic compounds, for example low molecular weight molecules, oligomers or polymers, are simply embedded in the inorganic matrices. On the contrary, the second class corresponds to the hybrid systems in which organic and inorganic components are both connected through the stronger covalent or ionic-covalent chemical bonds. Additionally, it is crucial to have in mind that the doped-materials (class I) involve mostly a host-guest relationship with included species, whereas the functionalized ones (class II) imply a deeper relationship, since supplementary organic compounds participate in this materials [1].

Despite all the potential applications of doped-mesostructured thin films (class I), such as: incorporation of dyes and fluorescence-based compounds; synthesis of hybrid polymers-POMTFs (Periodic Organic-inorganic Mesoporous Thin Films) or living cells encapsulation, the localization of the organic components in the micellar part or/and in the opened pores of mesostructured thin films may strongly limit their potential applications, mainly because of the high tendency to leach the organic molecules. Thus, most often it is necessary to graft the organic components to the matrix via stronger chemical bonds, like covalent or ionic-covalent ones. Due to this limitations only the second class of the hybrid inorganic-organic mesostructured thin films is going to be discussed herein.

Functionalized hybrid mesoporous thin films - grafting routes

Two grafting routes are commonly used to incorporate the organic moieties into the structure of POMTFs: the “one-pot” synthesis and the post-functionalization (*Fig. 1*). The first one, *i.e.* “one-pot” synthesis, involves a

co-condensation step that occurs between a functional organic precursor, in general organosilane, and an inorganic precursor (typically TEOS or TMOS, less frequently TMOs - Transition Metal Oxides), in the presence of the template. In this case the mesostructuration process, meaning the formation of mesostructures, and functionalization step take place at the same time. In the second grafting method, namely *the* post-functionalization route, the chemical modification occurs when mesostructuration and calcination steps are already finished. Functionalization of these materials can be achieved via the impregnation from the solution or via vapor treatment by means of chemical bonds formation with silanol or M-OH groups that cover the pore surface of the mesostructured thin film. The “one-pot” synthesis is dedicated mostly to functionalize silica POMTFs, whereas the post-functionalization technique can be successfully used with silica and TMOs matrices. Nevertheless, the “one-pot” synthesis of the transition metal oxide, either via the use of organosilane precursors or with applying a complexing/chelating agent, has been recently reported [2].

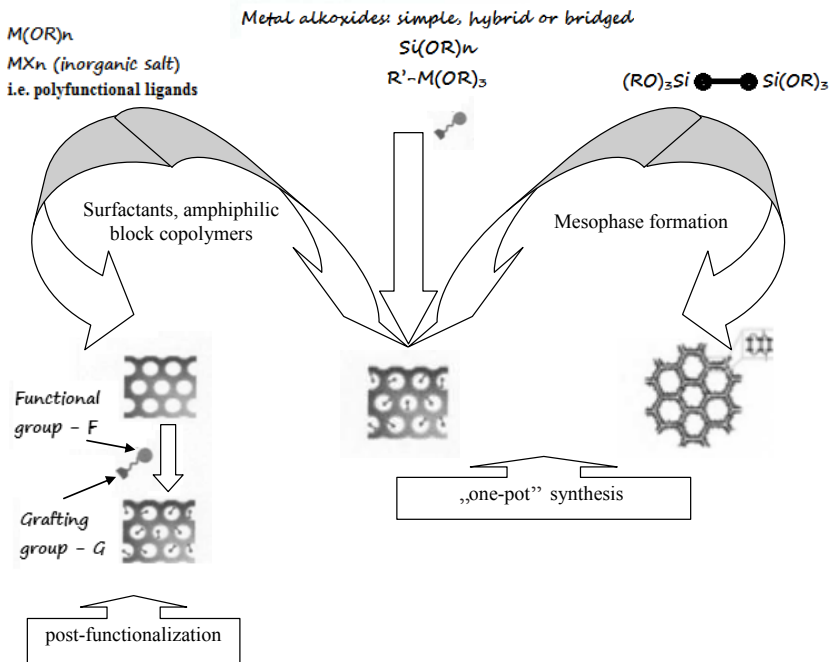


Figure 1. Grafting routes

Despite the fact that mainly the post-functionalization technique is exploited to modify properties of mesoporous molecular sieves (e.g. reviews [2, 3]), the most frequent route leading to the functional POMTFs is the “one-pot” synthesis. In fact, this approach allows to synthesize POMTFs bearing an enormous choice of the organic functionalities (e.g. [4]). These functional groups can be chemically inert, like alkyl chains or aromatic groups, as well as more reactive: aminoalkyl, methacryloxypropyl, cyanoalkyl, etc.

The main features of the “one-pot” and post-functionalization grafting routes are listed in the Table 1.

Table 1. “One-pot” synthesis versus post-functionalization [5]

“One-pot” synthesis	Post-functionalization
Tailor compatibility R-MX _n and MX _n	Tailor surface-R-MX _n interactions and reactivity
Network consolidation temperature limited by the thermal stability of organic groups	High pre-consolidation temperature (calcination step possible) before grafting, leading to a more stable inorganic network
Localization of organic groups in the pores and/or embedded in the framework, depending on the nature of the organic groups	Organic groups grafted mostly on the pore surface
Important role of organic groups in the mesostructuration process (e.g., polarity determination, condensation catalyst, co-surfactant, etc.)	Mesostructure determined before the incorporation of the organic groups
Relatively homogeneous dispersion of organic groups	Pore blocking possible
Limited by chemical compatibility	Limited by diffusion and pore blocking effects
One-pot synthesis, one or more functions in one synthesis, lower control of dispersion	One post-grafting, one function, successive functionalization possible

In general, the “one-pot” synthesis with a co-condensation step leads to a more homogeneous distribution (dispersion) of the organic functionalities inside the mesoporous matrices together with a high level of the stoichiometry control. The final materials exhibit only a small decrease of the pore sizes and pore volume when comparing with their non-functionalized counterparts. The

influence of the organic functions generally limits the organic/metal molar ratio, often being restricted to 20%. However, higher loadings of organosilanes, namely to 50% or even to 100%, may be achieved in the POMTFs synthesis either by a careful control of hydrolysis-condensation steps or by using the hybrid bridged silsesquioxanes [4, 5].

On the other hand, the post-functionalization route overcomes some difficulties related to the “one-pot” synthesis. Since the mesostructuration and grafting processes are two distinct steps, the direct influence of the organic functionalities during the synthesis can be eliminated. Moreover, the thermal treatment at high temperatures ($> 500^{\circ}\text{C}$) favors the formation of more stable matrices. That can be permitted only when organic functionalities are not present in the synthesized material. Of course, the post-functionalization method has also some drawbacks. It is worth mentioning that it often leads to a quite low loading and an inhomogeneous distribution of the functional groups inside the matrices. Furthermore, a decrease of the pore volume occurs quite often and sometimes, in extreme cases, a complete closure of the pores may happen [4]. In addition, depending on the post-grafting (impregnation) conditions, the inorganic network can partially suffer some damages derived from the capillary stress or the chemical cleavage of M-O-M bonds. Recently, the vapor infiltration treatment was successfully tested as an alternative route, leading to the materials without reduced pore sizes and with an increased mechanical strength [5].

Although the majority of the functionalized mesostructured thin films are obtained via “one-pot” and post-functionalization pathways, combined routes have been also investigated. This combined approach may occur especially when organosilanes are not commercially available. Instead of synthesizing the desired organosilanes before the film synthesis, some authors elaborated the procedure of obtaining hybrid thin films through co-condensation or post-functionalization technique with an organosilane bearing a reactive function (typically amino [6] thiol, [7] isocyano [8] groups). In this type of functionalization, after the removal of surfactant, the post-modification step takes place. It involves the interaction between the reactive function anchored into thin films and the organic molecules, like fluorescein derivatives, ferrocenecarboxylic acid [6], azobenzene derivatives [8] or α -cyclodextrin [7]. This combined approach connects the advantages of both: “one-pot” and post-functionalization pathways, allowing to limit the influence of organosilanes (often bulky) on the mesostructuration process and, at the same time, to avoid the synthesis of a too intricate organosilanes.

Functionalized hybrid mesoporous thin films – co-condensation or „one-pot” synthesis

The “one-pot” synthesis has been almost exclusively used to synthesize the silica-based hybrid mesostructured thin films via the co-condensation of organosilanes with TEOS or TMOS. However, Soler-Illia *et al.* [9, 10] reported the “one-pot” synthesis of highly ordered hybrid mesoporous thin films ($M_{1-x}(SiR)_xO_2$) obtained by the co-condensation of organotrialkoxysilanes ($R-Si(OEt)_3$, where R = propylamine, propylthiol and phenyl) with transition metal chlorides ($MC1_4$ with M = Zr or Ti). Such a new mixed oxide hybrid framework allows a further selective functionalization with metal chelating agents, leading to the bifunctional materials.

Although the “one-pot” synthesis presents several advantages when comparing to the post-grafting, it is perceived to be somehow more complicated. Several difficulties exist in addition to the controlling of the main parameters related to the EISA (evaporation-induced self assembly) process. For example, the presence of organosilanes, that present different reaction rates and self-assembling, can modify or even hinder the mesostructuration. Moreover, an increased amount of organosilanes in the reaction mixture favors condensation process to the cross-linking co-condensation reactions with the silica precursors. As the consequence it leads to an inhomogeneous distribution of different organic functionalities in the framework. In addition to that, the temperature of the network consolidation step has to be adapted to the organic compounds present inside the matrices.

Additionally, in some cases, the precursor may be insoluble, regardless the hydrolysis time. To overcome this problem, a pre-hydrolysis step of the organosilane in a weak acidic medium [11] and/or the use of a co-solvent are required. However, the choice of the co-solvent is also restricted by virtue of the limitations other than its dissolving properties. It has to be borne in mind that the co-solvent must not only dissolve the desired organofunctional molecule, but also has to be miscible with the starting sol without causing any organosilane gelation. Furthermore, it cannot affect in any way neither the film optical quality nor the mesostructuration. In addition, the co-solvent must present evaporation ability close to that of ethanol and assure a proper wettability towards the coating substrates. According to the literature, the most commonly employed co-solvent is the tetrahydrofuran alone or in a mixture with ethanol.

As it was already mentioned, the majority of hybrid POMTFs are obtained by the one step co-condensation process, where organosilanes and inorganic precursors (TEOS/TMOS) are mixed simultaneously in the initial sol. However, this one step co-condensation synthesis gives usually poorly organized hybrid

POMTFs, especially at high loading of organosilanes. Thus, an approach leading to well-ordered hybrid POMTFs with a high content of organosilanes has been developed [12].

Alternative “one-pot” synthesis was highlighted by Matheron *et al.* [13, 14]. This synthesis pathway is based on a pre hydrolysis-condensation step of TEOS, followed by the addition of organosilanes just prior the sol deposition. These conditions considerably limit the condensation of organosilanes before the film deposition and, in consequence, do not disrupt significantly the mesostructuration process.

The most of the commonly used organosilanes are monosilylated compounds, with a general formula: $F-S-Si(OR)_3$. Such molecules possess two different groups, one carrying the functionality and the other being the condensable groups. Both groups simultaneously interact with two different regions of the mesostructure. The condensable $-OR$ groups allow the formation of chemical bonds between the molecule and the framework. Generally, the localization of the functionality F is mainly governed by the „philicity” concept (i.e. “like” dissolves „like” or similar). Therefore, it is important to stress, that the localization of organosilanes is strongly governed by their physico-chemical properties. Several factors have to be taken into account, such as: the hydrophilic/hydrophobic balance of the organosilane molecule, the number of anchoring functions $(-OR)_3$, the length and the nature of the spacing groups (S - groups between the functionality F and the anchoring function $-Si(OR)_3$), the nature of the functionality F (hydrophobic, hydrophilic, ionic, polar, nonpolar, aromatic, etc.).

An increasing tendency is observed in the synthesis with probes presenting multiple trialkoxysilane functionalities. They are mainly incorporated inside the inorganic network, as was observed with multisilylated rare earth complexes [15], or they can even compose the walls of the framework, as observed with hybrid bridged silsesquioxanes [16], leading to the mesostructured thin films with organosilanes concentrations as high as 100%.

It is worth mentioning, that mesoporosity can be introduced into the materials’ structure by applying the synthesis that involves an appropriate templating agent. Surfactant molecules are commonly used as structure directing agents. In particular, their ability to form micelles is strongly demanded during synthesis of mesoporous materials. It is generally agreed that two kinds of sites are available when a molecule is solubilized inside surfactant micelles: one is near the polar head and the other one lies between alkyl chains in the hydrophobic core of the micelles [17]. It has been shown [18] that during the synthesis with CTAB as a template, the first sites that are occupied by aromatic compounds

lie near the polar head of the surfactant, probably due to specific interaction between the π system and the quaternary ammonium ion [19]. Once the first sites are saturated, the solubilization occurs in the hydrophobic part of the micelles, inducing a decrease of the curvature of the micelles geometry and causing a phase transition. However, the length and the nature of the spacing group (S) in organosilane may somehow hinder the natural placement of the hydrophobic functionality inside the micelles. For instance, with the same functionality (i.e. phenyl group) and the same relative amount of probes, no variation of mesophases was observed with the phenyltriethoxysilane, on the contrary to its counterpart with the (2-phenylethyl)trimethoxysilane (Fig. 2) [20].

Two main solubilizing sites: one (1^{st}) near the polar heads, the other (2^{nd}) inside the organic part

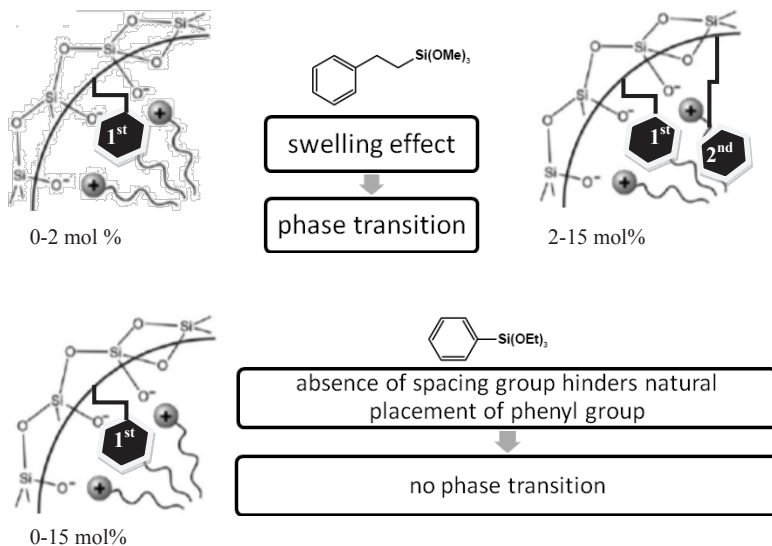


Figure. 2. Solubilization sites for phenyltriethoxysilane and (2-phenylethyl)trimethoxysilane cases [4]

The changes in the lattice parameters, that occur with an increasing amount of organosilanes, may be considered as a reliable indication of its preferential localization at the ionic interface, particularly near the polar heads of the micelles [20]. In the system CTAB-TEOS, the incorporation of a positively charged organosilane, namely 2-(trimethoxysilyethyl)pyridinium, induced the formation of a 2D-hexagonal phase ($p6m$), regardless of the loading ratio. However, the

authors observed a progressive increase of the interplanar distances $d(01)$ with the increasing incorporation of the protonated ammonium functions (Fig. 3). This observation also occurred with the other two positively charged groups that were studied (*i.e.* 3-(2,4-dinitrophenylamino)propyltriethoxysilane and 3-aminopropyltriethoxysilane). These results could be primarily attributed to the cationic character of the incorporated functions.

2D Hex $p6m$	1 mol%	8 mol%	15 mol%
	$d(01) = 3.7\text{nm}$	$d(01) = 4.1\text{ nm}$	$d(01) = 4.5\text{ nm}$

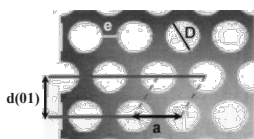



Figure 3. Increase of d -spacing with the quantity of 2-(trimethoxysilyethyl)pyridinium

The addition of increasing amounts of dibenzoylmethane/quinizarine derivatives for a fixed CTAB/silica molar ratio induces mesostructural evolutions in thin films. The following sequence was observed: cubic phase ($Pm3m$) < mixture of cubic ($Pm3m$) and 2D-hexagonal ($p6m$) < pure 2D-hexagonal phase < lamellar phase (Table 2). Such phase transitions are explained in terms of variation in the packing parameter g . The increase of the packing parameter can be due to the solubilization of large species, preferentially in the hydrophobic part of micelles during evaporation of solvents, leading to an increase of the total volume that is associated to the surfactant chain. This mechanism is supported by the UV-visible experiments performed on the hybrid thin films [21]. In this case, the incorporation of the large species causes direct phase transitions without modifications of the lattice parameters.

It worthy to add that co-solvent effect allows the formation of a mesophase for conditions at which mesostructured thin films are not usually obtained (*i.e.*, very low surfactant on silica ratio). The synthesis of mesoporous thin films with 10% mol of perfluoroalkylsilanes with long chains, typically tridecafluoro-1,1,2,2-tetrahydrooctyltriethoxysilane and heptadecafluoro-1,1,2,2-tetrahydrodecytrimethoxysilane, have been accomplished with sol containing a molar ratio CTACl/Si as low as 0.004. It is remarkable to point out (*i.e.* following the phase diagram of CTAB/Si/H₂O ternary system) that as a rule the lowest ratio CTAB/Si leading to the formation of mesostructured thin films is equal to 0.10. Moreover

for this last ratio, we could expect only a 3D hex mesophase ($P6_3/mmc$), which is a structure with a higher curvature of the micellar interface than the 2D-hexagonal phase ($p6m$) observed with the addition of the perfluoroalkylsilanes [21]. This result suggests that perfluoroalkylsilanes also act as a structure-directing agent when the reactant was mixed with a small amount of surfactant. Unquestionably, hydrolyzed perfluoroalkylsilanes carrying hydrophilic silanol head groups and long hydrophobic perfluoroalkyl chains can be clearly amphiphilic molecules.

Table 2. Phase transition according to the changes in the packing parameter g

		Packing parameter g				
		$g = V/a_0 \cdot l$				
						
		where a_0 = area of polar head; l = length of the alkyl chain; v = volume of the hydrophobic part				
α	<1/3	1/3 - 1/2	1/2 - 2/3	~1	>1	
Structures	Spherical micelles	Cylindrical micelles	3D Vesicles, flexible bilayers	Lamellae, planar bilayers	Inverse micelles	
Typical surfactant	single chain surfactant with a large polar head, e.g. $C_nH_{2n+1}N(C_2H_5)_3X$ (n=12-18), $18B_{4,3-17}$, C_{m-8-1} (n=12-18)	single chain surfactant with a small polar head, e.g. $C_nH_{2n+1}N(CH_3)_3X$ (n=8-18)	single chain surfactant with a small polar head, e.g. $C_{16}H_{33}(CH_2)_3N(CH_2)(C_6H_5)$, Gemini C_{m-8-1}	double chain surfactant and a small polar head, e.g. $C_nH_{2n+1}(CH_2)_3N(CH_2)_3X$ (n=20,22), $C_{16-2-16}$	double chain surfactant and a small polar head, e.g.	
Mesophase	SBA-6	SBA-7	MCM-41	MCM-48	MCM-50	FDU-2
	SBA-1	SBA-2	SBA-3	SBA-4		

Post-functionalization route

The other route leading to hybrid POMTFs consists of post-grafting organic functions onto stabilized inorganic (mainly silica, titania, ITO or opal) network. The difference of reactivity between silica and TMOs implies to differentiate these

two matrices towards post-functionalization. Indeed, grafting on silica matrices involves covalent bonds due to condensation reactions with organosilanes species which are also able to react on themselves. On the contrary, TMOs matrices are functionalized via ionic-covalent bonds with complexing/chelating agents which can only react with inorganic matrices. Moreover, the strength of bonds, from ionic-covalent to covalent, influences dramatically the properties of the resulting hybrid matrices in terms of diffusion, accessibility, homogeneity. The grafting of silica could be considered as irreversible while functionalization of TMOs is based on complexation equilibrium. Such differences render silica matrices much more sensitive to pore blocking due to extensive condensation of silica species. On the other hand, silica has shown a small hydrolytical stability and chemical durability, which represent a serious treat for several applications, whereas TMOs (e.g. titania) mesoporous films are much more water resistant [22].

Outlook

Due to its well defined pore network and surface reactivity, mesoporous silica thin films are especially widely studied for the absorption and separation of the biological molecules. In particular, hybrid mesoporous silica thin films has generated substantial interests [23-26]. Different mesoporous materials were investigated in applications such as high surface area catalysis [27-30], molecular sieves [31-34], gas sensors [35], opto-electronic devices [36-39] and drug delivery [40-44]. However, up to now the main issue remains the control of the morphology (pore size distribution, pore interconnectivity, etc). Additionally, it should be pointed out that synthesis routes toward these materials are not yet fully optimized and the synergy between sol-gel methods, supramolecular templating, and new macroscale templating techniques is needed to resolve this problem. Hierarchically ordered porous films present an enormous potential in such diverse and modern scientific fields as lab-on-chip components, membranes, heterogeneous catalysis and photocatalysis, drug carriers, (macro)molecule sensing, cell and tissue culture/regeneration [45]. However, full exploitation in such areas as development of robust, highly reproducible, and low-cost synthesis methods has to be achieved.

Acknowledgement

This paper was written with partial support from National Science Centre (Polish Ministry of Scientific Research and Information Technology) grant No. N204 538839; 2010-2013.

Glossary

2D	two-dimensional
3D	three-dimensional
CTAB	cetyltrimethylammonium bromide
CTACl	cetyltrimethylammonium chloride
EISA	evaporation induced self-assembly
FDU-2	mesoporous molecular sieve, cubic structure, Fm3m
Hex	hexagonal
ITO	indium tin oxide
MCM	Mobil Composition of Matter
MCM-41	Hexagonally-ordered Mesoporous Silicas from MCM family
MCM-48	MCM family representative with cubic structure
MCM-50	MCM family representative with lamellar structure
POMTFs	Periodic Organic-inorganic Mesoporous Thin Films
SBA	Santa Barbara Amorphous
SBA-1	mesoporous molecular sieve, cubic structure, Pm3n
SBA-2	mesoporous molecular sieve, hexagonal structure,, P6 ₃ /mmc
SBA-3	mesoporous molecular sieve, 2D hexagonal structure,, P6mm
SBA-6	mesoporous molecular sieve, cubic structure,, Pm3n
SBA-7	mesoporous molecular sieve, hexagonal structure,, P6 ₃ /mmc
SBA-15	mesoporous molecular sieve, 2D hexagonal structure,, P6mm
TEOS	tetraethoxy orthosilicate
TMOs	Transition Metal Oxides
TMOS	tetramethoxy orthosilicate

References

1. Sanchez. C., Ribot, F., *New J. Chem.* 1994;18:1007.
2. Hoffmann, F., Cornelius, M., Moreli, J., and Froba, M. *Angewandte Chemie-International Edition* 2006;45(20):3216.
3. Stein, A., Melde, B. J., and Schroden, R. C. *Advanced Materials* 2000;12(9):1403.
4. Nicole, L., Boissiere, C, Grosso, D., Quach, A., and Sanchez, C. *Journal of Materials Chemistry* 2005;15(35-36):3598.
5. Soler-Illia, G. J. A. A. and Innocenzi, P. *Chemistry-A European Journal* 2006;12(17):4478.

6. Fattakhova-Rohlfing, D., Rathousky, J., Rohlfing, Y., Bartels, O., and Wark, M. *Langmuir* 2005;2(24):11320.
7. Palaniappan, A., Li, X., Tay, F. E. H., Li, J., and Su, X. D. *Sensors & Actuators B: Chemical* 2006;119(1):220.
8. Sierocki, P., Maas, H., Dragut, P., Richardt, G., Vogtle, F., Cola, L., Brouwer, F. A. M., and Zink, J. I. *Journal of Physical Chemistry B* 2006;110(48):24390.
9. Soler-Illia, G. J. A. A., Angelome, P. C., and Bozzano, P. *Chemical Communications* 2004;(24):2854.
10. Angelome, P. C. and Soler-Illia, G. J. A. A. *Journal of Materials Chemistry* 2005;15(35-36):3903.
11. Jung, J., Bae, J. Y. and Bae, B. S. *Journal of Materials Chemistry* 2004;14(13):1988.
12. Fan, H. Y., Lu, Y. F., Stump, A., Reed, S. T., Baer, T., Schunk, R., Perez, L. V., Lopez, G. P., and Brinker, C. J. *Nature* 2000;405(6782):56; Fan, H. Y., Reed, S., Baer, T., Schunk, R., Lopez, G. P., and Brinker, C. J. *Microporous & Mesoporous Materials* 2001;44:625.
13. Matheron, M., Bourgeois, A., Brunet-Bruneau, A., Albouy, P. A., Biteau, J., Gacoin, T., and Boilot, J. P. *Journal of Materials Chemistry* 2005;15(44):4741; Matheron, M., Bourgeois, A., Gacoin, T., Brunet-Bruneau, A., Albouy, P. A., Boilot, J. P., Biteau, J., and Lacan, P. *Thin Solid Films* 2006;495(1-2):175.
14. Matheron, M., Gacoin, T., and Boilot, J. P. *Soft Matter* 2007;3:223.
15. Innocenzi, P., Falcaro, P., Schergna, S., Maggini, M., Menna, E., Amenitsch, H., Soler-Illia, G. J. A. A., Grosso, D., and Sanchez, C. *Journal of Materials Chemistry* 2004;14(12):1838.
16. Pai, R. A. and Watkins, J. J. *Advanced Materials* 2006;18(2):241.
17. Nagarajan, R. *Current Opinion in Colloid & Interface Science* 1997;2(3):282; *ibid*, 1996;1(3):391.
18. Desplantier-Giscard, D., Galarneau, A., Di Renzo, F., and Fajula, F. *Studies in Surface Science & Catalysis* 2001;135:06P27.
19. Kumpf, R. A. and Dougherty, D. A. *Science* 1993;261:1708; Kim, K. S., Lee, J. Y., Lee, S. J., Ha, T.-K., and Kim, D. H. *Journal of the American Chemical Society* 1994;116:7399.
20. Cagnol, F., Grosso, D., and Sanchez, C. *Chemical Communications* 2004;15:1742.
21. Quach, A., Escax, V., Nicole, L., Goldner, P., Guillot-Noel, O., Aschehoug, P., Hesemann, P., Moreau, J., Gourier, D., and Sanchez, C. *Journal of Materials Chemistry* 2007;17:2552.

22. Zhao, Y., Sheng, X., Zhai, J., Jiang, L., Yang, C., Sun, Z., Li, Y., Zhu, D. *Chem. Phys. Chem.* 2007;8:856–861.
23. Lu Y., Ganguli R., Drewien C. A., Anderson M. T., Brinker C. J., Gong W., Guo Y., Soyeyz H., Dunn B., Huang M. H., Zink J. I. *Nature* 1997;389:364–368.
24. Zhao D., Yang P., Melosh N., Feng J., Chmelka B. F., Stucky G. D. *Adv. Mater.* 1998;10:1380–1385.
25. Wan Y., Shi Y., Zhao D. *Chem. Commun.* 2007;9:897–926.
26. Sanchez C., Boissiere C., Grosso D., Laberty C., Nicole L. *Chem. Mater.* 2008;20:682–737.
27. Maschmeyer T., Rey F., Sankar G., Thomas J. M. *Nature* 1995;378:159–162.
28. Liu J., Yang Q., Kapoor M. P., Setoyama N., Inagaki S., Yang J., Zhang L. J. *Phys. Chem. B* 2005;109:12250–12256.
29. Wan Y., Wang H., Zhao Q., Klingstedt M., Terasaki O., Zhao D. *J. Am. Chem. Soc* 2009;131:4541–4550.
30. Thomas J. M., Hernandez-Garrido J. C., Raja R., Bell R. G. *Phys. Chem. Chem. Phys* 2009;11:2799–2825.
31. Kresge C. T., Leonowicz M. E., Roth W. J., Vartuli J. C., Beck J. S. *Nature* 1992;359:710–712.
32. Tanev P. T., Pinnavaia T.J. *Chem.Mater* 1996;8:2068–2079.
33. Bagshaw S. A., Prouzet E., Pinnavaia T. J. *Science* 1995;269:1242–1244.
34. Yiu H. H. P., Wright P. A. *J. Mater. Chem.* 2005;15:3690–3700.
35. Rossinyol E., Arbiol J., Peir F., Cornet A., Morante J. R., Tian B., Bo T., Zhao D. *Sens. Actuators B: Chem* 2005;109:57–63.
36. Scott B. J., Wirnsberger G., Stucky G. D. *Chem. Mater.* 2001;13:3140–3150.
37. Yamada T., Zhou H., Uchida H., Honma I., Katsube T. *J. Phys. Chem. B* 2004;108:13341–13346.
38. Yamada T., Zhou H.-S., Uchida H., Tomita M., Ueno Y., Ichino T., Honma I., Asai K., Katsube T. *Adv. Mater.* 2002;14:812–815.
39. Sel O., Sallard S., Brezesinski T., Rathousky J., Dunphy D. R., Collord A., Smarsly B. M. *Adv. Funct. Mater.* 2007;17:3241–3250.
40. Mal N. K., Fujiwara M., Tanaka Y. *Nature* 2003;421:350–353.
41. Munoz B., Ramila A., Perez-Pariente J., Diaz I., Vallet-Regi M. *Chem. Mater.* 2002;15:500–503.
42. Vallet-Regi M., Ramila A., del Real R. P., Perez-Pariente J. *Chem. Mater.* 2000;13:308–311.

43. Lai C.-Y., Trewyn B. G., Jeftinija D. M., Jeftinija K., Xu S., Jeftinija S., Lin V. S. Y. *J. Am. Chem. Soc* 2003;125:4451–4459
44. Slowing I. I., Trewyn B. G., Giri S., Lin V. S.-Y. *Adv. Funct. Mater.* 2007;17:1225–1236.
45. Innocenzi P., Malfatti L. and Soler-Illia G. J. A. A. *Chem. Mater.* 2011;23:2501–2509

Chapter 15

Terpyridine as molecular receptor in functional polymers

Szymon Jasiocki and Grzegorz Schroeder

*Adam Mickiewicz University, Faculty of Chemistry,
Grunwaldzka 6, 60-780 Poznań, Poland*

Supramolecular chemistry has become one of the major field of present chemical research since Lehn, Pedersen and Cram received the Nobel prize in 1987. Their studies in selective host-guest chemistry have become the concept of supramolecular chemistry [1]. The basic processes in supramolecular chemistry like self-recognition and self-assembly are based on the non-covalent interactions. These interactions (hydrogen bonding, ligand-metal coordination, π - π interactions) are weaker than covalent bonds and usually reversible. Inter- and intramolecular non-covalent interactions are highly important for most biological processes. Nature is therefore the model for artificial supramolecular phenomena.

N-Heterocycles are generally known for their complexing ability toward transition metal ions in their low oxidation states, such as iron(II), cobalt(II), copper(II), nickel(II), and ruthenium(II). Effective formation and stability of those complexes entitle these ligands to be molecular receptors for such metal ions. These properties, initially utilized in analytical chemistry, gave rise metal coordination to be used extensively in supramolecular chemistry. In particular, chelating ligands based on pyridine are of interest, since they allow the construction of defined supramolecular architectures and possess an increased stability compared to hydrogen bonding.

The most important are 2-2'-bipyridine and 2,2':6',2''-terpyridine (Tpy), which act as bidentate and tridentate chelating agents, respectively. Metal complexes of terpyridine as well as bipyridine are widely discussed by Schubert et al. [2-5]. Bipyridines were synthesized and utilized earlier than terpyridines which was attributed to synthetic difficulties especially for substituted terpyridines, necessarily to obtain building blocks. Terpyridines were first discovered by Morgan and Burstall in the 1930s as a byproduct of pyridine condensation with anhydrous FeCl_3 [6]. The structure of 2':6',2''-terpyridine and its metal complex structure is presented in Fig. 1.

The most common coordination geometry of terpyridine–metal complexes is distorted octahedron. However the geometry depends on the nature of the metal ion used and other geometries are obtained (square planar for Pt^{2+} or Pd^{2+} [7]). The octahedral geometry requires the complex stoichiometry to be two tridentate terpyridines for metal ion or one terpyridine with additional ligands attached to the metal center.

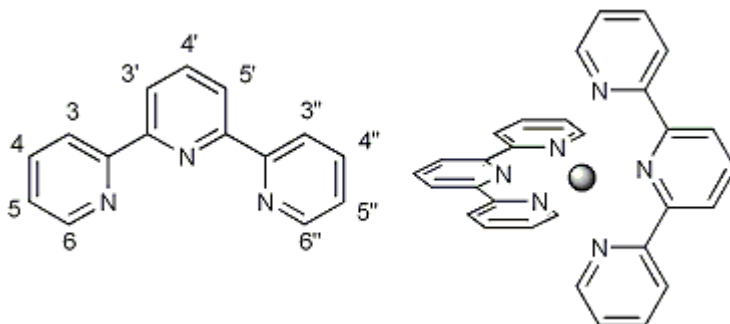


Figure 1. 2,2':6',2'' terpyridine (left) and bis-terpyridine-metal octahedral complex (right).

There are other than 2,2':6',2''-terpyridine-metal complexes forming supramolecular assemblies reported, namely 3,2':6',3''-terpyridine [8] and 4,2':6',4''-terpyridine [9,10] (Fig. 2). However, the coordination character of those structures is different and is not discussed here. This review is devoted only to 2,2':6',2''-terpyridine and its complexes, the ligand is therefore abbreviated to terpyridine.

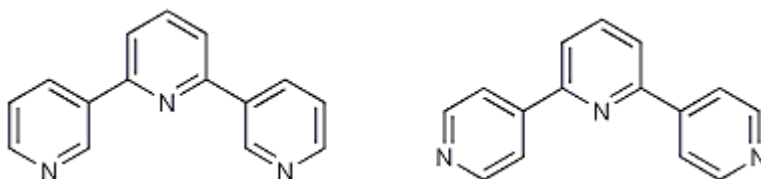


Figure 2. Structures of 3,2':6',3''-terpyridine (left) and 4,2':6',4''-terpyridine (right).

4'-Functionalized terpyridines are versatile building blocks for supramolecular assemblies and polymers. One of the most popular substrate for functionalization is 4'-chloroterpyridine. Numerous reactions are carried between 4'-chloroterpyridine and alcohols in polar, aprotic solvent (for example DMSO)

using KOH or similar base (Fig. 3) [2]. The reaction of 4'-chloroterpyridine with dihydroxy compounds produces telechelic bisterpyridine ligands, which can be self-assembled with various transition metal ions.

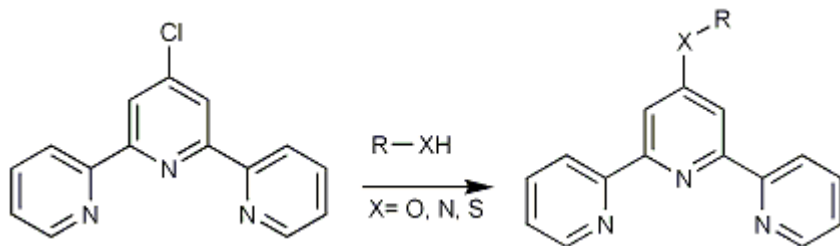


Figure 3. General strategy for functionalization of 4'-chloroterpyridine.

Using functionalized terpyridine molecules, especially functionalized in 4' position, systems containing two (dyads), three (triads), and more terpyridine-metal complex units can be created (Fig. 4). The coordination of metal ion by two terpyridine moieties from two separate molecules combine them together. Building blocks containing two terpyridine groups within the molecule structure lead to linear assemblies. Building blocks consisted of more terpyridine units produce higher dimensionality of assemblies.

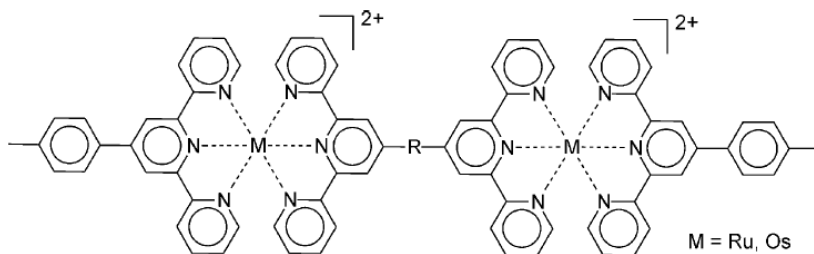


Figure 4. Schematic representation of a dyad [4].

Depending on the coordination metal ion employed, these assemblies can be homonuclear or heteronuclear (the same or different metal ion). Building blocks where two and more terpyridine moieties are conjugated produce grid-type supramolecular structures (Figs. 5 and 6).

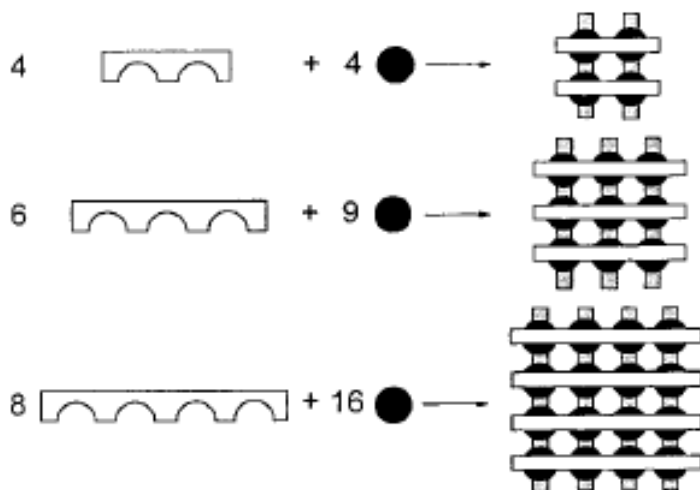


Figure 5. Schematic representation of the self-assembly process of $[2 \times 2]$, $[3 \times 3]$ and $[4 \times 4]$ grid-type architectures [11].

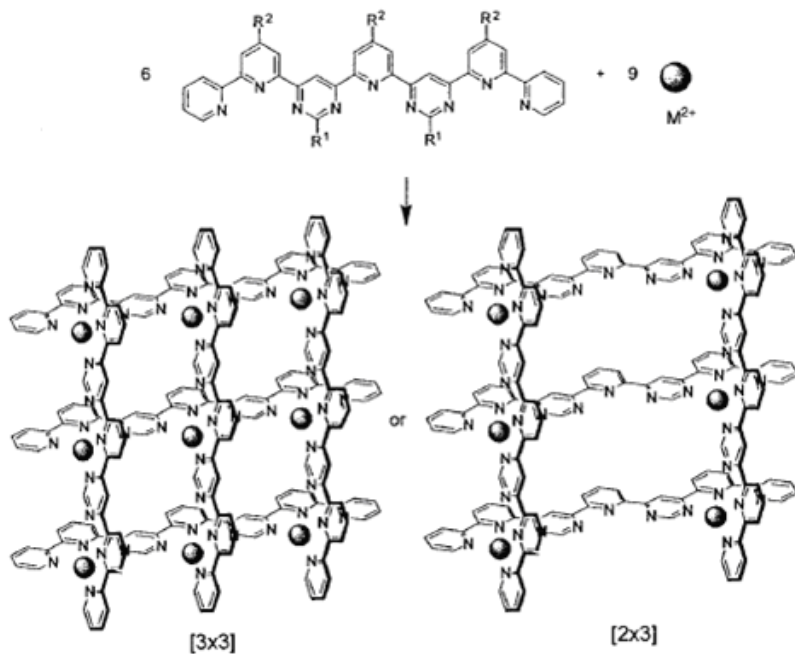


Figure 6. The self-assembly of a $[3 \times 3]$ grid (left) and a $[2 \times 3]$ grid (right) [11].

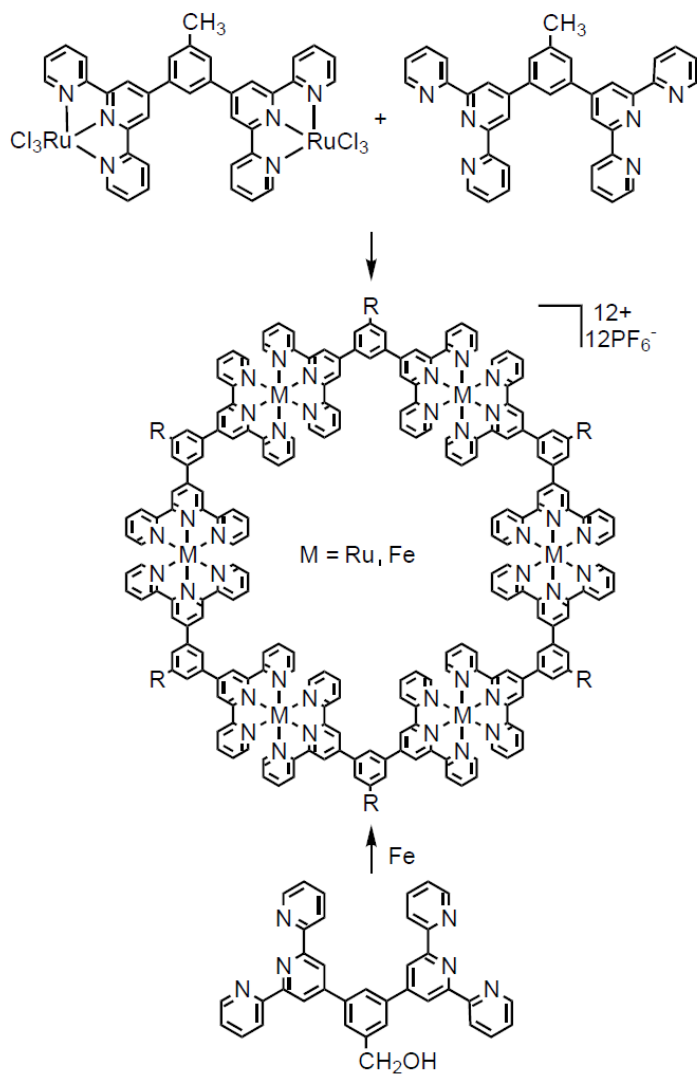


Figure 7. Two approaches of the hexameric metallomacrocycle synthesis [13].

However, the structure obtained depends strongly on the ligand substituent, the metal ion, the counterion, the solvent, and the reaction conditions [11]. More examples of grid-type assemblies are compiled in paper [4]. Another type of oligomeric assemblies are macrocycles. Directed construction of such frameworks can be obtained due to the desired angular terpyridine-based building blocks [12-15]. An example of hexameric macrocycle consisted of equimolar amount of bis-(terpyridinyl) ligand and coordination metal is presented in the Fig. 7 [13]. This structure is acquired using two synthetic strategies. In the first directed assembly of bismetallated and nonmetallated ligands occur, in the latter self-assembly of nonmetallated monomers is obtained upon the addition of metal ions. The identical structure was confirmed by TEM experiment.

An interesting illustration of assembly-disassembly process generating macromolecular superstructure is presented in Figs. 5, 7 and 8 [15].

This reversible process of molecular imprinting mimics the natural biosystems, especially for recognition process. The flexible 114-membered macrocycle in the presence of Fe^{2+} ions gives purple-coloured inner macrocyclic complex. Decomplexation occurs quantitatively upon potassium carbonate in DMF treatment. The metal free compound can be changed into complex again, therefore is very attractive for high conversion complexation purposes.

The layer-by-layer method was applied for fabrication of self-assembled Fe-TPBI (terpyridine-functionalized perylene bisimide Fe complex) multilayers on gold substrate [16]. AFM measurements indicate that the assembled metal-ligand chains grow approximately perpendicular to the gold surface. Time-resolved spectroscopy measurements seem to indicate that the energy absorbed by the multilayer is promptly dissipated to the gold surface by ultrafast processes (Fig. 9).

An example of reversible functionalization of the surface utilizing click chemistry of acetylene and azide groups is reported by Haensch et al. [17]. To the azide terminated silane monolayer on the substrate, the acetylene functionalized terpyridine-metal complex was covalently bonded (Fig. 10).

By the choice of the coordinating metal ion, different optical surface properties could be obtained. A subsequent decomplexation with hydrochloric acid gave the free ligand monolayer on the surface. This could be performed also by the addition of a strong competing ligand as hydroxyethyl ethylenediamine triacetic acid. However, in case of the silane monolayers its limited stability toward basic environments does not allow this approach. Decomplexation step allow a versatile method to reversibly functionalize surfaces. Terpyridine containing polymers can be obtained by coordination of different transition metal ions as cuprum(II) [18], lanthanides [19], and cadmium(II) [20].

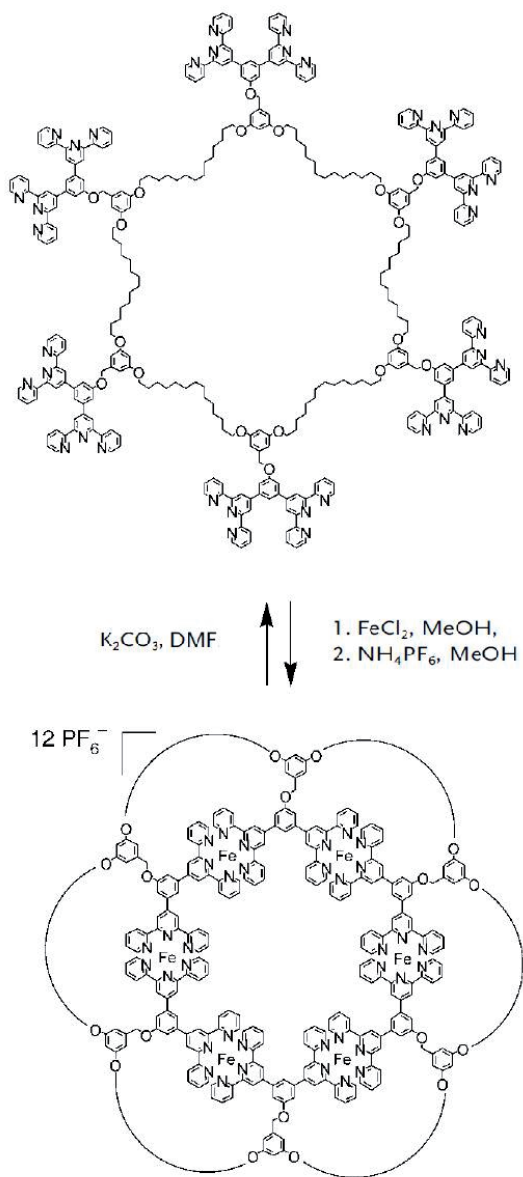


Figure 8. Metalation and demetalation process of the hexameric macrocycle [15].

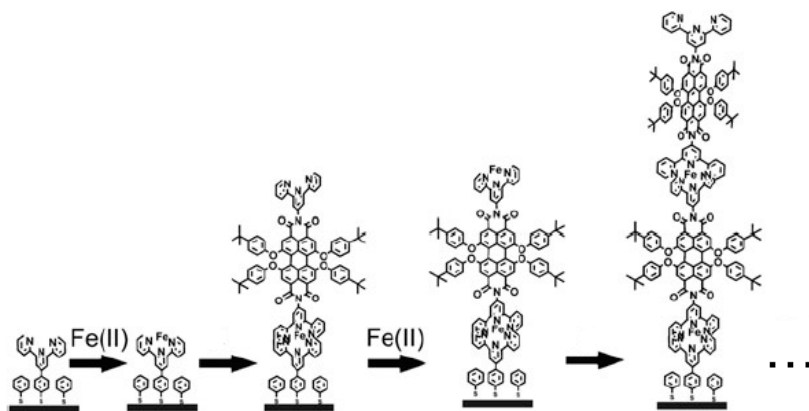


Figure 9. Schematic representation of supramolecular self-assembled Fe-TPBI multilayers formation [16].

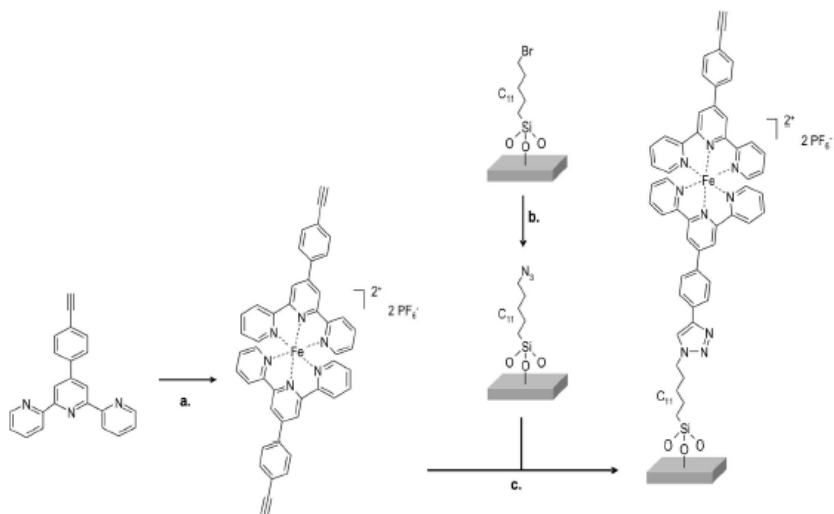


Figure 10. Schematic representation of the synthesis of the acetylene functionalized Fe(II) bis-terpyridine [17].

Mixed ligand metal-organic complexes with 4'-(3-pyridyl)-2,2':6',2''-terpyridine (pytpy) and diphenic acid (H_2dpa) or 4,5-imidazoledicarboxylic acid (H_3IDC) have been reported [21, 22]. Different coordination modes refers also to dpa^{2-} ligand and a one-dimensional helical chain is a one-dimensional double layer chain. Additionally π - π interactions of aromatic rings in the terpyridine molecules allow these structures to be extended into higher dimensionality. The most significant difference between the two analogous complexes $[Cd(HIDC)(pytpy)]$ (1) and $[Zn(HIDC)(pytpy)] \cdot (H_2O)$ (2) results from the pytpy ligand different π - π interactions [22]. As a consequence the chains are connected into 3-D and 2-D supramolecular structures.

Another example of terpyridine-based polymer is polyimide with 5,5''-bis(bromomethyl)-terpyridine incorporated into the main chain [23]. Such substituted terpyridine was polymerized with a designated aromatic diimide resulting in a resin product insoluble in water (Fig. 11).

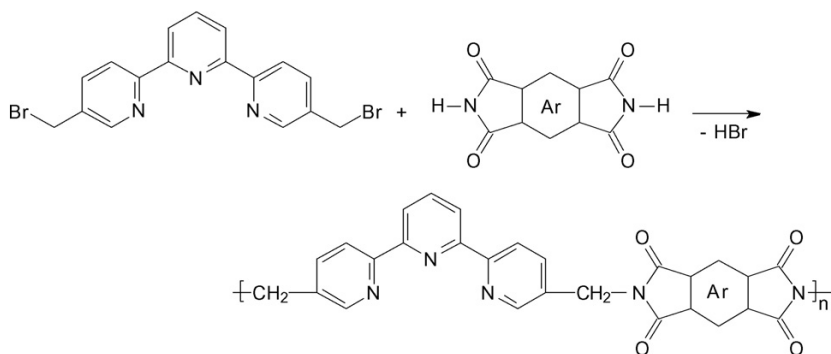


Figure 11. Scheme of synthesis of terpyridine-based polyimides [23].

The terpyridine-based polyimide polymer was fabricated and utilized as a sorbent in solid-phase extraction (SPE) toward heavy metals. This type extraction is resulted from insolubility of the material in water and is proceeded due to the coordination of terpyridine moieties. Polymer is characterized with high capability (8mg of metal/g of sorbent) and reusability. Adsorbed metal ion can be extracted with inorganic diluted acid. There is also possibility to gain selectivity toward metal ion changing pH. The pH influence at the metal concentration of $1.5 \times 10^{-1} \text{ moldm}^{-3}$ after 24h is given in Fig. 12.

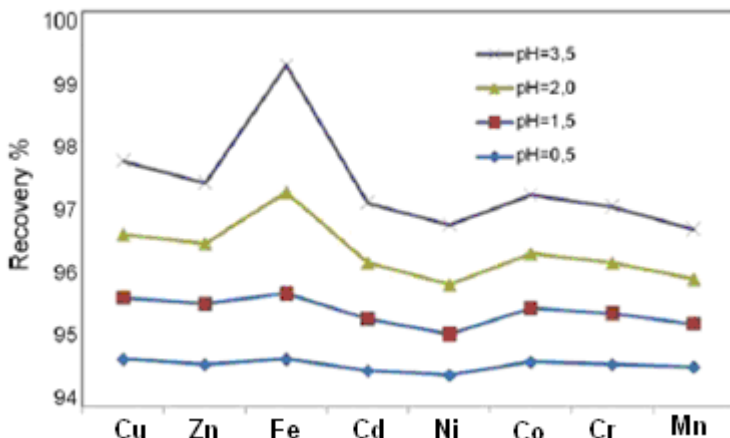


Figure 12. The pH dependency of simultaneous sorption of metals for the polyimide polymer [23].

A group of macromolecular building blocks based on polyether chain terminated with terpyridine molecules have been synthesized by Chiper et al. [24]. The nature of poly(tetrahydrofuran), poly(2-ethyl-2-oxazoline) or Pluronics chain used (Fig. 13) gives the possibility to synthesize metallo-supramolecular chain extended polymers upon metal complex formation. The properties of the obtained polymers depend on the metal ions and the counter ions used. Additionally thermosensitive properties of the Pluronics provide multiresponsive character of these polymer structures.

Ditopic ligands containing terpyridine moieties form coordination polymers with transition metal ions. Disregarding the counterions these polymers can be treated as positively charged polyelectrolytes. Applying well-known layer-by-layer electrostatic self-assembly method, ultrathin film on the planar substrate utilizing these metallosupramolecular polyelectrolytes (MEPE) and poly(styrene) sulfonate was formed (Fig.14) [25]. X-ray reflectometry, ellipsometry and UV-Vis methods confirmed formation of Fe(II)-MEPE/PSS and Ni(II)-MEPE/PSS films consisted of two monolayers per deposition. There is no metal ion exchange observed for these monolayers.

The next example are thin films fabricated employing the coordinative self-assembly [26-28]. The basic of this method is the synthesized polymer with terpyridine moieties incorporated in side chains, which acts as a polytopic ligand. The terpyridine groups allow immobilization of the polymer chain on the surface, while they form complexes with metal ions (Fig. 15).

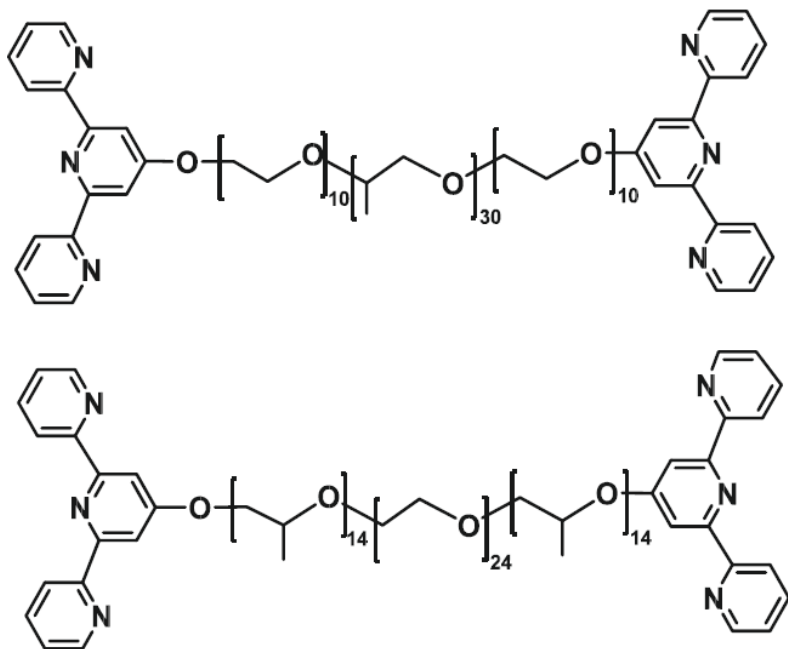


Figure 13. Chemical structures of bis-terpyridine Pluronics® [24].

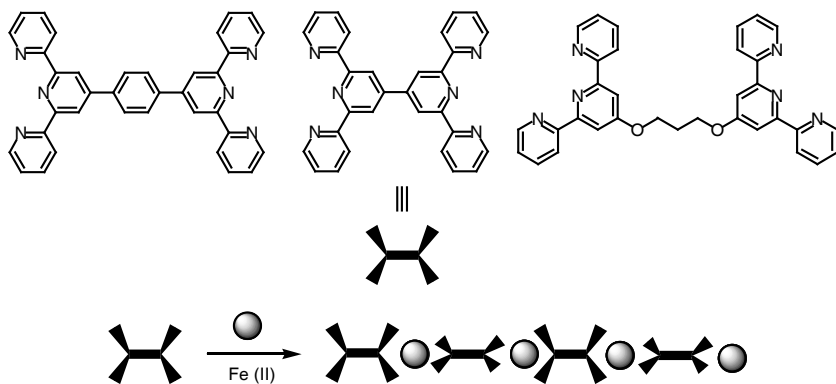


Figure 14. Bis-terpyridine ligands as metallosupramolecular polymer formation [25].

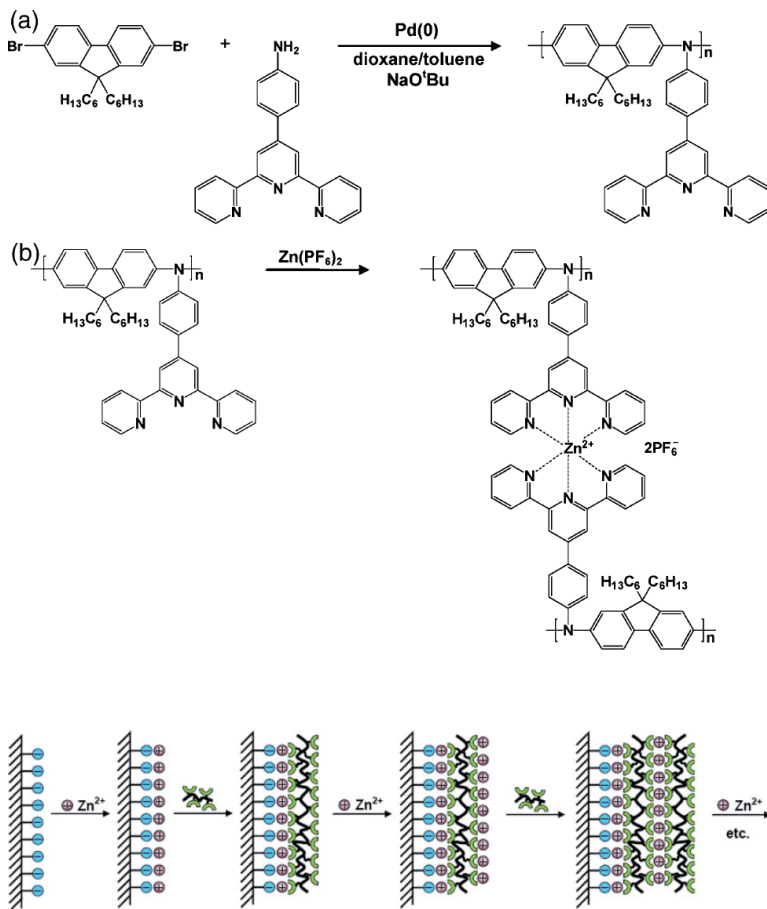


Figure 15. Top: Synthesis of poly(imino)fluorene-tpy a) and complex formation with zinc cation b); Bottom: Zinc coordination-polymer network formation via sequential assembly process on a solid substrate [26].

The structure of such fabricated thin film is rigid and porous comparable with metal-organic frameworks. The application of arylene groups in the polymer chain enables reversible oxidation processes, which depending on the potential applied are indicated by color change. In this particular example the poly(imino)fluorene is used and the color alters from yellow (neutral state) through red to blue (with the potential ranging from 310mV to 560 mV) as the oxidation state increases. Spectroelectrochemical measurements indicate that the switching time at different potentials

is up to 500 ms. This provides these coordinative thin films to be electrochromic and fast-switching materials. Morphology study of this kind of films was carried using scanning electron microscopy (SEM). The surface structure of thin film formed by zinc and polyiminocarbazolyene complex (a) and a cross-section of functionalized ITO glass substrate (b) after 12 dipping cycles show Maier [28]. The surface of the film is smooth, with some aggregates, and the thickness is 47nm, three times less than the indium-tin oxide coating, which is also visible in the picture. The film thickness depends on the complex solubility and the stability constant.

Terpyridine-metal complex units might be used as a core of dendrimer (especially for connecting dendrons) as well as can be incorporated in dendrimer arms or terminal group. (Figs. 17 and 18).

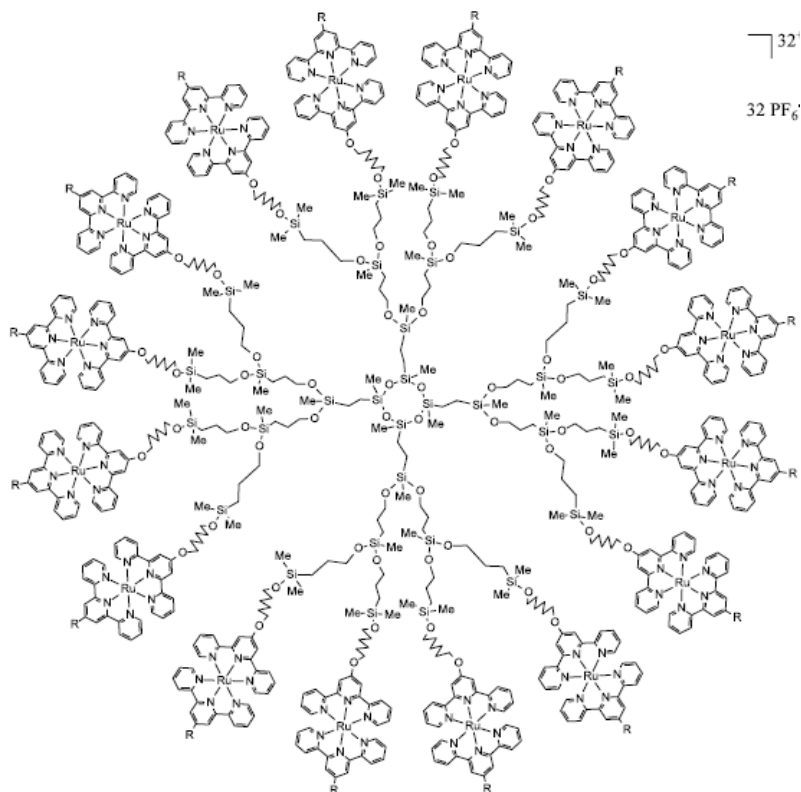


Figure 17. Terpyridine-Ru(II) complexed carbosilane 3-rd generation terpyridine dendrimer [29].

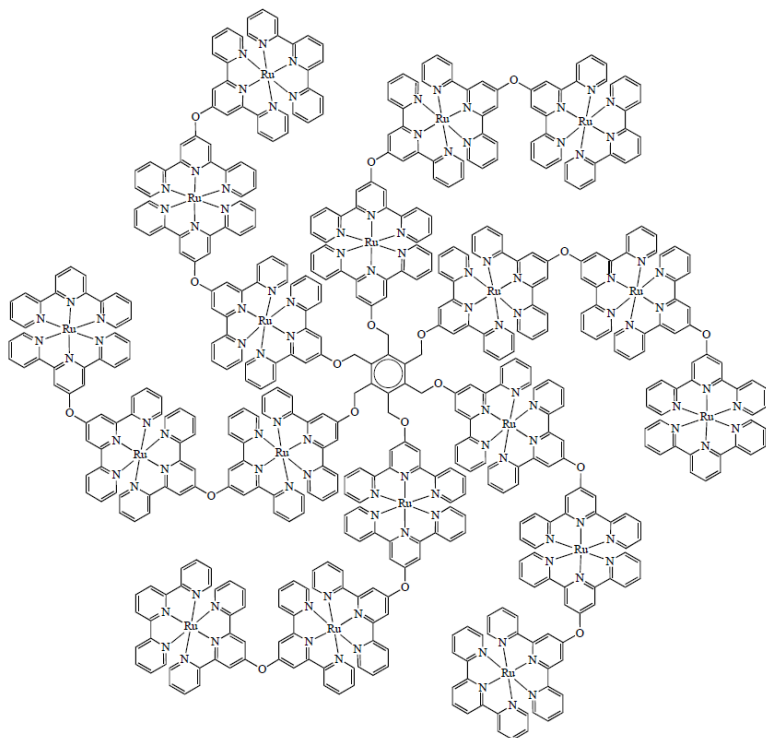


Figure 18. Star-shaped dendrimer with 18 $Ru(Tpy)_2$ complexes [30].

In the first case, metal-complex based core enables a convenient approach for convergent synthesis of dendrimers. Metal containing dendrimers are of special interest because they can be potentially useful as catalysts or light-harvesting units. The terpyridine groups on dendrimers accepted the ruthenium chloride ions on the mild condition that resulted in the paramagnetic ruthenium complex. Subsequent addition of terpyridine to the ruthenium-terpyridine complex on the dendritic periphery produced bis(terpyridine)ruthenium(II) complex which revealed diamagnetic property [29].

A novel polymer-supported terpyridine-palladium complex have been developed through ionic bonds to sulfonate group, which efficiently catalyzed the Suzuki–Miyaura cross-coupling reaction of aryl halides with aryl boronic acids in water under aerobic conditions to give the corresponding biaryls in high to excellent yield. This catalyst was recovered and reused several times without any loss of catalytic activity [31] (Fig 19).

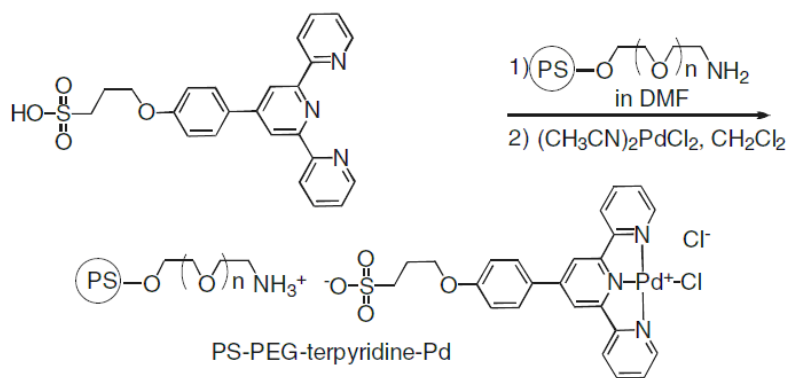


Figure 19. PS-PEG-terpyridine Pd²⁺ ionic complex [31].

The possibility to combine synthetic and natural binding systems brings a new generation supramolecular architectures. One of well-known systems is biotin bound to avidin and streptavidin proteins. It is a strong non-covalent binding system (Figs. 20 and 21). This association of receptors opens new of biosensor-building blocks as well as other applications as nonreactors or drug delivery systems [32].

A one-dimensional metal-organic protein framework is reported [33]. This resulted from the self-assembly of streptavidin protein-linker and tetrabiotinylated connector based on terpyridine-Fe²⁺ complex (Fig. 21). The conjunction of transition metal receptor as terpyridine with biotin allows the process of controlled protein aggregation. This assembly, in the presence of calcium ions, was used as a template for biomineralization of calcite to yield millimeter-sized bundles.

A combination of polytopic ligands containing transition metal binding site (terpyridine unit) and specifically lithium ion binding site (trispirotetrahydrofuranly unit) is presented in Fig. 22 [34]. The terpyridine acts here as an endoreceptor selectively coordinating Cu⁺ or Fe²⁺ ions inside the molecule while Li⁺ ions are bound to the peripheral exoreceptors. Both receptors are binding to the metal ions independently.

Among the approaches to supramolecular polymers is the use of self-complementary multiple hydrogen bonding units that are characterized by increased stability compared to single hydrogen bonds [35, 36] (Fig. 23). The quadruple hydrogen-bonding interactions of ureidopyrimidinone moieties at one end of molecule and coordination of transition metal ions by terpyridine moieties at the other end provide extended supramolecular polymer network.

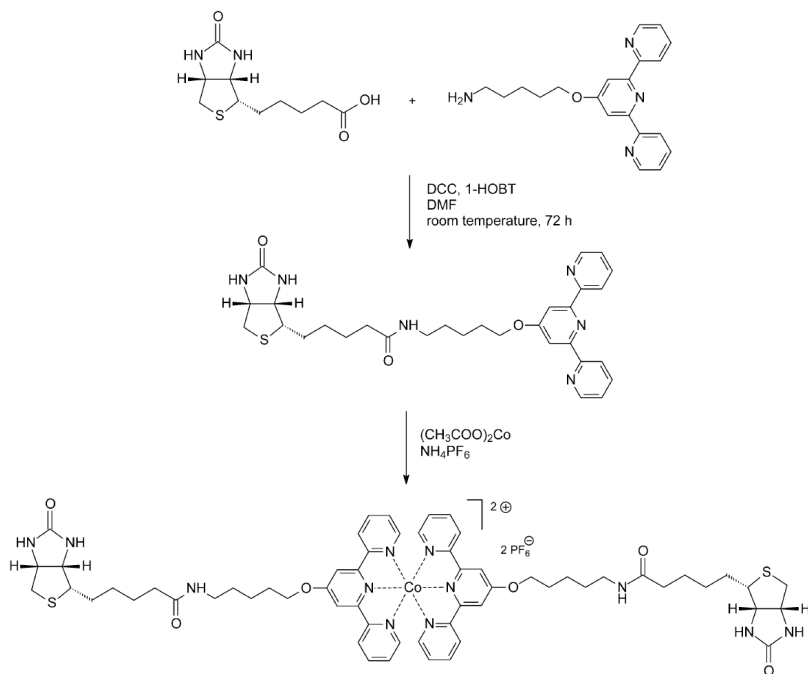


Figure 20. Synthesis of the biotin-functionalized terpyridine and complexation with cobalt(II) ions [32].

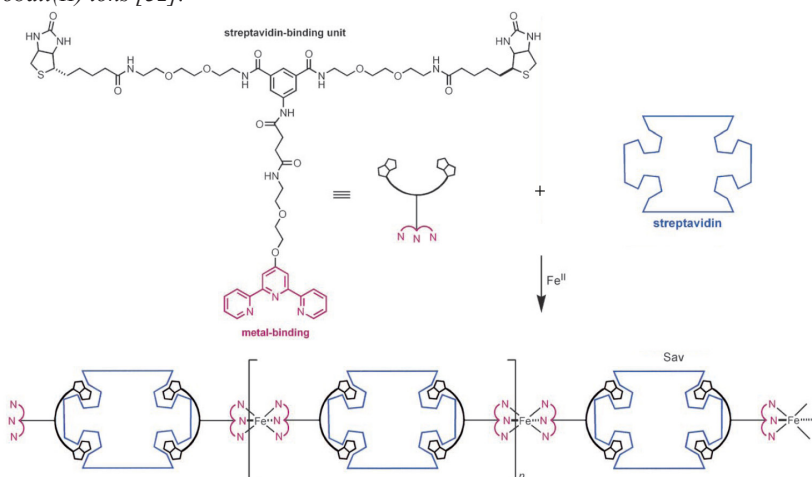


Figure 21. A linear polymer formation in the presence of streptavidin and Fe^{2+} ions [33].

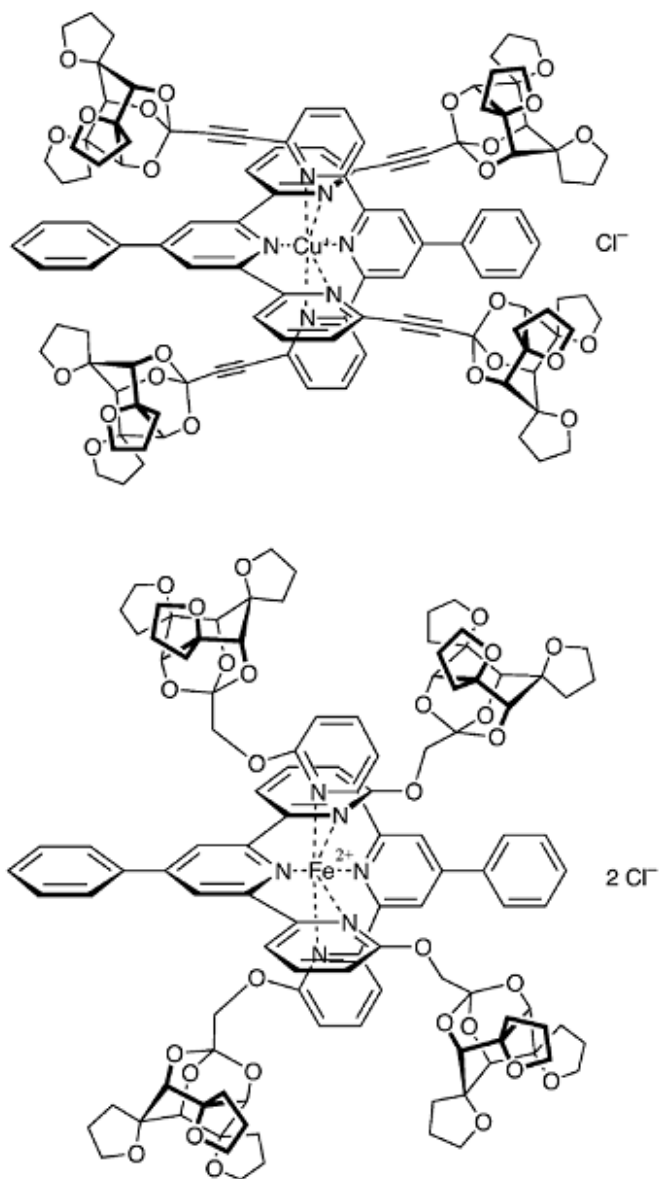


Figure 22. Complex derivatives of terpyridine with Cu^+ and Fe^{2+} [34].

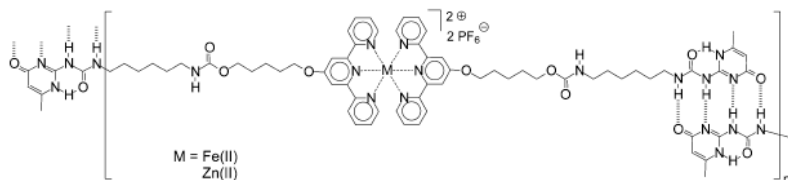


Figure 23. Metallo-supramolecular polymer formed by hydrogen bonds [35, 36].

Polytopic bis-terpyridine ligands with cyclam containing spacer were presented by Gasnier et. al. [37, 38]. The presence of cyclam complexing macrocycle enables the incorporation of additional metal ions into the polymer chain (Fig. 24). Two different types of metal complexes in the same polymer chain result in noteworthy electrochromic properties as well as reversible sol-gel transition upon redox conditions. Although the ligand itself is not a gelator, addition of two molar equivalents of metal ion produces colored gel in case of Co^{2+} . It is not observed when metalation is performed with one molar equivalent of metal ions and cyclam centers remain metal-free. However, an important role of anions and solvents in liquid phase or gel formation is underlined. Another property worth noting is the oxidation process of $(\text{Co}_2\text{L})_n$ polymer which proceeds through $\text{Co}^{2+}(\text{tpy})_2$ to $\text{Co}^{3+}(\text{tpy})_2$ conversion at 0,4 V and $\text{Co}^{2+}(\text{cyclam})$ to $\text{Co}^{3+}(\text{cyclam})$ afterward at 1V potential. Each step is indicated by a color change and entirely reversible. Also phase transition from liquid to gel is observed upon oxidation process. It is mainly attributed to positive charge increase [38].

Terpyridine is one of the most applicable ligands for the formation of supramolecular and polymeric architectures by means of metal coordination chemistry [38-56]. This is due to strong and directed metal bonding that allows complex systems to be formed. The terpyridine- Fe^{2+} binding constants are $K_1 = 1,26 \cdot 10^7 \text{M}^{-1}$ and $K_2 = 6,31 \cdot 10^{13} \text{M}^{-1}$ [57]. One of the advantages of terpyridine-metal complex is the reversibility under certain conditions. This makes these compounds convenient materials for introduction into polymers. Electronic, optical or catalytic properties of terpyridine-metal complexes allow functional materials to be fabricated. However, there is still much effort to be made for the common application of these materials.

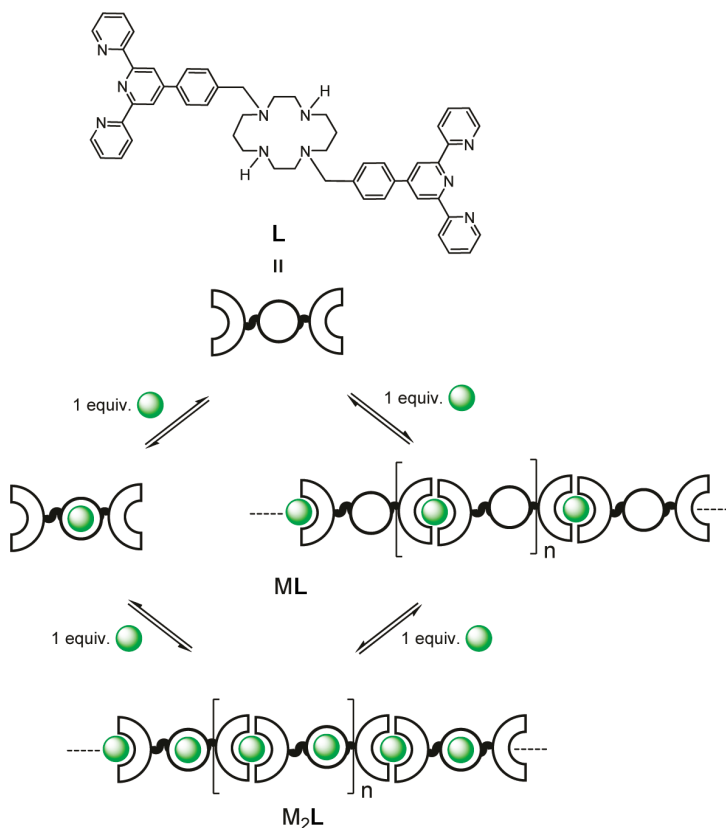


Figure 24. Structure of the L ligand; formation of the M_2L metallopolymers (where M : Co^{2+} , Ni^{2+} , or Cu^{2+}) through different ML intermediate complexes [37].

References

1. J.-M. Lehn, *Supramolecular chemistry. Concepts and Perspectives*, Wiley-VCH, 1995
2. U. S. Schubert, A. Winter, G. R. Newkome, *Terpyridine-based Materials: For Catalytic, Optoelectronic and Life Science Applications*, Wiley-VCH, 2011
3. P.R. Anders, U.S. Schubert, New functional polymers and materials based on 2,2':6',2''-terpyridine metal complexes, *Adv. Mater.*, 2004, 16, 1043-1068
4. H. Hofmeier, U.S. Schubert, Recent development in the supramolecular

- chemistry of terpyridine-metal complexes, *Chem. Soc. Rev.*, 2004, 33, 373-399
5. U.S. Schubert, C. Eschbaumer, *Macromolecules containing bipyridine and terpyridine metal complexes: Towards metallosupramolecular polymers*, *Angew. Chem. Int. Ed.*, 2002, 41, 2892-2926
 6. G.T. Morgan, F.H. Burstall, *Dehydrogenation of pyridine by anhydrous ferric chloride*, *J. Chem. Soc.*, 1932, 20-30
 7. I. Eryazici, C.N. Moorefield, G.R. Newkome, *Square-planar Pd(II), Pt(II), and Au(III) terpyridine complexes: Their syntheses, physical properties, supramolecular constructs, and biomedical activities*, *Chem. Rev.*, 2008, 108, 1834-1895
 8. J. Granifo, M. Vargas, M.T. Garland, A. Ibáñez, R. Gaviño, R. Baggio, *The novel ligand 4'-phenyl-3,2':6',3''-terpyridine (L) and the supramolecular structure of the dinuclear complex $[\text{Zn}_2(\mu\text{-L})(\text{acac})_4] \cdot \text{H}_2\text{O}$ (acac = acetylacetonato)*, *Inorg. Chem. Comm.*, 2008, 11, 1388-1391
 9. L. Hou, D. Li, *A new ligand 4'-phenyl-4,2':6',4''-terpyridine and its 1D helical zinc(II) coordination polymer: syntheses, structures and photoluminescent properties*, *Inorg. Chem. Comm.*, 2005, 8, 190-193
 10. G.W.V. Cave, C.L. Raston, *Helical polymeric network of $[\text{ZnCl}_2(4'\text{-aryl-4,2'-6',4''-terpyridine)]_n$* , *J. Supramol. Chem.*, 2002, 2, 317-319
 11. E. Breuning, G. S. Hanan, F. J. Romero-Salguero, A. M. Garcia, P. N. W. Baxter, J.-M. Lehn, E. W., K. Rissanen, H. Nierengarten, A. van Dorsseleer, *Self-Assembly, Characterisation, and Crystal Structure of Multinuclear Metal Complexes of the $[2 \times 3]$ and $[3 \times 3]$, Grid-Type*, *Chem.-Eur. J.*, 2002, 8, 3458-3466
 12. G. R. Newkome, T. J. Cho, C. N. Moorefield, G. R. Baker, M. J. Saunders, R. Cush, P. S. Russo, *Angew. Chem.* 1999, 111, 3899–3903; *Angew. Chem. Int. Ed.*, 1999, 38, 3717–3721.
 13. G. R. Newkome, T. J. Cho, C. N. Moorefield, R. Cush, P. S. Russo, L. A. Godínez, M. J. Saunders and P. Mohapatra, *Hexagonal Terpyridine - Ruthenium and -Iron Macrocyclic Complexes by Stepwise and Self-Assembly Procedures*, *Chem.-Eur. J.*, 2002, 8, 2946–2954.
 14. G. R. Newkome, T. J. Cho, C. N. Moorefield, P. P. Mohapatra, L. A. Godínez, *Towards Ordered Architectures: Self-Assembly and Stepwise Procedures to the Hexameric Metallomacrocycles $[\text{Arylbis}(\text{terpyridinyl})_6\text{Fe II } 6\text{-n-RuII } n]$ (n = 0,2,3,5)*, *Chem. Eur. J.*, 2004, 10, 1493 – 1500
 15. P. Wang, C. N. Moorefield, G. R. Newkome, *Nanofabrication: Reversible*

- Self-Assembly of an Imbedded Hexameric Metallomacrocycle within a Macromolecular Superstructure, *Angew. Chem. Int. Ed.*, 2005, 44, 1679–1683
16. N. Tuccitto, I. Delfanti, V. Torrisi, F. Scandola, C. Chiorboli, V. Stepanenko, F. Würthner, A. Licciardello, Supramolecular self-assembled multilayers of terpyridine-functionalized perylene bisimide metal complexes, *Phys. Chem. Chem. Phys.*, 2009, 11, 4033–4038
 17. C. Haensch, M. Chiper, C. Ulbricht, A. Winter, S. Hoepfener, U.S. Schubert, Reversible supramolecular functionalization of surfaces: Terpyridine ligands as versatile building blocks for noncovalent architectures, *Langmuir*, 2008, 24, 12981–12985
 18. H.Z. Xie, D.Y. Wei, Syntheses and characterization of two 1D Cu(II) coordination polymers with 2,2':6',2''-terpyridine ligand, *Russ. J. Coord. Chem.*, 2011, 37, 600–605
 19. Q.-R. Wu, J.-J. Wang, H.-M. Hu, Y.-Q. Shangguan, F. Fu, M.-L. Yang, F.-X. Dong, G.-L. Xue, A series of lanthanide coordination polymers with 4'-(4- carboxyphenyl)-2,2':6',2''-terpyridine: Syntheses, crystal structures and luminescence properties, *Inorg. Chem. Comm.*, 2011, 14, 484–488
 20. Q.-R. Wu, J.-J. Wang, H.-M. Hu, B.-C. Wang, X.-L. Wu, F. Fu, D.-S. Li, M.-L. Yang, G.-L. Xue, Two novel cadmium(II) coordination polymers based on bis-functionalized ligand 4'-(4-carboxyphenyl)-2, 2':6', 2''-terpyridine, *Inorg. Chem. Comm.*, 2011, 13, 715–719
 21. L. Gou, T. Qin, H.-M. Hu, X.-L. Chen, B.-C. Wang, Q.-R. Wu, B. Zhang, Z.-X. Tang, Syntheses and characterizations of two metal-organic polymers derived from pyridyl substituted terpyridine and 4,5-imidazole dicarboxylate, *J. Coord. Chem.*, 2008, 61, 3943–3952
 22. L. Gou, B. Zhang, H.-M. Hu, X.-L. Chen, B.-C. Wang, Q.-R. Wu, T. Qin, Z.-X. Tang, Syntheses and characterization of two novel cadmium(II) coordination polymers derived from pyridyl substituted terpyridine and diphenate mixed ligands, *J. Mol. Struct.*, 2008, 889, 244–250
 23. S. Köytepe, S. Erdoğan, T. Seçkin, Synthesis of polyimide from 5,5''-bis(bromomethyl)-2,2':6',2''-terpyridine and investigation of the polymer sorption behavior towards some metal ions *J. Hazard. Mater.*, 2009, 162, 695–702
 24. M. Chiper, R. Hoogenboom, U.S. Schubert, New terpyridine macroligands as potential synthons for supramolecular assemblies, *Europ. Polym. J.*, 2010, 46, 260–269
 25. M. Schütte, C. Stolle, D. G. Kurth, *Metallosupramolecular Chemistry*

- in Two Dimensions, *Supramol. Chem.*, 2003, 15, 549
26. A. Maier, A.R. Rabindranath, B. Tiede, Fast-switching electrochromic films of zinc polyiminofluorene-terpyridine prepared upon coordinative supramolecular assembly, *Adv. Mater.*, 2009, 21, 959-963
 27. A. Maier, A.R. Rabindranath, B. Tiede, Coordinative supramolecular assembly of electrochromic films based on metal ion complexes of polyiminofluorene with terpyridine substituent groups, *Chem. Mater.*, 2009, 21, 3668-3676
 28. A. Maier, H. Fakhrnabavi, A.R. Rabindranath, B. Tiede, Supramolecular assembly of electrochromic films of terpyridine- functionalized polyiminocarbazolyene metal complexes, *J. Mater. Chem.*, 2011, 21, 5795-5804
 29. C. Kim, H. Kim, 2,2':6',2''-Terpyridine and bis(2,2':6',2''-terpyridine) ruthenium(II) complex on the dendritic periphery, *J. Organomet. Chem.*, 2003, 673, 77-83
 30. E.C. Constable, P. Harverson, Convergent synthesis of an octadecaruthenium metallodendrimer, *Inorg. Chim. Acta*, 1996, 252, 9-11
 31. T. Suzuka, T. Nagamine, K. Ogihara, M. Higa, Suzuki-miyaura cross-coupling reaction in water with polymer-supported terpyridine palladium complex under aerobic conditions, *Catal. Lett.*, 2010, 139, 85-89
 32. H. Hofmeier, J. Pahnke, C.H. Weidl, U.S. Schubert, Combined biotin-terpyridine systems: A new versatile bridge between biology, polymer science and metallo-supramolecular chemistry, *Biomacromolecules*, 2004, 5, 2055-2064
 33. S. Burazerovic, J. Gradinaru, J. Pierron, and T. R. Ward, Hierarchical Self-Assembly of One-Dimensional Streptavidin Bundles as a Collagen Mimetic for the Biomineralization of Calcite, *Angew. Chem. Int. Ed.*, 2007, 46, 5510 –5514
 34. D.G. Hilmey, L.A. Paquette, Exo- and Endo-Receptors in One. A Novel Class of Supramolecular Structures Housing Transition-Metal-Binding Bi- and Terpyridine Units alongside Lithium Ion-Selective Trispirotetrahydrofuranyl Components, *J. Org. Chem.*, 2004, 69, 3262-3270
 35. H. Hofmeier, R. Hoogenboom, M.E.L. Wouters, U.S. Schubert, High molecular weight supramolecular polymers containing both terpyridine metal complexes and ureidopyrimidinone quadruple hydrogen-bonding units in the main chain, *J. Am. Chem. Soc.*, 2005, 127, 2913-2921

36. H. Hofmeier, A. El-Ghayoury, A.P.H.J. Schenning, U.S. Schubert, New supramolecular polymers containing both terpyridine metal complexes and quadruple hydrogen bonding units, *Chem. Comm.*, 2004, 10, 318-319
37. A. Gasnier, G. Royal, P. Terech, Metallo-supramolecular gels based on a multitopic cyclam bis-terpyridine platform, *Langmuir* 2009, 25, 8751-8762
38. A. Gasnier, C. Bucher, J.-C. Moutet, G. Royal, E. Saint-Aman, P. Terech, Redox-responsive metallo-supramolecular polymers and gels containing bis-terpyridine appended cyclam ligand, *Macromol. Symp.*, 2011, 304, 87-92
39. R. Shunmugam, G.J. Gabriel, K.A. Aamer, G.N. Tew, Metal-ligand-containing polymers: Terpyridine as the supramolecular unit, *Macromol. Rapid Commun.* 2010, 31, 784-793.
40. K.A. Aamer, G.N. Tew, Supramolecular polymers containing terpyridine-metal complexes in the side chain, *Macromolecules*, 2007, 40, 2737-2744.
41. F. Camerel, R. Ziessel, B. Donnio, D. Guillon, New Engineering of an iron-terpyridine complex with supramolecular gels and mesomorphic properties, *J. Chem.*, 2006, 30, 135-139
42. F.S. Han, M. Higuchi, Y. Akasaka, Y. Otsuka, D.G. Kurth, Preparation, characterization, and electrochromic properties of novel Co(II)-bis-2,2':6',2''-terpyridine metallo-supramolecular polymers, *Thin Solid Films*, 2008, 516, 2469-2473
43. C. Mugesana, P. Guillet, S. Hoepfener, U.S. Schubert, C.-A. Fustin, J.-F. Gohy, Metallo-supramolecular diblock copolymers based on heteroleptic cobalt(III) and nickel(II) bis-terpyridine complexes, *Chem. Comm.*, 2010, 46, 1296-1298.
44. A. Gasnier, J.-M. Barbe, C. Bucher, F. Denat, J.-C. Moutet, E. Saint-Aman, P. Terech, G. Royal, Acid-base-driven interconversion between a mononuclear complex and supramolecular coordination polymers in a terpyridine-functionalized dioxocyclam ligand, *Inorg. Chem.*, 2008, 47, 1862-1864
45. Wild, A., Hornig, S., Schlütter, F., Vitz, J., Friebe, C., Hager, M.D., Winter, A., Schubert, U.S. Complexation of terpyridine-containing dextrans: Toward water-soluble supramolecular structures, *Macromol. Rapid Comm.*, 2010, 31, 921-927
46. W. Huang, H. Qian, C-H...X hydrogen-bond-mediated supramolecular frameworks: Syntheses and crystal structures of hydrochlorate

- hexafluorophosphate and hydrochlorate tetrafluoroborate of 4'-chloro-2,2':6',2''-terpyridine, *J. Mol. Struct.*, 2007, 832, 108-116
47. M. Chiper, D. Fournier, R. Hoogenboom, U.S. Schubert, Thermosensitive and switchable terpyridine-functionalized metallo-supramolecular poly(N-isopropylacrylamide), *Macromol. Rapid Comm.*, 2008, 29, 1640-1647
 48. A. Winter, C. Friebe, M.D. Hager, U.S. Schubert, Advancing the solid state properties of metallo-supramolecular materials: Poly(ϵ -caprolactone) modified π -conjugated bis(terpyridine)s and their Zn(II) based metallo-polymers, *Macromol. Rapid Comm.*, 2008, 29 1679-1686
 49. M. Kudera, C. Eschbaumer, H.E. Gaub, U.S. Schubert, Analysis of Metallo-Supramolecular Systems Using Single-Molecule Force Spectroscopy, *Adv. Funct. Mat.*, 2003, 13, 615-620
 50. A. Jain, J. Wang, E.R. Mashack, B.S.J. Winkel, K.J. Brewer, Multifunctional DNA interactions of Ru-Pt mixed metal supramolecular complexes with substituted terpyridine ligands, *Inorg. Chem.*, 2009, 48, 9077-9084
 51. H. Hofmeier, E. Herdtweck, U.S. Schubert, Asymmetric bipyridine-terpyridine-copper(II) complexes: An approach for new supramolecular architectures, *Z. Anorg. Allg. Chem.*, 2004, 630, 683-688
 52. J. Lombard, J.-C. Leprêtre, J. Chauvin, M.-N. Collomb, A. Deronzier, Photoredox vs. energy transfer in a Ru(II)-Fe(II) supramolecular complex built with an heteroditopic bipyridine-terpyridine ligand, *Dalton Trans.*, 2008, 658-666
 53. W. Huang, H. Qian, Supramolecular frameworks composed of Ru(II), Cu(II), Zn(II), Ni(II) and Fe(II) complexes having tridentate 4'-chloro-2,2':6',2''-terpyridine ligand and 1:1 or 1:2 ratios of metal and ligand, *J. Mol. Struct.*, 2008, 874, 64-76
 54. E.C. Constable, M.D. Ward, Synthesis and co-ordination behaviour of 6',6''-bis(2-pyridyl)-2,2' : 4,4'' : 2'',2'''-quaterpyridine; 'back-to-back' 2,2' : 6',2''-terpyridine, *J. Chem. Soc., Dalton Trans.*, 1990, 1405-1409
 55. P. R. Andres, R. Lunkwitz, G. R. Pabst, K. Böhn, D. Wouters, S. Schmatloch, U. S. Schubert, New 4'-Functionalized 2,2':6',2''-Terpyridines for Applications in Macromolecular Chemistry and Nanoscience, *Eur. J. Org. Chem.*, 2003, 3769-3776
 56. U. S. Schubert, C. Eschbaumer, O. Hienb, P.R. Andres, 4'-Functionalized 2,2':6',2''-terpyridines as building blocks for supramolecular chemistry and nanoscience, *Tetrahedron Lett.*, 2001, 42, 4705-4707

57. R.H. Holyer, C.D. Hubbard, S.F.A. Kettle, R.G. Wilkins, The kinetics of replacement reactions of complexes of the transition metals with 2,2',2''-terpyridine, *Inorg. Chem.*, 1966, 5, 622-625

Chapter 16

Supramolecular complexes of terpenes and their derivatives with cyclodextrins

Leonid Yakovishin¹, Vladimir Grishkovets², Grzegorz Schroeder³
and Volodymyr Rybachenko⁴

¹*Sevastopol National Technical University, Universitetskaya Str., 33,
Sevastopol, 99053, Crimea, Ukraine*

²*V.I. Vernadsky Taurida National University, Vernadsky Ave., 4,
Simferopol, 95007, Crimea, Ukraine*

³*Adam Mickiewicz University, Faculty of Chemistry,
Grunwaldzka 6, 60-780 Poznań, Poland*

⁴*L.M. Litvinenko Institute of Physical Organic and Coal Chemistry NAS
of Ukraine, R. Luxemburg 70; 83-114 Donetsk, Ukraine*

Cyclodextrins (CD, Figure 1) are the cyclic oligosaccharides composed of several *D*-glucopyranose moieties. The latter ones are linked by $\alpha(1\rightarrow 4)$ -glycoside bonds. Cyclodextrin molecules have the shape of torus or hollow truncated cone. The inner cavity of cyclodextrins is hydrophobic, while their front surfaces are hydrophilic. The primary OH-groups make a full circle on the narrow front surface. The wide front surface includes secondary OH-groups. Cyclodextrins are got by fermentative hydrolysis of starch. The most important are α -CD, β -CD, and γ -CD, among which the most accessible is β -CD (Figure 2). There exist cyclodextrins with large circles. Their molecules consist of several dozens of glucose moieties [1–8].

The peculiarities of cyclodextrins structure determine their ability to make complexes with polar non-organic ions and non-polar organic molecules. That is why cyclodextrins are widely used for molecular capsulation of different drugs. Such supramolecular complexes can be used for address delivery, controlled release, solvability increase, expansion of biological activity spectrum of drugs, stability increase, drug dose and side-effect reduction [1, 2, 5, 6, 9, 10–12]. Cyclodextrins can be treated as molecular receptors [7], as catalysts imitating ferments [8, 12, 13], can be used in chromatography [1, 3, 8, 12, 14, 15].

Cyclodextrins are considered to be non-toxic substances [1, 12]. This advantage allows to widely use them in pharmaceutical, cosmetic, and food industry [1, 8, 12]. β -CD is a food additive E459 [16]. But it is necessary to take into account that the profile of their toxicity varies depending on the way of their introduction into the organism [12, 17]. Subcutaneous injection of heavy doses of β -CD causes animals' weight and leaver mass reduction, as well as displays nephrotoxicity [17, 18]. Parenteral administration of β -CD leads rats to nephrosis [19].

The stable complexation is provided by the steric correspondence of the guest molecule and cyclodextrin cavity. It is known that high-energy water release from the inner cavity (Figure 3), hydrophobic effects and Van der Waals interactions are one of the most important conditions for cyclodextrin clathrates formation [1].

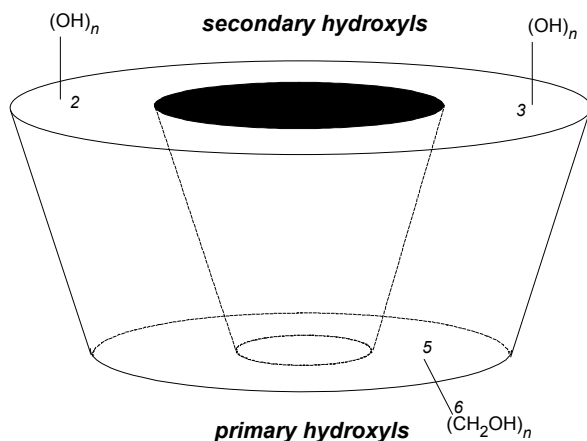
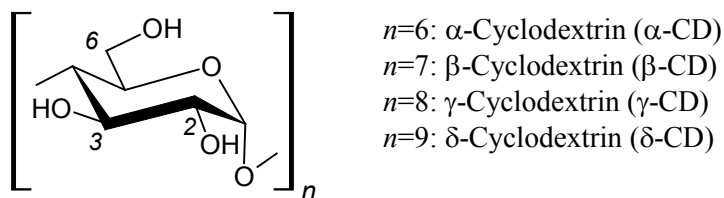


Figure 1. Cyclodextrins.

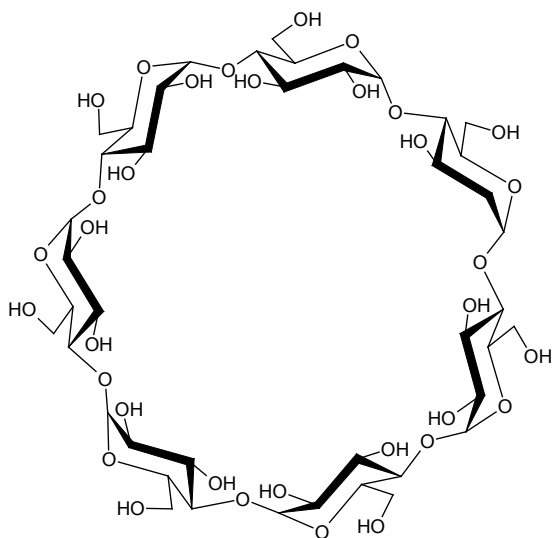


Figure 2. β -Cyclodextrin (β -CD).

Primary and secondary cyclodextrin OH-groups have different activity, that is why they can be exposed to selective modification [20]. Thus, variable derivatives of cyclodextrins have been got [9, 21–23].

With the purpose of probable drugs cyclodextrin complexes with some terpenoids and their derivatives have been obtained.

1. Cyclodextrins complexes with mono- and sesquiterpenoids

Cyclodextrins are known to be fixators of essential oils [1, 5]. Complexation of β -CD with fir needle oil, rich in bornyl acetate **1** (Table 1), has been investigated by the thermogravimetry, IR and NMR spectroscopy methods [24–26]. It was shown that bornyl acetate makes an inner-spheric complex of 1:1 ratio with β -CD. In this complex the borneol moiety sites in the β -CD inner cavity completely. Acetyl fragment gets out of cavity and makes an intermolecular H-bond with one of the CH_2OH -groups of the front surface of β -CD (Figure 4). This conclusion was made by Sevastianova Ye.V. et al. on the basis of spin-lattice relaxation change T_1 of ^{13}C nuclei. The common immobilization of fir needle oil and alkaline proteinase has been carried out by means of β -CD [24, 26, 27].

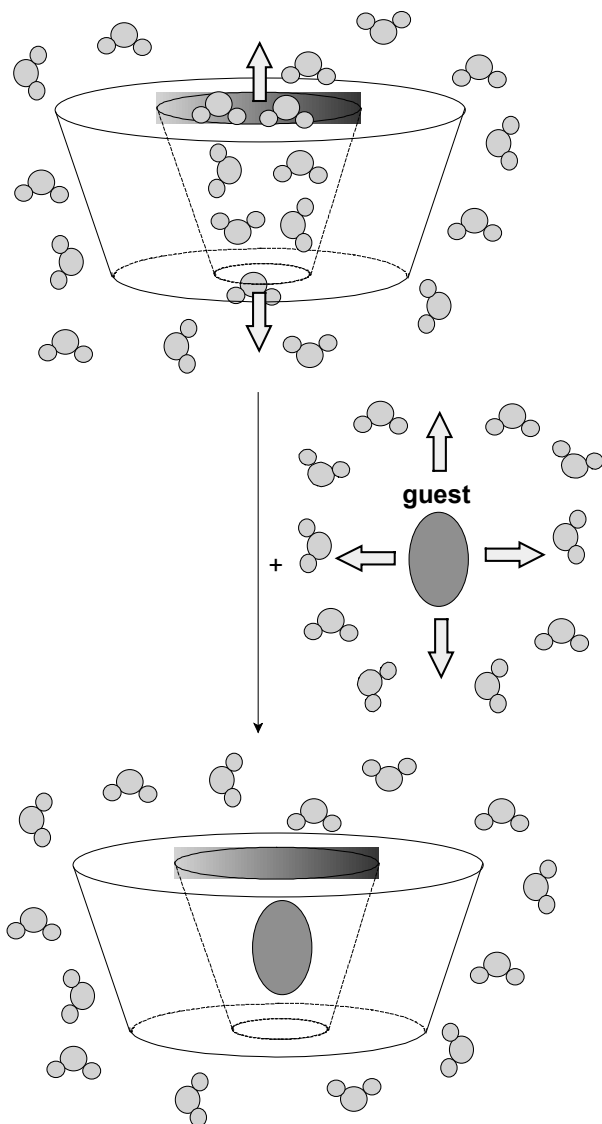


Figure 3. Formation of inclusion complex cyclodextrin–guest.

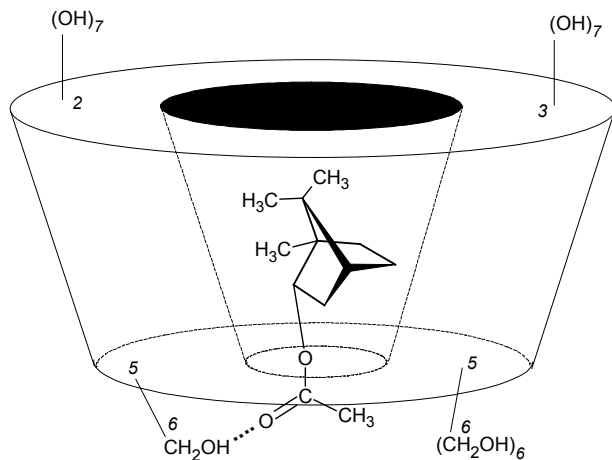
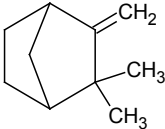
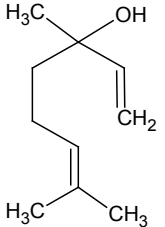
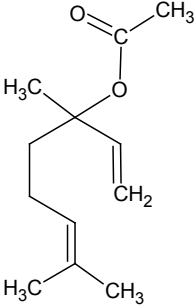
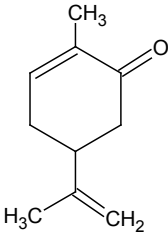
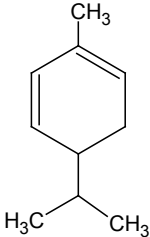


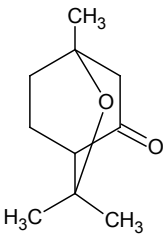
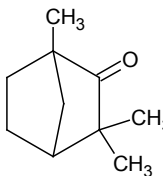
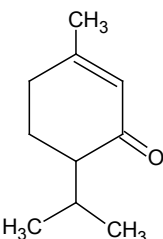
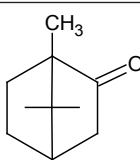
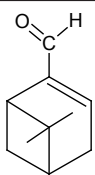
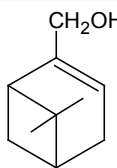
Figure 4. Schematic view of bornyl acetate complex with β -CD.

Table 1. Monoterpenes and monoterpenoids, used for complexation with cyclodextrins

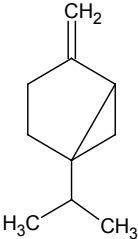
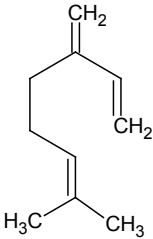
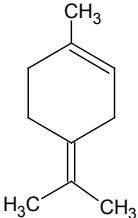
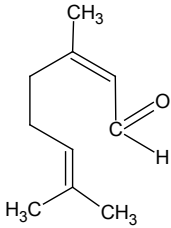
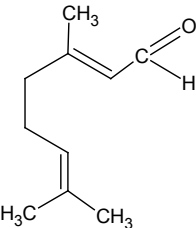
Compound	Structure	References
1 Bornyl acetate		[24–26, 43]
2 α -Pinene		[28, 30, 42, 43]
3 Limonene		[28, 30, 40, 42, 43]

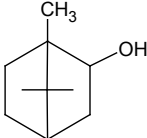
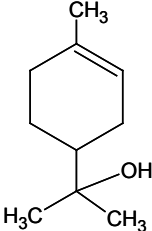
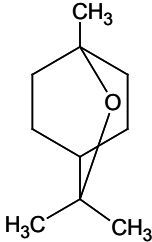
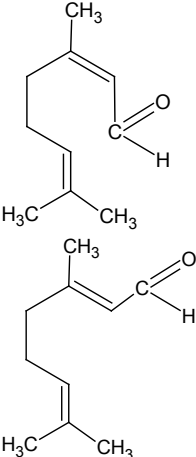
4	Camphene		[28, 30, 43]
5	Linalool		[28, 30, 40-43]
6	Linalyl acetate		[28]
7	Carvone		[28, 30, 41, 43]
8	α -Phellandrene		[28, 30]

9	Menthol		[29, 40, 43]
10	Isomenthol		[29, 43]
11	Neomenthol		[29]
12	Neoisomenthol		[29]
13	Menthone (<i>trans</i> -menthone)		[29, 30, 40, 43, 45, 46]
14	Isomenthone (<i>cis</i> -menthone)		[29, 30]

15	3-Oxo-1,8-cineole		[29]
16	Fenchone		[30, 40, 41, 43, 45, 46]
17	Piperitone		[30]
18	Camphor		[30, 32–41, 43, 44]
19	Myrtenal		[30]
20	Myrtenol		[30]

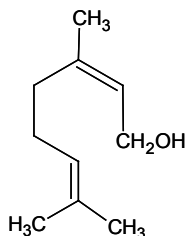
21	β -Citronellol trifluoroacetate		[30]
22	<i>trans</i> -Pinocarveol		[30]
23	Geraniol		[41, 43]
24	γ -Terpinene		[41, 42]
25	β -Pinene		[42]

26	Sabinene		[42]
27	β -Myrcene		[42, 43]
28	Terpinolene		[42]
29	Neral		[42]
30	Geranial		[42]

31	Borneol		[43–46]
32	Terpineol		[43]
33	Cineole (eucalyptol)		[43]
34	Citral (neral 29 and geranial 30 mixture)		[43]

35

Nerol



[45, 46]

The complexes of cinnamon oil inclusion with β -CD has been got [28]. The oil contains terpenoids (α -pinene (2), limonene (3), camphene (4), linalool (5), linalyl acetate (6), carvone (7), and α -phellandrene (8); Table 1) and other essential compounds. Maximum efficiency of cinnamon oil inclusion into β -CD was reached under the 15:85 percentage (117 mg of oil per 1 g of β -CD).

The molecular dynamics and mechanics methods allowed to make calculations for the complexes of 1:1 ratio made by the γ -CD derivatives and terpenoids of menthan type (by menthol (9), isomenthol (10), neomenthol (11), neoisomenthol (12), menthone (13), isomenthone (14), and 3-oxo-1,8-cineole (15); Table 1) [29]. Herewith, it was established that the nature and configuration of substituent at the C-3 atom of terpenoid molecule determine complexation energy and explain the reason of enantioselectivity variety relatively to terpenoids among the investigated derivatives of γ -CD. The methyl group configuration of C-3 terpenoids influences the chiral identification less.

Cyclodextrins and their derivatives interact with terpenes and terpenoids enantioselectively. Sorbents based on modified cyclodextrins are used for chromatographic identification of essential oils' components. Capillary gas chromatography on the basis of cyclodextrins was used to analyze terpenoids' enantiomers (camphene (4), α -pinene (2), limonene (3), α -phellandrene (8), carvone (7), fenchone (16), menthone (13), isomenthone (14), piperitone (17), camphor (18), myrtenal (19), myrtenol (20), β -citronellol trifluoroacetate (21), *trans*-pinocarveol (22), and linalool (5); Table 1) [30].

In the review [31] of photochemical transformations of terpenoids with cyclodextrins and without them is given. It was shown that the cyclodextrine nature and terpenoid nature affect the nature of photolytes and their complexes. Thus, the photolysis of α -ionone complex with α -CD (Figure 5) produces *retro*- α -ionone, and the complex with β -CD gives the products of acyclic shift. The differences are probably caused by the dimensions of cyclodextrins' inner cavity. Complexation influences the photolysis rate and the direction of reaggregation. The conclusion of formation of inner terpenoid complexes with cyclodextrins

was made on the basis of ^1H NMR method. Herewith, the strong-field proton shift of β -CD's H-3 and H-5 protons directed into the inner hydrophobic cavity.

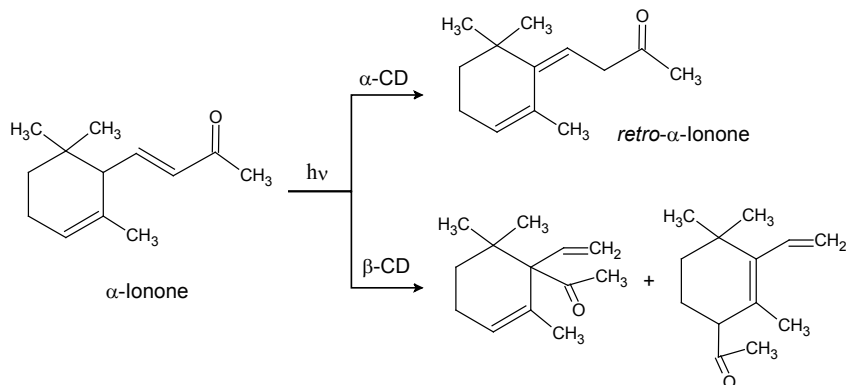


Figure 7. Scheme of α -ionone photolysis in the complexes with α -CD and β -CD.

Much attention in reviews is paid to camphor (**18**, Table 1) clathration by cyclodextrins and their derivatives. The NMR method was effectively used for the study of camphor enantiomers complexation with α -CD. The complexes were made by the camphor molecule and two molecules of α -CD (Figure 6) [32, 33]. For the (*1S,4S*)-camphor the complexation free energy makes $-7,95\pm 0,09$ kcal/mol, and for the (*1R,4R*)-camphor it is $-7,61\pm 0,06$ kcal/mol [32]. Thus, the most stable complex is made by (*1S,4S*)-camphor.

By means of X-ray crystallography and molecular dynamics method it was shown that camphor sites inside the cavity formed by the α -CD dimer of the "head-to-head" type [34]. The complexes are stabilized by hydrogen bonds made by the carbonyl camphor group and secondary OH-groups at C-2 and C-3 glucose remains of α -CD, or by the carbonyl camphor group and water molecule located about the ring of primary α -CD OH-groups.

Unlike α -CD, β -CD and γ -CD make complexes of 1:1 ratio with camphor [35]. α -CD, β -CD, and their permethylated derivatives are used as chiral additives for the HPLC camphor [36]. In [37] it was displayed that under the conditions of GLC and HPLC, β -CD does not identify camphor enantiomers and makes 1:1 complexes with them. On the contrary, α -CD bounds selectively to camphor enantiomers and makes 2:1 complexes. Complexation of camphor enantiomers with α -CD has been studied by the NMR [38] and calorimetry [39] methods. It was discovered that camphor incapsulation by α -CD leads to the complex of 1:2 ratio, herewith the main role hydrophobic interactions play in it

[39]. The K_{ass} for (+)-camphor complex was $6,16 \times 10^5 \text{ M}^{-2}$, and for (-)-camphor complex – $3,18 \times 10^5 \text{ M}^{-2}$ (at 298 K) [39]. Therefore, the (+)-camphor complex turned out to be most stable.

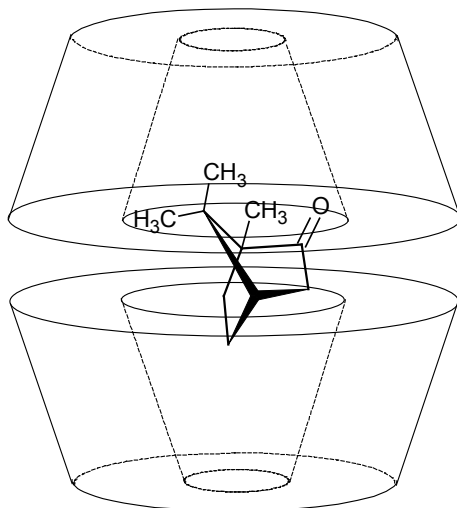


Figure 6. Schematic view of camphor complex with α -CD.

The solubility method, X-ray diffractometry, and thermal analyses helped to investigate the interaction of α -CD and β -CD with twelve components of essential oils. Among them there were triterpenoids (camphor (**18**), limonene (**3**), linalool (**5**), menthol (**9**), menthone (**13**), and fenchone (**16**); Table 1) [40]. All the terpenoids make 1:2 complexes with α -CD, and 1:1 complexes with β -CD. The stability constants (K_s, M^{-1}) of the α -CD complexes with terpenoids in water at 25°C range as follows:

$$K_s(\text{limonene}) > K_s(\text{menthol}) > K_s(\text{linalool}) > K_s(\text{camphor}) > K_s(\text{menthone}) > K_s(\text{fenchone}).$$

The stability constants (K_s, M^{-1}) of the β -CD complexes with terpenoids in water at 25°C range in the following way:

$$K_s(\text{methol}) > K_s(\text{limonene}) > K_s(\text{menthone}) > K_s(\text{camphor}) > K_s(\text{fenchone}).$$

Thus, limonene bounds to α -CD best of all, and menthol complexates better

with β -CD. In general, the stability constants of the β -CD complexes appeared higher. It indicates its better ability to make inclusive complexes. It was shown that the fugacity and photooxidation ability of substances reduces under the condition of complexation.

The method of chemical precipitation enabled to study the complexation between β -CD and monoterpenoids of insecticide properties (linalool (**5**), *S*-carvone (**7**), camphor (**18**), geraniol (**23**), γ -terpinene (**24**), and fenchone (**16**); Table 1) [41]. Incapsulation of linalool and γ -terpinene was higher when the mass ratio reached 3,33:1 (β -CD : terpenoid). For the *S*-carvone, camphor, geraniol, and fenchone the best encapsulation was measured at the 6,66:1 ratio. Maximum inclusive efficiency was reached for camphor (52%) and geraniol (34%) by using 10 g of β -CD, and linalool (31% per 5 g β -CD) as well.

Incapsulation of lemon oil into β -CD has been carried out [42]. It is discovered the composition of oil terpene substances (α - and β -pinene (**2** and **25**), sabinene (**26**), β -myrcene (**27**), limonene (**3**), γ -terpinene (**24**), terpinolene (**28**), linalool (**5**), neral (**29**), and geraniol (**30**); Table 1) in the complex does not change essentially depending on the mixing time and drying type.

The authors of [43] give the order of terpene and terpenoid (Table 1) molecules siting into β -CD in aqueous medium. The range was made by means of statistical analysis: (-)-borneol (**31**) > terpineol (**32**) > (+)-camphor (**18**) > (-)-carvone (**7**) = geraniol (**23**) = (\pm)-linalool (**5**) = cineole (**33**) = (-)-fenchone (**16**) > (+)-isomenthol (**10**) = citral (**34**) > (-)-menthone (**13**) > (+)-menthol (**9**) > (+)-limonene (**3**) = (-)-bornyl acetate (**1**) > (+)-camphene (**4**) > (-)- α -pinene (**2**) > myrcene (**27**).

The complexes of borneol (**31**) and camphor (**18**) enantiomers with β -CD, the primary alcoholic groups modified: 6-*O*-phenyl- β -CD, 6-*O*-(4-formylphenyl)- β -CD, 6-*O*-(4-nitrophenyl)- β -CD, 6-*O*-(4-bromophenyl)- β -CD, 6-*O*-(4-chlorophenyl)- β -CD, and 6-*O*-(4-hydroxybenzoyl)- β -CD (Figure 7) [44]. Clathration was studied by microcalorimetry titration in aqueous solution. The stability constants and complexes' thermo dynamical parameters were defined. The most stable clathrates are the ones of borneol. Herewith, the highest stability constant was reached by the (+)-borneol complex with 6-*O*-(4-chlorophenyl)- β -CD ($K_s=133450\pm 2450$ M⁻¹). The borneol molecule penetrates deeper into the cyclodextrins' cavity, and raises enthalpy by strong hydrophobic and Van der Waals interactions. The β -CD modification leads to improvement of guest molecules linking. The most enantioselective towards camphor was 6-*O*-(4-chlorophenyl)- β -CD. The stability constant of its complex with (+)-camphor is 449760 ± 490 M⁻¹, it is four times higher than the one with (-)-camphor ($K_s=12405\pm 545$ M⁻¹).

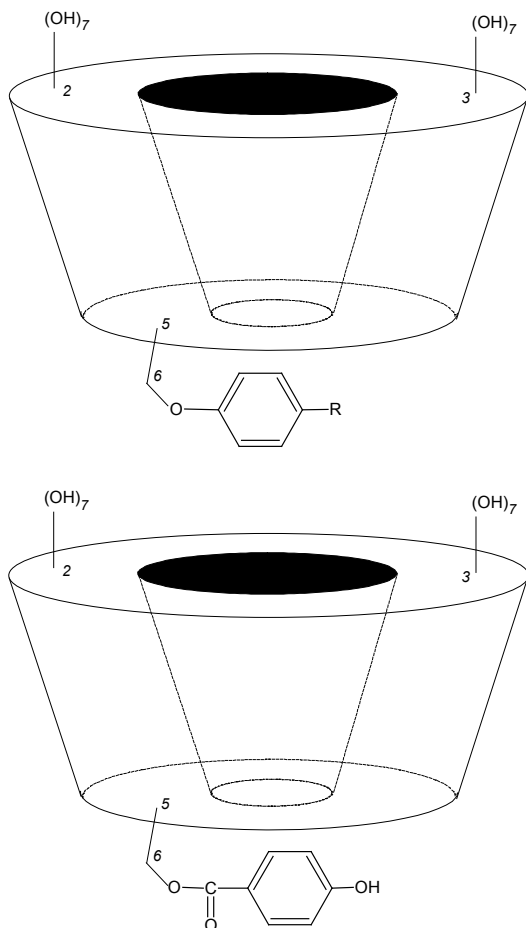


Figure 7. Modified β -CD ($R=H, CHO, NO_2, Br, Cl$).

The modified cyclodextrins have been suggested as sensors for terpenes, terpenoids, and steroids detecting [45, 46]. In particular, β -CD having a moiety of sodium anthranilate and γ -CD modified by two moieties of sodium anthranilate (Figure 8) have been investigated to define nerol (**35**), (-)-menthol (**13**), (-)- and (+)-fenchones (**16**), and (-)-borneol (**31**) (Table 1) [45, 46]. Complexation changes the fluorescence intensity. The moiety of sodium anthranilate can be a spacer narrowing the inner cavity of cyclodextrin and contributes to the

1:1 complex formation (Figure 9). Besides, it can serve as a hydrophobic cap closing the narrow ring of cyclodextrin (Figure 9) [45]. It has been discovered that the β -CD, modified by one moiety of sodium anthranilate only, has a higher sensibility to terpenoids than to steroids [45]. On the contrary, γ -CD with two moieties of sodium anthranilate is more sensitive to steroids [46].

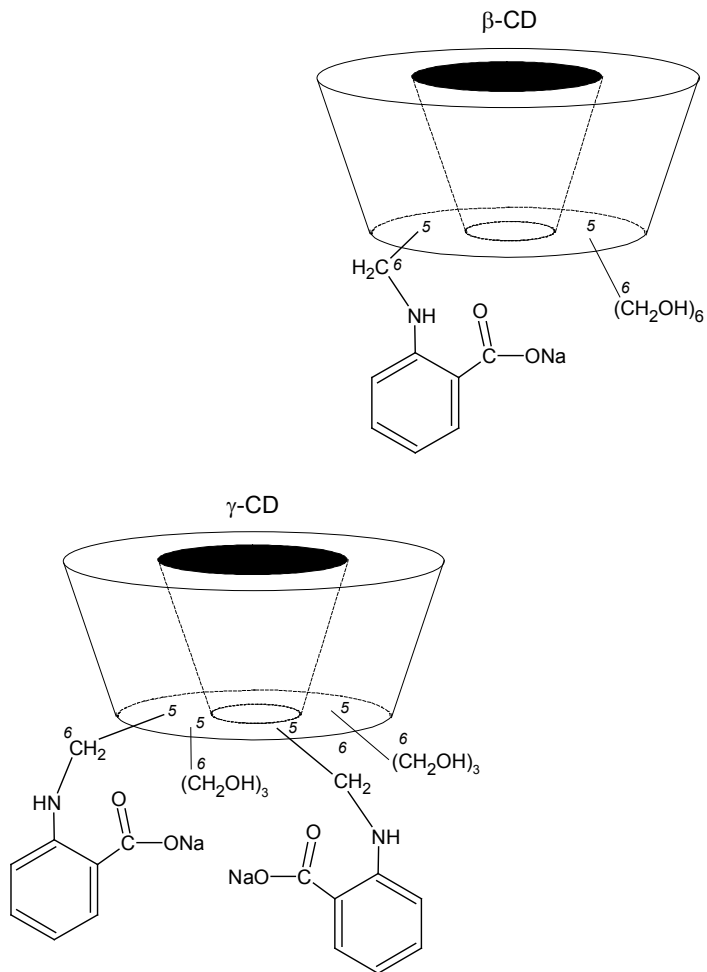


Figure 8. β - and γ -CD modified by the moieties of sodium anthranilate.

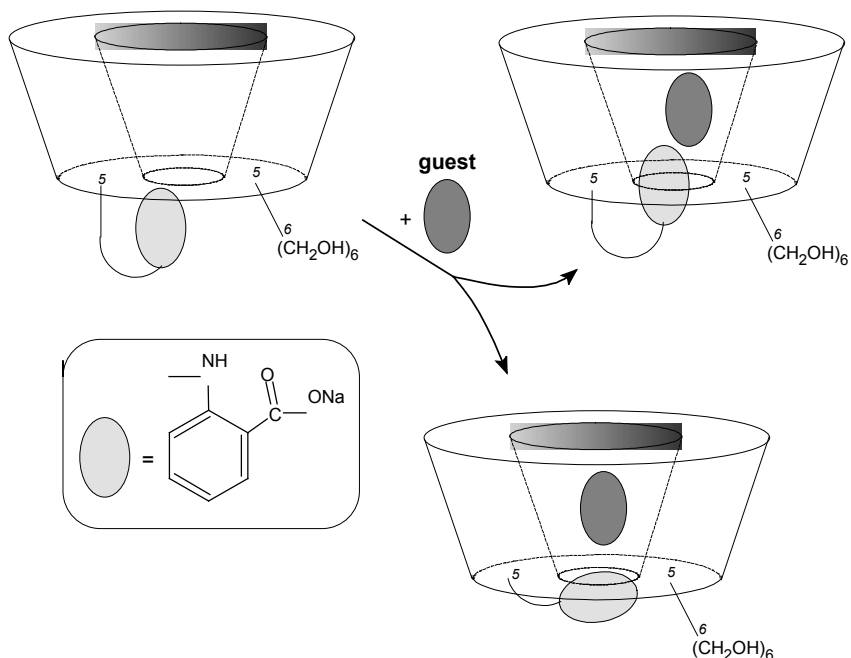


Figure 9. The role of moiety of sodium anthranilate in the complexation with guest.

The clathrate of sesquiterpenoid of euplotin C (Figure 10) extracted from marine ciliate *Euplotes crassus*, with heptakis(2,6-di-*O*-methyl)- β -CD [47, 48]. The complex has been studied by the spectroscopy methods of ¹H NMR, electrospray ionization mass spectrometry and by molecular mechanics. The method of NMR titration and the presence of complex ion peak $[M^{\text{euplotin}} + M^{\text{cyclodextrin}} + \text{Na}]^+$ confirms the 1:1 composition of the complex. In the mass spectrum the peak of ion $[M^{\text{euplotin}} + 2M^{\text{cyclodextrin}} + 2\text{Na}]^{2+}$ of low intensity corresponding to the 1:2 complex formation. The latter was affirmed by NMR titration as well. But the complex of 1:2 ratio is formed under the great abundance of cyclodextrin. In the clathrate of the 1:1 composition the euplotin molecule penetrates deeply into the cavity of modified β -CD at the side of wide ring (Figure 10). Prenyl moiety of euplotin C molecule sites at the narrow ring, the dihydropyranic ring is included into cyclodextrin cavity, and both acetyl group and protons at the C-4 and C-5 atoms of cyclopentane ring are beyond the big ring.

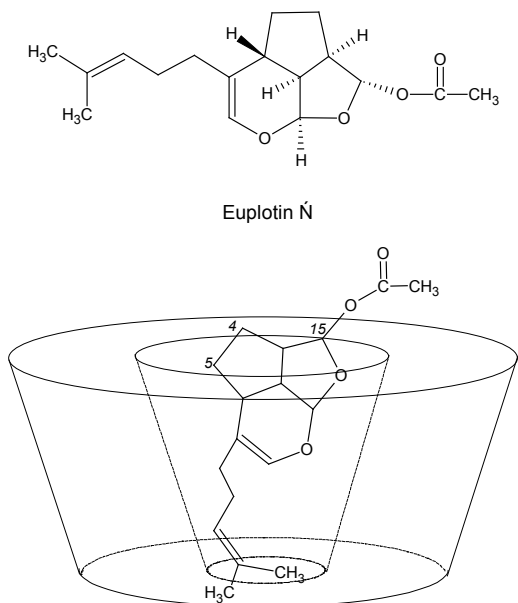
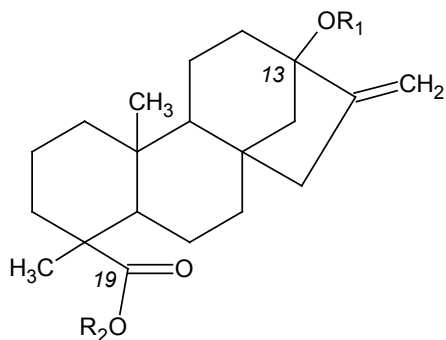


Figure 10. Schematic representation of euplotin C complex.

2. Cyclodextrins complexes with diterpene glycosides

The solubilizing effect of γ -CD in relation to steviolmonoside and steviolbioside (Figure 11), got by saponification of rubusoside and stevioside respectively [49]. Stevioside is a diterpene glycoside *Stevia rebaudiana* Bertoni (Compositae) [50], and rubusoside is *Rubus suavissimus* S. Lee (Rosaceae) [51]. α - and β -CD do not have a solubilizing effect. The authors of [49] explained this fact by the absence of complexation because of small dimensions of these cyclodextrins' inner cavities. They discovered an explicit stimulation of steviolmonoside and steviolbioside 1,4- α -transglucosylation in the presence of γ -CD as well.

Molecular complexes of diterpene glycosides rebaudiosides A, C, and D with γ -CD, which are steviol glycosides as well (Figure 11) and are contained in *Stevia rebaudiana* [52]. All the complexes are of 1:1 ratio. The process of clathrates formation has been studied by NMR methods (¹H, ¹³C cross polarized magic angle spinning), by differential scanning calorimetry, IR Fourier and Raman spectrometry. Besides, the analysis of phase solvability has been carried out.



	R ₁	R ₂
Steviol	H	H
Stevioside	β -D-Glc _p -(1→2)- β -D-Glc _p	β -D-Glc _p
Rubusoside	β -D-Glc _p	β -D-Glc _p
Steviolmonoside	β -D-Glc _p	H
Steviolbioside	β -D-Glc _p -(1→2)- β -D-Glc _p β -D-Glc _p -(1→2)- β -D-Glc _p	H
Rebaudioside A	3 ↑ 1 β -D-Glc _p α -L-Rha _p -(1→2)- β -D-Glc _p	β -D-Glc _p
Rebaudioside C	3 ↑ 1 β -D-Glc _p	β -D-Glc
Rebaudioside D	β -D-Glc _p -(1→2)- β -D-Glc _p 3 ↑ 1 β -D-Glc _p	β -D-Glc _p -(1→2)- β -D-Glc _p

Figure 11. Steviol glucosides.

The stability constants (M^{-1}) of complexes in water at 25°C range as follows:

$$K_s(\text{rebaudioside D}) > K_s(\text{rebaudioside C}) > K_s(\text{rebaudioside A})$$

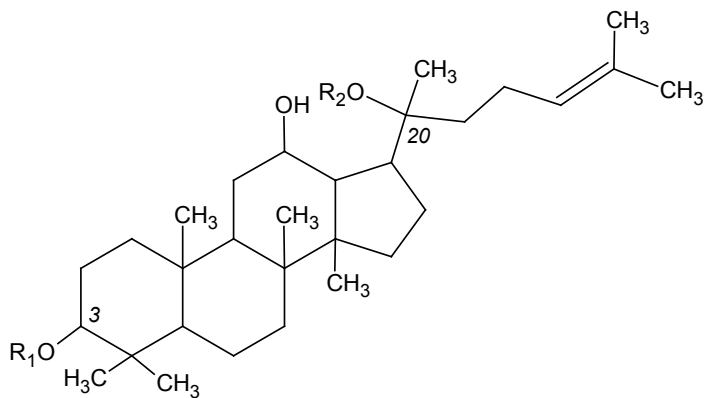
Thus, the rebaudioside D complex is the most stable ($K_s=1091 M^{-1}$). It is probably connected with the additional glucose moiety appearance in the carbohydrate chain at the C-19 atom in the molecule of this glycoside. But the glycoside solubility of rebaudioside A in the presence of cyclodextrin increases best (12,75 times).

3. Cyclodextrins complexes with triterpene glycosides

Recently, the 1:1 complexes of dammarane triterpene glycoside 20-*O*-(β -*D*-glucopyranosyl)-20(*S*)-protopanaxadiol (IH901, Figure 12) with β -CD and hydroxypropyl- β -CD has been got [53]. The IH901 glycoside is a metabolite of ginsenoside Rb₁ (Figure 12), one of the main saponins of *Panax ginseng* C.A. Meyer (Araliaceae) roots [54]. The investigation of complexes has been carried out by means of IR Fourier spectrometry, X-ray diffraction, differential scanning calorimetry, and scanning electronic microscopy. The stability constants of IH901 complexes with β -CD and hydroxypropyl- β -CD were calculated with the help of phase diagrams of solubility. They are equal to $4,52 \pm 0,340$ and $0,68 \pm 0,037$ ($\times 10^{-3} M^{-1}$) respectively. Thus, the complex with β -CD turned out to be 6 times more stable. Less stability of the complex with hydroxypropyl- β -CD can be explained by the steric difficulties caused by its hydroxypropyl groups. They can prevent guest molecules from entering the cyclodextrin's inner cavity. This effect was shown earlier for the aspartame complexes [55].

Previously, it was discovered that β -CD, heptakis-2,6-*O*-dimethyl-, heptakis-2,3,6-*O*-trimethyl- and heptakis-2,6-*O*-dihydroxypropyl- β -CD, γ -CD and octakis-2,6-*O*-dihydroxypropyl- γ -CD inhibit catalytic activity of dipotassium glycyrrhizinate. It is explained by the formation of clathrate 1:1 complexes (Figure 13) [56]. Inhibition did not take place for α -CD. Evidently, the small cavity of this cyclodextrin does not allow glycyrrhizic acid to site in it. The importance of H-bonds, Van der Waals and hydrophobic interactions for the complexation was shown. Glycyrrhizic acid is the main triterpene saponin of licorice *Glycyrrhiza glabra* L., and is 3-*O*- β -*D*-glucuronopyranosyl-(1 \rightarrow 2)-*O*- β -*D*-glucuronopyranoside of glycyrrhetic acid [54].

The modification of β -CD electrolyte used for capillary electrophoresis of monoammonium glycyrrhizinate (glycyrram, Figure 14) was carried out. It caused essential changes of the electrophorogramme profile [57]. It can be connected with complexation.



	R ₁	R ₂
Ginsenoside Rb ₁	β -D-Glc _p -(1→2)-β-D-Glc _p	β -D-Glc _p -(1→6)-β-D-Glc _p
IH901	H	β -D-Glc _p

Figure 12. Ginsenoside Rb₁ and its metabolite IH901.

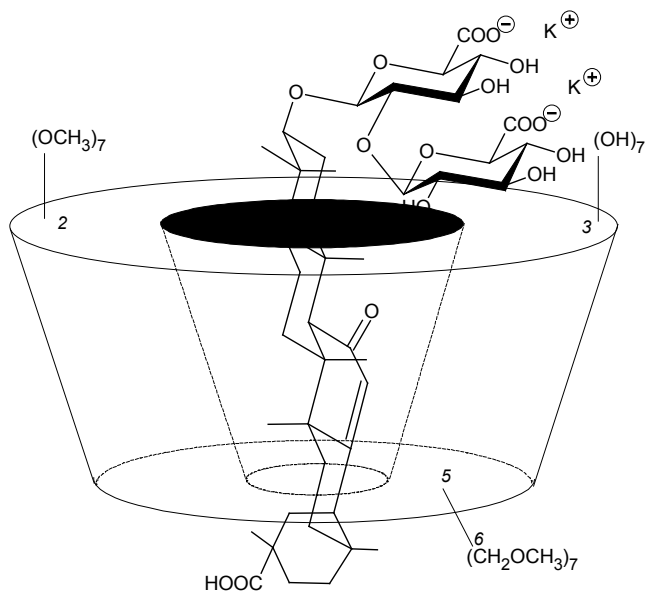


Figure 13. Schematic representation of dipotassium glycyrrhizinate complex with heptakis-2,6-O-dimethyl-β-CD.

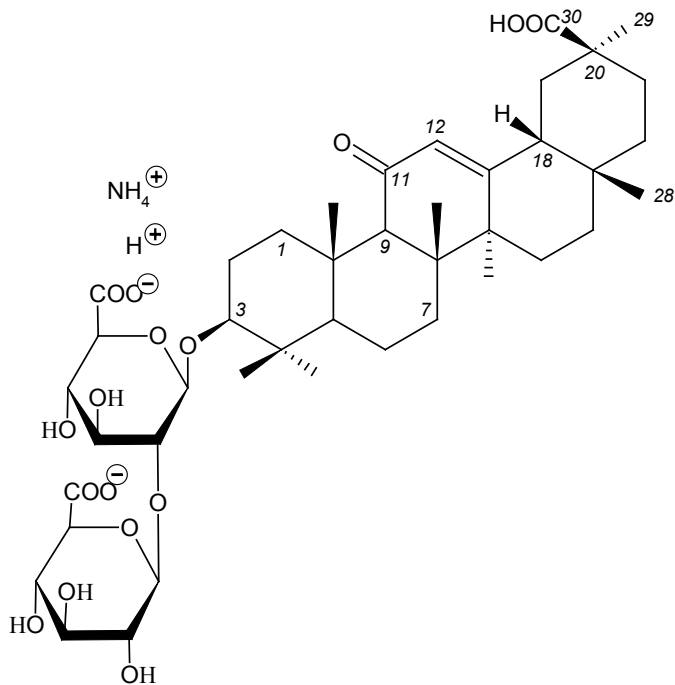


Figure 14. Monoammonium glycyrrhizinate (glycyrram).

By means of UV and IR Fourier spectrometry (Figure 15) the complexation of glycyrram (Figure 14) with β -CD has been investigated [58]. The method of isomolar series showed glycyrram makes a 1:1 clathrate complex with β -CD (Figure 16). The complexation is accompanied by hypochromic effect. The complex is formed on account of H-bonds and non-valent interactions. The influence of glycyrram, β -CD, and their complex on *Avena sativa* L. seeds' germination and on the fish *Poecilia reticulata* has been considered. The complex proved to be non-ichthyotoxic and did not suppress seeds' germination [59].

Such triterpene glycosides as α -hederin (hederagenin 3-*O*- α -L-rhamnopyranosyl-(1 \rightarrow 2)-*O*- α -L-arabinopyranoside, Figure 17), and its 28-*O*- α -L-rhamnopyranosyl-(1 \rightarrow 4)-*O*- β -D-glucopyranosyl-(1 \rightarrow 6)-*O*- β -D-glucopyranosyl ester (hederasaponin C, Figure 17) have been suggested as promising molecular complexing agents [60]. α -Hederin and hederasaponin C were discovered in representatives of most species of the ivy genus *Hedera* L., in which they are dominant saponins [54, 61–64]. Both glycosides are the

components of cough medicines containing extract of *Hedera helix* L. leaves [54, 65–67]. Herewith, the main therapeutic effect of ivy medicines is determined by the presence of α -hederin [67].

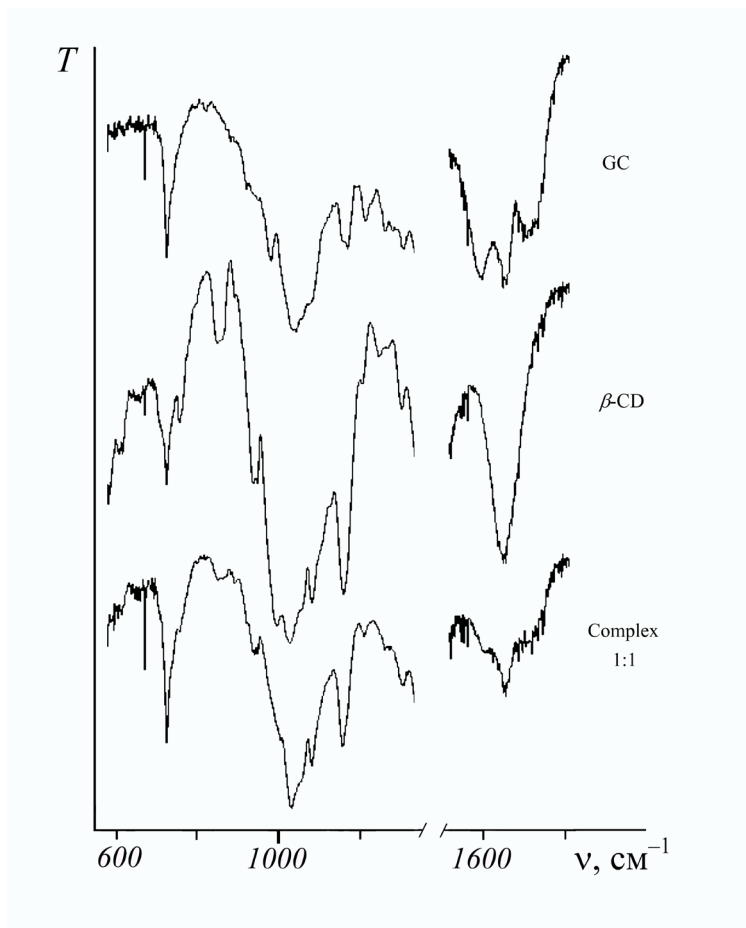


Figure 15. Fragments of IR Fourier spectra of glycyrram (GC), β -CD, and their complex.

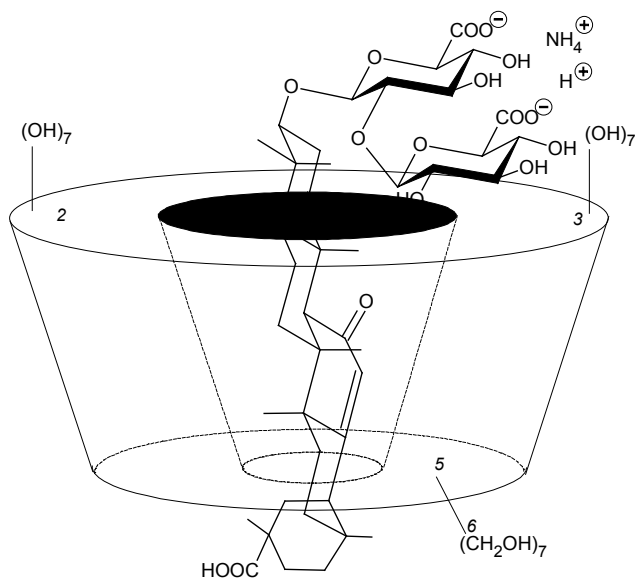


Figure 16. Schematic representation of monoammonium glycyrrhizinate (glycyrram) complex with β -CD.

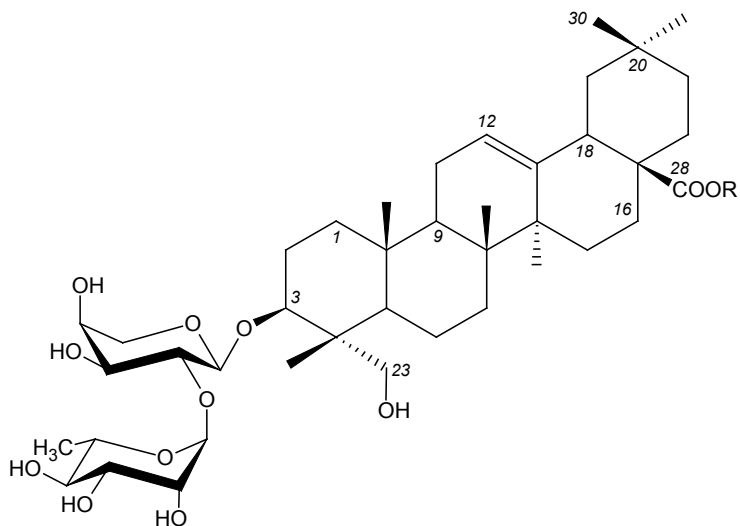


Figure 17. α -Hederin ($R=H$) and hederasaponin C ($R=\leftarrow\beta\text{Glc}_p-(6\leftarrow 1)-\beta\text{Glc}_p-(4\leftarrow 1)-\alpha\text{Rha}_p$).

Toxicity of triterpene glycosides causes plants' growth and development reduction, that is why glycosides are the factors of allelopathic interaction in plant association. Besides, triterpene glycosides display toxicity towards fishes and mollusks [54, 68–70]. Herewith, usually bidesmosidic glycosides display low toxicity explained by the absence of free carboxylic group at the C-17 atom in their aglicones. On the contrary, glycosides with a free carboxylic group have a high activity. α -Hederin is a monodesmosidic glycoside having a high biological activity.

Recently, we managed to get a molecular complex of α -hederin with β -CD. Its impact on *Avena sativa* L. seeds germination has been studied. It was discovered that the 1:1 complex is less phytotoxic than individual glycoside. The seeds' germination under complex effect reached 84%. The viability of seeds, previously cultivated by α -hederin, was 68% only. The very β -CD blocked germination to some extent (it reached 80%). The germination of seeds in distilled water (control set) was 92 %. The decrement of ichthyotoxicity of α -hederin making complex with β -CD was observed. The incubation time

$t_{LD_{100}}$, during which 100 % fatality of the fish *Poecilia reticulata* took place, on average was about 25 min for α -hederin, and reached 173 min for its complex.

References

1. Steed J.W., Atwood J.L. Supramolecular chemistry. – Chichester: John Wiley & Sons, Ltd, 2000. – 745 p.
2. Challa R., Ahuja A., Ali J., Khar R.K. Cyclodextrins in drug delivery: an updated review, AAPS Pharm. Sci. Tech. – 2005. Vol. 6, No 2. – P. E329–E357.
3. Li S., Purdy W.C. Cyclodextrins and their applications in analytical chemistry, Chem. Rev. – 1992. – Vol. 92. – P. 1457–1470.
4. Singh R., Bharti N., Madan J., Hiremath S.N. Characterization of cyclodextrin inclusion complexes – a review, J. Pharm. Sci. Tech. – 2010. – Vol. 2. – P. 171–183.
5. Belikov V.G., Kompantseva E.V., Botezat-Belyi Yu.K. Cyclodextrins and their inclusion compounds with drugs (review), Pharm. Chem. J. – 1986. – Vol. 20, No 5. – P. 299–306.
6. Uekama K., Hirayama F., Irie T. Cyclodextrin drug carrier systems, Chem. Rev. – 1998. – Vol. 98. – P. 2045–2076.
7. Zorky P.M., Lubnina I.E. Supramolecular chemistry: origin, evolution and prospects, MSU Vestnik. Ser. 2. Chem. – 1999. – Vol. 40, No 5. – P. 300–307.

8. Szejtli J. Introduction and general overview of cyclodextrin chemistry, *Chem. Rev.* – 1998. – Vol. 98. – P. 1743–1753.
9. Kompantseva E.V., Gavrilin M.V., Ushakova L.S. β -Cyclodextrin derivatives and their applications in pharmacology (a review), *Pharm. Chem. J.* – 1996. – Vol. 30, No 4. – P. 258–262.
10. Astakhova A.V., Demina N.B. Modern drug technologies: synthesis, characterization, and use of inclusion complexes between drugs and cyclodextrins (a review), *Pharm. Chem. J.* – 2004. – Vol. 38, No 2. – P. 105–108.
11. Brewster M.E., Loftsson T. Cyclodextrins as pharmaceutical solubilizers, *Adv. Drug Deliv. Rev.* – 2007. – Vol. 59. – P. 645–666.
12. Del Valle E.M.M. Cyclodextrins and their uses: a review, *Proc. Biochem.* – 2004. – Vol. 39. – P.1033–1046.
13. Breslow R., Dong S.D. Biomimetic reactions catalyzed by cyclodextrins and their derivatives, *Chem. Rev.* – 1998. – Vol. 98. – P. 1997–2011.
14. Sumina E.G. Organized nanosystems in thin-layer chromatography, *Sorb. Chromatogr. Proc.* – 2010. – Vol. 10, No. 1. – P. 150–160.
15. Sumina E.G., Atayan V.Z., Shtykov S.N. Application of cyclodextrin mobile phases in thin-layer chromatography of organic reagents of xanthenic and quinolinic rows, *Sorb. Chromatogr. Proc.* – 2008. – Vol. 8, No. 1. – P. 83–93.
16. Sarafanova L.A. Nutritional additives: Encyclopedia. – Saint-Petersburg: GIOR, 2004. – 808 p.
17. Gould S., Scott R.C. 2-Hydroxypropyl- β -cyclodextrin (HP- β -CD): A toxicology review, *Food Chem. Toxicol.* – 2005. – Vol. 43. – P. 1451–1459.
18. Perrin J.H., Field F.P., Hansen D.A., Mufson R.A., Torosian G. β -Cyclodextrin as an aid to peritoneal dialysis. Renal toxicity of β -cyclodextrin in the rat, *Res. Commun. Chem. Pathol. Pharmacol.* – 1978. – Vol. 19. – P. 373–376.
19. Frank D. W., Gray J. E., Weaver R. N. Cyclodextrin nephrosis in the rat, *Am. J. Pathol.* – 1976. – Vol. 83. – P. 367–382.
20. Riabov S.V., Lebedev A.F., Kercha Yu.Yu. Selective functionalisation of cyclodextrins, *Polym. J.* – 2007. – Vol. 29, No. 1. – P. 48–51.
21. Riabov S.V., Voitenko Z.V., Kisel A.I., Lebedev A.F., Kercha Yu.Yu., Laptiy S.V. Modification of β -cyclodextrin by isoindole derivatives, *Polym. J.* – 2005. – Vol. 27, No. 4. – P. 232–235.
22. Riabov S.V., Kercha Yu.Yu., Kobrina L.V., Kobylinskyy S.N., Laptiy S.V. Synthesis and sorption properties of the cyclodextrin based

- polymers, *Polym. J.* – 2006. – Vol. 28, No. 1. – P. 47–52.
23. Riabov S.V., Lebedev A.F., Laptiy S.V. Synthesis of cyclodextrin derivatives having triethoxysilyl groups, *Polym. J.* – 2006. – Vol. 28, No. 1. – P. 53–55.
 24. Sevastyanova E.V., Davidenko T.I., Shapiro Yu.E., Pyhteeva E.G. Immobilization of fir oil, *Pharm. Chem. J.* – 1994. – Vol. 28, No. 3. – P. 59–63.
 25. Davidenko T.I., Romanovskaya I.I., Andronati S.A. Immobilization of biologically active compounds, *Microbiol. Biotechnol.* – 2009. – No. 6. – P. 8–22.
 26. Romanovskaya I.I., Davidenko T.I., Dekina S.S., Pashkin I.I., Andronati S.A. Immobilization of biologically active substances with the aim of creating potential diagnostic and medicinal agents, *J. Org. Pharm. Chem.* – 2009. – Vol. 7, No. 3. – P. 69–78.
 27. Davidenko T.I. Immobilization of enzymic preparation, *Odessa Nat. Univer. Herald, ser. Chem.* – 2003. – Vol. 8, No. 4. – P. 135–147.
 28. Petrovi G.M., Stojanovi G.S., Radulovi N.S. Encapsulation of cinnamon oil in β -cyclodextrin, *J. Med. Plant. Res.* – 2010. – Vol. 4. – P. 1382–1390.
 29. Bicchi C., Brunelli C., Cravotto G., Rubiolo P., Galli M., Mendicuti F. Cyclodextrin derivatives in enantiomer GC separation of volatiles. Part XXI: Complexation of some terpenoids with 2-*O*-acetyl-3-*O*-methyl- and 2-*O*-methyl-3-*O*-acetyl-6-*O*-*t*-hexyldimethylsilyl- γ -cyclodextrins: Molecular Mechanics and Molecular Dynamics, *J. Sep. Sci.* – 2003. – Vol. 26, No. 17, P. 1479–1490.
 30. König W.A., Krebber R., Evers P., Bruhn G. Stereochemical analysis of constituents of essential oils and flavor compounds by enantioselective capillary gas chromatography, *J. High Resolut. Chromatogr.* – 1990. – Vol. 13, No. 5. – P. 328–332.
 31. Luzina O.A., Polyakov N.E., Salahutdinov N.F., Korchagina D.V., Barhash V.A. Study inclusion complexes of some terpenoids with β -cyclodextrin by NMR, *Chem. Comput. Simul. Butlerov Commun.* – 2002. – No. 7. – P. 39–44.
 32. Dodziuk H., Ejchart A., Lukin O., Vysotsky M.O. ^1H and ^{13}C NMR and molecular dynamics study of chiral recognition of camphor enantiomers by α -cyclodextrin, *J. Org. Chem.* – 1999. – Vol. 64. – P. 1503–1507.
 33. Anczewski W., Dodziuk H., Ejchart A. Manifestation of chiral recognition of camphor enantiomers by alpha-cyclodextrin in longitudinal and transverse relaxation rates of the corresponding 1:2

- complexes and determination of the orientation of the guest inside the host capsule, *Chirality*. – 2003. – Vol. 15. – P. 654–659.
34. Kokkinou A., Tsorteki F., Karpusas M., Papakyriakou A., Bethanis K., Mentzafos D. Study of the inclusion of the (*R*)- and (*S*)-camphor enantiomers in α -cyclodextrin by X-ray crystallography and molecular dynamics, *Carbohydr. Res.* – 2010. – Vol. 345, No. 8. – P. 1034–1040.
 35. Simova S., Berger S. Diffusion Measurements vs. chemical shift titration for determination of association constants on the example of camphor–cyclodextrin complexes, *J. Inclus. Phenom. Macrocyclic Chem.* – 2005. – Vol. 53, No. 3. – P. 163–170.
 36. Bielejewska A., Nowakowski R., Duszczyk K., Sybilska D. Joint use of cyclodextrin additives in chiral discrimination by reversed-phase high-performance liquid chromatography: temperature effects, *J. Chromatogr. A.* – 1999. – Vol. 840, No. 2. – P. 159–170.
 37. Asztemborska M., Bielejewska A., Duszczyk K., Sybilska D. Comparative study on camphor enantiomers behavior under the conditions of gas–liquid chromatography and reversed-phase high-performance liquid chromatography systems modified with α - and β -cyclodextrins, *J. Chromatogr. A.* – 2000. – Vol. 874, No. 1. – P. 73–80.
 38. Bernatowicz P., Nowakowski M., Dodziuk H., Ejchart A. Determination of association constants at moderately fast chemical exchange: Complexation of camphor enantiomers by α -cyclodextrin, *J. Magn. Reson.* – 2006. – Vol. 181, No. 2. – P. 304–309.
 39. Schmidtchen F.P. The anatomy of the energetics of molecular recognition by calorimetry: chiral discrimination of camphor by α -cyclodextrin, *Chem. Eur. J.* – 2002. – Vol. 8. – P. 3522–3529.
 40. Ikeda Y., Matsumoto K., Kunihiro K., Fuwa T., Uekama K. Inclusion complexation of essential oils with α - and β -cyclodextrins, *J. Pharm. Soc. Japan.* – 1982. – Vol. 102, No. 1. – P. 83–88.
 41. López M.D., Pascual-Villalobos M.J. Analysis of monoterpenoids in inclusion complexes with β -cyclodextrin and study on ratio effect in these microcapsules, *Julius-Kühn-Archiv.* – 2010. – Vol. 425. – P. 705–709.
 42. Bhandari B.R., D'Arcy B.R., Padukka I. Encapsulation of lemon oil by paste method using β -cyclodextrin: encapsulation efficiency and profile of oil volatiles, *J. Agric. Food Chem.* – 1999. – Vol. 47, No. 12. – P. 5194–5197.
 43. Donze C., Coleman A.W. β -CD inclusion complexes: relative selectivity of terpene and aromatic guest molecules studied by competitive

- inclusion experiments, *J. Inclus. Phenom. Mol. Recogn. Chem.* – 1993. – Vol. 16, No. 1. – P. 1–15.
44. Liu Y., Yang E.-C., Yang Y.-W., Zhang H.-Y., Fan Z., Ding F., Cao R. Thermodynamics of the molecular and chiral recognition of cycloalkanols and camphor by modified β -cyclodextrins possessing simple aromatic tethers, *J. Org. Chem.* – 2004. – Vol. 69. – P. 173–180.
 45. Hamada F., Kondo Y., Ishikawa K., Ito H., Suzuki I., Osa T., Ueno A. Host-guest sensory system of sodium anthranilate-modified β -cyclodextrin: molecular recognition properties, *J. Incl. Phenom. Mol. Recogn. Chem.* – 1994. – Vol. 17, No. 3. – P. 267–275.
 46. Hamada F., Ishikawa K., Ito R., Shibuya H., Hamai S., Suzuki I., Osa T., Ueno A. Spacer effect of appended moieties for molecular recognition in doubly-sodium anthranilate modified γ -cyclodextrin, *J. Incl. Phenom. Mol. Recogn. Chem.* – 1994. – Vol. 20, No. 1. – P. 43–51.
 47. Guella G., Callone E., Mancini I., Uccello-Barretta G., Balzano F., Dini F. Chemical and structural properties of the inclusion complex of euplotin C with heptakis(2,6-di-O-methyl)- β -cyclodextrin through NMR spectroscopy, electrospray mass spectrometry and molecular mechanics investigations, *Eur. J. Org. Chem.* – 2004. – Vol. 2004, No. 6. – P. 1308–1317.
 48. Guella G., Skropeta D., Di Giuseppe G., Dini F. Structures, biological activities and phylogenetic relationships of terpenoids from marine ciliates of the genus *Euplotes*, *Mar. Drugs.* – 2010. – Vol. 8, No. 7. – P. 2080–2116.
 49. Ohtani K., Aikawa Y., Fujisawa Y., Kasai R., Tanaka O., Yamasaki K. Solubilization of steviolbioside and steviolmonoside with gamma-cyclodextrin and its application to selective syntheses of better sweet glycosides from stevioside and rubusoside, *Chem. Pharm. Bull.* – 1991. – Vol. 39. – P. 3172–3174.
 50. Madan S., Ahmad S., Singh G.N., Kohli K., Kumar Y., Singh R., Garg M. *Stevia rebaudiana* (Bert.) Bertoni – a review, *Ind. J. Nat. Prod. Resour.* – 2010. – Vol. 1, No. 3. – P. 267–286.
 51. Chou G., Xu S.-J., Liu D., Koh G.Y., Zhang J., Liu Z. Quantitative and fingerprint analyses of chinese sweet tea plant (*Rubus suavissimus* S. Lee), *J. Agric. Food Chem.* – 2009. – Vol. 57, No. 3. – P. 1076–1083.
 52. Upreti M., Strassburger K., Chen Y.L., Wu S., Prakash I. Solubility enhancement of steviol glycosides and characterization of their inclusion complexes with gamma-cyclodextrin, *Int. J. Mol. Sci.* – 2011. – Vol. 12. – P. 7529–7553.

53. Lee P.S., Han J.-Y., Song T.W., Sung J.H., Kwon O.-S., Song S., Chung Y.B. Physicochemical characteristics and bioavailability of a novel intestinal metabolite of ginseng saponin (IH901) complexed with β -cyclodextrin, *Int. J. Pharm.* – Vol. 316, No. 1–2. – P. 29–36.
54. Hostettmann K., Marston A. Saponins. – Cambridge: Cambridge University Press, 1995. – 548 p.
55. Prankerd R., Stone H., Sloan K., Perrin J. Degradation of aspartame in acidic aqueous media and its stabilization by complexation with cyclodextrins or modified cyclodextrins, *Int. J. Pharm.* – 1992. – Vol. 88. – P. 189–199.
56. Tamagaki S., Koide M., Takahashi M., Mizushima T., Ukawa J., Tagaki W. Inhibitory effects of cyclodextrins by inclusion on the catalytic activity of glycyrrhizinate for the hydrolysis of a nonionic ester surfactant, *J. Chem. Soc., Perkin Trans. 2.* – 1996. – P. 1257–1260.
57. Gavrilin M.V., Senchenko S.P., Tamirjan A.M., Pechenova A.V. Improved methods of assessing the quality of the roots and the licorice syrup, *Chem. Plant Raw Mater.* – 2009. – No. 4. – P. 147–150.
58. Yakovishin L.A., Grishkovets V.I. Molecular complexation of monoammonium glycyrrhizate (glycyrram) with β -cyclodextrin, *Abstr. of Int. conf. «Modern problems of chemistry of natural compounds».* – Tashkent (Uzbekistan). – 2010. – P. 171.
59. Yakovishin L.A., Grishkovets V.I., Belash D.Yu., Yarovoy I.R., Korzh E.N., Kopytov Yu.P. Supramolecular complex of monoammonium glycyrrhizate (glycyrram) with β -cyclodextrin, *Abstr. of sci. conf. «Biologically active substances: fundamental and applied problems».* – Novy Svet (Ukraine). – 2011. – P. 226.
60. Yakovishin L.A., Grishkovets V.I., Schroeder G., Borisenko N.I. Molecular complexation of ivy saponins with some drugs and biologically active substances. In *Functionalized molecules – synthesis, properties and application*, Ed. V.I. Rybachenko. – Donetsk: Schidnyj vydavnyczyj dim, 2010. – 226 p. – Chapter 4. – P. 85–103.
61. Mshvildadze V., Elias R., Faure R., Rondeau D., Debrauwer L., Dekanosidze G., Kemertelidze E., Balansard G. Triterpenoid saponins from the leaves of *Hedera pastuchowii*, *Chem. Pharm. Bull.* – 2004. – Vol. 52, No. 12. – P. 1411–1415.
62. Mshvildadze V., Elias R., Faure R., Debrauwer L., Dekanosidze G., Kemertelidze E., Balansard G. Triterpenoid saponins from berries of *Hedera colchica*, *Chem. Pharm. Bull.* – 2001. – Vol. 49, No. 6. – P. 752–754.

63. Elias R., Diaz-Lanza A. M., Vidal-Ollivier E., Balansard G., Faure R., Babadjamian A. Triterpenoid saponins from the leaves of *Hedera helix*, *J. Nat. Prod.* – 1991. – Vol. 54, No. 1. – P. 98–103.
64. Grishkovets V.I., Sidorov D.Yu., Yakovishin L.A., Arnautov N.N., Shashkov A.S., Chirva V.Ya. Triterpene glycosides of *Hedera canariensis*. I. Structures of glycosides L-A, L-B₁, L-B₂, L-C, L-D, L-E₁₁, L-G₁, L-G₂, L-G₃, L-G₄, L-H₁, L-H₂, and L-I₁ from the leaves of *Hedera canariensis*, *Chem. Nat. Comp.* – 1996. – Vol. 32, No. 3. – P. 360–365.
65. Büechi S., Bolli R. Efeu – expektorans, mukolytikum und broncholytikum. Botanische und klinische aspekte, *Phytotheraphie.* – 2003. – No. 3. – S. 19–22.
66. Yakovishin L.A., Grishkovets V.I. Triterpene glycosides of the medicinal preparation Hedelix[®], *Chem. Nat. Comp.* – 2003. – Vol. 39, No. 5. – P. 508–509.
67. Sieben A., Prenner L., Sorkalla T., Wolf A., Jakobs D., Runkel F., Haberlein H. α -Hederin, but not hederacoside C and hederagenin from *Hedera helix*, affects the binding behavior, dynamics, and regulation of β 2-adrenergic receptors, *Biochemistry.* – 2009. – 48, No. 15. – P. 3477–3482.
68. Waller G.R., Jurzysta M., Trohne R.L.Z. Root saponins from alfalfa (*Medicago sativa* L.) and their allelopathic activity on weeds and wheat, *Allelopathy J.* – 1995. – Vol. 2, No. 1. – P. 21–30.
69. Podolak I., Galanty A., Sobolewska D. Saponins as cytotoxic agents: a review, *Phytochem. Rev.* – 2010. – Vol. 9. – P. 425–474.
70. Yakovishin L.A., Ertahova V.A., Bazyura E.A. Influence of the triterpene glycosides and their complexes on mollusks, *Ukr. Bioorg. Acta.* – 2006. – Vol. 4, No. 2. – P. 22–26.

Chapter 17

Mesoporous material as assisted matrix for MALDI-TOF MS

Szymon Jasiocki, Izabela Nowak and Grzegorz Schroeder

Adam Mickiewicz University, Faculty of Chemistry,

Grunwaldzka 6, 60-780 Poznań, Poland

Matrix-assisted laser desorption/ionization time-of-flight mass spectrometry (MALDI-TOF MS), since its development [1,2], has been widely applied for the analyses of various high molecular species like proteins/peptides [3,4], oligosaccharides [5,6], oligonucleotides [7,8] synthetic polymers [9,10] or molecular receptors. However, the utility of this method is limited for the small molecule (<500 Da) analyses because of the interference of the matrix, which mixed with an analyte, produces its own background in the low-molecular mass region.

New approaches to solve this problem have been developed. The idea is either to eliminate the matrix or use materials that generate no background ions in the analyte m/z region. Desorption/ionization on porous silicon (DIOS) is a suitable method for small molecules analyses because requires no addition of matrix [11]. Graphene used as a novel matrix is effective for desorption/ionization for nonpolar compounds [12]. Oxidized carbon nanotubes can provide both qualitative and quantitative determination of low molecular compounds [13]. Other idea is application of metal-phtalocyanines which form matrix-analyte adducts, easily detected in analysis both in the negative and positive ion mode [14]. One of the method is usage of modified mesoporous materials SBA-15 as assisted matrix [15].

In the typical synthesis of modified mesoporous materials SBA-15 process, a triblock copolymer poly(ethyleneoxide)-poly(propylene oxide)-poly(ethylene oxide) BASF P123 (HO(EO)₂₀(PO)₇₀(EO)₂₀H), P105 (HO(EO)₃₇(PO)₅₆(EO)₃₇H), P94 (HO(EO)₂₁(PO)₄₇(EO)₂₁H), L64 (HO(EO)₁₃(PO)₃₀(EO)₁₃H) or L43 (HO(EO)₇(PO)₁₉(EO)₇H) was dispersed in water mixed with HCl under stirring. Once the triblock copolymer was completely dissolved, tetraethyl orthosilicate (TEOS) was added to the resulting homogeneous solution under vigorous stirring in order to achieve TEOS/copolymer molar ratio of 120. The composition of the reaction mixture was: 0.09 mmol Pluronic : 10.8 mmol TEOS : 0.12 mol

HCl : 3.3 mol H₂O. The stirring was continued for 8 h and then the resultant mixture was aged at 373 K for 16 h without stirring. The as-prepared sample was recovered by filtration, washed with a copious amount of water and air-dried at 333 K. After calcination at 823 K for 8 h in air the mesoporous sample was finally obtained.

The resulting SBA-15 samples were denoted as SBA-15-X, where X stands for Pluronic type. All samples studied in this work are summarized in Table 1.

Table 1. Parameters of the studied SBA-15

Method/parameter	SBA-15-X				
	43	64	94	105	123
XRD/ Cell parameter a ₀ (nm)	~6.8	8.2	9.8	10.5	11.4
N ₂ ads./ Surface area. BET (m ² g ⁻¹)	740	800	740	780	680
Pore diameter (nm)	2.8	4.3	5.8	6.6	7.8
Pore volume. (cm ³ g ⁻¹)	0.46	0.43	0.50	0.51	0.58
XRD + N ₂ ads. / Wall thickness (nm)	~4.0	3.9	4.0	3.9	4.1

The transmission electron micrographs (TEM) were taken on a JEOL-2000 operated at 80 keV (Fig. 1).

The interactions of molecules as protein/peptides with solid surface [16, 17] are predominantly determined by the hydrophobic and electrostatic forces, which are two main types of driving forces in controlling the immobilization process and capacity of biomolecules into porous hosts [18]. Other influencing factors may include the pore structure of hosts (such as the pore symmetry and pore diameters), the experimental conditions (such as the choice of buffer solutions), and the nature of protein/peptides, etc. It has been shown that a selective adsorption of proteins can be achieved in the macroporous structures through modulating the surface charge of materials [19, 20].

The matrix in MALDI MS methods performs two important functions: it absorbs photon energy from the laser beam and transfers it into excitation energy of the solid system, and it serves as a solvent for the analyte, so that the intermolecular forces are reduced and aggregation of the analyte molecules is held to a minimum. Typical MALDI matrix as: CHCA, sinapic acids, DBH, DAN, DHAP, 3-HPA, THAP, HABA, MBT, CICCA or FCCA are characterized by: a strong light absorption property at the wavelength of the laser flux, the

ability to form micro-crystals with the sample, a low sublimation temperature, which facilitates the formation of an instantaneous high-pressure plume of matrix-sample material during the laser pulse duration, and the participation in some kind of a photochemical reaction so that the sample molecules can be ionized with high yields. The use of mixed matrices of classical compounds and mesoporous material opens up new possibilities for mass spectrometry analytical. Mesoporous materials isolate analytes than conventional MALDI matrices.

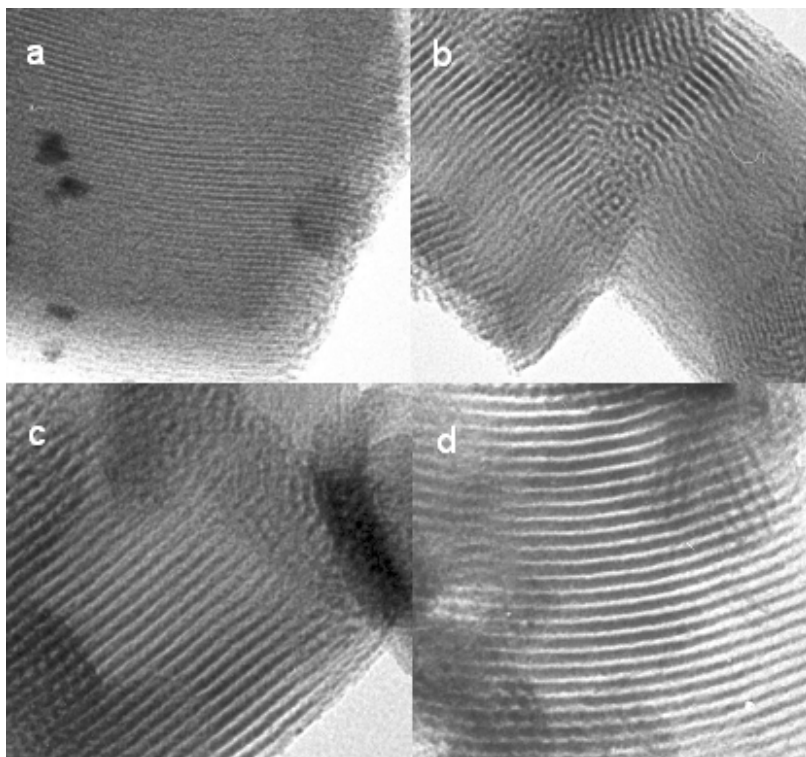


Figure 1. TEM images of SBA-15- a) 43, b) 64, c) 105 and d) 123 with the pore size of: 2.8; 4.3; 6.6 and 7.3 nm respectively.

obtained from the BASF surfactants:

L43; $(HO(EO)_7(PO)_{19}(EO)_7H)$;

L64; $(HO(EO)_{13}(PO)_{30}(EO)_{13}H)$;

P105; $(HO(EO)_{37}(PO)_{56}(EO)_{37}H)$ and

P123; $(HO(EO)_{20}(PO)_{70}(EO)_{20}H)$.

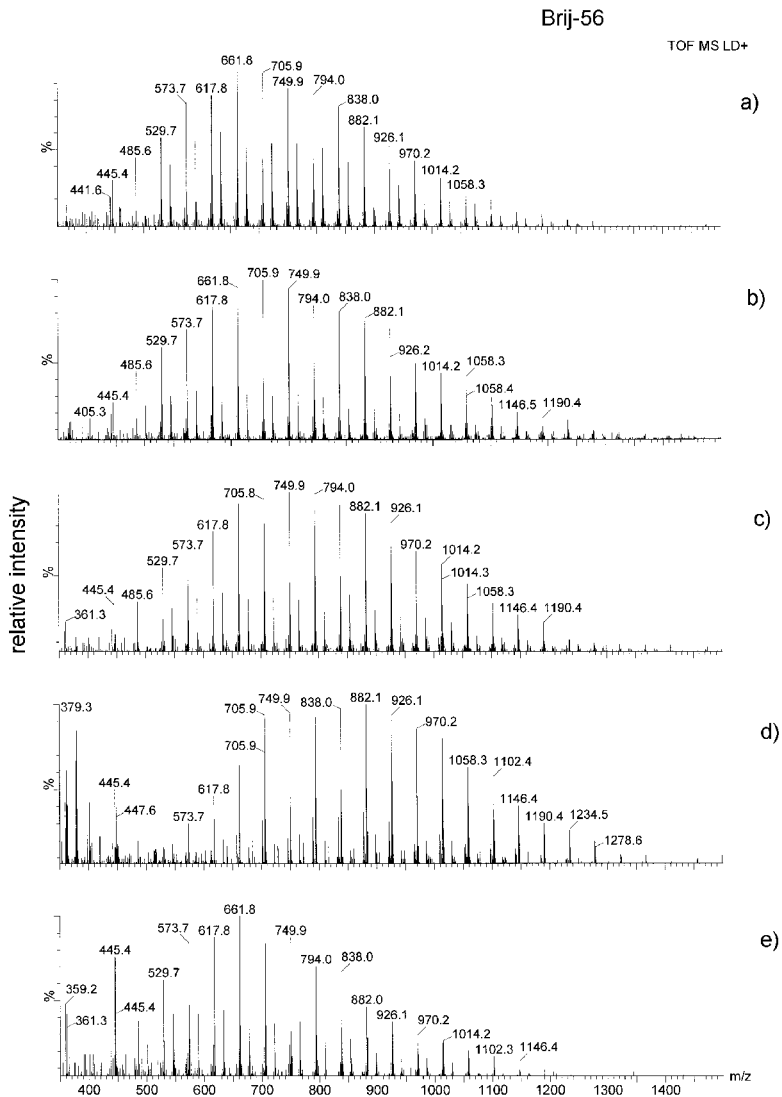


Figure 3. MALDI-TOF spectra of Brij-56 with SBA-15-105 a), SBA-15-94 b), SBA-15-64 c), SBA-15-43 d) and without SBA-15 e).

PEG 350

TOF MS LD+

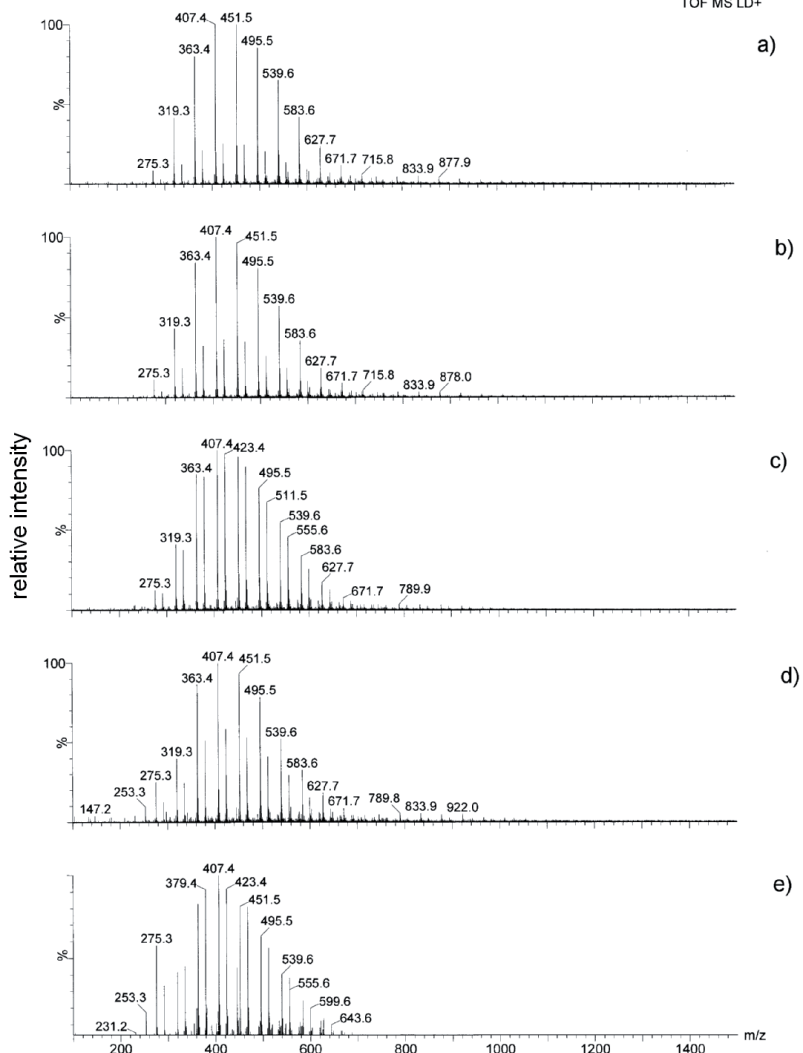


Figure 4. MALDI-TOF spectra of PEG-350 with SBA-15-105 a), SBA-15-94 b), SBA-15-64 c), SBA-15-43 d) and without SBA-15 e).

Triton X-100

TOF MS LD+

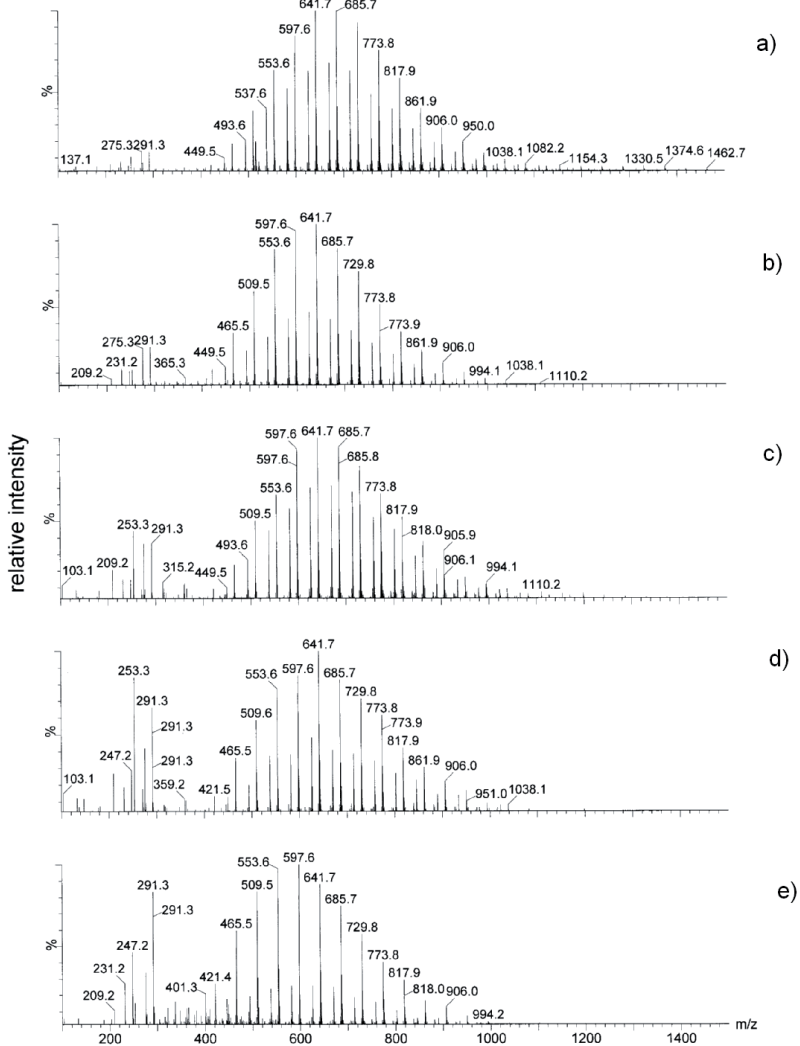


Figure 5. MALDI-TOF spectra of Triton X-100 with SBA-15-105 a), SBA-15-94 b), SBA-15-64 c), SBA-15-43 d) and without SBA-15 e).

In a series of MALDI-TOF spectra of Brij-56 (Fig. 3) we observe a shift of the maximum of the signal intensities distribution. The shift is toward lower m/z values with increasing SBA-15 pore diameters. It is a consequence of the increasing amount of short-chained detergent molecules adsorbed in pores that undergo evaporation to the gas state.

Eventually the signal intensities distribution for sample with SBA-15-105 (Fig. 3a), with the largest pore diameter studied, is the most similar to the that one in the spectrum in the Fig. 3e, for the sample without SBA-15, with the maximum at m/z 661.8 assigned to $[M+Na]^+$ ion ($n=9$). The relationship between m/z maximum and pore diameter is illustrated in the Fig 6.

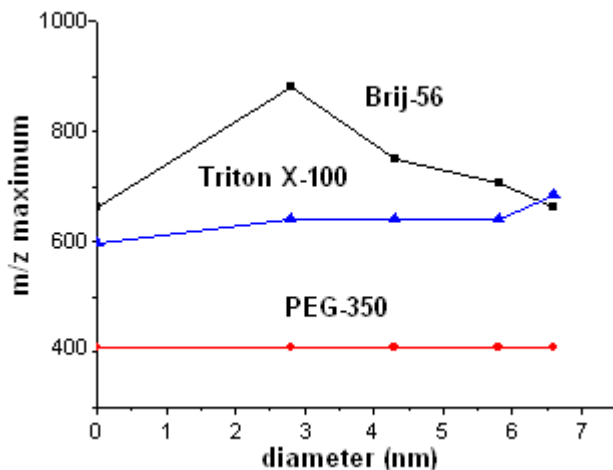


Figure 6. The relationship plot between the pore diameter and the m/z maximum value of Brij-56, PEG-350 and Triton X-100.

In the case of Triton X-100 such a shift is slight toward higher m/z value which can be explained by a steric hindrance of the large hydrophobic group which prevents molecules from adsorption in pores. It occurs for the largest pore diameter, with the maximum at m/z 685.7 assigned to $[M+K]^+$ ion ($n=10$). This shift is absent for PEG-350 and the maximum is constant at m/z 407.4 assigned to $[M+Na]^+$ ion ($n=8$). However, there are noticeable differences in low m/z parts of the spectra (Figs. 4 and 5). The intensities of the signals in low m/z region decrease with the increasing pore diameters. Molecules responsible for these signals are adsorbed in mesoporous matrix and are not evacuated from the pores in the experiment conditions. As a result spectrum is cleaner.

It is noteworthy that there are differences in the $[M+Na]^+$ and $[M+K]^+$ ion intensities ratios in all detergents spectra. For Brij-56 and PEG-350 we observed higher intensities of $[M+Na]^+$ signals than $[M+K]^+$, however this ratio is reversed for Triton X-100 (Fig.7).

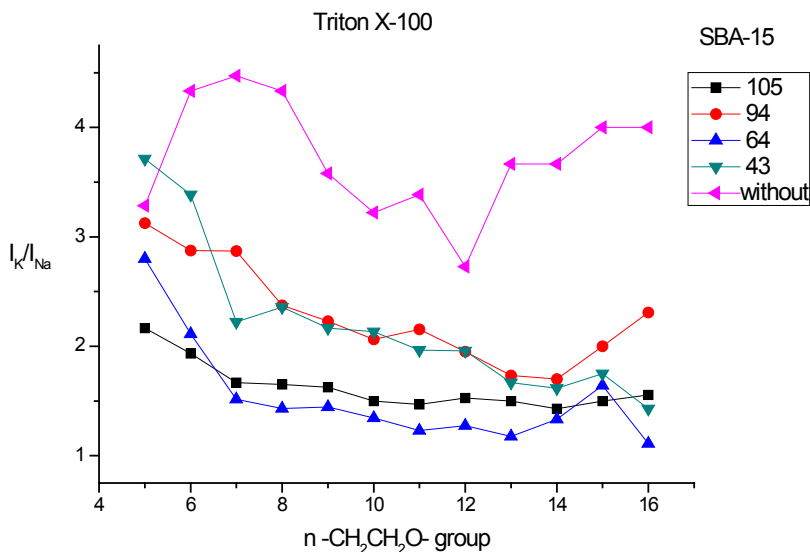


Figure 7. The plot of $[M+Na]^+$ and $[M+K]^+$ ions intensity ratios dependency on the detergent chain length of Triton X-100.

This experiment proved that SBA-15 material can be successfully utilized as a matrix and this technique is suitable for the analysis of small molecules like detergents. Mesoporous silica molecular sieves demonstrated several advantages compared with DHB such as less background interference ions, higher homogeneity and reproducibility of the spectra.

Acknowledgement

Financial support from Ministry of Science and Higher Education (Grant no. N N 204 029 636) is acknowledged.

References

1. Karas M.; Hillenkamp F., Laser Desorption Ionization of Proteins with Molecular Masses Exceeding 10,000 Daltons, *Anal. Chem.*, 1988, 60,

- 2299-2301.
2. Tanaka M.; Waiki H.; Ido Y.; Akita S.; Yoshida T., Protein and Polymer Analyses up to m/z 10,000 by Laser Ionization Time-of-Flight Mass Spectrometry, *Rapid Commun. Mass Spectrom.*, 1988, 2, 151-153.
 3. Chaurand P., Luetzenkirchen F., Spengler B., Peptide and protein identification by matrix-assisted laser desorption ionization (MALDI) and MALDI-post-source decay time-of-flight mass spectrometry, *J. Am. Soc. Mass Spectrom.*, 1999, 10, 91-103.
 4. Pierson J., Norris J.L., Aerni, H.-R., Svenningsson P., Caprioli R.M., Andr n P.E., Molecular Profiling of Experimental Parkinson's Disease: Direct Analysis of Peptides and Proteins on Brain Tissue Sections by MALDI Mass Spectrometry, *J. Proteome Research*, 2004, 3, 289-295.
 5. Wang J., Sporns P., Low N.H., Analysis of food oligosaccharides using MALDI-MS: Quantification of fructooligosaccharides, *J. Agric. Food Chem.*, 1999, 47, 1549-1557.
 6. Finke B., Stahl B., Pfenninger A., Karas M., Daniel H., Sawatzki G., Analysis of high-molecular-weight oligosaccharides from human milk by liquid chromatography and MALDI-MS, *Anal. Chem.*, 1999, 71, 3755-3762.
 7. Li Y., Tang K., Little D.P., K ster H., Hunter R.L., McIver Jr. R.T., High-resolution MALDI Fourier transform mass spectrometry of oligonucleotides, *Anal. Chem.*, 1996, 68, 2090-2096.
 8. Little D.P., Cornish T.J., O'Donnell M.J., Braun, A., Cotter R.J., K stet H., MALDI on a Chip: Analysis of Arrays of Low-Femtomole to Subfemtomole Quantities of Synthetic Oligonucleotides and DNA Diagnostic Products Dispensed by a Piezoelectric Pipet, *Anal. Chem.*, 1996, 69, 4540-4546.
 9. Nielen M.W.F., Maldic time-of-flight mass spectrometry of synthetic polymers, *Mass Spectrom. Rev.*, 1999, 18, 309-344.
 10. Trimpin S., Keune S., R der H.J., M llen K., Solvent-Free MALDI-MS: Developmental Improvements in the Reliability and the Potential of MALDI in the Analysis of Synthetic Polymers and Giant Organic Molecules, *J. Am. Soc. Mass Spectrom.*, 2006, 17, 661-671.
 11. Kraj A., Dylag T., Gorecka-Drzazga A., Bargiel S., Dziuban J., Silberring J., *Acta Biochim. Pol.*, 2003, 50, 783-787.
 12. Dong X., Cheng J., Li J., Wang Y., Graphene as a Novel Matrix for the Analysis of Small Molecules by MALDI-TOF MS, *Anal. Chem.*, 2010, 82, 6208-6214.
 13. Pan C., Xu S., Hu L., Su X., Ou J., Zou H., Guo Z., Zhang Y., Guo

- B., Using Oxidized Carbon Nanotubes as Matrix for Analysis of Small Molecules by MALDI-TOF MS, *J. Am. Soc. Mass Spectrom.*, 2005, 16, 883–892.
14. Zhang S., Liu J., Chen Y., Xiong S., Wang G., Chen J., Yang G., A Novel Strategy for MALDI-TOF MS Analysis of Small Molecules, *J. Am. Soc. Mass Spectrom.*, 2010, 21, 154-160.
 15. Li X., Wu X., Kim J. M., Kim S. S., Jin M., Li D., MALDI-TOF-MS analysis of small molecules using modified mesoporous material SBA-15 as assisted matrix, *J. Am. Soc. Spectrom.*, 2009, 20, 2167.
 16. Wei Y., Latour R. A., Determination of adsorption free energy for peptide-surface interactions by SPR spectroscopy, *Langmuir*, 2008, 24, 6721—6729.
 17. Wei Y., Latour R. A., Benchmark experimental data set and assessment of adsorption free energy for peptide-surface interactions, *Langmuir* 2009, 25, 5637-5646.
 18. Qiao S. Z., Yu C. Z., Xing W., Hu Q. H., Djojoputro H., Lu G. Q., Synthesis and Bio-adsorptive Properties of Large-Pore Periodic Mesoporous Organosilica Rods, *Chem. Mater.* 2005, 17, 6172—6176.
 19. Qian K., Wan J., Qiao L., Huang X., Tang J., Wang Y., Kong J., Yang P., Yu C., Liu B., Macroporous material as novel catalysts for efficient and controllable proteolysis, *Anal. Chem.*, 2009, 81, 5749-5756.
 20. Qian K., Wan J., Liu F., Girault H. H., Liu B., Yu C., Toward Intelligent Nanosize Bioreactors: A pH-Switchable, Channel-Equipped, Functional Polymer Nanocontainer, *ACS Nano*, 2009, 3, 3656-3662.

Chapter 18

Phosphono peptides and their host-guest chemistry. ESI MS study

Piotr Młynarz^a, Bernadeta Lasek^b, Paweł Kafarski^a, Tomasz Kozik^b
and Grzegorz Schroeder^b

^a *Wrocław University of Technology, Faculty of Chemistry,
Wybrzeże Wyspiańskiego 27, 50-370 Wrocław*

^b *Adam Mickiewicz University, Faculty of Chemistry,
Grunwaldzka 6, 60-780 Poznań, Poland*

1. Introduction

The term “phosphono peptides” was introduced by Martell in 1975, although this class of compounds was recognized about 30 years earlier. These compounds are regarded as structural analogues of peptides in which carboxylic moiety was replaced by phosphonic entity. Therefore they may act as peptide antagonists and thus exhibit various physiologic activity. Due to these properties phosphono peptides are used in agriculture and medicine, with antibacterial properties being the most intensively exploited [1].

Hexaaza-macrocyclic ligands containing polyamine and Schiff base fragments are widely described in literature [2-7]. This group of compounds attracts a special attention because, depending on their structure, they possess suitable cavities ready for incorporation of structurally diverse organic or inorganic molecules, especially negatively charged ones, such as: phosphate anions, dicarboxylic organic acids and acidic amino acids. Moreover, ready formation of hydrogen bonds between anionic groups of guest molecule and host amine groups with *pK* values ranging from 3 to 9.5 allowed determining stability constants of associated molecules [8-11].

Above findings prompted us to apply both groups of described compounds in supramolecular research. The first step was to study the fragmentation properties of phosphono peptides, which could aspire to be the guest molecules being negatively charged if compared with their peptide counterparts. These studies supplement already reported studies of organophosphorous compounds [12-17] and the detailed MS studies concerning peptides possessing Glu, Pro,

Asp and Leu residues [18, 19, 20, 21]. All phosphono peptides were synthesised and purified as described in literature [22].

In the second step host-guest chemistry studies showed selectivity in binding of ditopic, dinegative compounds by both studied receptors. Additionally, as it was expected, the molecules possessing branched side chain revealed lower affinity for both receptors with the binding being dependent on position of branching and size of the side chain. Competition experiment carried out with both receptors showed that polyamine macrocycle exhibited stronger binding abilities than its Schiff base analogue [23]. Formation of host-guest molecular complexes protects phosphono peptides against its fragmentation, what might indicate existence of strong intermolecular interaction published.

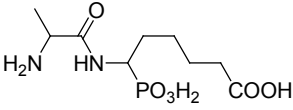
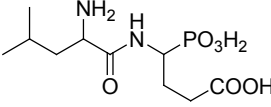
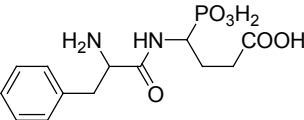
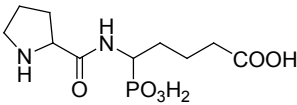
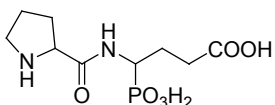
2. ESI mass spectrometry of phosphono peptides

2.1. Phosphono peptide ESI-MS fragmentation

The studied phosphono peptides due to their structural diversity were divided into six groups: Xaa-Yaa(COOH)PO₃H₂ (where Xaa, Yaa are any amino acid residues); Gly-Yaa-PO₃H₂; Ala-YaaPO₃H₂; Val-YaaPO₃H₂, Leu-YaaPO₃H₂, Pro-YaaPO₃H₂. In general, each of these groups over cone voltage 30 eV underwent deprotonation, dehydration, peptide bond cleavage and dimerization (Scheme 1). In the last process interaction between both terminal phosphonate groups are proposed (*vide supra*) [24], although complementary phosphonate-ammonium binding can not be excluded. For the latter interaction the polymeric supramolecular formation should be noticeable, but under the studied conditions they were not observed. Similarly, proton may be located either on amino or phosphonic group in other fragmentation species.

With exception of Gly-YaaPO₃H₂ (Table 2) all the examined dipeptides possessed individual characteristic fragmentation patterns, which depended on the structure of both side chains present in their structures. Thus, cleavage of bonds between C_α-C=O in N-terminal amino acid and CH₂-COOH in P-terminal aminophosphonate of the Xaa-Yaa(COOH)PO₃H₂ resulted in formation of a very specific molecular entities for all studied compound of this class (Table 1; Scheme 2). The less abundant, but noticeable, were also the signals originated from amide bond cleavage, dehydration and dimerization.

Table 1. The major peaks in the ESI mass spectra of phosphono peptides containing P-terminal analogues of acidic amino acids recorded at various cone voltages.

Phosphono peptides	cv [eV]	[M-H] ⁻	[M-H-H ₂ O] ⁻	[M-Xaa] ⁻	[M-H-NH ₂ CHR ₁ -COOH] ⁻	[M ₂ -H] ⁻
 1A	30	281	263		192	563
	70	281	263	210	192	563
	90	281	263		192	563
	130	281	263		192	563
 8Leu	30	295	277		164	591
	70	295	277		164	591
	90	295	277		164	591
	130	295	277		164	591
 3H	30	329	311		164	659
	70	329	311		164	659
	90	329	311		164	659
	130	329	311		164	659
 4P	30	293	275		178	587
	70	293	275		178	587
	90	293	275		178	587
	130	293	275		178	587
 5P	30	279	261		164	
	70	279	261		164	
	90	279	261		164	559
	130	279	261		164	559

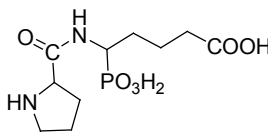
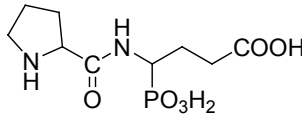
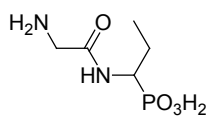
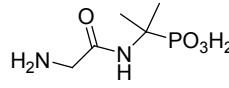
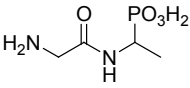
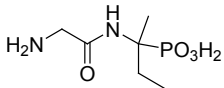
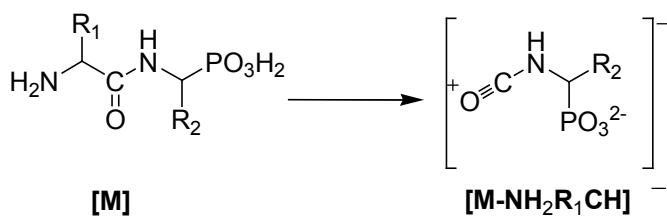
	30	293	275	587
	70	293	275	587
	90	293	275	587
	130	293	275	587
4P	<hr/>			
	30	279	261	
	70	279	261	
	90	279	261	559
	130	279	261	559
5P	<hr/>			

Table 2. The major peaks in the ESI mass spectra of phosphono peptides containing N-terminal glycine at various cone voltages.

Phosphono peptides	cv [eV]	[M-H] ⁻	[M-H-H ₂ O] ⁻	[M-Gly] ⁻	[M ₂ -H] ⁻
	30	195	177	138	391
	70	195	177	138	391
	90	195	177	138	391
	130	195	177	138	391
2G	<hr/>				
	30	195	177	138	391
	70	195	177	138	391
	90	195	177	138	391
	130	195	177	138	391
4G	<hr/>				

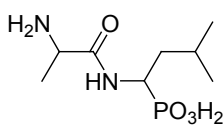
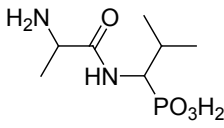
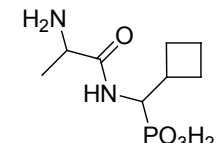
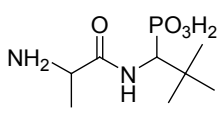
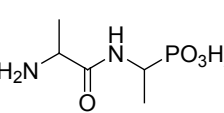
	30	181	163	124	363
	70	181	163	124	363
	90	181	163	124	363
	5G	130	181	163	124
	30	209	191	152	
	70	209	191	152	
	90	209	191	152	
	1G	130	209	191	152

The Ala-Yaa-PO₃H₂, Val-Yaa-PO₃H₂ and Leu-Yaa-PO₃H₂ phosphono dipeptides (Tables 3, 4 and 5) displayed analogous trend resulting presented on the Scheme 1. Additionally, similar as for Xaa-Yaa(COOH)PO₃H₂ molecules, characteristic detachment of NH₂CHR₁ fragment with mono or double deprotonation was observed (Scheme 3).



Scheme 3.

Table 3. The major peaks in the ESI mass spectra of phosphono peptides containing N-terminal alanine at various cone voltages.

Phosphono peptides	cv [eV]	[M-H] ⁻	[M-H-H ₂ O] ⁻	[M-Ala] ⁻	[M-2H-CH(CH ₃)NH ₂] ⁻	[M ₂ -H] ⁻
 3A	30	237				475
	70	237	219	166		475
	90	237	219	166		475
	130	237	219	166		475
 4A	30	223				447
	70	223	205	152		447
	90	223	205	152		447
	130	223	205	152		447
 2A	30	235	217(§)			471
	70	235	217	164		471
	90	235	217	164		471
	130	235	217	164		471
 8A	30	237				475
	70	237	219	166	192	475
	90	237	219	166	192	475
	130	237	219	166	192	475
 11A	30	195	177	124		391
	70	195	177	124	150	391
	90	195	177	124	150	391
	130	195	177	124	150	391

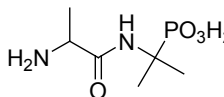
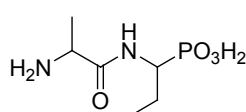
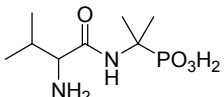
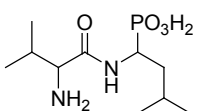
	30	209	191	138	164	
	70	209	191	138	164	
13A	90	209	191	138		
	130	209	191	138		
	30	209	191			419
	70	209	191	138	164	419
14A	90	209	191	138	164	419
	130	209	191	138	164	419

Table 4. The major peaks in the ESI mass spectra of phosphono peptides containing N-terminal valine at various cone voltages.

Phosphono peptides	cv [eV]	[M-H] ⁺	[M-H-H ₂ O] ⁺	[M-Val] ⁺	[M-2H-Val-NH] ⁺	[M-2H-NH ₂ R ₁ CH] ⁺	[M ₂ -H] ⁺
	30	237	219			164	475
	70	237	219	138	121	164	475
	90	237	219	138	121	164	475
	130	237	219	138	121		475
	30	265	247				
	70	265	247	166			
	90	265	247	166			
	130	265	247				

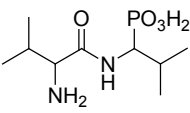
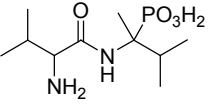
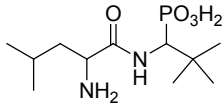
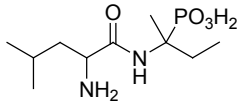
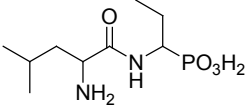
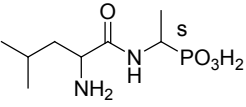
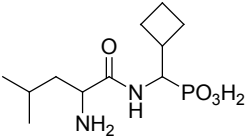
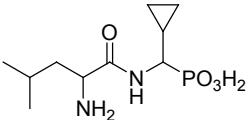
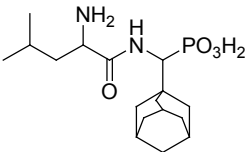
	30	251	233		503	
	70	251	233		503	
	90	251	233		503	
	130	251	233		503	
3V						
	30	265			192	531
	70	265	247	166	192	531
	90	265	247	166	192	531
	130	265	247	166	192	531
4V						

Table 5. The major peaks in the ESI mass spectra of phosphono peptides containing N-terminal leucine at various cone voltages.

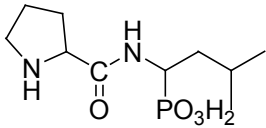
Phosphono peptides	c_v [eV]	[M-H] ⁺	[M-H-H ₂ O] ⁺	[M-Leu] ⁺	[M-NH ₂ R ₁ CH] ⁺	[M ₂ -H] ⁺
	30	279	261			559
	70	279	261	166		559
	90	279	261	166		559
	130	279	261	166		559
1L						
	30	265				531
	70	265	247	152		531
	90	265	247	152		531
	130	265	247	152		531
2L						

	30	251	233		503	
	70	251	233	138	503	
	90	251	233	138	503	
	130	251	233	138	503	
4L						
	30	237	219	124	475	
	70	237	219	124	475	
	90	237	219	124	475	
	130	237	219	124	475	
5L						
	30	277			555	
	70	277	259	164	555	
	90	277	259	164	555	
	130	277	259	164	555	
10L						
	30	263	245	150		
	70	263	245	150		
	90	263	245	150		
	130	263	245	150		
11L						
	30	357			272	715
	70	357	339	244	272	715
	90	357	339	244	272	715
	130	357	339	244	272	715
12L						

For Val containing peptide **1V** one more fragmentation process (Table 4) with detachment of Val-NH+2H⁺ entity was observed. Also, the course of amide bond cleavage noticeable for that group of peptides was less efficient than that present for other phosphono peptides. The last class of the studied peptides comprised of N-prolyl phosphono peptide. Its fragmentation pattern (Table 6)

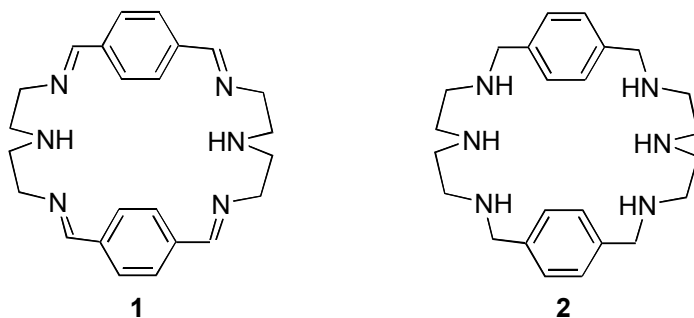
closely resemble that observed for N-alanyl phosphono peptides with formation of $[M-NH_2R_1CH]^-$ unit.

Table 6. The major peaks in the ESI mass spectra of phosphono peptides containing N-terminal proline at various cone voltages.

Phosphono peptides	cv [eV]	$[M-H]^-$	$[M-H-H_2O]^-$	$[M-Pro]^-$	$[M_2-H]$
 1P	30	263			527
	70	263	245	166	527
	90	263	245	166	527
	130	263	245	166	527

2.2. Phosphono peptide host-guest chemistry

The complexation of phosphono peptides by well known host molecules host **1** and **2** (Scheme 4) was then studied (Table 7).



Scheme 4.

Both receptors showed the same tendency in phosphono peptides binding. In general, formation of the molecular monocationic complexes was observed. However, the affinities of certain groups of these peptides for receptor molecules were diverse. For example, in the case of those containing analogues of acidic amino acids (existing as dinegative anions), the length between phosphonic and carboxylic moieties, which are spanning between two amine groups of the macrocycles, was the crucial factor. Thus, the most optimal intermolecular interactions with opposite amino groups of receptor **1** possessed peptide

1A (for structure see Table 1), which contains four methylene groups in the aminophosphonate side chain, and peptide **4P** having three methylene group (Table 1). If considering complexation abilities of mononegative peptides of the structures: Ala-XaaPO₃H₂ and Leu-XaaPO₃H₂ the crucial element influencing their binding to host molecule **1** was the presence of variable type of branching in side chain of the P-terminal residue. This, most probably, results from close proximity of this chain to the anchoring phosphonic unit. On the other hand, peptides having N-terminal Gly and Val did not demonstrate the same dependence being bound with similar affinities. The obtained data demonstrate that the N-terminal residue has no influence on the mode of binding as also revealed by competition studies. In addition, the presence of host molecules protected phosphono peptides from fragmentation, which may indicate that they are strongly bound under the ESI conditions [25].

Table 7. The ESI-MS studies of complexation of phosphono peptides by macrocyclic receptor **1**.

Guest molecules and their complexation ratio	Molecular weight of guest	Molecular weight of formed complexes	The observed signal (M+H) ⁺ and their complexation ratio
1A	282	685	686
8L	296	699	700
3H	330	733	734
1A:8L:3H (1:1:1)			686:700:734 (1:0.5:0.5)
2G	196	599	600
4G	196	599	600
5G	181	584	585
2G:4G:5G (1:1:1)			600:600:585 (1:1:1)
3A	238	641	642
4A	224	627	628
8A	238	641	642
11A	196	599	600
3A:4A:8A:11A (1:1:1:1)			642:628:642:600 (0.5:0.8:0.8:1)
1L	280	683	684
2L	266	669	670
4L	251	654	655
5L	237	640	641
1L:2L:4L:5L (1:1:1:1)			684:670:655:641 (0.5:0.8:0.8:1)

2P	236	639	640
4P	294	697	678
5P	280	683	684
2P:4P:5P (1:1:1)			640:678:684 (0.5:1:0.1)
2V	266	669	670
3V	252	655	656
4V	266	669	670
2V:3V:4V (1:1:1)			670:658:670 (1:1:1)

When comparing the binding properties of receptors **1** and **2** it is clearly seen that receptor **2** interacted with guest molecules more efficiently than receptor **1** (Table 8). This phenomenon most likely results from that the higher number of amine groups in **2**, which allow to achieve a better fit of guest molecule into the macrocycle cavity because of more flexible placement of negatively charged groups.

Table 8. The competition studies of two receptor and one guest molecules.

Supramolecular components	Molecular weight of guest	Molecular weight of formed complexes with receptor 1	Molecular weight of formed complexes with receptor 2	The observed signal (M+H) ⁺ and their complexation ratio
1A+1+R2 (10:1:1)	282	685	692	686:693(0.7:1)
8L+1+2 (10:1:1)	296	699	706	700:707 (0.8:1)
3H+1+2 (10:1:1)	330	733	740	734:741 (0.6:1)
2G+1+2 (10:1:1)	196	599	606	600:607 (0.7:1)

The ESI-MS spectrometry studies revealed the existence of general trend of fragmentation, characteristic for all the studied phosphono peptides. Moreover, when taking into consideration the presence of characteristic residues at the N-terminus and P-terminus of Xaa-YaaPO₃H₂ dipeptide it is possible to create a representative model of fragmentation, which indicates the differences in strength of bonds between their C-C, C-P atoms.

Supramolecular studies provided information about binding of these peptides

to commonly used aza-macrocyclic receptors **1** and **2**. These studies indicated preferential binding of the peptides containing analogues of acid amino acids, which possess an additional carboxylic group in side chain. This may result from the best adaptation of these peptides to the binding cavities of both receptors, however, the exact molecular mode of binding has to be determined. Comparison of both macrocycles have shown that the receptor **2** having six amino groups was more efficient host molecule for phosphono peptides than analogous Schiff base **1**. Quite interestingly, the tight binding resulted in significant protection of the studied phosphono peptides against defragmentation.

Acknowledgement

The authors would like to thank Polish Ministry of Science and Higher Education for financial support by grant No. R0501601.

References

1. P. Kafarski and B. Lejczak in "Aminophosphonic and Aminophosphinic Acids Chemistry and Biological Activity" eds. V. P. Kukhar and H. R. Hudson, John Wiley & Sons, LTD, 2000, pp 407-442.
2. J. Jazwinski, J.-M. Lehn, R. Meric, J.-P. Virneron, M. Cesario, J. Guilhem, C. Pescard, *Tetrahedron Lett.*, 28 (1987) 3489-3492.
3. R. W. Hay, T. Clifford, D. T. Richens, P. Lightfoot, *Polyhedron* 19 (2000) 1485-1492.
4. J. Gao, A. E. Martell, J. Reibenspies, *Inorg. Chim. Acta*, 329 (2002) 122-128.
5. J. Gao, A. E. Martell, J. Reibenspies, *Inorg. Chim. Acta*, 335 (2002) 125-129.
6. T. Lu, S. Chen, Z. Mao, A. E. Martell, L. Ji, *Inorg. Chem. Commun.*, 6 (2003) 1068-1070.
7. D. A Rockcliffe, A. E. Martell, *J. Mol. Cat. A*, 106 (1996) 211-221.
8. D. A Nation, J. Reibenspies, A. E. Martell, *Inorg. Chem.*, 35 (1996) 4597-4603.
9. A. E. Martell, R. J. Motekaitis, Q. Lu, D. A. Nation, *Polyhedron*, 18 (1999) 3203-3218.
10. Q. Lu, R. J. Motekaitis, J. Reibenspies, A. E. Martell, *Inorg. Chem.*, 34 (1995) 4958-4964.
11. J. Huang, Sh.-A. li, D.-X. Yang, W.-Y. Sun, W.-X. Tang, *Bioorg. Med. Chem.*, 12 (2004) 529-535.
12. Z. Moldovan, S. Nicoara, M. Culea, O. Cozar, I. Fenesan, P. Vegh, J.J. Rios, *J. Mol. Struct.*, 348 (1995) 393-396

13. G. Schroeder, N. Lyapchenko, P. Przybylski, B. Brzeziński, T. Kozik, A. Burzyńska, P. Kafarski, *J. Mol. Struct.*, 750 (2005) 142-151.
14. N. Lyapchenko, G. Schroeder, P. Przybylski, A. Burzyńska, P. Kafarski, B. Brzeziński *J. Mol. Struct.*, 782 (2006) 183-190.
15. A. Filippi, M. Speranza, A. Paladini, R. De Carolis, a. Giardini-Guidoni, A. Lagana, M. Satta, *J. Mass Spectrom.* 41 (2006) 98-102.
16. D. N. Tripathi, K. S. Pandey, A. Bhattacharya, R. Vaidyanathaswamy, *Anal. Chem.* 64 (1992) 823-824.
17. H. Fang, m.-j. Fang, Ch.-j. Zhu, L.-n. Liu, Y.-f. Zhao, *Rapid Comm. Mass Spectrom.* **21** (2007) 3629-3634.
18. A. G. Harrison, *J. Mass. Spectrom.* 38 (2003) 174-187.
19. D. Maux, Ch. Enjalbal, J. Martinem, J.-L. Aubagnac, *Rapid Comm. Mass Spectrom.* **16** (2002) 1470-1475.
20. A. G. Harrison, *Int. J. Mass. Spectrom.* 255-256 (2006) 111-112.
21. C. Terier, J. Doumit, J. Frey, *Amino Acids*, 10 (1996) 273-276.
22. P. Kafarski, B. Lejczaj and P. Mastalerz, *Can. J. Chem* 60 (1982) 3081-3084.
23. P. Mlynarz, A. Rydzewska, S. Sliwińska, M. Szymczyk, *Phosphorous Sulphur and Silicon*, , 184 (2009) 1496-1501.
24. O. Picazo, I. Alkorta, J. Elguero, O. Mo, M. Yanez, *J. Phys. Org. Chem.*, 18 (2005) 491-497.
25. E. Leize, A. Jaffrezic, A. Van Dorsselaer, *J. Mass. Spectrom.*, 31 (1996) 537-544.

Наукове видання

МОЛЕКУЛЯРНІ РЕЦЕПТОРИ

(англійською мовою)

Збірник наукових праць

Підписано до друку 20.12.2011. Формат 60x84/16. Папір офісний.

Гарнітура Times New Roman. Друк-лазерний. Ум.друк.арк. 22,55

Обл.-вид.арк. 24. Тираж 200.

Видавниче підприємство «Східний видавничий дім»
(Державне свідоцтво № ДК 697 от 30.11.2001)
83086, г. Донецьк, вул. Артема, 45
тел./факс (062) 338-06-97, 337-04-80
e-mail: svd@stels.net

M 75 Molecular receptors : [collected research papers] / Edited by V.I. Rybachenko. – Donetsk : «East Publisher House» Ltd, 2011. – 200 с.

ISBN 978-966-317-108-1

Functional materials with molecular receptors is a new direction in chemistry. The book presents the results of basic research on various types of molecular receptors. Discusses not only the synthesis, properties and application of these systems but also the research methods appropriate to describe the molecular receptors and their complexes.

Функціональні матеріали на підставі молекулярних рецепторів є новий напрямок в хімії. У книзі представлені результати фундаментальних досліджень різних типів молекулярних рецепторів. Обговорюється не тільки синтез, властивості і застосування цих систем, а й методи досліджень, що підходять для опису молекулярних рецепторів і їх комплексів.

УДК 541.1+547

ББК 24.2

M 75

